THE ROLE OF THE NEUREGULINS IN THE NUCLEUS

A thesis submitted to the University of Kent for the degree of Doctor of Philosophy

Ming Wang

2010

Declaration

No part of this thesis has been submitted in support of an application for any degree or other qualification of the University of Kent, or any other University or Institution of learning.

Signed: 

Date: 25/10/2010

Acknowledgements

I would like to thank my supervisor Professor Bill Gullick for his advice, encouragement, guidance and support throughout this project. Many sincere thanks to all the members of the 'Gullick lab' past and present for their help and friendship. I am also grateful to Ray Newsam and Ian Brown for their help with microscopy techniques and imaging softwares.

This work would not have been possible without the support of my family, in particular my mother for her constant encouragement, love and support, for which I will never forget.

List of figures

List of tables

Abstract

The neuregulins (NRGs) are ligands for receptor tyrosine kinases of the ErbB family. The *NRG* gene family consists of four members, *NRG1- 4* encoding different isoforms due to alternative splicing. NRG signalling has been implicated in normal development and in the pathology of many diseases. Using immunohistochemical staining of tissue arrays, we detected that NRG1α and 1β localised to the cell nuclei of a range of normal and human cancer tissues. The β3 isoform of NRG1 localised to two subnuclear compartments: nucleoli and spliceosomes. We tagged NRG1β3 with photoactivateable GFP and demonstrated that the fusion protein re-localised from nucleoli to spliceosomes over a ninety minute period. Using wild type NRG1β3 and its two mutants which localised exclusively to spliceosomes or to nucleoli, we explored the possible functions of intranuclear NRG1β3 in each of these compartments separately. We showed using an array capable of detecting 42 receptor tyrosine kinases that wild type NRG1 and a mutant exclusively localising to spliceosomes increased phosphorylation and/or expression of the ErbB4 and ErbB2 receptors. Using a transcriptomic analysis the same two constructs induced expression of messenger RNA of Heat Shock Protein 70B' and we confirmed its increased expression at the protein level using western blot analysis. This data supports the hypothesis that intranuclear NRGs could activate receptor signalling and alter gene expression when localised in spliceosomes.

Abbreviations

ABC	Avidin-Biotin Complex
ADAM	A disintegrin and metalloprotease
APS	ammonium persulfate
AR	amphiregulin
ARIA	acetylcholine receptor-inducing activity
AS MDW	Application Solution Multidimensional Workstation
bp	base pair
BrdU	bromodeoxyuridine
BSA	bovine serum albumin
BTC	betacellulin
cDNA	complementary DNA
CIAP	Calf Intestinal Alkaline Phosphatase
CNS	central nervous system
CRD	cysteine-rich domain
DAB	3,3' diaminobenzidine tetrachloride
DCIS	ductal carcinoma *in situ*
DEPC	diethylpyrocarbonate
DMEM	Dulbecco's modified Eagle's medium
DMSO	dimethyl sulfoxide
DNA	deoxyribonucleic acid
Dox	doxycycline
dNTP	deoxynucleotide triphosphate
ECD	extracellular domain
ECL	enhanced chemiluminescence
EDTA	ethylene diamine tetra acetic acid
EGF	epidermal growth factor
EGFP	enhanced green fluorescence protein
EGFR	epidermal growth factor receptor
EGTA	ethylene glycol tetraacetic acid
EPR	epiregulin
ER	endoplasmic reticulum
ERAD	endoplasmic reticulum associated degradation
FA	formaldehyde agarose

FACS	fluorescent activated cell sorter
FBS	foetal bovine serum
FGF	fibroblast growth factor
GAPDH	glyceraldehyde phosphate dehydrogenase
GFP	green fluorescent protein
GGF	glial growth factor
GH	growth hormone
GPCR	G-protein coupled receptors
Grb2	growth-factor-receptor bound-2
HBD	heparin-binding domain
HB-EGF	heparin-binding EGF
HRG	heregulin
HRP	horse radish peroxidase
HSP	heat shock protein
ICD	intracytoplasmic domain
IEGs	immediate-early genes
IF	immunofluorescence
Ig	immunoglobulin
IGF1R	insulin-like growth factor 1 receptor
IHC	immunohistochemistry
Jak2	Janus tyrosine kinase 2
Kb	kilo bases
kDa	kilo Dalton
LB	Luria-Bertani
MAPK	mitogen-activated protein kinase
MIG6	mitogen-induced gene 6
mAb	monoclonal antibody
mM	millimolar
mRNA	messenger ribonucleic acid
NDF	neu differentiation factor
ng	nanogram
NLS	nuclear localisation sequence
NRG	neuregulin
NSCLC	non-small-cell lung cancer
NTAK	neural and thymus-derived activator of ErbB kinases

PAGE	polyacrylamide gel electrophoresis
PAFP	photoactivatable fluorescent proteins
PDGF	platelet-derived growth factor
PBS	phosphate buffered saline
PCNA	proliferating cell nuclear antigen
PCR	polymerase chain reaction
PDZ	Psd-95/Dlg/ZO1
PI3K	phosphatidylinositol 3-kinase
PMT	photo multiplier tube
PNS	peripheral nervous system
Prl	prolactin
PSD-95	postsynaptic density protein-95
PTB	phosphotyrosine binding domain
PTP	protein tyrosine phosphatase
RNA	ribonucleic acid
rpm	revolutions per minute
RTK	receptor tyrosine kinase
RT-PCR	reverse transcriptase-polymerase chain reaction
SDS	sodium dodecyl sulphate
SE	standard deviation
SH2	Src homology 2
Shc	Src-homology-2-containing
SOCS5	suppressor of cytokine signalling-5
STAT3	signal transducers and activators of transcription 3
TACE	TNFα converting enzyme
TAE	tris acid EDTA
TEMED	N,N,N,N'-Tetra-methyl-ethylenediamine
Tet	tetracycline
TGF-α	transforming growth factor-α
TKI	tyrosine kinase inhibitor
Tm	melting temperature
TNFα	tumour necrosis factor α
V	voltage
VEGF	vascular endothelial growth factor
WB	western blot

Chapter 1. Introduction

1.1 Cell signalling

All cells receive and respond to signals from their surroundings. Many unicellular eukaryotes respond to signalling molecules secreted by other cells, allowing cell-cell communication. In multicellular organisms, the behaviour of each individual cell is tightly regulated by a variety of signalling molecules that are secreted or expressed on the surface of one cell and bind to receptors expressed by a target cell. These signals integrate and coordinate the functions of individual cells that make up complex organisms. The binding of signalling molecules (including steroid hormones, neurotransmitters, peptide hormones, and growth factors) to their receptors initiates a chain of intracellular reactions that regulate virtually all aspects of cell behaviour, including metabolism, movement, proliferation, and survival. Most ligands responsible for cell-cell signalling bind to receptors on the surface of their target cells, while other ligands such as steroid hormones bind to receptors that are intracellular proteins located in the cytosol or the nucleus. Among the wide variety of signalling molecules in animals, the polypeptide growth factors play critical roles in controlling animal cell growth and differentiation. As might be expected, abnormalities in growth factor signalling are the basis for a variety of diseases, including many kinds of cancer.

1.2 Receptor tyrosine kinases

The receptor tyrosine kinase (RTK) family includes the receptors for most polypeptide growth factors. Approximately 20 different RTK families have been identified including the insulin receptor and the receptors for many growth factors such as epidermal growth factor (EGF), platelet-derived growth factor (PDGF), fibroblast growth factor (FGF) and vascular endothelial growth factor (VEGF). All RTKs share a similar structure: a ligand-binding extracellular domain, a single transmembrane domain, and an intracellular tyrosine kinase domain which possesses catalytic activity and sites for protein-protein interactions (Fischer, 1999). The extracellular domains of RTKs exhibit

a variety of conserved elements, including immunoglobin (Ig)-like domains and cysteine-rich domains. The majority of RTKs are largely monomeric in the absence of ligands. Ligand binding to the extracellular domain leads to conformational changes that induce and stabilise receptor dimerisation (Heldin, 1995). The transmembrane domain of RTKs is primarily α-helical in structure and anchors the receptor in the correct orientation with respect to the membrane. The cytoplasmic domain comprises a well-conserved bilobular protein tyrosine kinase region containing an amino-terminal lobe and a carboxy-terminal lobe (Hubbard and Till, 2000). Adenosine triphosphate (ATP) binds in the cleft between the two lobes, and the tyrosine-containing substrate binds to the carboxy-terminal lobe. Phosphorylation of distinct tyrosine residues on the activated receptor creates binding sites for Src homology 2 (SH2) (Waksman *et al.*, 1992) and phosphotyrosine-binding (PTB) domain-containing molecules (Eck *et al.*, 1996). Some of these molecules are, in turn, phosphorylated, leading to their activation or to interact with other downstream signalling proteins, resulting in the assembly of activated signalling complexes at the membrane (Cohen *et al.*, 1995). These signalling cascades induced by RTK activation convey the signal from the cell surface to the nucleus, where gene expression is regulated.

RTKs are regulators of a variety of different biologic effects including cell growth, movement, differentiation and survival. Also, they have a long history of involvement in human cancer: amplification, overexpression or somatic mutations resulting in increased receptor signalling have been observed in at least ten RTK families (Bennasroune et al., 2004). Mutations in the extracellular domain have been described in several RTK families that result in constitutive receptor dimerisation. Similarly, mutations in the kinase domains of RTKs give rise to activated receptors associated with various human diseases. An increased understanding of RTK signalling and function will provide insights for drug targeting strategies for cancer treatments.

1.3 The ErbB family

The ErbB receptors belong to subclass I of the superfamily of receptor tyrosine kinases. There are four members of the ErbB family, including the epidermal growth factor receptor (EGFR) (also known as ErbB1 or HER1), ErbB2 (HER2), ErbB3 (HER3), and ErbB4 (HER4). Like other RTKs, each of these ErbB receptors possesses an

extracellular ligand-binding region, a single transmembrane helix, and a cytoplasmic region that contains the tyrosine kinase domain. Recent studies have also highlighted the role of the juxtamembrane region, the cytoplasmic segment of the receptor that connects the transmembrane helix to the tyrosine kinase domain (Jura et al., 2009; Red Brewer et al., 2009), which has been demonstrated to be essential in stabilising formation of the tyrosine kinase dimer. The extracellular domains of ErbB receptors in common contain two ligand-binding (L) domains and two cysteine-rich (CR) domains which are arranged in an alternating fashion (Figure 1-1). These domains are less conserved among ErbB receptors providing a rationale for their different specificity in ligand binding (Yarden, 2001). The intracellular tyrosine kinase domains of ErbB receptors show a high degree of homology.

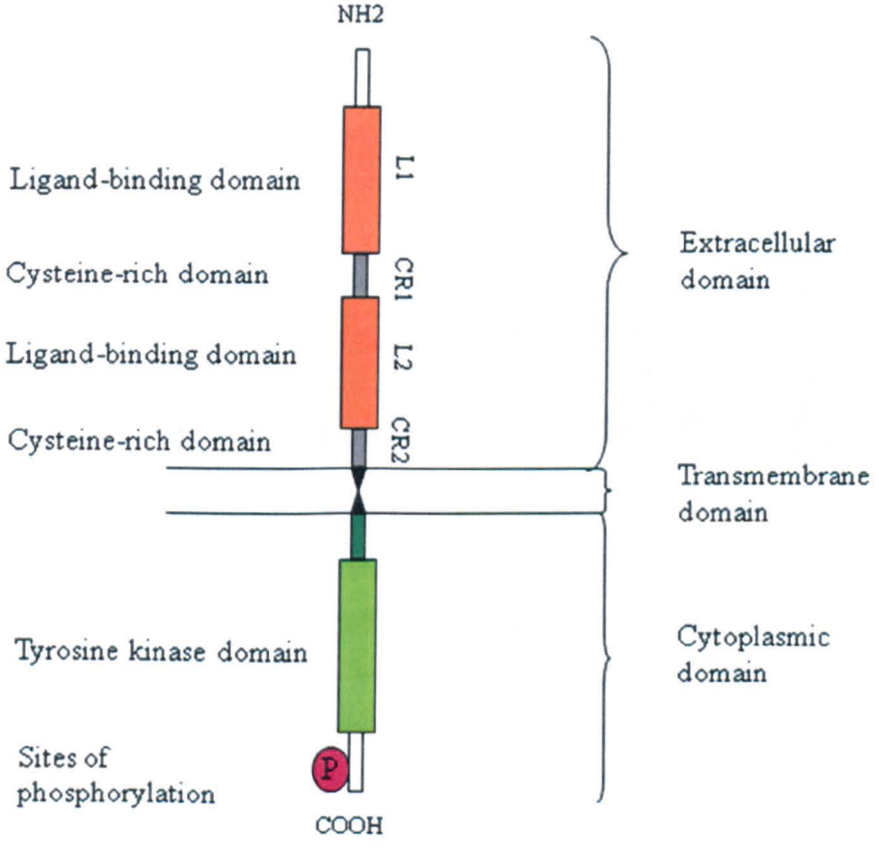

Figure 1-1. Schematic structure of EGFR. The two CR domains are shown in grey and the two L domains are shown in orange. The juxtamembrane is shown in dark green. The tyrosine kinase domain is shown in light green and the carboxy terminal region containing phosphorylation sites is represented by the red circle. Figure adapted from Gullick, 2001.

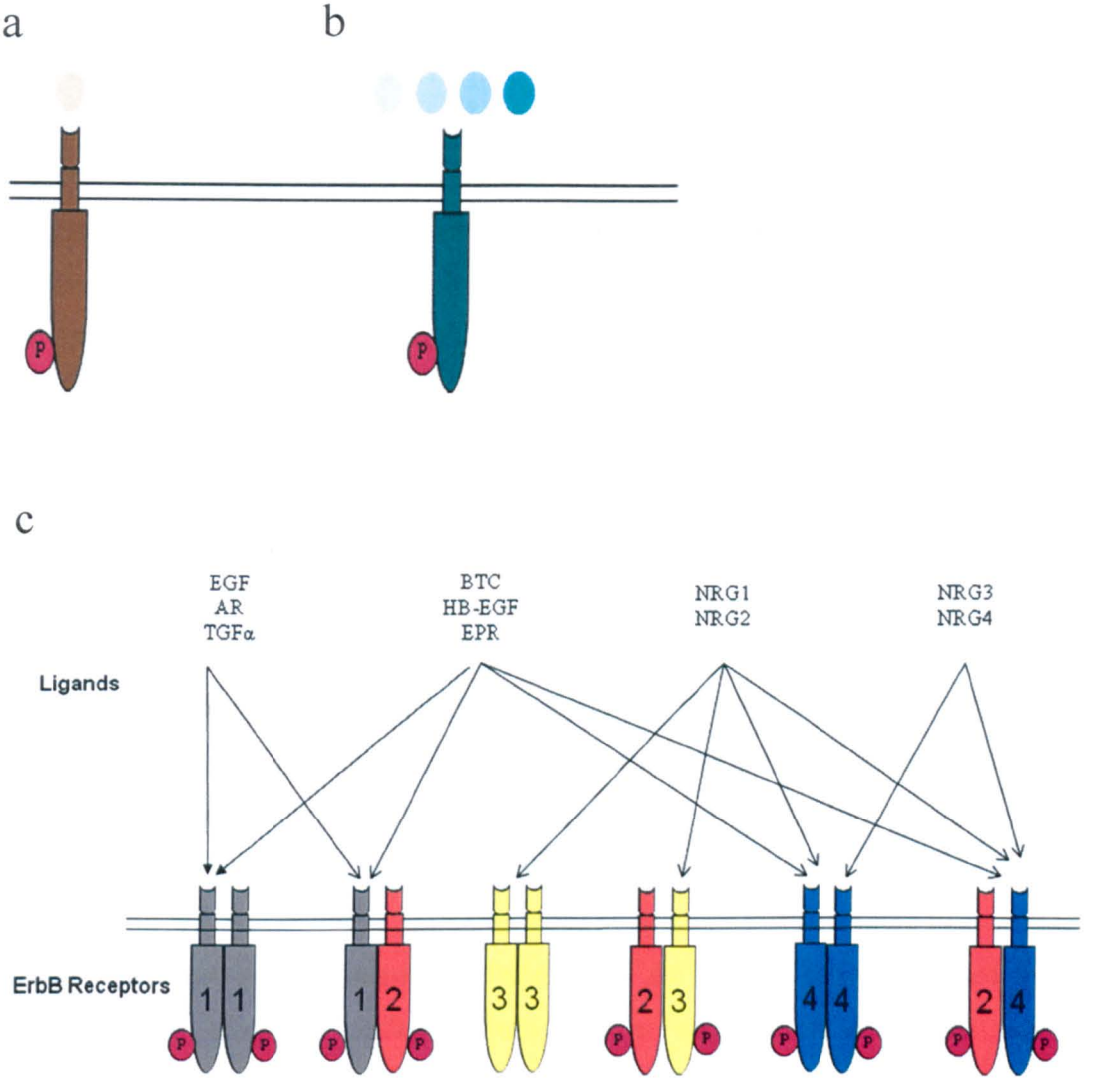

Figure 1-2. Diagrammatic representation of the evolution of ErbB receptor family and their ligands from (a) *Caenorhabditis elegans*, through (b) *Drosophila melanogaster*, and to (c) vertebrates. In vertebrates, the ErbB receptor family consists of four members and there are two variations within this family: ErbB2 that does not bind any known ligand, and ErbB3 that lacks kinase activity. ErbB ligands are divided into four categories based on their binding specificity to ErbB receptors. Figure adapted from Stein and Staros, 2000.

The vertebrate ErbB family has evolved from a single ligand-receptor combination in *Caenorhabditis elegans*, through *Drosophila melanogaster* with one receptor and four ligands, to vertebrates, where four ErbB receptors and multiple ligands are expressed (Figure 1-2). A trend leading to expanded signalling is observed during evolution. This evolutionary process, as suggested by Amit et al., greatly enhances reproducibility and reliability of the signalling required in multicellular organisms (Amit et al., 2007).

1.4 ErbB ligands

ErbB receptors are activated by binding the growth factors of the EGF-family to their extracellular domains. Proteins that belong to the EGF-family are characterised by the presence of an EGF-like domain. The EGF-like domain, composed of three intramolecular disulphide bonds formed between six conserved cysteine residues, confers the binding specificities of each ligand to the receptors. With respect to their binding specificity to ErbB receptors, EGF-related growth factors could be divided into four categories (Figure 1-2c). The first group includes EGF, transforming growth factor-α (TGFα) and amphiregulin (AR), which bind only to the EGF receptor. The second group includes heparin-binding EGF (HB-EGF), betacellulin (BTC) and epiregulin (EPR) which can bind both the EGFR and ErbB4. The third group includes neuregulin1 (NRG1) and 2 (NRG2) which both bind to ErbB3 and ErbB4. The last group consists of neuregulin 3 (NRG3) and 4 (NRG4) which bind specifically to the ErbB4. EGF family ligands are distinguished from non-ligand EGF motifs based on the presence of a splice site between the fourth and fifth cysteines within the six cysteine EGF-module and are relative close to a putative transmembrane region of the potential ligand (Stein and Staros, 2000). Based on these criteria it is possible more ligands exist. Epigen, the most recently identified member of the family, is characterised by its relatively low receptor binding affinity but a very potent mitogenic activity (Kochupurakkal *et al.*, 2005). Other potential ligands including tomoregulin 1 and 2 (Eib and Martens, 1996), neuroglycan-C (Kinugasa *et al.*, 2004), and mucin 3, 4, 12, and 17 also have been reported. No direct ligand for ErbB2 has been described (Olayioye *et al.*, 1998). Figure 1-3 is a tree diagram with labelled ligand families as branches (Stein and Staros, 2006). Generally, the tree segregates into EGF receptor ligands and ErbB3/ErbB4 ligands, paralleling the evolution of the receptors. Another feature worth noting is the pairing of the ligands (TGFα/BTC, AR/HB-EGF, and EPR/EGF) which reflects gene duplication events. Interestingly, within each pair, the receptor binding specificity is different, with one more specific for the EGF receptor, while the other has broader receptor specificity.

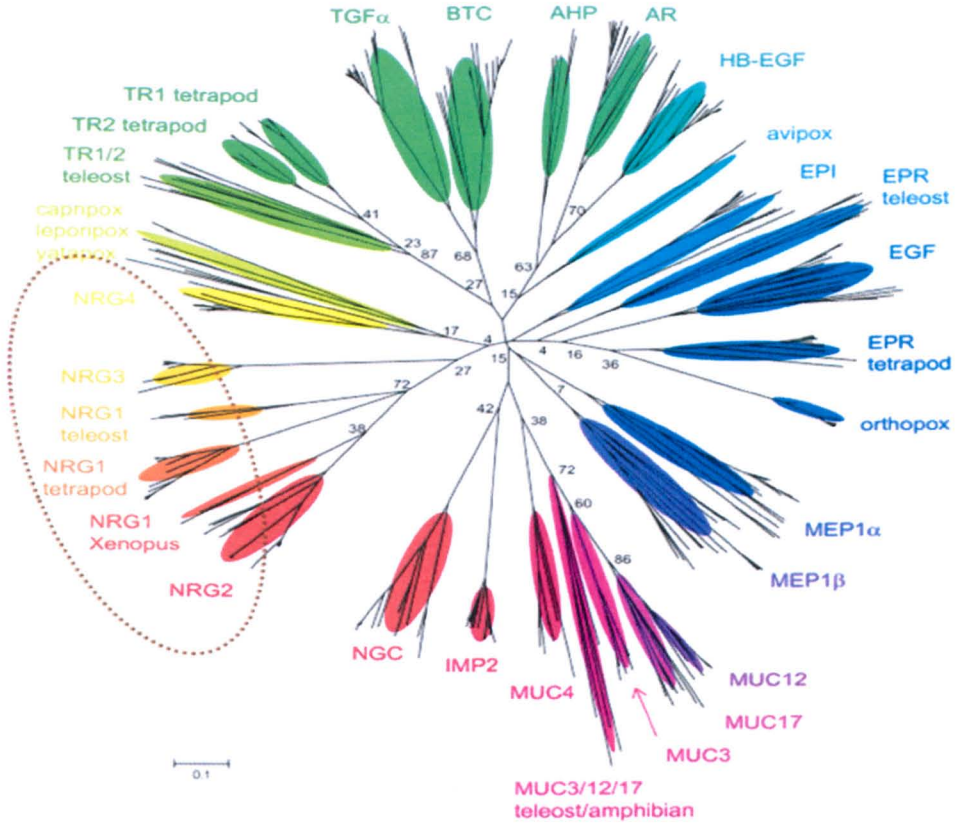

Figure 1-3. Relationships among the ErbB ligand family with the neuregulin family circled. Figure adapted from Stein and Staros, 2006.

1.5 Receptor dimerisation

Binding of ligands to the extracellular domains of ErbB receptors results in receptor homo- or hetero-dimerisation. Individual receptor parings can consist of two molecules of the same type, called homodimers, or two molecules of different types, termed a heterodimer. Based on the crystal structures of EGFR, ErbB2 and ErbB3 extracellular domains, the process of ligand-induced receptor dimerisation has been further understood (Garrett et al., 2002; Ogiso et al., 2002). As mentioned earlier, the extracellular domain of ErbB receptors consists of four subdomains. L1 and L2 are involved in ligand binding, whereas CR1 and CR2 are cysteine-rich domains (Figure 1-4a). In the unoccupied state, the receptor is largely monomeric. The recently resolved EGFR dimer of 2:2 stoichiometry reveals that the ligands are located on opposite sides of the dimer, which is different from other ligand:RTK complexes. It also reveals that the liganded ErbB structure comprises a dimerisation arm, which is a β-hairpin loop projecting away from the ligand binding site. This dimerisation arm mediates

interactions between receptor dimers. Prior to ligand binding, CR1 and CR2 are connected through intramolecular bonding involving the dimerisation arm, thus keeping L1 and L2 at distance and preventing the formation of a ligand binding site (Figure 1-4b). In a ligand-bound state L1 and L2 are brought together leading to the separation of CR1 and CR2 (Figure 1-4d). This conformational change exposes the dimerisation arm to the exterior allowing it to interact with the CR1 of its dimerisation partner leading to the formation of a dimer composed of two 2:2 receptor:ligand complexes (Figure 1-4e).

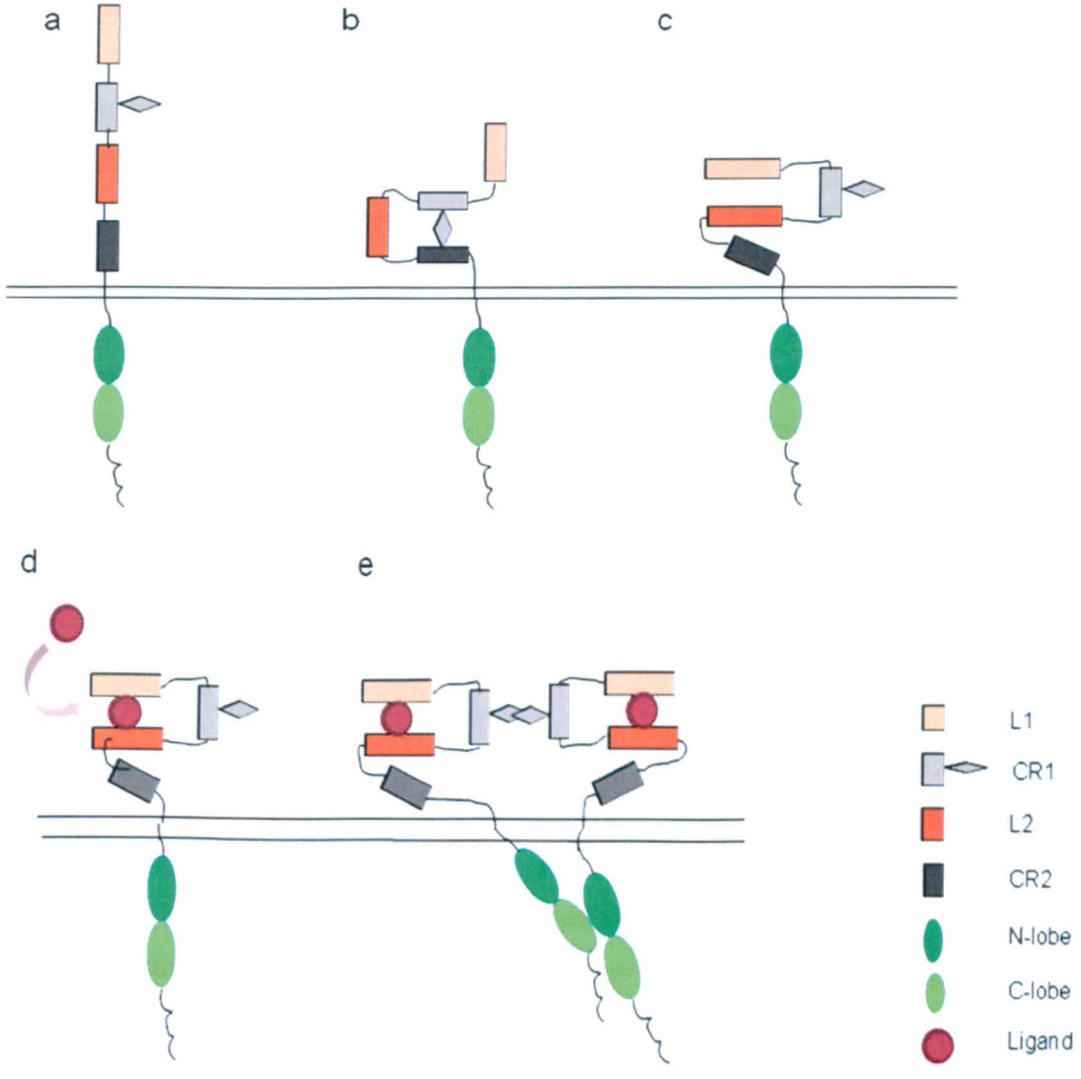

Figure 1-4. Schematic representations for ligand-dependent dimerisation and activation of an ErbB receptor. (a) The domain structure; (b) inactive monomer; (c) ErbB2 has a fixed conformation that resembles the ligand-activated state of other ErbB receptors; (d) monomer in active conformation; and (e) dimer. Figure adapted from Zhang et al., 2006.

The structure of the ErbB2 extracellular region shows significant differences to the other ErbB receptors (Figure 1-4c). In the absence of a ligand, domains L1 and L2 of ErbB2 are very close and this interaction makes ligand binding impossible, explaining why ErbB2 has no ligand. The constitutive exposure of the ErbB2 dimerisation arm also explains why ErbB2 has an enhanced ability to form heterodimers and is considered as a favourite partner for all other ErbB receptors.

Binding of an EGF-like ligand to the extracellular domain of ErbB receptors induces a conformational alternation not only of the extracellular domain which mediates receptor dimerisation but also the intracellular domain resulting in an activated kinase. As mentioned earlier, the ErbB kinase domain comprises two lobes: the N-terminal lobe and the C-terminal lobe. Extracellular domain dimerisation brings the kinase domains together, with the C-lobe of one kinase serving as the activator of the other kinase domain by binding to the N-lobe of its dimer partner (Figure 1-4e) (Zhang et al., 2006). It is believed that the receptors are flexible at the region between the transmembrane domain and the N-lobe implying that the receptors can switch positions to activate each other. ErbB3 has been generally considered as kinase-inactive due to the lack of several key conserved residues. However, recent findings demonstrate that despite these sequence alterations, ErbB3 retains sufficient kinase activity to transphosphorylate the receptor's intracellular domain when in a heterodimeric state (Shi et al., 2010a).

1.6 Signalling pathways downstream of ErbB receptors

The signalling pathways downstream of ErbB receptors are complex and diverse (Figure 1-5). Even though all possible homo- and heterodimeric receptor complexes between members of the ErbB family have been identified in different systems (Olayioye *et al.*, 2000), evidence has suggested that a given ErbB receptor combination can discriminate among signalling by different ligands. The following experiment illustrates the importance of the ligand identity in determining the signalling pathways engaged. ErbB4 transfected cells were treated with different ligands BTC, NRG1 and NRG2 individually (Sweeney and Carraway, 2000). Even though the cells all exhibited similar ErbB4 receptor dimerisation, different signalling molecules were recruited to the activated ErbB4 proteins (Figure 1-6). The preferential recruitment of p85 to NRG1 and NRG2 stimulated receptors is associated with cell survival or motility, whereas the

preferential recruitment of Shc to BTC stimulated receptors is linked to cell growth and differentiation. The underlying mechanism of differential recruitment and activation of intracellular signalling molecules has not been elucidated. However, the experimental results above strongly suggested that different ligands can elicit different usage of ErbB phosphorylation sites or recruit different signalling proteins to activated receptors, thereby stimulating distinct signalling pathways. As shown in Figure 1-5, the signalling molecules recruited by activated ErbB tyrosine kinase receptors are diverse, including adaptor proteins such as Shc and Grb2, kinases such as c-Src and phosphatidylinositol 3-kinase (PI3K), protein tyrosine phosphatases such as SHP1 and SHP2, and the Cbl E3 ubiquitin ligase (Yaffe, 2002). As expected these signalling molecules, in turn, drive different cellular responses.

Even if the same signalling molecules are recruited to the activated ErbB receptors, there are examples of preferential modulation of specific pathways. For instance, all four ErbB receptors can activate PI3K pathways by recruiting p85 regulatory subunit to the activated receptor (Soltoff and Cantley, 1996). However, different mechanisms are used. p85 binds to EGFR and ErbB2 indirectly through adaptor proteins, whereas a specific subunit of p85 binds directly to ErbB3 or one of the ErbB4 isoforms (Elenius et al., 1999; Fedi et al., 1994). Due to the presence of multiple binding sites for p85, ErbB3 is the most efficient activator of PI3K (Prigent and Gullick, 1994).

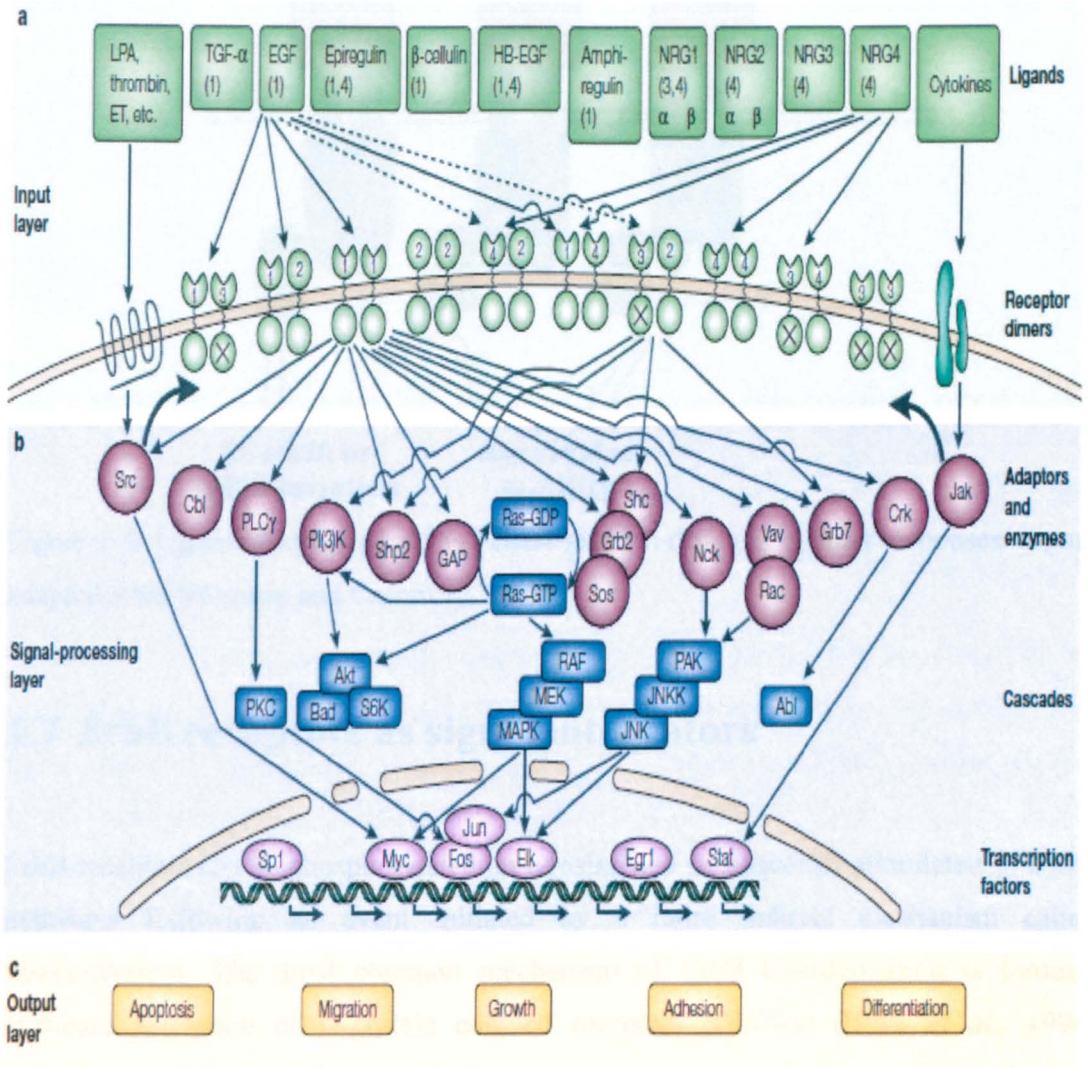

Figure 1-5. Overview of the ErbB signalling pathways. The ErbB signalling network consists of three layers: (a) ligands and their cognate receptor combinations comprise the input layer, (b) diverse signalling molecules that are activated upon receptor activation comprises the signal-processing layer, and the output is involved in regulation of gene expression (c) which then activate responses ranging from cell division to differentiation to apoptosis. Figure taken from Yarden and Sliwkowski, 2001.

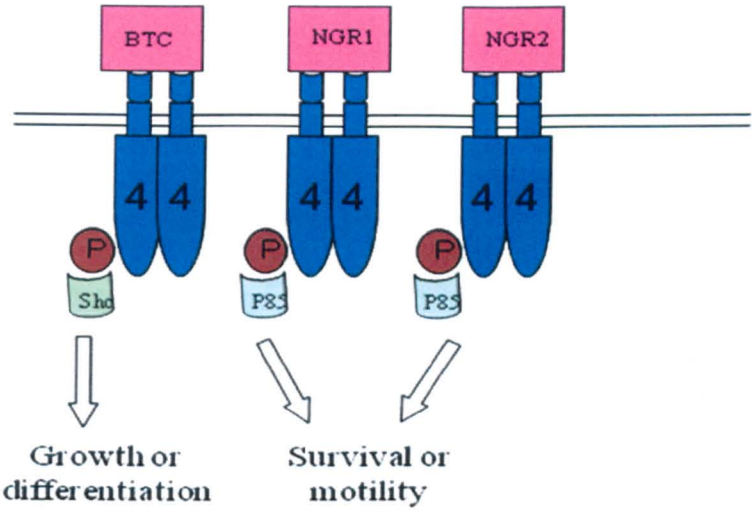

Figure 1-6. Ligand discrimination by ErbB4 leads to different cellular responses. Figure adapted from Sweeney and Carraway, 2000.

1.7 ErbB receptors as signal integrators

ErbB receptors can be phosphorylated on tyrosine and subsequently stimulate signalling pathways following an event initiated by a more indirect mechanism called transactivation. The most common mechanism of ErbB transactivation is through upstream activation of G-protein coupled receptors (GPCRs) (Daub *et al.*, 1996; Donepudi and Resh, 2008). A disintegrin and metalloproteinase (ADAM), which is activated in cells treated with a GPCR ligand, cleaves EGF-like ligand precursors. The mature ErbB ligands are released and activate their cognate receptors on the cell surface (Figure 1-7). GPCRs can also transactivate the ErbB family through c-Src, a non-receptor tyrosine kinase that associates with both the plasma membrane and endosomal compartments (Donepudi and Resh, 2008). In the case of EGFR, c-Src co-localises with ligand-activated EGFR in endosomes and prolongs the EGFR activation. In addition to GPCRs, many other ligand/receptor systems have been reported to transactivate the ErbB family (Joo *et al.*, 2008). For example, cytokines, such as growth hormone (GH) and prolactin (Prl), can indirectly activate ErbB receptors through Janus tyrosine kinase 2 (Jak2), which phosphorylates specific tyrosine residues in the cytoplasmic domains of EGFR or ErbB2. Transactivation of the ErbB family by other receptor families implies its central role of converging signals for different biological responses and could represent part of the success of therapeutics that target these receptors (Normanno et al., 2006).

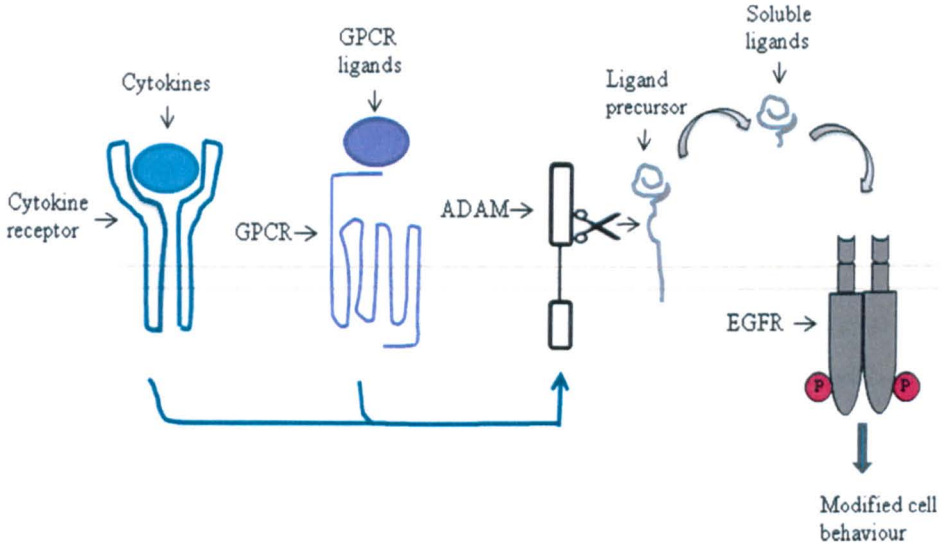

Figure 1-7. Transactivation of the ErbB family. Activation of GPCRs and cytokine receptors lead to ADAM activation, which cleaves ErbB pro-ligands. The mature ErbB ligands that are subsequently released activate their cognate receptors. Figure adapted from Donepudi and Resh, 2008.

1.8 System regulations

Not only could the ligand-receptor complex initiate various signalling pathways but also their biological consequences can feed back to the ErbB signalling network. If the feedback could amplify and prolong the active state of signalling pathways, it is referred to as positive-feedback. Negative feedback results in signal attenuation.

ErbB2, acting as a co-receptor in the dimerisation complex with all the other receptors in this family, is considered as a positive regulator due to its effect on increasing the ligand binding affinity and the duration of signalling (Gullick, 2001). Autocrine signalling is another aspect of positive regulation. As the mitogen-activated protein kinase (MAPK) pathway is initiated by ErbB receptor activation, transcription of several ErbB ligands such as TGFα and HB-EGF are up-regulated within the same cell (Ciardiello and Tortora, 2003). These ligands can then stimulate more receptors thus amplifying their signalling. Recently findings demonstrated that the juxtamembrane region of EGFR plays an essential positive role in stabilising formation of the kinase dimer (Hubbard, 2009) and thus could be considered as a component of positive control

of the system.

With respect to the negative feedback exerted on the ErbB system, multiple molecular mechanisms participate in signal attenuation at different levels. At the receptor level, targeting surface receptors for degradation is an effective mechanism to attenuate the signalling. After being activated by the ligands, EGFR can go through an internalisation process, either being degraded or being recycled largely depending on pH stability of ligand–receptor interaction. For example, the interaction between EGF and EGFR is stable at endosomal pH and results in lysosomal degradation. Whereas interaction of TGFα and EGFR is more pH sensitive, resulting in dissociation in the endosome and recycling of EGFR to the cell membrane (Wiley, 2003). In general however, ligand induced endocytosis downregulates growth factor signalling.

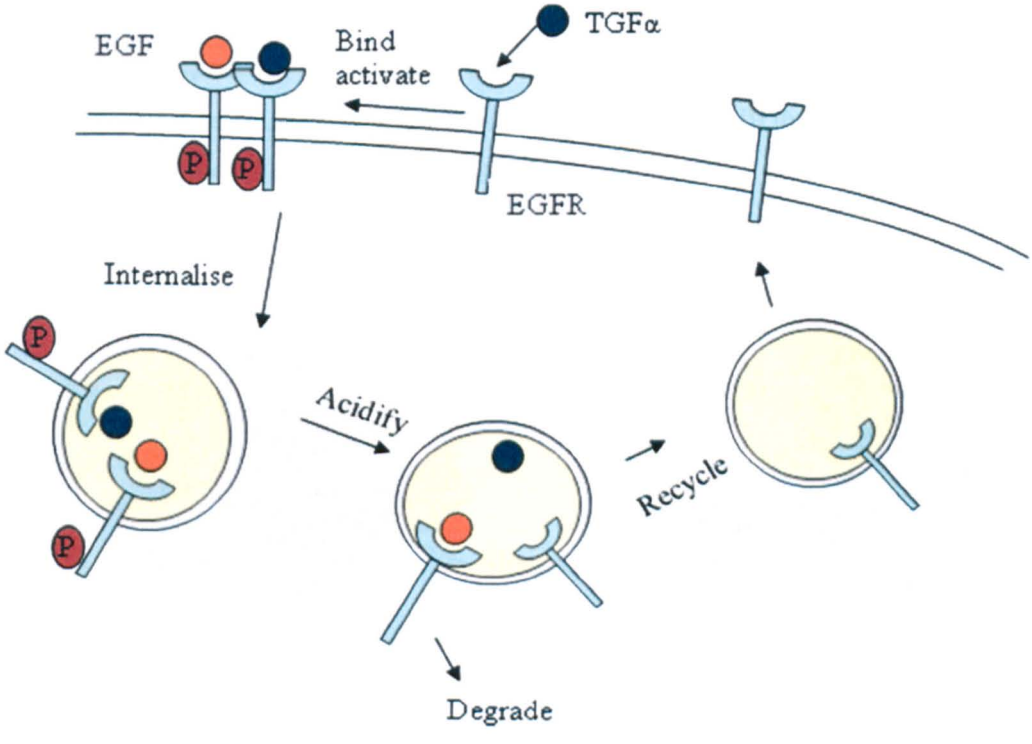

Figure 1-8. Trafficking of EGFR. Upon ligand binding EGFR is activated and internalised. Dissociation occurs in the acidified endosomal compartment. The ultimate fate of EGFR is determined by the properties of the ligands. Figure adapted from Wiley, 2003.

Signal attenuation also occurs at the transcription level. Unlike the pre-existing mechanism above, there are a group of molecules that are newly synthesised after the activation of ErbB by their ligands. For instance, upon binding of the EGF-like ligands, ErbB receptors become phosphorylated followed by initiation of the MAPK pathway. Phosphorylated MAPK translocates to the nucleus to direct phosphorylate transcription factors, which activate transcription of immediate-early genes (IEGs). IEGs regulate a second wave of transcription (Amit et al., 2007). A broad range of proteins including transcription repressors are then transcriptionally induced to feedback and inhibit the activity of ErbB receptors. One such example is the suppressor of cytokine signalling-5 (SOCS5) which is up-regulated by EGF binding (Kario *et al.*, 2005). This accelerates EGFR degradation, decreases its lifetime and leads to a significant reduction in the levels of receptor. There are also inducible adaptor proteins such as MIG6 (mitogen-induced gene 6), whose C-terminal region overlaps the distal surface of the C-lobe of the kinase domain (Figure 1-9) (Zhang et al., 2007). Thus, binding of MIG6 to an EGFR kinase domain can prevent both the activation of kinase domains and downstream signalling by activated kinase domains. Residues in EGFR located at the MIG6-binding interface are conserved, suggesting that MIG6 will also bind to other EGFR family members (Zhang et al., 2006).

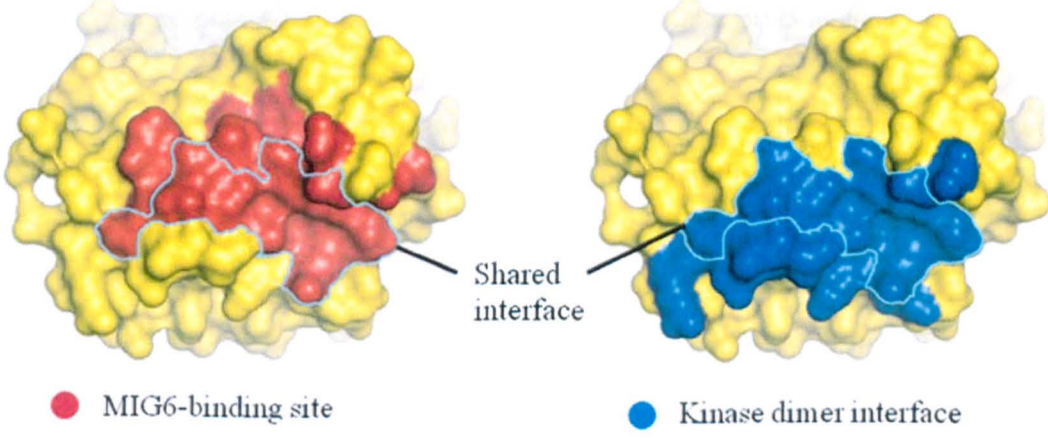

Figure 1-9. Comparison of the MIG6 binding interface and the EGFR kinase domain dimer interface on the C-lobe. A large proportion of the surface is shared by the two interfaces (outlined). Figure taken from Zhang et al, 2007.

1.9 EGF-like ligands in development and in human cancers

The important and sometimes essential roles of EGF-like ligands in development of different organs are supported by the analysis of genetically modified mice. For example, in mice lacking the expression of EGF and TGFα the prostate does not develop normally (Abbott *et al.*, 2003). Different members of the EGF-family of growth factors, like EGF, HB-EGF and TGFα, are expressed throughout the central and peripheral nervous system where they regulate cellular activities such as proliferation, migration and differentiation (Xian and Zhou, 2004). Although knockout mice for the *TGFα* gene presented abnormalities in the skin, hair and eye, the absence of the *TGFα* gene did not significantly affect the development or function of the nervous system in these animals. These results suggest that other ErbB ligands may compensate for defects in TGFα function in the nervous system. In agreement with these findings, individual null mutations for *EGF*, *AR* and *TGFα* did not affect mammary gland development (Luetteke *et al.*, 1999). However, triple knockout mice lacking expression of EGF, AR and TGFα showed aberrant mammary gland growth. Taken together, these studies demonstrate that, while there is functional redundancy in the roles of these ErbB ligands, some ligands make specific contributions implying that functional differentiation of specific tissues/organs requires the cooperation of multiple ErbB ligands.

The contribution of each ErbB family member to cancer cell behaviour is generally regulated by a combination of its level of expression and the availability of its cognate ligands in the tumour microevironment. The ability of ErbB ligands to induce *in vivo* transformation has been investigated in different transgenic mice models. In particular, TGFα overexpression has been demonstrated to induce transformation in different tissues (Sandgren et al., 1995). Furthermore, several studies that have shown overexpression of ErbB ligands in various human carcinomas suggest their important role in the pathogenesis of several human tumour types. When 76 cases of breast carcinoma were investigated, overexpression of HB-EGF was found in 71.80% of the carcinoma cases but only slightly in normal mammary glands (Ito *et al.*, 2001). Interestingly, its expression was inversely related to biological aggressiveness of the breast carcinoma suggesting that HB-EGF may play a crucial role in the early stage of this carcinoma. TGFα overexpression has been demonstrated in essentially all

carcinoma types, with many tumours showing overexpression (Salomon *et al.*, 1995). Expression of AR is found in different carcinoma types as well but these tend to display a more differentiated phenotype (Saeki *et al.*, 1992). Coexpression of different EGF-like ligands also occurs in human carcinomas. Normanno *et al.* have demonstrated that coexpression of TGFα, AR and/or NRG occurs in human colon, breast, lung, ovarian and gastric carcinoma (Normanno et al., 2001). Recently, a study carried out in our laboratory established an expression profile of the four ErbB receptors and eleven EGF-like ligands using immunohistochemical staining in one hundred cases of breast cancer. The statistical analysis revealed a strong association between the expression of any member of the family and all other members (McIntyre et al., 2010), suggesting that coexpression of different EGF-like growth factors is a common phenomenon in human carcinogenesis. Taken together, these findings suggest that ErbB ligands are involved in the pathogenesis of human carcinoma and it has important implications for both prognostic and therapeutic applications.

1.10 ErbB receptors in development and in human cancer

Similar to the experiments with regard to EGF-like ligand functions, specific roles of ErbB receptors in different organs and tissues have been suggested using mouse models with null mutations. Null mutations in genes that encode ErbB receptors were embryonic lethal. More specifically, null mutations of *EGFR* lead to abnormalities in multiple organs including the skin, lung, pancreas, gastrointestinal tract and central nervous system (Miettinen et al., 1995; Sibilia et al., 1998; Sibilia and Wagner, 1995; Threadgill et al., 1995). *ErbB2* and *ErbB4* knockout mice had similar phenotypes with lethal defects in cardiac and neural structures (Lee *et al.*, 1995; Leu *et al.*, 2003). In the case of *ErbB3*, most knockout mouse embryos exhibited cardiac abnormalities with defective valves as well as neural crest defects and reduction in Schwann cells (Erickson *et al.*, 1997). These data indicate that ErbB receptors are critically involved in regulating specific aspects of embryogenesis and development. Although their full roles may not be revealed as there is likely to be compensation by the remaining receptors in the family, ErbB receptors play essential roles during the development of the mammary gland in adult organisms. Evidence has suggested that the four ErbB receptors are differentially expressed during the development of the mammary gland. The EGFR and

ErbB2 receptors are required during ductal morphogenesis (Fowler et al., 1995; Jones and Stern, 1999), whereas the ErbB3 and ErbB4 receptors are preferentially expressed through alveolar morphogenesis and lactation (Troyer and Lee, 2001).

The aberrant signalling by ErbB receptors is involved in a wide range of human tumours. Constitutive activation of ErbBs has been shown to be important for malignant transformation and tumour proliferation. In most cases, gene amplification, overexpression, or mutations are responsible for the transforming ability of ErbBs (Robertson *et al.*, 2000).

EGFR overexpression has been reported in diverse tumours, such as lung, pancreas, ovarian and bladder cancers and the frequency of EGFR expression in carcinomas is wide ranging (Salomon *et al.*, 1995). EGFR signalling can also be altered through small in frame deletions or point mutations in the tyrosine kinase domains (Lynch *et al.*, 2004). This mutation is associated with increased kinase activity or ligand-independent constitutive activity. Another frequent EGFR mutation is characterised by a deletion mutation in the extracellular domain of the receptor (Pedersen *et al.*, 2001). Due to lacking the dimerisation arm this mutant is constitutively active at the plasma membrane.

Overexpression of ErbB2 due to gene amplification is found in 25-30% of breast cancers (Slamon *et al.*, 1987) and less frequently in other cancer types and has been associated with a poor prognosis for breast and ovarian cancer patients. The transforming effect of ErbB2 when overexpressed has been confirmed in transgenic mouse models (Ursini-Siegel *et al.*, 2007). Even though overexpression appears to be the main mechanism by which ErbB2 mediates tumorigenesis in these cancers, either in frame insertion or missense mutations in the kinase domain of the receptor have also been reported in lung cancer patients (Stephens *et al.*, 2004). These ErbB2 mutations are associated with increased kinase activity and transformation *in vitro* (Wang et al., 2006b).

The levels and the frequency of expression of ErbB3 in human carcinomas are generally comparable to EGFR (Normanno *et al.*, 2003). Even though ErbB3 mutations are rarely found in tumours (Jeong *et al.*, 2006), ErbB3 is an essential partner for ErbB2 in the transformation process; indeed without ErbB3, ErbB2 overexpression alone is

insufficient to promote tumour cell proliferation (Holbro *et al.*, 2003). Tumours from breast cancer patients with ErbB2 overexpression have up-regulation of ErbB3 (Siegel *et al.*, 1999). It also has been shown that ErbB3 is involved in coupling EGFR to the PI3K pathway in non-small-cell lung cancer (NSCLC) cell lines with EGFR mutations (Engelman *et al.*, 2005).

ErbB4 expression has been found in different tumours, such as breast, ovarian, squamous cell, oesophageal, bladder and pancreatic cancer (Normanno et al., 2003; Srinivasan et al., 1998). Instead of overactivity in tumorigenesis, ErbB4 is more often associated with anti-proliferation, differentiation or reduced tumorigenesis in cancer cells (Sartor *et al.*, 2001). Somatic mutation of the kinase domain of ErbB4 occurs at low frequency in some common human cancers, but how ErbB4 mutations contribute to the development of human cancers is not clear yet (Soung *et al.*, 2006). A recent study revealed ErbB4 mutations in 19% of cases of melanoma samples and melanoma cells expressing mutant ErbB4 had reduced cell growth after inhibition of ErbB4 activity (Prickett et al., 2009).

Another mechanism of aberrant ErbB signalling is the activation of autocrine growth factor loops that drive uncontrolled cell growth. Switching from paracrine to autocrine signalling is frequently described for cells expressing the ErbB receptors (Derynck *et al.*, 1987). In lung cancer patients, cases that demonstrated high expression of growth factors with co-expression of receptors were observed in more advanced stage tumours and was associated with a significantly poorer prognosis, for both TGFα and EGF (Tateishi *et al.*, 1990). Similarly, an autocrine interaction of NRG1 and ErbB2 and ErbB3 stimulates cell proliferation in some tumours arising from Schwann cells (Hansen *et al.*, 2006). This potent mechanism of activation occurs when an ErbB receptor is overexpressed in the presence of its cognate ligand or when overexpression of the ligand occurs in the presence of its cognate receptor.

1.11 ErbB receptors as targets for cancer therapy

1.11.1 Intervention strategies

There are several sites in growth factor-regulated pathways where therapeutic intervention might be possible: the synthesis and the secretion of the growth factor,

binding to the receptor, the synthesis and activation of the receptor, and proteins involved in the intracellular signal transduction (Figure 1-10). The most promising and well studied strategies to inhibit receptor function are monoclonal antibodies (mAbs) and small molecules tyrosine kinase inhibitors (TKIs).

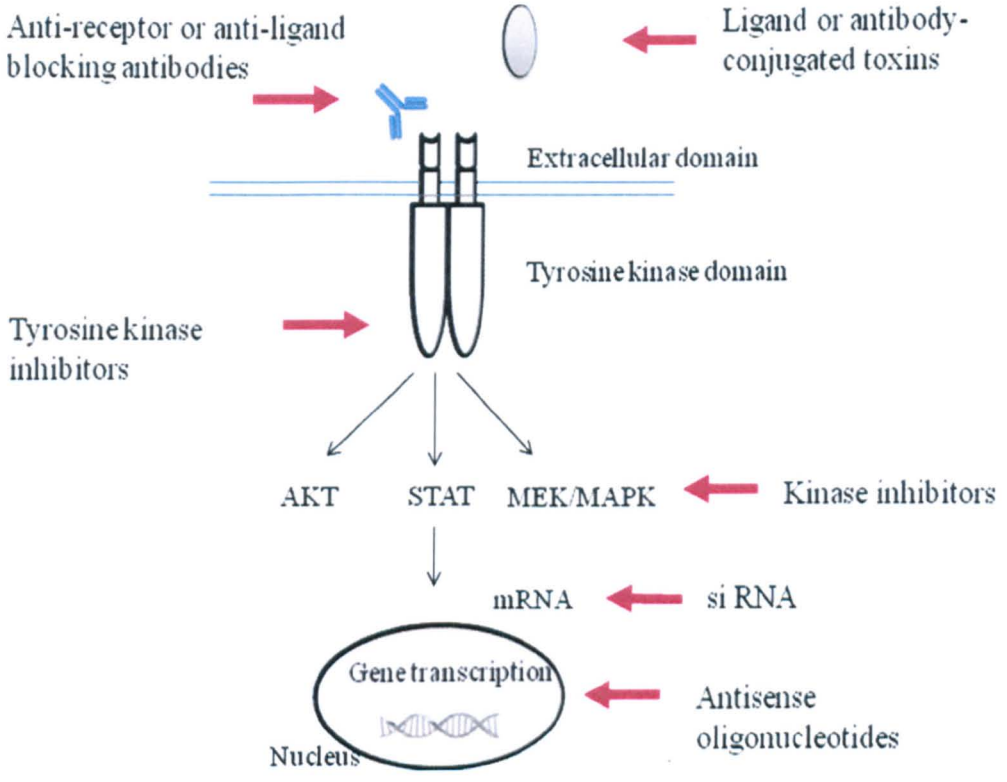

Figure 1-10. Potential sites for therapeutic intervention in ErbB signalling pathways. Figure adapted from Motoyama et al, 2002.

Anti-RTK mAbs work by blocking the ligand-receptor interaction and therefore inhibiting ligand activated RTK signalling and increasing RTK downregulation and internalisation. Among the numerous mAbs developed against EGFR, Cetuximab is the first one approved for clinical use. Cetuximab is a chimeric (mouse/human) monoclonal antibody able to bind to EGFR with higher affinity compared to TGFα or EGF (Kim *et al.*, 2001) and is capable of promoting EGFR internalisation and subsequent degradation. Cetuximab has been approved to treat patients with advanced metastatic colorectal cancer. The monoclonal anti-ErbB2 antibody Trastuzumab (also known as Herceptin) induces tumour regression in approximately 30-35% of patients with ErbB2 overexpressed metastatic breast cancer when used as a single agent (Tokunaga *et al.*, 2006). Trastuzumab binds to the extracellular domain of ErbB2, but the mechanisms of responses to Trastuzumab are not well understood.

TKIs share the same target of mAbs but exploiting different mechanisms by targeting the intrinsic tyrosine kinase activity and thereby block receptor phosphorylation and activation of downstream signalling pathways. For example, Gefitinib is able to bind strongly to EGFR and it is able to inhibit tumour cell growth and enhance the antitumour effects of chemotherapy in preclinical studies (Baselga and Averbuch, 2000). This drug has been approved for the treatment for selected patients with NSCLC (Thatcher et al., 2005). There are also TKIs that are able to simultaneously block all the ErbB family members. Canertinib is a pan-ErbB inhibitor, which has been shown to target a cysteine residue in the ATP-binding pocket of EGFR and ErbB2. Tumour samples that were treated with Canertinib showed a strong decrease in EGFR phosphorylation (Citri et al., 2002; Nyati et al., 2004). Moreover, Canertinib is able to induce ubiquitination and degradation of ErbB2, thus interfering with the EGFR/ErbB2 dimerisation process, which partially explains its strong activity observed in preclinical models (Citri et al., 2002).

The treatment of tumour cells with these agents affects many of the intracellular pathways that are essential for cancer development and progression. In preclinical models, treatment of tumour cells with ErbB-targeted TKIs and antibodies rapidly downregulates PI3K-AKT and MAPK signalling and, as a consequence, blocks the proliferation of tumour cell lines and xenografts in nude mice (Motoyama et al., 2002). A few studies have shown that these pathways are downregulated in tumours from treated patients (Daneshmand et al., 2003). In this context, it is important to note the toxicity reported for ErbB targeted drugs is correlated with known functions of EGFR and ErbB2 in normal physiology.

1.11.2 Resistance to ErbB targeted therapeutics

During the process of cancer development, cells acquire multiple mutations, each of which contribute to and are necessary for full malignancy (Hanahan and Weinberg, 2000). For example, most NSCLC patients who showed clinical responses to treatment with Gefitinib and Erlotinib (both of which are TKIs) had tumours with somatic mutations in the EGFR kinase domain (Lynch et al., 2004; Paez et al., 2004). The recent identification of additional mutations in NSCLC patients whose tumours displayed drug-sensitive mutations and who initially responded to TKI treatment might explain some of the acquired resistance to EGFR inhibitors (Pao et al., 2005). Biochemical analyses of transfected cells and growth inhibition studies with lung cancer cell lines

demonstrated that the T790M mutation in the kinase domain of EGFR conferred resistance to EGFR mutants usually sensitive to either Gefitinib or Erlotinib.

In contrast to EGFR-mutant lung cancers that are responsive initially to TKI therapy, only approximately one-third of patients with ErbB2 overexpressing metastatic breast cancer respond to Trastuzumab (Vogel et al., 2002). Several theories have been proposed to explain the clinical results, including the existence of compensatory pathways and signalling aberrations downstream of ErbB2. It has been shown experimentally that Trastuzumab cannot block the proliferation of tumour cells that have autocrine EGFR activation (Lane et al., 2000), and it cannot prevent the ligand-induced formation of ErbB2-containing heterodimers and the activation of downstream signalling pathways (Motoyama et al., 2002). These results suggested that ErbB ligands facilitate escape from Trastuzumab though the activation of alternative ErbB homo and heterodimers. As Trastuzumab binds to the domain of ErbB2 which is not involved in receptor dimerisation, this explains why ErbB ligands can induce the formation of ErbB2 containing heterodimers in the presence of the antibody.

Aberrant activation of other RTKs, for example, insulin like growth factor-1 receptor (IGF1R) (Laban et al., 2003) or fibroblast growth factor receptor family members (Adnane et al., 1991), also occurs in various types of cancer. These alterations have shown impact on response to ErbB targeted agents. Indeed, activation of the IGF1R in ErbB2 overexpressing breast cancer cells rendered initially Trastuzumab-sensitive cells resistant to the antibody (Lu et al., 2001). Moreover, co-targeting ErbB2 and IGF1R revealed a synergistic effect on cell growth in ErbB2 overexpressing MCF-7 breast cancer cells (Camirand et al., 2002).

The antiproliferative effect of ErbB targeted therapeutics often correlates with the downregulation of MAPK and PI3K-AKT pathways. It has been suggested that persistent activation of these pathways caused by aberrations downstream of the receptors might have a role in resistance to Trastuzumab, as well as EGFR-directed inhibitors (Janmaat et al., 2003). In fact, activation of AKT, or loss or mutation of the lipid phosphatase PTEN, the negative regulator of PI3K, have been found to be important causes of tumour cell resistance (She et al., 2003). Therefore, such mutations might have an important role in modulating the efficacy of ErbB directed therapies.

1.11.3 The future of ErbB receptor-targeted therapy

It is clear that the ErbB family has significant oncogenic potential in several common cancers. Increased understanding of the structure and signalling characteristics of the ErbB RTK family has now provided further insight into the development of ErbB-targeted inhibitors. The discovery of kinase domain mutations in EGFR and its impact on response to ErbB targeted therapeutics emphasise that we need more knowledge on how the mutated receptors contribute to tumourigenesis. Turning to combination strategies, the finding that ErbB3 induction caused escape of inhibition by TKI therapy in ErbB2 overexpressing breast cancers (Sergina et al., 2007) gives further insight into breast cancer resistance to therapy. In this work it was demonstrated that AKT-driven feedback signalling re-established ErbB3 signalling by inducing a forward shift in the ErbB3 phosphorylation-dephosphorylation steady-state equilibrium. The significant role of ErbB3 in ErbB2 induced tumourigenesis reveals that the ErbB2/ErbB3 signalling complex represents the principal oncogenic unit in ErbB2 amplified breast cancers and effective treatment of this cancer subtype requires the effective inactivation of this oncogenic complex. Efforts are now ongoing to develop more potent TKIs and combinations of TKIs with inhibitors of ErbB3 effectors, such as PI3K inhibitors or Akt inhibitors, to silence ErbB2/ErbB3 signalling effectively. Also, the importance of IGF1R in maintaining strong activation of the PI3K-AKT pathway, and its potential to interfere with ErbB targeted inhibitors, indicate it is logical to consider combining anti-ErbB agents with an IGF1R inhibitor (Mitsiades et al., 2004). The PI3K-AKT pathway can be activated by many different mechanisms and these could also be targeted together with ErbB RTKs (Mills et al., 2003).

The success of the first decade of ErbB targeting agents has identified new questions and challenges to be met in the coming decade. By continuing exchange of information between basic and clinical studies, we will be able to identify further factors that underlie clinical response to ErbB targeted therapeutics. Our increasing knowledge will contribute not only to development of novel therapeutics, but also allow us to optimally use those already in the clinic.

1.12 Neuregulins

1.12.1 *NRG* genes

Neuregulin [(NRG, also called heregulin, Neu differentiation factor (NDF), glial growth factor (GGF), and acetylcholine receptor-inducing activity (ARIA)] was first cloned and characterised in rat and in human as a putative ligand for the ErbB2 receptor (Holmes et al., 1992; Peles et al., 1992; Wen et al., 1994). Despite the various names given by different research groups, they are derived from a single gene, *neuregulin1* (*NRG1*). Soon after the identification of the *NRG1* gene, three other genes which encode related proteins were discovered. Now, the neuregulin family consists of four members, NRG1, NRG2 (also called NTAK, for neural and thymus-derived activator of ErbB kinases, and Don-1) (Carraway *et al.*, 1997), NRG3 (Zhang *et al.*, 1997) and NRG4 (Harari *et al.*, 1999). As a result of the alternative splicing of the mRNA products of these *NRG* genes, at least 26 different NRG isoforms exist in different species (Hayes and Gullick, 2008).

In general, different types of NRG and its isoforms display specificities in terms of the tissue expression, receptor binding and biological functions. NRG1 isoforms are predominantly expressed in many parenchymal organs such as breast, prostate, heart, skeletal muscle, lung, liver, kidney, salivary gland, small intestine, spleen, brain, and in the embryonic nervous system (Carraway and Burden, 1995). NRG2 is highly expressed in restricted regions of the brain, (Busfield *et al.*, 1997) and its expression levels increase with development (Longart *et al.*, 2004). In skeletal muscles, NRG2 protein is concentrated at synaptic sites and is associated with synaptic differentiation (Rimer *et al.*, 2004). NRG3 is expressed in both the embryonic and postnatal nervous system (Zhang *et al.*, 1997). Recently, NRG3 expression has been found in the dermal mesenchyme of the mammary gland of the embryonic mouse, suggesting a potential role of NRG3 in establishing the mammary lineage (Howard, 2008). NRG4 mRNA transcripts are detected in the adult pancreas and muscle (Harari *et al.*, 1999). Using immunohistochemical staining, NRG4 expression is detected in human breast (Dunn *et al.*, 2004) and prostate cancer tissues (Hayes *et al.*, 2007).

As mentioned above, NRG was originally isolated as a ligand for ErbB2. However, NRG does not bind directly to ErbB2 but instead interacts with ErbB3 and ErbB4. NRG1 and NRG2 are direct ligands of both ErbB3 and ErbB4, whereas NRG3 and

NRG4 can only activate ErbB4. NRG proteins are the only ligands capable of activating all four ErbB receptors by heterodimerisation, which allows a broader range of biological effects to be induced by these ligands. It has been suggested that the different cellular responses to NRG are dependent on the expression of ErbB receptors in a particular cell type (Qian et al., 1994). Furthermore, transactivation of other receptors may contribute to the actions of NRG, as shown in Figure 1-7. Adding further complexity to the NRG signalling pathway and the diversity of *NRG* genes and isoforms and their wide tissue distribution is gene splicing and posttranslational modification.

1.12.2 *NRG* splicing

NRG1

Human *NRG1* is located on chromosome 8, in the p22-p11 region (Lee and Wood, 1993). This gene is about 1.4 megabases long with less than 0.3% encoding proteins (Stefansson *et al.*, 2002). Due to its rich alternative splicing and the use of multiple promoters, at least 15 different NRG isoforms are derived from the single *NRG1* gene (Steinthorsdottir *et al.*, 2004). They are classified based on the N-terminal sequence (type I, II or III), the type of EGF-like domain (α, β or γ), and the variations in the cytoplasmic domain (a, b and c) (Figure 1-11). The NRG isoforms display a variety of N-terminal sequences. Type II and Type III NRG possess hydrophobic stretches in the N-terminus, while Type I has a signal-anchor sequence within the transmembrane domain (Falls, 2003). Furthermore, the first 21 amino acids of NRG1 have a putative nuclear localisation sequence (NLS) (KGKKKER; residues 13-18) (Holmes *et al.*, 1992) which is important for protein trafficking and sorting.

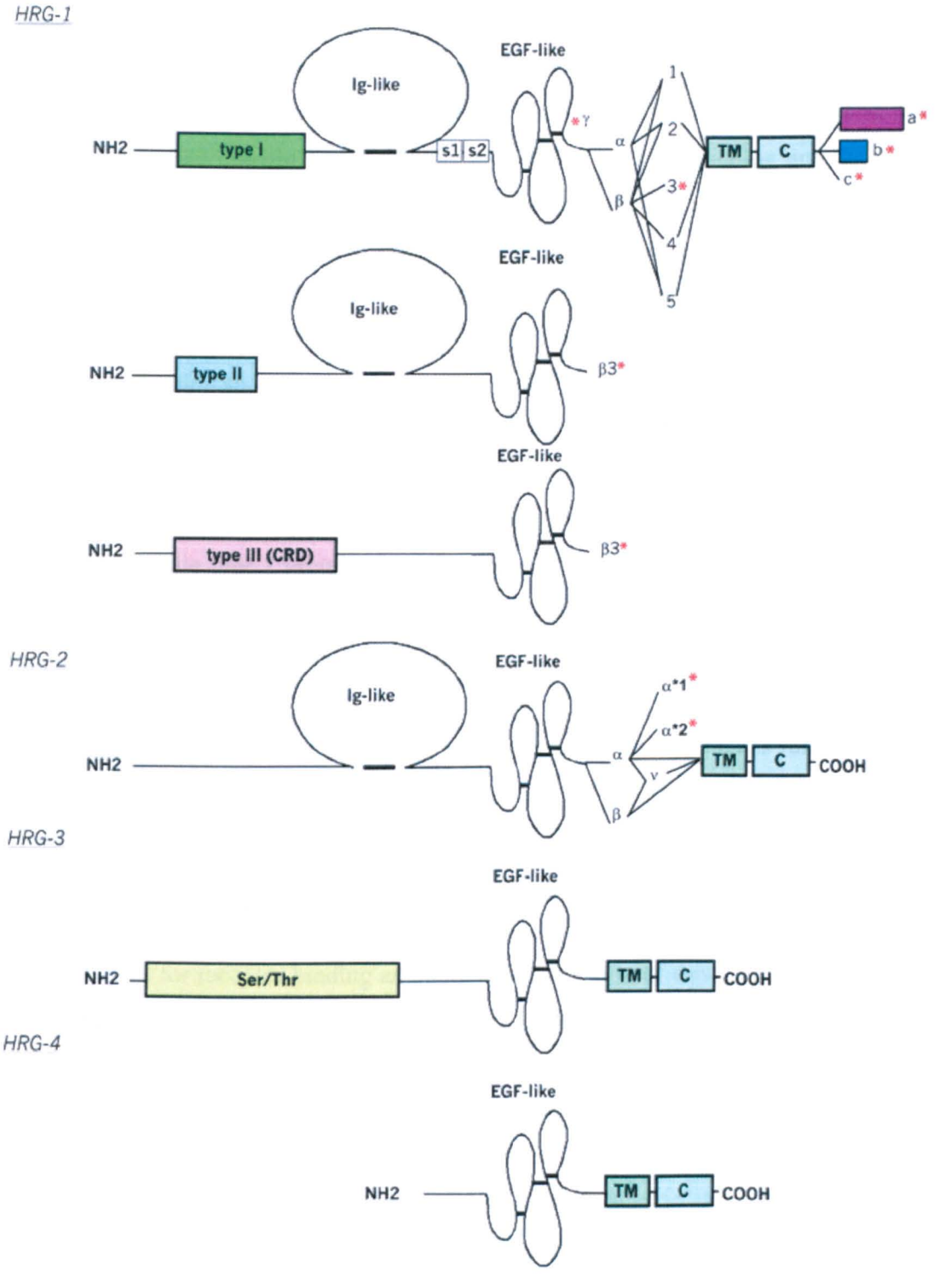

Figure 1-11. Schematic representation of neuregulin1-4 isoform structures. Asterisks indicate the position of stop codons. Figure adapted from Breuleux, 2007.

Type I (e.g., NRG, ARIA) and type II (e.g., GGF) NRG1s both contain an immunoglobulin (Ig)-like domain N-terminal to the EGF-like motif (Figure 1-11). A disulphide bond formed between two cysteines is conserved in all Ig-like domains. Even though the Ig-like domain is not directly involved in receptor binding and activation, evidence suggests that this domain is important for efficient interaction of EGF-like domain with the ErbB receptors (Eto *et al.*, 2006). Furthermore, the Ig-like domain facilitates the localisation of NRGs at the extracellular matrix thus modifying the concentration of the growth factors at their site of action (Meier *et al.*, 1998). Another nuclear localisation sequence has been reported to be present in the Ig-domain of NRG1 which is sufficient for nuclear targeting (Breuleux *et al.*, 2006). Type III NRG1 lacks the Ig-like domain, but contains a cysteine-rich domain (CRD). As a result, type III NRG1 proteins have a cytosolic N-terminus and the CRD is embedded in the plasma membrane. While type I proteins contain a glycosylation site between the Ig-like and the EGF-like domain, type II proteins lack this domain. This region is subjected to modifications by both N-linked and O-linked sugars (Burgess *et al.*, 1995).

As aforementioned, the three disulphide bonds formed by six cysteines residues define the EGF-like domain which is found in many transmembrane proteins. Four of the six cysteine residues composed of the major part of the EGF-like domain are shared by all isoforms of NRG. Conservation of this complete domain in all NRG proteins explains the similar receptor specificities of this ligand family. This motif of NRG is essential and sufficient for receptor binding and activation. Deletion of this domain abolished its ability to bind the receptors (Jones *et al.*, 1999). Type I NRG1 is further subdivided into α, β and γ isoforms based on the variations on the sequence between the fourth and the sixth cysteine residues in the EGF-like domain. This C-terminal portion of the EGF-like domain is associated with differences in the receptor binding affinities. For example, even though the α and the β isoform of NRG1 both bind to the ErbB3 and ErbB4 receptors, the β isoform shows approximately ten-fold higher binding affinity than the α isoform (Lu *et al.*, 1995). The γ isoform contains a stop codon after the fourth cysteine residue. The truncated EGF-like domain of NRG1γ suggests that it cannot bind or activate the receptors but what function it has remains enigmatic.

Next to the EGF-like domain is the juxtamembrane domain. Five differently spliced NRG1 variants (1-5) exist here providing a high degree of diversity in this region. The extracellular juxtamembrane region of NRG1 has been implicated in surface sorting and

the regulation of the cleavage of transmembrane NRGs (Montero *et al.*, 2007). Proteolytic cleavage at the proteolysis site in the ectodomain releases the Type I/II NRG1s as soluble secreted molecules (Figure 1-12). Alternatively, there are proteins lacking the transmembrane domain such as NRG1β3 which has a stop codon C-terminal to the EGF-like domain.

The 157 amino acid long cytoplasmic tail of NRG1 is followed by two variable regions (a or b) with different lengths, or by a stop codon (c). The cytoplasmic domains exhibit great similarity (>85%) among human, rat and chicken NRG molecules implying a functional role for this region. Both *in vivo* and *in vitro* studies have shown that the intracellular domain of NRG regulates proteolytic cleavage of the extracellular domain (Liu *et al.*, 1998). Also, there is evidence suggesting that the cytoplasmic tail is necessary for the receptor-independent apoptosis-inducing properties of neuregulins (Montero et al., 2007).

NRG2

The human *NRG2* gene was mapped to chromosome 5, in the q23-33 region. This gene encodes 15 exons, coding for 9 known isoforms (Ring *et al.*, 1999). Even though the overall structure of NRG2 looks similar to that of NRG1, the sequence homology of each domain is relatively low (Higashiyama et al., 1997). Alternative splicing within the EGF-like domain of the *NRG2* gene also results in α and β isoforms. The presence of the region between the EGF-like domain and the transmembrane domain gives rise to the v isoform. In addition to membrane-bound NRG2 proteins, secreted forms also exist as the result of translational frameshifts occurring in the C-terminal region of the EGF-like domain leading to the truncated proteins α*1 and α*2. Unlike NRG1, no variation seems to occur in the cytoplasmic tail of NRG2.

NRG3

The *NRG3* gene was mapped to chromosome 10, in the q22-q23 region (Gizatullin *et al.*, 2000). Ten exons were first identified in the mouse gene. Recently, a new isoform with two additional 5' exons was identified and this transcript is produced by alternative promoter usage (Carteron *et al.*, 2006). In our work using bioinformatics and polymerase chain reaction (PCR) (Smart and Gullick, unpublished) we have preliminary evidence of several other splice variant including some which contain stop codons upstream to the EGF domain. As shown in Figure 1-11, in contrast to many of the

NRG1 family members, the Ig-like domain is absent in the extracellular domain of NRG3. Instead, NRG3 contains a Ser/Thr-rich region N-terminal to the EGF-like domain. This region is involved in O-linked glycosylation.

NRG4

Recently, Hayes et al. (2007) has identified five alternative spliced isoforms of NRG4 (NRG4 A1, NRG4 A2, NRG4 B1, NRG4 B2 and NRG4 B3) (Figure 1-13). Transmembrane sequences are present in NRG4 A type but not in B type isoforms. Only A1 and A2 isoforms contain the intact EGF-like domain. The C-terminus of NRG4 isoforms varies in length. The intracellular domain of the A1 isoform is encoded from two exons, where that of A2 is encoded from a different exon which contains a predicted PDZ (Psd-95/Dlg/ZO1) binding domain. The B1 and B2 isoforms have a single residue encoded from different exons. B3 has a 21 amino acid sequence which contains a predicted Src kinase phosphorylation site. NRG4 shows little homology to other NRGs aside the EGF-like domain and does not have any recognisable structural motifs at the N-terminus even in the transmembrane region, where the high sequence homology is shared with the other three NRGs (Harari *et al.*, 1999).

1.12.3 Proteolytic processing of NRG ligands

Proteolytic cleavage of transmembrane precursors (often called "proNRGs") is mediated by "A disintegrin and metalloproteinase" (ADAM) family members. ADAMs are also membrane-anchored molecules and these metalloproteinases are considered to be responsible for the ectodomain shedding of many membrane proteins, including cytokine receptors, growth factors and growth factor receptors (Zhou *et al.*, 2006). ADAM17 is the most extensively investigated ADAM protein and is known to release soluble TNFα (tumour necrosis factor α) from its membrane precursor, proTNFα, which permits TNFα paracrine signalling. Thus, ADAM17 is also called TACE (TNFα converting enzyme). Experiments carried out in cells expressing an inactive form of ADAM17 indicate that cleavage of proNRGα2c is defective, illustrating the involvement of this protease in NRG proteolytic processing (Montero *et al.*, 2000). Another member of the ADAM family, ADAM19/meltrin-β also participates in the proteolytic processing of membrane-anchored NRGs. However, ADAM19 affects the processing of NRGβ1 and β4 but not that of NRGα2 suggesting that this protease has a preference for β-type NRGs as substrates (Shirakabe *et al.*, 2001).

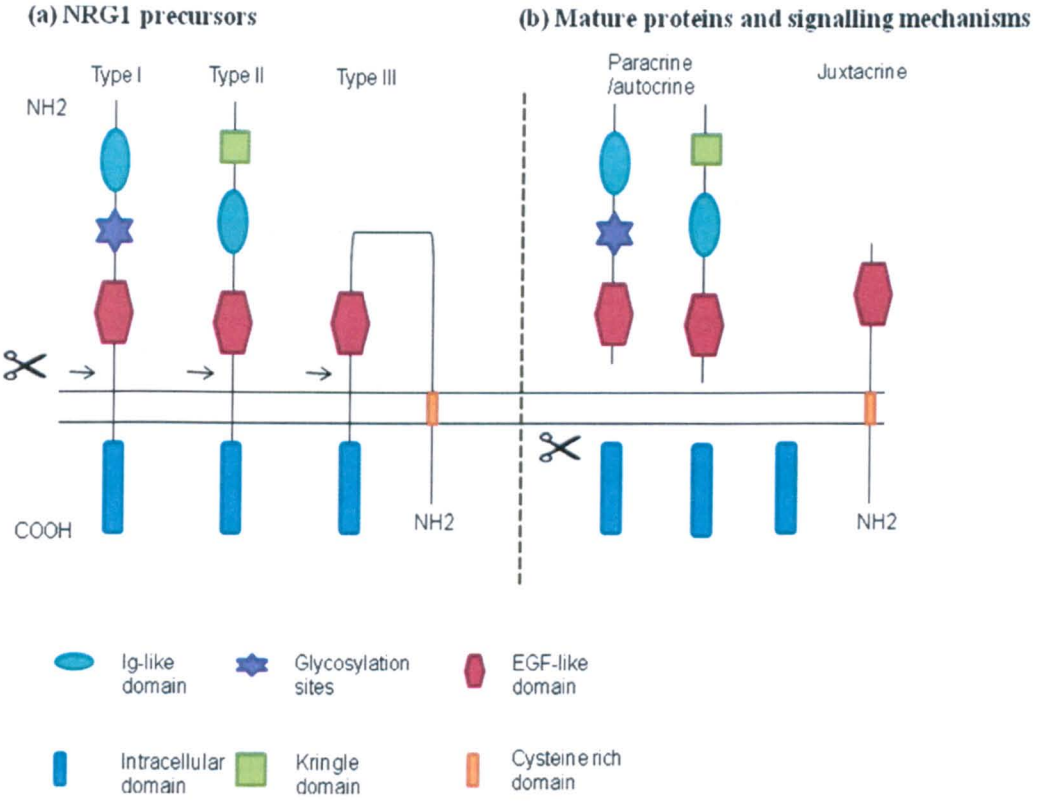

Figure 1-12. Schematic diagram of NRG1 isoforms: membrane orientation and signalling. (a) Type I and II NRG1s are synthesised as single transmembrane proteins; Type III has two transmembrane domains. (b) Upon proteolytic cleavages at the juxtamembrane, Type I and II NRG1s are released as secreted molecules, acting in a paracrine/autocrine fashion. Type III remains membrane-bound through its cysteine rich domain and functions as a juxtacrine signal. The cytoplasmic domain undergoes further cleavage and is translocated to the nucleus. Other, truncated, splice variants are also produced. Figure adapted from Montero et al, 2007.

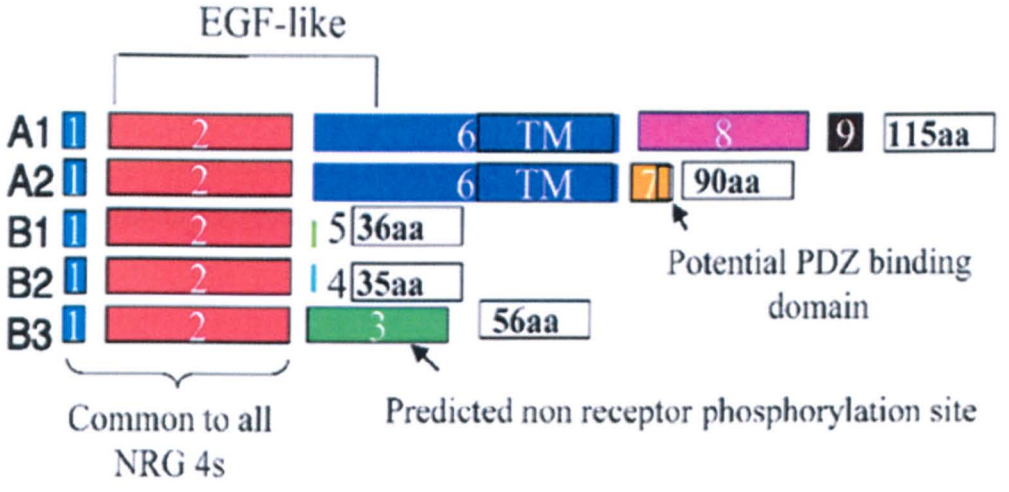

Figure 1-13. Schematic diagram of NRG4 coding regions. Figure taken from Hayes et al, 2007.

Accumulating evidence indicates that proteolytic release of NRG ligands is a regulated process, even though the mechanisms underlying activation of these proteases have not been elucidated. Studies suggest that the cytoplasmic domain of ADAM17 may act as a signal transducer that regulates shedding by ADAM17 in response to intracellular activities. Upon growth factor stimulation, ADAM17 is phosphorylated on a specific residue though activation of the extracellular signal-regulated kinases 1 and 2 (ERK1/ERK2) and MAPK signalling pathways (Fan *et al.*, 2003). ADAMs can also be activated by GPCRs which require second messengers, such as the elevation of intracellular calcium influx and activation of protein kinase C (Diaz-Rodriguez *et al.*, 2000). Studies on the expression and function of NRGs have indicated that cleavage of transmembrane NRGs may be an essential step in the physiological actions of these factors. As the ErbB pathway is a target for anti-cancer drugs, the upstream activators of ErbB ligands, their sheddases, have been considered as new drug targets in the ErbB pathway. Indeed, targeting ADAM-mediated ligand cleavage has been shown to inhibit ErbB3 and EGFR pathways in NSCLC (Kataoka, 2009).

1.13 NRG signalling mechanisms

In general, cell-cell communication regulates basic cellular activities that are important for the development of tissues and organs. Typically, a ligand can activate receptors on

the cell of its origin (autocrine signalling) or can be released into the cell milieu where it interacts with the cell surface receptors of the adjacent cells (paracrine signalling). Autocrine signalling occurs among the same types of cells, whereas paracrine signalling affects either the same cell type or a different cell type. Juxtacrine signalling is described as when activating receptors in the target cell, the ligand remains associated with the plasma membrane of the signalling cell (Figure 1-14).

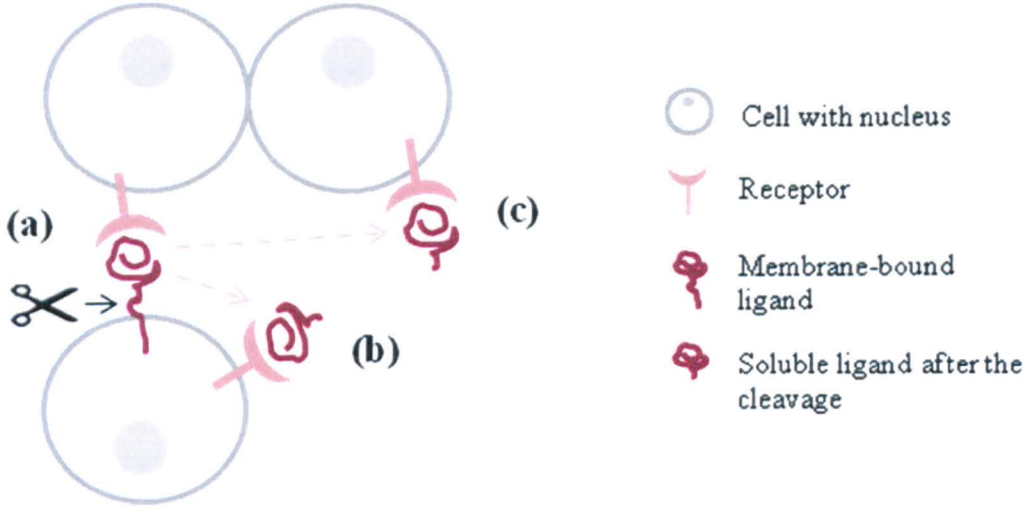

Figure 1-14. Juxtacrine (a), autocrine (b) and paracrine (c) signalling mechanisms.

1.13.1 Paracrine signalling

Proteins that serve as paracrine signals generally follow the secretory pathway. The path has its origins in the rough endoplasmic reticulum. The protein then proceeds through many compartments of the Golgi apparatus and finally ends up in a vesicle that fuses with the plasma membrane, releasing the protein outside of the cell. The NRGIIβ3 isoform, which lacks the transmembrane domain C-terminal to the EGF-like domain (Figure 1-11), is suggested to follow this pathway supported by the evidence that NRGIIβ3 is efficiently released into the medium when expressed by transfection in fibroblast cells (Marchionni *et al.*, 1993). To serve as paracrine signals other transmembrane proNRGs are proteolytic cleaved and released as soluble proteins allowing a further level of regulation in the system. The significance of NRG1 paracrine signalling is well illustrated in heart development. For normal cardiac morphogenesis the endocardium must signal to cells in the myocardium which is not in direct contact. In the fetal heart, NRG1 is produced by the endocardial endothelium, while its receptor

ErbB4 is expressed in myocardial cells. This requires a paracrine type of signal. In the genetically altered mouse model, cytoplasmic tail-deleted transmembrane NRGs show the same cardiac phenotype as NRG1-null mice demonstrated by the absence of normal trabeculation of the ventricles (Gassmann *et al.*, 1995). The explanation for the similarity in the cardiac phenotypes is that the cytoplasmic tail-deleted mutant, unlike wild type NRG isoforms, is resistant to proteolytic release of its extracellular domain ligand and demonstrates that a paracrine NRG signal is required for endocardial induction of myocardial differentiation (Liu *et al.*, 1998). Once released, NRG1 binds to ErbB4 on cardiomyocytes that, after homodimerisation with ErbB4 or heterodimerisation with phosphorylated ErbB2, leads to activation of PI3K signalling pathway (Lemmens *et al.*, 2007). Just as NRGs mediate signalling in the heart's early development, paracrine signalling of NRGs are also critical in the adult heart and in the adult nervous system (Falls, 2003; Gullick, 2001).

1.13.2 Autocrine signalling

Autocrine signalling of NRG that regulates cell proliferation and differentiation has been reported in different tissues and in various types of carcinomas. In response to axon damage, Schwann cells that secret NRG1 also have the expression of ErbB2 and ErbB3 co-ordinately regulated, suggesting an autocrine interaction of Schwann cell NRG1 and ErbB receptors (Birchmeier, 2009). Similarly, developing muscle which produces NRG1 also expresses ErbB2 and ErbB3. NRG1 induces ErbB2/ErbB3 heterodimers on the muscle cell surface to provide a local signal that activates synaptic expression of acetylcholine receptor, suggesting autocrine regulation of neuromuscular synapse development (Moscoso *et al.*, 1995). Autocrine signalling of NRG is also common in transformed cells (Gollamudi *et al.*, 2004), in many breast cancer cell lines (Lupu *et al.*, 1996), and in majority of ovarian cancer and colon cancer cells (Gilmour *et al.*, 2002). Many breast tumour cells synthesise NRG themselves. In fact, NRG was originally purified from MDA-MB-231 breast epithelial cell conditioned medium (Peles *et al.*, 1992). Endogenous NRG has been shown to be involved in breast cancer tumour progression and correlates with a more malignant phenotype (Lupu et al., 1996; Tsai et al., 2003). Using a series of breast epithelial cell lines (derived from a single, clonal cell line) that covers the complete spectrum of tumour progression from normal cells to cancer cells capable of metastasis, Li et al. have demonstrated that malignant progression is associated with the development of a proliferative autocrine NRG signalling loop (Li et al., 2004). As the cells progress to malignancy, they express higher

levels of ErbBs and secrete high levels of NRG in to the culture media, resulting in high basal levels of ErbB receptor phosphorylation. In summary, sustained ErbB receptor activation through the autocrine effects of NRG is a key promoter of cell proliferation and is involved in tumour progression.

1.13.3 Juxtacrine signalling

As shown in Figure 1-12, the cysteine-rich domain encoded by the type III specific N-terminal exon forms a second transmembrane domain. As a result, type III NRG1 has a cytosolic N-terminus and has a membrane-tethered EGF-like domain. This form of the molecule is therefore restricted to signalling via cell-cell interactions. Following proteolytic cleavage this form of NRG1 may now signal to adjacent cells in a juxtacrine manner. The expression of type III NRG1 isoforms is restricted to the nervous system. Defects in animals lacking type III NRG include retraction of nerve terminals from newly formed synapses, absence of Schwann cells from peripheral nerves and loss of motor and sensory neurons (Wang *et al.*, 2001).

Soluble forms of NRGs have demonstrated biological activity. The expression of proNRGs as membrane bound proteins raises the question of whether these factors are active in their membrane-anchored form. Several *in vitro* studies indicate that membrane-bound factors of the EGF family including proTGFα and proHB-EGF retain biological activity in their transmembrane forms (Baselga *et al.*, 1996). There is evidence that membrane-bound NRGs are also functional ligands capable of activating receptors in neighbouring cells via a juxtacrine mechanism. Membrane-bound NRGs can be detected on the surface of MDA-MB-231 human breast cancer cells and this form of the molecule can establish contact with ErbB3-expressing cells and induce ErbB2 phosphorylation and increases DNA synthesis in cells overexpressing ErbB2 (Aguilar and Slamon, 2001). Montero et al. showed that NRGα2c in its transmembrane form is able to cause tyrosine phosphorylation of ErbB2, ErbB3 and ErbB4 when expressed in MCF-7 breast cancer cell line (Montero et al., 2007). Taken together, these studies demonstrated that transmembrane neuregulins are functionally active and suggested it is capable of playing a role in cell-cell communication and subsequent signal transduction *in vivo*.

1.13.4 Back signalling of NRG

Bao et al. proposed that type III NRG1 is a bidirectional signalling protein that functions as a ligand that activates ErbB receptors and as a functional fragment that modulates the behaviour of type III NRG1-expressing neurons (Bao et al., 2003). In this case, transmembrane type III NRG1 interacts with ErbB4 receptors on the surface of neighbouring cells. As a result, the ErbB receptors are activated and the conventional "forward signalling" occurs. Binding of the EGF-like domain to ErbB receptors also stimulates the cleavage of NRG1 possibly in both the external juxtamembrane region releasing the EGF-like domain and in the intramembrane region that releases the C-terminal of the intracellular domain (ICD). In contrast to the cleavage of NRG transmembrane precursors which is mediated by metalloproteinase, the processing of type III NRG1 involves a γ-secretase catalysed activity. Subsequent to cleavage, the ICD translocates to the nucleus where it contributes to the transcriptional regulation of gene expression. By binding to a zinc-finger transcription factor Eos, nuclear translocation of ICD increases the transcriptional activity of postsynaptic density protein-95 (PSD-95). This ICD-Eos nuclear signalling is important in regulating neuronal survival and in synaptic maturation and maintenance (Bao *et al.*, 2003). These findings suggest that the ICD of the NRG1 has the ability to interact with transcriptional regulators in the nucleus and control gene expression in cells expressing the NRG proteins. Deregulated synaptic transmission has been implicated in schizophrenia and a loss of synapses has been observed in patients with Alzheimer disease (Nathan and Muller, 2001; Rowan *et al.*, 2003). Understanding how this "back signalling" of NRG contributes to synaptic plasticity will provide further insight into its potential roles in these pathological conditions.

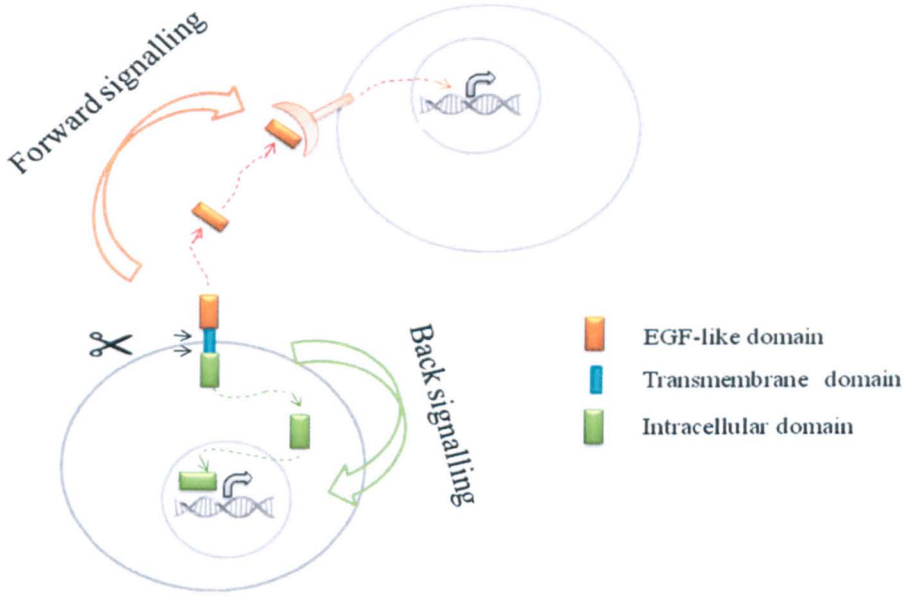

Figure 1-15. Schematic diagram of bidirectional signalling of type III NRG1. Forward signalling occurs when membrane-bound type III NRG1 activates its cognate receptors on the surface of neighbouring cells. This stimulates proteolytic release and translocation of the intracellular domain of type III NRG1 to the nucleus (back signalling). Figure adapted from Bao et al, 2003.

1.13.5 Nuclear localisation of NRG

Mounting evidence has suggested that ligands do not only act by initiating surface receptor mediated signalling but may also be involved in alternative signalling pathways. Many signalling molecules from different families with growth regulatory activity have been reported to be present within the cell nucleus. Perhaps the best studied are the fibroblast growth factors (Olsnes et al., 2003). Nuclear localisation of platelet derived growth factor, vascular endothelial growth factor, hepatoma growth factor, growth hormone, prolactin and several of the cytokines have also been reported in various cell lines and tissues (Jans and Hassan, 1998). In addition, several ligands of the ErbB receptors have been reported to be found inside the nucleus, including EGF (Bryant and Stow, 2005), BTC (Srinivasan et al., 1999), HB-EGF, and both the human AR (Johnson et al., 1991) and its rat equivalent called Schwannoma derived growth factor (Kimura, 1993). Moreover, Schwannoma derived growth factor was shown to depend on translocation to the nucleus to induce its mitogenic activity. Another member of the ErbB receptor ligand family, HB-EGF was also capable of translocation to the cell nucleus and plays a role in disease progression in various cancers (Adam et al., 2003).

The first evidence of nuclear localisation of NRG1 was reported by Li et al. (Li et al., 1996b). Using immunofluorescence microscopy, electron microscopy autoradiography, and SDS-PAGE analysis of nuclear fractions, they showed that the NRG1β1 isoform was internalised and translocated to the nucleus of SKBR-3 breast cancer cells as an intact molecule. Moreover, nuclear NRG1β1 was demonstrated to modulate the activity of c-myc, a critical regulator of cell cycle progression, differentiation, and malignant transformation, as well as stimulating cancer cell proliferation *in vitro*. Since then several groups have presented evidence of nuclear localisation of NRGs. Immunohistochemistry staining showed nuclear localisation of NRG precursors in papillary thyroid carcinomas but not in normal thyroid tissue (Fluge et al., 2000). Nuclear staining for NRG has also been observed in medulloblastomas (Gilbertson et al., 1998). Recently, when sixty cases of pre-invasive ductal carcinoma in situ (DCIS) were examined, nuclear expression of NRG1α, NRG1β and NRG3 has been shown in 40-50% of the cases (Marshall et al., 2006). An antibody specific for a splice variant of NRG4 showed intense staining of the nucleus in rat salivary gland tissue (Hayes et al., 2007). Therefore, a systemic study is needed to examine the subcellular localisation of the NRGs in tissues of different physiological conditions.

Based on the observations of NRGs in the nucleus of various tissues and the diversity of NRG splicing variants, questions have arisen concerning the functions of intranuclear localised NRGs. Due to the low resolution of immunohistochemical staining used in the studies described above, the subnuclear structures that NRG1β localised to could not be resolved. To provide further insight into the intranuclear expression of NRG1, green fluorescent protein (GFP)-tagged NRG1β3 was examined in different cell lines including fibroblasts or epithelial cells and using cells from human, rodents or dog. High-resolution confocal microscopy showed that NRG1β3 localised to nucleoli alone, to SC35-positive spliceosomes alone or a combination of both patterns in one cell. Importantly, localisation of NRG1β3 to either structures was receptor independent, as it occurs in cells lacking its cognate receptors, ErbB3 and ErbB4, and was unaffected by removal of the EGF-like receptor binding domain (Golding et al., 2004). When NRG1β3 expressing live cells were followed by time-lapse microscopy, it was noticed that the distribution of this protein changed over 2h from a nucleolar pattern to a speckled pattern and vice versa (Figure 1-16).

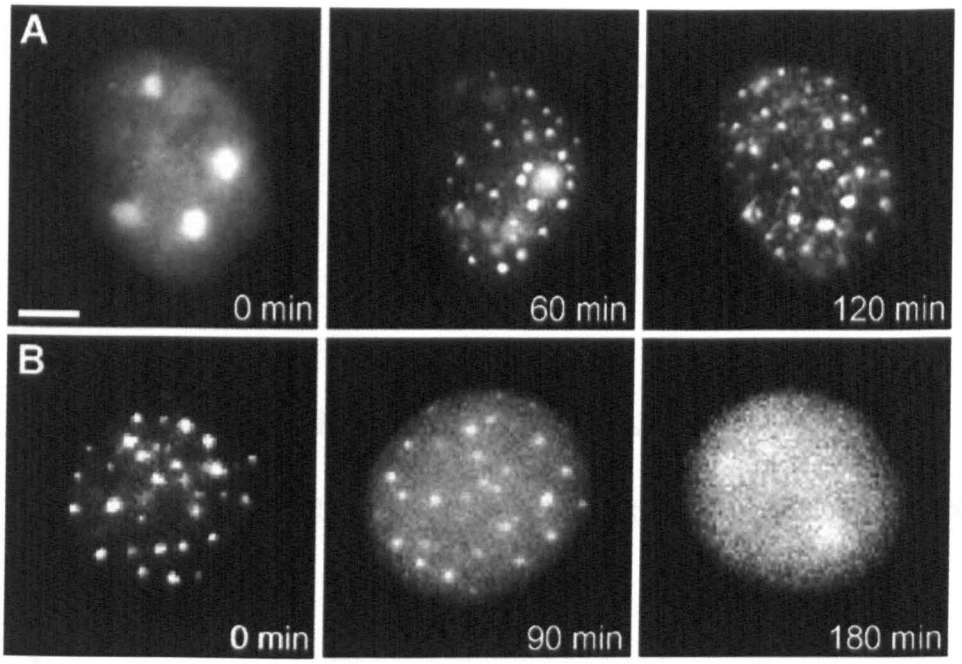

Figure 1-16. Localisation patterns of GFP-tagged NRG1β3 interconvert. Live NR6 cells expressing NRG1β3GFP was filmed by time-lapse microscopy. Nuclear localisation of NRG1β3GFP changes from the nucleolar pattern to the speckle pattern (panel A) or vice versa (panel B). Figure taken from Golding et al, 2004.

a.

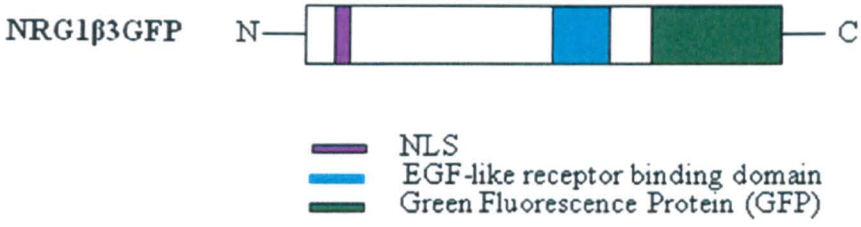

b.

14--16

1-21 MSERKEGRGKGKGKKKERGSG

56 67 69 79

49-79 AGSKLVLRCETSSEYSSLRFKWFKNGNELNR

c.

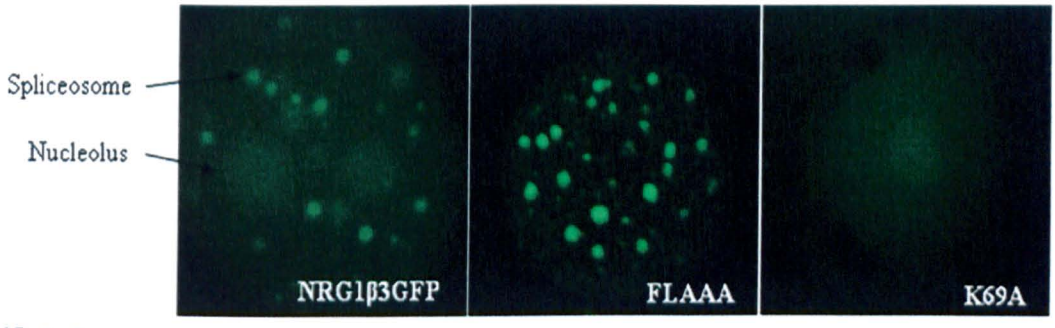

	NRG1β3GFP	FLAAA	K69A
Nucleolar localisation	+	-	+
Spliceosome localisation	+	+	-

Figure 1-17. Nuclear localisation of NRG1β3GFP and its mutants in transfected COS-7 cells. (a) Schematic representation of GFP tagged NRG1β3 fusion protein. The putative nuclear localisation sequence is shown in purple, the EGF-like receptor binding domain in blue and the attached GFP in green. (b) Amino acid sequences of the first 21 amino acids and 49-79 region of wild type NRG1β3. Residues in red are responsible for either nucleolar (14-16) or spliceosome localisation (56, 67, 69 and 79). (c) Transfection of COS-7 cells with wild type NRG1β3GFP and the two mutants which could localise only in nucleoli (FLAAA, named as the three consecutive lysines at position 14-16 were mutated to alanines) or only at spliceosomes (K69A, named as lysine 79 was mutated to alanine). Either subnuclear localisation occurred (+) or not (-).

To identify the regions that mediate targeting of NRG1β3 to nucleoli and spliceosomes, Golding et al. examined a panel of deletion mutants (Golding et al., 2004). Their work demonstrated that the first 21 amino acids of the N-terminus were essential for nucleolar localisation, while targeting to nuclear speckles required residues 49-79. Breuleux et al. reported essentially similar results using the NRG1α splice variant (Breuleux et al., 2006). Further mutational analysis determined the specific amino acids required within each subnuclear localisation sequence. Substitution of alanine for lysine at the third position in the KKK sequence within the putative NLS, when in conjunction with a further substitution of either of the first two positions hinders nucleolar localisation, indicating that these three residues (14, 15 and 16) are important for nucleolar localisation (Figure 1-17). Another mutational analysis done by Dr Carol Trim (a postdoctoral fellow in this laboratory) identified four positively charged residues that were required for spliceosome localisation. Molecular modelling suggests that three of them may form a binding site for interaction with other structures within the spliceosome (Wang et al., submitted, 2010). In a yeast two hybrid system, Breuleux et al. identified positive interactions of NRG1α with nuclear proteins implicated in different biological functions including pre-mRNA splicing (Breuleux et al., 2006).

The observation that NRG1β3 localises to nucleoli and spliceosomes raises the question of the functions of the intranuclear NRG. The importance of these subnuclear structures in ribosomal biogenesis and pre-mRNA splicing (Leung *et al.*, 2003) implies that NRG1β3 may have specific activities inside the nucleus. The mutants that target NRG1β3 exclusively to nucleoli and spliceosome allowed us to investigate its possible functions associated with each subnuclear structure.

1.14 Aims

This project aims to explore the observation of intranuclear expression of one of the neuregulin growth factors, NRG1β3

1. The frequency of intranuclear expression of NRG1 in a range of normal and tumour tissues will be determined using immunohistochemical staining in tissue arrays obtained from SuperBioChips (ethical approval granted by the Research Ethics (Human Participants) Committee of the University of Kent).
2. To determine whether the NRG1 found in two different compartments in the nucleus (spliceosomes and nucleoli) moves from one location to the other or is degraded and re-synthesised, using photoactivatable GFP tagged NRG1β3.
3. To address the possible function of intranuclear NRG.
    a. To establish a MCF-7 Tet-Off cell line in which NRG1β3GFP expression can be induced.
    b. To look at the amount of 28S and 18S ribosomal RNA as an assay for possible effects on nucleoli function.
    c. To observe the effects of nuclear localisation of NRG1 on cell growth rates.
    d. To develop a splicing assay in cells expressing the intranuclear NRG1 or ErbB4 splicing variants.
    e. To perform a kinomic analysis to examine the differential expression and/or phosphorylation of RTKs stimulated by intranuclear expression of NRG1.
    f. To perform a transcriptomic analysis to look for genes up or down regulated by intranuclear expression of NRG1.
4. To examine the localisation pattern of ErbB3 when coexpressed with NRG1β3.

Chapter 2. Materials and Methods

2.1 Cell culture

2.1.1 Cell lines utilised in this study

The MCF-7 Tet-Off cell line was a gift from Dr Paul Edwards (Cambridge, UK). The stable cell line HEK-293-ErbB3 was obtained from Dr Greg Plowman (California, USA). The NIH3T3 stable cell line transfected with ErbB4 (NIH3T3-ErbB4) was a gift from Dr Bruce Cohen (Bristol Myers Squib, USA) and the cell lines COS-7, HEK-293, HT-29, MCF-7, and T47D were originally obtained from Cancer Research UK (London, UK).

Table 2-1. Cell lines used in this study. Information about their source and morphology.

Cell line	Species	Morphology	Derived from
COS-7	Monkey	Fibroblast	African green monkey kidney fibroblast-like cell line
HEK-293	Human	Fibroblast	Primary embryonic kidney cells transformed by sheared human adenovirus
HT-29	Human	Epithelial	Colon carcinoma
MCF-7	Human	Epithelial	Breast Adenocarcinoma
NIH3T3	Mouse	Fibroblast	Swiss mouse embryos
T47D	Human	Epithelial	Breast ductal carcinoma

2.1.2 Starting cell culture from frozen stocks

The vial of cells was thawed in a 37°C water bath with gentle agitation. Immediately upon thawing, the outside of the vial was wiped with 70% ethanol. The following operations were carried out in a laminar flow tissue culture hood under strict aseptic conditions. The contents of the vial were transferred to a 15ml conical centrifuge tube containing 4ml of pre-warmed medium. The mix was centrifuged at 1,000rpm for 5min. The supernatant was carefully aspirated and the cells were resuspended in complete medium. The cell suspension was mixed thoroughly and added to a T25 tissue culture flask (Sarstedt Inc., USA). The flask was gently rocked to distribute the cells evenly

over the growth surface and was incubated at 37°C in an atmosphere of 95% air and 5% CO_2. The next day, the cells were examined under a microscope. If the cells were well attached and confluent, they were passaged for use. If the majority of cells were not well attached culturing was continued. Culture was expanded as needed.

2.1.3 Freezing cell line cultures

To ensure a renewable source of cells frozen aliquots were prepared. To prepare frozen stocks cells were trypsinised using 0.3ml of trypsin-ethylene diamine tetra acetic acid (EDTA) (0.05% trypsin, 0.53mM sodium EDTA) (Invitrogen, UK) and resuspended in 3ml of 10% dimethyl sulfoxide (DMSO) (Sigma, UK) in 90% Fetal Bovine Serum (FBS) (Invitrogen, UK). Cells were aliquoted into individual sterile cryovials (NUNC, USA). Vials were frozen at –20°C for 1-2h and then transferred to -80°C to freeze overnight. The following day, vials were placed in liquid nitrogen storage. Two or more weeks later, a vial of frozen cells was plated to confirm viability.

2.1.4 Routine culture and maintenance of cell lines

All cell lines used in this study were grown as adherent monolayers. Standard tissue culture techniques were used. The cell lines were grown in Dulbecco's modified Eagle's medium (DMEM) supplemented with 10% FBS, L-Glutamine (1%) and penicillin-streptomycin (1%) all from Invitrogen, UK. Cells were incubated at 37°C in an atmosphere of 95% air and 5% CO_2 using T25 tissue culture flasks then plated out for experiments. The cells were briefly washed in 1ml of trypsin-EDTA and replaced with 0.5ml of trypsin-EDTA and incubated for 1-5min until cells were detached from the flask. 5ml of fresh medium was added to the trypsinised cells, which were then resuspended in the medium and aliquoted out into flasks or dishes accordingly the experiments undertaken. For routine maintenance of cell lines 0.2ml of cells were pipetted into T25 tissue culture flasks containing 5ml of medium.

2.1.5 Transient transfections

Transient transfections were carried out in a number of different cell lines. Initially two transfection reagents were tried for each cell type and the most effective one was optimised further by varying the DNA to reagent ratio if needed.

Cells were plated one day before the transfection experiment so that they would reach

50–80% confluent after overnight incubation. The following transfection methods are based on cells growing in 35mm culture dishes.

2.1.5.1 FuGENE 6 transfection reagent

The starting volume of the reagent and the mass of DNA listed in Table 2-2 was based on a FuGENE 6 transfection reagent: DNA ratio of 3:1. 3µl of FuGENE 6 reagent was added to serum free medium to make a total volume of 100µl. After 5min incubation at room temperature, 2µg of DNA was added to the pre-diluted FuGENE 6 reagent. The mixture was incubated for a minimum of 15min at room temperature and then added dropwise to cells. Cells were returned to the incubator for 24-72h depending on the experiment purpose.

Table 2-2. Transfection setup using FuGENE 6 transfection reagent.

Type of dish or plate	Total medium volume per well or plate (ml)	FuGENE 6 Reagent (µl)	Mass of DNA (µg)	Approximate total volume of complex (µl)
60mm	4	6	2	200
35mm	2	3	2	100
24-well	0.5	0.6	0.2	20

2.1.5.2 Lipofectamine 2000 transfection reagent

4µg of DNA was diluted in 250µl of Opti-MEM® I Reduced Serum Medium (Invitrogen, UK). 10µl of Lipofectamine 2000 transfection reagent (Invitrogen, UK) was diluted in 250µl of Opti-MEM I Medium. After 5min incubation at room temperature, the diluted DNA was mixed with the diluted Lipofectamine 2000 transfection reagent. The mixture was incubated for 20min at room temperature. Complexes were added to cells and mixed gently. Cells were incubated at 37°C for 24-72h prior to testing for expression. To transfect cells in different tissue culture formats, the amounts of Lipofectamine 2000 transfection reagent, nucleic acid and medium were varied (Table 2-3).

Table 2-3. Transfection reaction setup using Lipofectamine 2000 transfection reagent.

Type of dish or plate	Volume of plating medium (ml)	Volume of dilution medium (µl)	Lipofectamine 2000 (µl)	Mass of DNA (µg)
60mm	4	2 x 500	20	8
35mm	2	2 x 250	10	4
24-well	0.5	2 x 50	2	0.5

2.1.6 Hemocytometer counting and cell viability

The hemocytometer (Marienfeld, Germany) consists of a thick glass microscope slide with two chambers, each of which is divided into nine squares with the dimension of 1x1mm. A cover glass (Marienfeld, Germany) is supported 0.1mm over these squares so that the total volume over each square is 1mm x 1mm x 0.1mm or $10^{-4}cm^3$. In total each large square has volume of 0.0001ml. Cell number was calculated by:

Cells/ml = average count per square x 10^4
Total cells = cells per ml x dilution factor x total volume of cell preparation from which the sample was taken.

The dye Trypan blue (Sigma, UK) was used to determine the number of viable cells present in a cell suspension. It is based on the principal that live cells possess an intact cellular membrane which can actively exclude dyes, whereas dead cells do not have such integrity and so are stained in a blue colour. 0.2ml of Trypan blue was diluted with 0.8ml of 1x phosphate buffered saline (PBS) to make a 1 in 5 dilution. Cover glass was placed over the hemocytometer chamber. 0.5ml of agitated cell suspension was mixed with an equal amount of diluted Trypan blue. With a glass Pasteur pipette (Sigma, UK) both chambers of the hemocytometer were filled by capillary action. The hemocytometer was placed on the stage of an inverted microscope. The number of non-blue cells in each of 9 squares of hemocytometer was counted. For cells on the boundaries, only cells intersecting two of the boundaries were counted. If over 10% of the cells represented clumps, all steps were repeated. If fewer than 200 or more than 500 cells were present in the 9 squares, the process was repeated with a more suitable dilution factor. Each count was repeated three times.

2.1.7 Isolation of individual colonies using cloning cylinders

Culture dishes containing clones were examined with an inverted microscope with a x10 objective. Once average size, healthy and well separated colonies were located, a circle around them was drawn on the bottom of the dish with a marker pen. Individual colonies were isolated and picked from the dish using 8mm x 8mm cloning cylinders (Millipore, UK).

The growth medium was removed and the cells were rinsed twice with PBS to remove any floating cells. A cloning cylinder was picked using curved tip forceps and the bottom of the cylinder was gently pressed into the silicone grease to make sure an even distribution of grease on the bottom of the cylinder. The cylinder was placed over a marked colony so that the cells were in the centre of the cylinder. The cylinder was gently pressed down to create a seal between the cylinder and the dish. Extra care was taken to not to slide the cylinder across the colony. 0.2ml of trypsin-EDTA was added to fill the cloning cylinder without making it overflow. The dish was returned to the incubator for 5min. Once cells began to round up and came off the dish bottom, they were transferred to a 96-well plate for further propagation in the presence of selective medium. After all of the desired clones were picked from the dish and the cloning cylinders were removed from the plate, fresh complete growth medium was added to the dish. The remaining clones were left to continue to grow.

2.2 RNA purification and analysis

RNA is highly susceptible to degradation so special care was taken when handling RNA. Whenever possible, sterile disposable plasticware was used. Non-disposable plasticware was thoroughly rinsed with 0.1M NaOH, 1mM EDTA followed by spraying RNase AWAY (Molecular BioProducts, USA) to remove nuclease and nucleic acid contamination. Glassware was filled with 0.1% diethylpyrocarbonate (DEPC) (Sigma, UK), allowed to stand overnight at 37°C and autoclaved to eliminate residual DEPC. Electrophoresis tanks were cleaned with 0.5% sodium dodecyl sulfate (SDS) detergent solution and rinsed with ethanol. All solutions were treated with 0.1% DEPC.

2.2.1 Total RNA extraction

To obtain optimal RNA yield, no more than $1x10^7$ cells were used as the starting material. Total RNA was extracted from animal cells using RNeasy Mini Kit (Qiagen, UK) according to the manufacturer's instructions. Purified RNA was stored at -70°C.

2.2.2 Determination of total RNA yield and quality

2.2.2.1 Yield and purity

The yield of total RNA obtained was determined spectrophotometrically at an absorbance of 260nm using the SmartSpec™ 3000 (Bio-Rad, UK). To ensure significance A_{260} readings should be greater than 0.15. Pure RNA should exhibit A_{260}/A_{280} ratios of 2.0. However, due to the variations between different starting materials and variations in performing the procedure, A_{260}/A_{280} ratios ranging from 1.7-2.0 was acceptable. Cuvettes were washed with 0.1M NaOH, 1mM EDTA followed by washing with RNase-free water. For accurate values, absorbance was measured in 10mM Tris-HCl, pH 7.5.

2.2.2.2 Formaldehyde agarose (FA) gel electrophoresis

The integrity of the purified RNA was determined by denaturing agarose gel electrophoresis. If the ribosomal RNA bands of a specific sample were not sharp but appeared as a smear, it was likely that the sample was degraded.

FA gel preparation

0.6g agarose was mixed with 10x FA gel buffer. RNase-free water was added to make up to 50ml. The mixture was microwaved for 1min to melt the agarose then cooled down to 60°C in a water bath. 0.9ml of 37% formaldehyde (Sigma, UK) and 5µl of SybR Green (Invitrogen, UK) were added before pouring onto the gel support. Prior to running, the gel was equilibrated in 1x FA gel running buffer for at least 30min.

RNA sample preparation for FA gel electrophoresis

1 volume of 5x RNA loading buffer was added to 4 volumes of RNA sample and mixed. The mixture was incubated for 5min at 65°C, chilled on ice and loaded onto the equilibrated FA gel.

Gel running conditions

Gels were run at 50-70 voltage (V) in 1x FA gel running buffer.

Quantification of RNA signals

Image processing of RNA gel pictures was performed by ImageJ software Ver. 1.38 (http://rsb.info.nih.gov/ij/). ImageJ is a public domain Java image processing program which allows quantifying band intensity.

Compositions of FA gel buffers

10x FA gel buffer

3-[N-morpholino]propanesulfonic acid	200mM
Sodium acetate	50mM
EDTA	10mM

1x FA gel running buffer

10x FA gel buffer	100 ml
37% (12.3M) formaldehyde	20 ml
RNase-free water	880 ml

5x RNA loading buffer

Saturated aqueous bromophenol blue solution	16µl
500 mM EDTA ,pH 8.0	80µl
37% formaldehyde	720µl
100% glycerol	2ml
Formamide	3ml
10x FA gel buffer	4ml
RNase-free water	100µl

2.3 cDNA synthesis by Reverse Transcriptase (RT-PCR)

SuperScript II Reverse Transcriptase (Invitrogen, UK) was used to reverse transcribe RNA obtained from various cell lines. The reaction was set up as follows:

Table 2-4. Two-step RT-PCR. Step one.

Component	Amount
Total RNA	5µg
Oligo(dt) 12-18 [0.5mg/ml]	1µl
DEPC water	to make a final volume of 10µl

The mixture was incubated at 70°C for 10min then chilled on ice for 2min. The following reagents were then added and incubated at 37°C for 90min.

Table 2-5. Two-step RT-PCR. Step two.

Components	Amount
5x First Strand Buffer	4µl
Dithiotheitol, 0.1M	2µl
dNTP mix [5mM each]	2µl
RNAsin	1µl
Superscript II RT	1µl

2.4 Cloning

2.4.1 Polymerase Chain Reaction (PCR)

2.4.1.1 Components

Taq DNA polymerase (Roche, UK) was used in PCR detection applications. For PCR cloning applications, *Pfu* DNA polymerase (Promega, UK) was used to enable the production of PCR products with high-fidelity and yield. For multiple reactions, 2 master mixes were prepared as described in Table 2-6 and Table 2-7 to keep the enzyme from interacting with primers and template during preparation of the reaction mixes. The volume of each Master Mix was 110% of the volume needed for all the samples. The extra volume allowed for losses during pipetting. For each reaction, 25µl Master Mix 1 was combined with 25µl Master Mix 2 in a thin-walled PCR tube on ice. The mixture was gently votexed to produce a homogeneous reaction and then centrifuged briefly to collect the solution at the bottom of the tube. In every set of PCR reactions a negative control was used in which template DNA was replaced by deionised H_2O to check for contamination. Thermal cycling was started immediately after this step.

Table 2-6. PCR Master Mix 1 components.

Component	Concentration	Volume
Water, PCR Grade		to make a final volume of 25µl
dNTP	200µM	1µl
Forward primer	5µM	5µl
Reverse primer	5µM	5µl
Template DNA	0.01-1µg/µl	variable
Final volume		25µl

Table 2-7. PCR Master Mix 2 components.

Component	Concentration	Amount
Water, PCR Grade		19.75µl
PCR reaction buffer with $MgCl_2$	10x	5µl
Taq DNA Polymerase	5U/µl	1.25µl
Final volume		25µl

2.4.1.2 Thermal cycling

Thermal cycling was carried out in the GeneAmp PCR System 9700 (Applied Biosystems, UK) and the thermal profile described in Table 2-8 was used to perform PCR.

Table 2-8. PCR thermal profile.

Step	Temperature	Time	Number of Cycles
Initial denaturation	95°C	2min	1 cycle
Denaturation	95°C	0.5–1min	
Annealing	42–65°C	0.5–1min	25–35 cycles
Extension	72°C	1min/kb	
Final Extension	72°C	5min	1 cycle
Soak	4 °C	indefinite	1 cycle

2.4.1.3 Primers used in this study

All the primers used in this study are listed in Table 2-9. The specificity of the primers that were designed manually was checked with the EMBL-GenBank database software using the Blast program. All the primers were synthesised by Lark Technologies, Inc. (Essex, UK).

Table 2-9. Primers used in this study.

Purpose	Name	Sequence 5'→3'
Cloning of mCherry	CherryF	GATCCCGCGGATGGTGAGCAAGGGCGAG
	CherryR	GATCGCGGCCGCCTTGTACAGCTCGTCCATGC
Cloning of NRG1β3-PAGFP Sequencing	NRG1β3F	CAAGTGAATTCATGTCCGAGCGCAAAGAA
	NRG1β3R	TACCAGGATCCTTCAGGCAGAGACAGAAAGG-
	NRG/PAGFP	GTGAATGGAGGGGAGTGCT
Mutagenesis	MP1	CGGCAAGCTGACCCCTGAAGTTCATCTGC
	MP2	CTGTCTCTGCCTGAA CGGGATCCACCGGTCGC
ErbB4 JM- isoforms detection (Gilmour *et al.*, 2001)	JM-F	CAGTGTGAGAAGATGGAAGAT
	JM-R	CTTTTTGATGATCTTCCTTCTAAC
ErbB4 CYT-isoforms detection (Gilmour *et al.*, 2001)	CYT-F	ATCTCTTGGATGAAGAGGATTTG
	CYT-R	GTCATCAAAAATCTCAGCAGTAGC
NRG1α detection	NRG1α-F	ACTGGTATGCCAGCCTCAAC
	NRG1α-R	CTCCAGTGAATCCAGGTTGG
Cloning of ErbB3	ErbB3F	ATGAGGGCGAACGACG
	ErbB3R	CGTTCTCTGGGCATTAGCC

2.4.2 Agarose gel electrophoresis

Agarose gel electrophoresis was employed to check the progression of a restriction enzyme digestion, to quickly determine the yield and purity of PCR reaction and to size fractionate DNA fragments, which then could be eluted from the gel. The percentage of agarose in the gel varied depending on the expected sizes of the fragments. 0.7% agarose gels were typically used for DNA molecules larger than 1kb, whereas 2% agarose gel was prepared for smaller DNA fragments. Prior to gel casting, dried agarose was dissolved in 50ml 1x Tris-acetate-EDTA (TAE) buffer by heating in a microwave for 1-2min until the agarose was dissolved. 5μl of SYBR Green was added to enable fluorescent visualization of the DNA fragments under ultraviolet (Lane et al.) light. The warm gel solution then was poured into a gel tank with casting comb in place and left for 20-30min to allow solidification. 1x TAE buffer was added to the gel tank until the buffer covered the agarose gel. The DNA samples were mixed with 5x loading dye (Promega, UK) and loaded into the sample wells along with the DNA ladder (Promega, UK) for fragment size determination. Electrophoresis usually was at 50-70V for 0.5-1h at room temperature, depending on the desired separation. After electrophoresis the gel was placed on a UV light box and a picture of the fluorescent SYBR Green-stained DNA separation pattern was taken with a Kodak camera, using the Bio-Rad bioimaging system (California, USA).

50x TAE buffer

Tris base	242g
Glacial acetic acid	57.1ml
EDTA	18.6g
dH2O	to a final volume of 1L

2.4.3 Purification of PCR products

The amplified products were run on an agarose gel and the DNA fragments were excised with a razor blade under the UV illuminator. Gel slices were weighed using the analytical balance and were purified using QIAEX II Gel Extraction Kit (Qiagen, UK), as per the manufacturer's instructions. The concentration of the purified product was determined by electrophoresis. Samples (2µl) were run on an agarose gel with 6x loading dye and compared to molecular weight markers (Promega, UK) of known concentrations.

2.4.4 Restriction enzyme digestions

For restriction enzyme digestions, all reactions were carried out in 20µl volumes, containing approximately 1µg DNA, 1x specific restriction buffer and 5 units of the restriction enzyme (Promega, UK). For simultaneous digestion with two enzymes a suitable buffer was chosen. Digestion was carried out at 37°C for 1-4h. Reaction mixtures were electrophoresed on an agarose gel along with markers and then purified by the QIAquick PCR Purification Kit (Qiagen, UK), as per the manufacturer's instructions.

Table 2-10. Restriction digestion reaction setup.

Components	Amount
Sterile deionised water	16.3µl
10x buffer	2µl
Acetylated BSA (10µg/µl)	0.2µl
DNA (1µg/µl)	1µl
Restriction enzyme (10u/µl)	0.5µl
Final volume	20µl

2.4.5 Dephosphorylation of the linearised vector

Digested vectors were treated with Calf Intestinal Alkaline Phosphatase (CIAP) (Promega, UK) to remove the phosphate group from the 5'-ends to prevent self-ligation of the vector. Sufficient CIAP was diluted in CIAP 1x reaction buffer (Promega, UK) to a final concentration of 0.01U/µl. Each picomole of DNA ends required 0.01U CIAP

(1μg of 1,000bp DNA = 1.52pmol DNA = 3.03pmol of ends). The reaction mixture was incubated at 37°C for 30min. Another aliquot of diluted CIAP (equivalent to the amount used in Table 2-11) was added and the incubation continued at 37°C for an additional 30min. 300μl of CIAP stop buffer was then added to the reaction mixture.

Table 2-11. Dephosphorylation reaction setup.

Component	Amount
DNA	up to 10pmol
CIAP 10x reaction buffer	5μl
Diluted CIAP (0.01u/μl)	5μl
Final	50μl

CIAP stop buffer

Tris-HCl (pH 7.5)	10mM
EDTA (pH 7.5)	1mM
NaCl	200mM
SDS	0.5%

TE buffer

Tris-HCl (pH 8.0)	10mM
EDTA	1mM

2.4.6 Ligation of plasmid vector and insert DNA

Various vector: insert DNA ratios were tested in order to find the optimum ratio for a particular vector and insert. In most cases, either a 1:1 or 3:1 molar ratio of vector: insert worked well. The following formula illustrates how to convert molar ratios to mass ratios.

(ng of vector × kb size of insert)/ kb size of vector × molar ratio of (insert/vector)
= ng of insert

Table 2-12 gives an example of a ligation reaction setup using a 1:1 molar ratio of vector: insert. The ligation reaction was incubated at 4°C overnight. T4 DNA ligase and ligase 10x buffer were purchased from Promega, UK.

Table 2-12. Ligation reaction setup.

Components	Amount
Vector DNA	3M
Insert DNA	1M
Ligase 10x buffer	1µl
T4 DNA Ligase	1µl
Nuclease-free water	to final volume of 10µl

2.4.7 Transformation of competent cells

Stocks of the antibiotics ampicillin (25mg/ml) and kanamycin (10mg/ml) (Sigma, UK) were made up in dH_2O, filter sterilised and stored at –20°C. Luria-Bertani (LB) (Sigma, UK) agar plates were made up with the addition of ampicillin (50µg/ml) or kanamycin (30µg/ml) and stored at 4°C. Selective plates were warmed at 37°C for 30min prior to use. The water bath was equilibrated to 42°C. Subcloning was undertaken according to the subcloning efficiency DH5α competent cells packet insert. Briefly, an aliquot of 50µl of DH5α cells (Invitrogen, UK) was thawed on ice. 1-10ng of DNA (approximately 1µl of the ligation reaction) was added to the DH5α competent cells and incubated on ice for 30min. The tube was then heated at 42°C for 45sec and returned to the ice for another 2min. 0.9ml of SOC medium (Invitrogen, UK) was then added and the mixture was shaked at 37°C for 1h. 50-100µl of each transformation reaction was plated on a prewarmed selective Lennox L agar plates supplemented with ampicillin or kanamycin for selection of recombinant clones. Two different volumes were plated to ensure that at least one plate would have well-spaced colonies. After experimental reactions were plated out, plates were incubated at 37°C overnight. 5ml of autoclaved LB (Sigma, UK) medium containing the appropriate antibiotic was added to sterile 50ml falcon tubes. Tubes were shaken overnight at 37°C in an orbital incubator shaker (Stuart Scientific, UK) at 225rpm. The amplified plasmid DNA was then extracted from the bacterial broth using the QIAprep Spin Miniprep Kit (Qiagen, UK) according to the manufacturer's instructions. Spectrophotometric determination of DNA concentrations were then undertaken using the SmartSpec™ 3000 (Bio-Rad, UK) at an absorbance of 260nm in a quartz curvette.

LB agar

NaCl	10g
Tryptone	10g
Yeast extract	5g
Agar	20g
dH2O	To a final volume of 1L

2.4.8 Confirmation of the presence and orientation of the inserted sequence

Plasmid DNA was either digested using appropriate restriction enzymes or screened by PCR to confirm the presence and orientation of the inserted fragment in the vector. Positive clones were sent to Lark Technologies, Inc. for sequencing to confirm that the sequences had not been altered by any cloning procedures.

Nucleotide sequence was translated into amino acid sequence using EMBOSS Transeq (http://www.ebi.ac.uk/emboss/transeq/) and aligned with protein database using WU-BLAST2 Protein Database Query (http://www.ebi.ac.uk/Tools/blast2/index.html).

2.4.9 Mutagenesis

Mutagenesis was performed using the QuickChange Site-Directed Mutagenesis Kit (Stratagene, UK) following the manufacturer's instructions. The mutagenic oligonucleotide primers were designed individually for each mutation. In general, primers were 25-45 bases in length with a melting temperature (Tm) of ≥75°C. The desired point mutation was close to the middle of the primer with ~10-15 bases of template-complementary sequence on both sides. Primers were optimised to have a minimum GC content of 40% and to terminate in one or more C or G bases at the 3'-end. Each reaction was a three-step procedure which introduced mutations at multiple sites using a single oligonucleotide per site. The primers were extended during thermal cycling by *Pfu* DNA polymerase. Incorporation of the oligonucleotide primers generated a mutated plasmid containing staggered nicks. Following thermal cycling, the product was treated with *Dpn* I. The *Dpn* I endonuclease was specific for methylated and hemi-methylated DNA and so digested the parental DNA template to select for mutation-containing synthesised DNA. The nicked vector DNA incorporating the desired mutation was then transformed into competent cells where the nicks were repaired. Colonies were then screened for desired mutations.

2.4.9.1 Mutant strand synthesis reaction

The ds-DNA template was prepared by standard Miniprep protocols. Each component (provided by the kit) of the mutant strand synthesis reaction was added in the order listed in Table 2-13:

Table 2-13. Mutant strand synthesis reaction components.

Components	Amount
10x QuikChange Multi reaction buffer	2.5μl
QuikSolution	0.2μl
ds-DNA template	100ng
Mutagenic primers	100ng
dNTP mix	1μl
QuikChange Multi enzyme	1μl
Double-distilled H_2O	to a final volume of 25μl

The reaction tubes were placed in the PCR machine and the cycling parameters were set up as follows:

Table 2-14. Mutagenesis thermal cycling profile.

Cycles	Temperature	Time
1	95 °C	30sec
12–18	95 °C	30sec
	55 °C	1min
	68 °C	1min/kb of plasmid length

2.4.9.2 *Dpn* I digestion of the amplification products

1μl of *Dpn* I restriction enzyme was added directly to each amplification reaction. Each reaction was mixed well by pipetting the solution up and down several times and was spun down in a microcentrifuge for 1min. Digestion of the parental ds-DNA was achieved by 1h incubation at 37°C.

2.4.9.3 Transformation of XL10-Gold ultracompetent cells

45μl of the ultracompetent cells were aliquoted into a prechilled 14-ml BD Falcon polypropylene round-bottom tube (BD Sciences, USA) for each reaction with the addition of 2μl of the β-mercaptoethanol mix provided with the kit. Each reaction tube was swirled every 2min for 10min. 1.5μl of the *Dpn* I-treated DNA was added to each tube of the ultracompetent cells. After incubation on ice for 30min, the tube was heat-pulsed in a 42°C water bath for 30sec and was then incubated on ice for 2min. Before 1h incubation at 37°C with shaking at 225rpm, to each tube was added 0.5ml of

42°C NZY$^+$ broth. 100µl of the transformation reaction was plated on pre-warmed LB-ampicillin agar plates. Each plate was incubated at 37°C for 16h.

NZY$^+$ broth	
Casein hydrolysate	10g
Yeast extract	5g
NaCl	5g
1M MgCl2	12.5ml
1M MgSO4	12.5ml
2M glucose	10ml
dH2O	to a final volume of 1L

2.4.10 TOPO TA cloning

TOPO TA Cloning Kit (Invitrogen, UK) was utilised for the direct insertion of Taq polymerase-amplified PCR products into a plasmid vector.

2.4.10.1 Setting up TOPO cloning reaction

PCR reaction was performed using Taq polymerase. The TOPO cloning reaction was set up as described in Table 2-15 and incubated for 5min at room temperature.

Table 2-15. TOPO cloning reaction setup.

Reagent	Amount
Fresh PCR product	0.5 – 4µl
Salt Solution	1µl
Water	add to a total volume of 5µl
TOPO vector	1µl
Final volume	6µl

2.4.10.2 Transforming competent cells

2µl of the TOPO Cloning reaction from the above step was added to a vial of DH5α competent cells. After 15min incubation on ice, the cells were heat-shocked for 30sec at 42°C in a water bath without shaking. After adding 250µl of SOC medium, the tube was shaked horizontally (200rpm) at 37°C for 1h. 10-50µl of the transformation reaction was spread on a prewarmed either ampicillin or kanamycin resistant plate which was coated with 40µl of 40mg/ml X-gal (Sigma, UK). Plates were incubated overnight at 37°C. White or light blue colonies were picked for analysis.

2.4.10.3 Analysing transformants

At least 6 white or light blue colonies were cultured overnight in LB media containing 50μg/ml ampicillin or 50μg/ml kanamycin. Plasmid DNA was isolated and analysed by either restriction digestions or PCR screening to confirm the presence and correct orientation of the insert. A patch plate was made at the same time to preserve the colonies for further analysis.

2.4.10.4 Plasmid storage

Once the correct clone was identified, a stock of plasmid DNA was stored at -20°C. A glycerol stock was also prepared for long term storage. The original colony was streaked out on LB plates containing 50μg/ml ampicillin or 50μg/ml kanamycin. A single colony was isolated and inoculated into 2ml of LB containing 50μg/ml ampicillin or 50μg/ml kanamycin. 850μl of culture was mixed with 150μl of sterile glycerol and transferred to a cryovial. The glycerol stocks were stored at -80°C.

2.4.11 Plasmids constructed in this study

2.4.11.1 pTRE2- NRG1β3GFP vector construction

To clone NRG1β3GFP into the Tet-Off response vector pTRE2, the pQBI25-fN1 vector which contains the NRG1β3GFP fragment was digested at *BamH* I and *Mlu* I restriction sites. The response vector pTRE2 was digested with the same restriction enzymes. After gel purification the response vector was ligated with the NRG1β3GFP insert and the ligation mixture was transformed into DH5α cells. The desired recombinant plasmid was identified by restriction analysis by choosing another two restriction sites (*Sac* II and *Not* I) outside the insertion but within the multiple cloning site in the pTRE2 vector. The orientation and the correct junctions were confirmed by sequencing.

2.4.11.2 Mammalian cherry vector pmCherry construction

To generate the mCherry fragment, mCherry was amplified from the bacterial vector pRSET-B mCherry (a gift from Dr. Dan Mulvihill, University of Kent, UK) using the primers CherryF 5'-GATCCCGCGGATGGTGAGCAAGGGCGAG-3' and CherryR 5' GATCGCGGCCGCCTTGTACAGCTCGTCCATGC-3'. This pair of primers contains two restriction sites, *Sac* II and *Not* I, at the 5' end and the 3' end, respectively. A couple of nucleotides were added to both ends of the primers to facilitate restriction digestions.

GC contents, melting temperatures and secondary structures of the primers were checked using the DNA calculator (http://www.sigma-genosys.com/calc/DNACalc.asp). The pEGFP-N1 vector was double digested with *Sac* II and *Not* I restriction enzymes to remove the EGFP fragment from the vector. Following PCR product digestions, the mCherry fragment was cloned into the digested pEGFP-N1 to create the mammalian expression vector pmCherry. Ligation was confirmed by PCR screening using CherryF and CherryR primers. DNA sequencing further verified the inserts.

2.4.11.3 Plasmid pNRG1β3-PAGFP construction

The pPAGFP plasmid was obtained as a kind gift from Dr. Lippincott-Schwartz (National Institute of Health, USA). The NRG1β3-PAGFP expression construct was made after first amplifying NRG1β3 from the vector pQBI25-fN1 using primers NRG1β3F: 5'-CAAGTGAATTCATGTCCGAGCGCAAAGAA-3' and NRG1β3R: 5'-TACCAGGATCCTTCAGGCAGAGACAGAAAGG-3'containing *EcoR* I (forward primer) and *BamH* I (reverse primer) restriction sites. Utilising these unique restriction sites, the NRG1β3 PCR product was ligated into the pPAGFP vector as an *EcoR* I and *BamH* I restriction digest fragment. Ligation was confirmed by PCR screening using NRG1β3F and NRG1β3R primers. The insert was sequenced from both the 5'- and 3' ends using universal primers CMV F and EBV R. Primer NRG/PAGFP: 5'-GTGAATGGAGGGGAGTGCT-3' was synthesised and used to sequence the junction of NRG1β3 and PAGFP. The QuikChange Site-directed Mutagenesis kit was used to rectify the random mutation resulting from subcloning. The mutagenesis primer MP1: 5'-CGGCAAGCTGACCCCTGAAGTTCATCTGC-3' was designed to remove the extra nucleotide. To further correct frame shift mutations, two nucleotides were introduced by site-directed mutagenesis reactions using primer MP2: 5'-CTGTCTCTGCCTGAACGGGATCCACCGGTCGC-3'. All mutagenesis results were confirmed by sequencing.

2.4.11.4 Plasmid pmCherry-ErbB3 construction

To construct the pmCherry-ErbB3 vector, ErbB3 was first amplified from its vector pBABE-puro ErbB3 using a pair of primers ErbB3F: 5'-ATGAGGGCGAACGACG-3' and ErbB3R: 5'-CGTTCTCTGGGCATTAGCC-3'. The amplified ErbB3 PCR product was then subcloned into the pCR2.1-TOPO vector using the TOPO TA cloning kit. Both of the pCherry vector and the pCR2.1-TOPO ErbB3 vector were digested at *Hind* III

and *EcoR* I restriction sites. Following gel purification the digested ErbB3 fragment was ligated into the pmCherry vector. Ligation was confirmed by PCR screening using primers ErbB3F and ErbB3R. The sequence of the correct insertion was confirmed by sequencing.

2.5 Western blotting

2.5.1 Cell lysis

Cells were plated into 35mm polystyrene tissue culture dishes and maintained until they were 70% confluent. To make cell lysates cells were washed twice with ice cold, 2mM ethylene glycol tetra-acetic acid (EGTA) in PBS and then lysed in 200µl of ice cold lysis buffer for 1-2min. The lysates were collected into 1.5ml eppendorf tubes using a cell scraper (Fisher Scientific, UK) and centrifuged at 14,000rpm for 10min in a Genofuge 16M centrifuge (Teche Cambridge, UK) at 4°C. If required the protein concentration was determined by the Bradford assay (Bradford, 1976) using BSA (Bio-Rad, UK) as the standard.

Lysis buffer

Tris HCl pH 7.4	0.05M
Triton X-100	1 %
EDTA	5mM
NaCl	0.15M
Phosphatase inhibitor cocktail 2 (Invitrogen, UK)	1 %
Protease inhibitor cocktail (Invitrogen, UK)	0.5 %

2.5.2 The standard Bradford assay

A 96-well plate assay protocol was followed from the Bradford reagent (Sigma, UK) instruction booklet. Briefly, the Bradford reagent was gently mixed and brought to room temperature. Protein concentration standards were created by serially diluting 2mg/ml Bovine Serum Albumin (BSA). 5 dilutions of the BSA protein standard were prepared within the linear range of the assay (0.1-1.4mg/ml). 5µl of the protein standards were added to separate wells in the 96-well plate. The unknown samples were prepared with an estimated concentration between 0.1-1.4mg/ml. 250µl of the Bradford reagent was added to each well being used and mixed on a shaker for 1min. Samples were incubated at room temperature for 15min. Absorbance was read at 595nm in a MRX Dynatech plate reader (Dynatech Laboratories, Inc., USA). The standard curve was plotted and

was used to calculate the concentration of unknown samples. The volume of each sample was then adjusted to account for different protein concentrations. 5x sample buffer was added to the cell lysate and boiled at 100°C for 5min in a heat block (Stuart Scientific, UK), then stored at –20°C.

5x Sample buffer

SDS	10%
Tris pH 6.8	1M
Bromophenol blue	0.015g
β-mercaptoethanol	10%
Glycerol	33%

2.5.3 Sodium dodecyl sulphate–polyacrylamide gel electrophoresis (SDS-PAGE)

The 'Mighty Small II' Mini Vertical Unit obtained from Amersham Biosciences (Little Chalfont, UK) was utilised to run SDS-PAGE gels. Gel plates were cleaned with acetone and assembled according to the supplier's instructions. For each SDS-PAGE gel, after sandwiching one white plate and one glass plate which were separated by spacers, 7% resolving gel were poured into the plate stack until ¾ full. An upper layer of water-saturated iso-butanol was added to the top of the gel to allow setting as a flat surface. Once the resolving gel was set, 3.75 % stacking gel was poured and a comb 1.5mm thick with sample wells 5mm across was inserted.

The gels were placed in a running tank filled with 1x running buffer. Samples were heated for 5min at 100°C. 30µl of the cell lysate was loaded into each well with a syringe. 5µl of dual colour molecular weight markers (M.W. 10-250kDa) (Bio-Rad, UK) was also loaded into a well on each gel. Electrophoresis was initially carried out at 60V though the stacking gel then the voltage was increased to 120 V though the resolving gel until the dye front reached the bottom of the gel.

7 % resolving gel

Acrylamide / Bis solution 29:1	7%
Tris-HCl pH 8.8, 2M	5.6µl
SDS	0.1%
N,N,N,N'-Tetra-methyl-ethylenediamine (TEMED)	15µl
10 % Ammonium persulfate (Dapson)	450µl

3.75 % stacking gel

Acrylamide / Bis solution 29:1	3.75%
Tris-HCl pH 6.8	0.1M
SDS	0.1%

1x running buffer

Tris- HCl	0.025M
Glycine	0.192M
SDS	1%

2.5.4 Electro blotting

The stacking gel was cut off and top left-hand corner of the resolving gel was nicked for orientation. Two pieces of 3mm filter paper (Whatman, UK) and one piece of nitrocellulose membrane (Amersham Biosciences, UK) were cut to the dimensions of the gel and soaked in the blotting buffer. The gel, filter paper and nitrocellulose were sandwiched together and placed in the Trans blot cell wet blotting tank (Bio-Rad, UK) filled with blotting buffer. Blotting was carried out either for 3h at 400mA or overnight at 100mA at room temperature.

10x running buffer

Tris-HCl	0.25M
Glycine	1.92M
SDS	10 %

Blotting buffer

10x running buffer	10 %
Methanol	10 %
SDS	0.1 %

2.5.5 Immunodetection

Ponceau S staining was used as a rapid and reversible staining method for locating protein bands on western blots. Blots were stained with Ponceau S staining solution and then rinsed off with PBS until the background was clean. The membranes were then shaken in the blocking buffer for 1h, washed in 0.1% Tween 20/PBS (Sigma, UK) and probed with a primary antibody in the blocking buffer for 1.5h. After washing in 0.1% Tween 20/PBS the membrane was probed with horse radish peroxidase (HRP) conjugated secondary antibody (DAKO, UK) for 1h. Visualisation was carried out using enhanced chemiluminescent (ECL) detection (Amersham Biosciences, UK) followed by exposure to X-ray film (Amersham Biosciences, UK) and the film was developed using a compact x4 hyperprocessor (Xograph imaging systems, UK).

Ponceau S staining solution

Ponceau S	0.2%
acetic acid	3%

Blocking buffer

Marvel	5%
Tween 20/PBS	0.5%

2.5.6 Antibodies used in this study

Table 2-16. List of antibodies used in this study. IF: immunofluorescence, IHC: immunohistochemistry, WB: western blotting.

Antibody	Specificity	Source	Application	Origin
RTJ2	ErbB3 intracellular domain	Mouse monoclonal	IHC, IF, WB	(Rajkumar *et al.*, 1996)
HFR1	ErbB4 intracellular domain	Mouse monoclonal	IF, WB	(Srinivasan *et al.*, 1998)
76HG	NRG1α	Rabbit polyclonal	IHC	(Qi *et al.*, 1994)
102HG	NRG1β	Rabbit polyclonal	IHC	(Srinivasan *et al.*, 1999)
122NRG3	NRG3 EGF-like domain	Rabbit polyclonal	IHC	(Dunn *et al.*, 2004)
136NRG3	NRG3 intracellular domain	Rabbit polyclonal	IHC	(Dunn et al., 2004)
PY20	Phosphotyrosine	Mouse monoclonal	IF, WB	Sigma ,UK
GFP3E1	Green fluorescent protein	Mouse monoclonal	WB	(Hunt & Geley, CRUK)
Hsp70'B	Hsp70B'	Mouse monoclonal	WB	Stressgen, UK
Tyr984	Phospho-ErbB4 (Tyr984)	Rabbit monoclonal	WB	Cell Signalling, UK

2.6 Immunofluorescence staining

Prior to seeding with cells the coverslips were placed in a 24-well plate. Cells were allowed to grow overnight. The following day media was removed from the 24-well plate. All the following procedures were carried out at room temperature. Cells were washed three times with PBS and then fixed with 4% paraformaldehyde/PBS for 10min. The fixative was then removed and the cells were washed three times with PBS. If required, cells were permeablised with 0.1% Triton X-100 (Sigma, UK) in PBS for 10min and washed. Cells were incubated in 1% BSA/PBS for 30min to block unspecific binding of the antibodies. The blocking buffer was removed by holding each coverslip on its edge with forceps and draining it onto a sheet of fibre-free paper. Cells were incubated with primary antibody at an appropriate dilution in 1% BSA/PBS solution for 1h in a humidified chamber. An omission of primary antibody was used as the control. The antibody solution was removed by aspiration. After three washes in PBS cells were incubated with secondary antibody at an appropriate dilution in 1% goat serum (Sigma,

UK) in 1% BSA/PBS for 1h in the dark. Following washing three times with PBS, cells were mounted by placing a drop of Mowiol on a microscope slide. Slides were wrapped in foil and stored at 4°C.

Mowiol mounting medium

Glycerol	6g
Mowiol 4-88	2.4g
0.2M Tris, pH 8.5	12ml
dH_2O	6ml

2.6.1 Bromodeoxyuridine (BrdU) immunofluorescence staining

For DNA synthesis analysis cells were incubated with 10mM BrdU (Sigma, UK) for 24h. Cells on coverslips were washed with PBS and fixed in 4% paraformaldehyde/PBS at room temperature for 10min. After three washes with PBS cells were permeablised with 0.1% Triton X-100 for 10min. DNA was denatured by incubating cells in 2N HCl for 30min at room temperature. The acid was then neutralised with 0.1M borate buffer, pH8.5. Cells were blocked for 30min in 1% BSA/PBS and incubated with a monoclonal anti-BrdU antibody (1:500) (Sigma, UK) for 1h at room temperature and then washed with PBS. Cells were further incubated with Alexa Fluor 546-conjugated secondary antibody (Sigma, UK) diluted 1:1000 in 1% goat serum in 1% BSA/PBS for 1h at room temperature in the dark. Following incubation, cells were washed with PBS. Coverslips were subsequently mounted with Mowiol.

2N HCl

10N HCl	20ml
Distilled water	80ml

0.1M Borate buffer, pH 8.5

Sodium borate	3.8g
Distilled water	100ml

2.7 Immunohistochemical staining

2.7.1 Tissue source

Tissue arrays were purchased from SuperBioChips (South Korea) unless specified. They were formalin fixed and paraffin-embedded. Human normal tissue array (AC1) contained 60 normal organ samples from non-cancer patients: skin, subcutis, breast, spleen, lymph node, skeletal muscle, lung, heart, aorta, salivary gland, liver, gallbladder,

pancreas, tonsil, oesophagus, stomach, small intestine, colon, kidney cortex, kidney medulla, uterus, prostate, placenta, umbilical cord, adrenal, thyroid, thymus, gray matter, white matter, and cerebellum. Human cancer tissue array (VB2) contained 146 samples of various cancers including lung (24), bone (16), soft tissue (25), melanoma (10), skin (3), breast (19), uterine cervix (26), endometrium (12) and ovary (11). AC1 and VB2 tissue arrays were immunohistochemically stained with the anti-NRG1α and anti-NRG1β antibodies.

Human breast cancer-normal array (CBB2) contained samples from 15 cancer patients and 15 normal patients with 2 cores each. Human breast cancer-metastasis-normal array (CBA3) contained 40 breast cancer cases, 10 metastatic cancer cases and 9 normal cases. CBB2 and CBA3 tissue arrays were immunohistochemically stained with the NRG3 122 and NRG3 133 antibodies by Laura Smart (a former PhD student in the laboratory). The tissue arrays containing 104 formalin fixed and paraffin embedded human breast cancer tissue cores were obtained from Professor Adrian Harris and Dr Russell Leek (Cancer Research UK, UK). They were immunohistochemically stained with the anti-NRG1α and anti-NRG1β antibodies by Emmet Mcintyre (another PhD student in the laboratory).

Ethical approval for the use of these tissues was granted by the Research Ethics (Human Participants) Committee or the University of Kent.

2.7.2 Staining procedure

1. De-paraffinisation and hydration
    - incubate in a dry oven at 60°C for 1h
    - dewax slides in Histoclear 1 for 4min, Histoclear 2 for 4min and Histoclear 3 for 4min
    - hydrate slides in 100% Ethanol 1, 100% Ethanol 2 and 70% Ethanol 3 for 4min each
    - immerse slides in tap water for 5min and place in PBS for 5min to equilibrate.
2. Quenching endogenous peroxidase
    - incubate in 3% hydrogen peroxide solution for 10min
    - wash slides in PBS for 5min x 3 times
3. Primary antibody

- incubate with primary antibody diluted in 3% hydrogen peroxide for 1h at room temperature

- wash slides with distilled water for 5min and place in PBS for 5min to equilibrate

4. Secondary antibody

- incubate for 30min at room temperature with Strep ABC complex/ HP from DAKO kit.

- wash slides with distilled water for 5min and place in PBS for 5min to equilibrate

5. Chomogenic reaction

- incubate slides in fresh DAB solution and wait for colour change (approximately 1-5min)

- wash in distilled water to stop the reaction

6. Counterstain

- in Gill's hematoxylin for 30sec

7. Dehydration, clearing and mount

- dehydrate slides in 70% Ethanol 1 for 4min, 100% Ethanol 2 for 4min and 100% Ethanol 3 for 10min

- clear slides in Histoclear 1 for 4min, Histoclear 2 for 4min, and Histoclear 3 for 10 min - mount the cover slide with DPX mounting medium (Fisher Scientific, UK)

2.7.3 Scoring

In this study, only the presence or absence of nuclear staining was recorded. Brown-coloured nuclear staining in tissues samples was evaluated by two observers and only obvious nuclear immunostaining was considered to be positive. All statistical tests were done using Microsoft Office Excel 2007.

2.8 Microscopy

2.8.1 Light microscopy

Tissue cultures were examined under the Olympus CKX31 inverted microscope. Tissue section staining was examined by two observers using double-headed upright microscopy (Olympus BX40, Germany). Photographs were taken using a Leica Leitz

DMRB microscope (Leica Microsystems, Germany).

2.8.2 Fluorescence microscopy

Green fluorescent live cells were visualised by the Leica AS MDW (Application Solution Multidimensional Workstation), which is a dedicated workstation for multi-dimensional cell imaging with temperature controlled at 37°C. CO_2 concentration and humidity in the specimen chamber were also well regulated. Cells were growing on 35mm glass bottom culture dishes suitable for live cell imaging. The culturing medium of the cells was removed and washed twice with 2ml of Hanks Balanced Salt Solution (HBSS, obtained from Gibco BRL, UK). The images were captured on the basis that they were representative of the majority of the cells.

2.8.3 Confocal microscopy

The following microscopy was performed on a Leica SP2 laser scanning confocal microscope.

2.8.3.1 GFP and cherry

For simultaneous imaging of GFP and cherry, GFP was excited using low intensity (13%) levels of the 488nm line of an argon ion laser. Emission was collected with a 505nm filter. The 546nm line of the helium-neon laser (power at 80%) was used for cherry excitation and its emission was collected with the 560nm filter.

2.8.3.2 Alexa Fluor 633

The 633nm line of the helium-neon laser (power at 60%) was used to excite the far-red-fluorescent Alexa Fluor 633 and its emission was collected with the 647nm filter.

2.8.3.3 PAGFP

Individual cells with PAGFP plasmids can be seen faintly with ultraviolet light and selected for photoactivation. The PAGFP photoactivation process was started by locating a target cell though the 10x objective and switching to the high magnification objective 63x oil immersion lens followed by zooming in on a region around the cell. This limited the confocal laser scanning to a more defined rectangular region. An initial

excitation scan at 488nm laser light confirmed the position of the cell within the rectangular region. ~2s of irradiation with 405nm laser light at a power of 20% photoactivated PAGFP within the cell. Immediately after each 405nm excitation scan, the rectangular region of interest was scanned with 488nm laser light. Pre- and post-photoactivation images were captured using low intensity (13%) levels of the 488nm line of an argon ion laser. Emission was collected with a 505nm filter.

2.9 Kinomic assay

The Human Phospho-RTK Array Kit with four membranes was purchased from R&D Systems (Minneapolis, USA).

2.9.1 Cell lysis

Cells were rinsed with PBS before adding 200µl of NP-40 lysis buffer. The lysates were transferred to sterile eppendorfs and pipetted up and down to resuspend and then gently rocked at 4°C for 30min. After being microcentrifuged at 14,000rpm for 5min, the supernatant was collected and stored at -80°C. The sample protein concentrations were determined using the Bradford assay. 200µg of total protein from each sample was incubated with the Human Phospho-RTK Array membranes.

NP-40 Lysis Buffer

NP-40	1%
Tris-HCl (pH 8.0)	20mM
NaCl	137mM
Glycerol	10%
EDTA	2mM
Sodium orthovanadate	1mM
Aprotinin	10µg/ml
Leupeptin	10µg/ml
Pepstatin	10µg/ml

2.9.2 Array blotting

The procedures were performed according to the manufacturer's protocol. Briefly, arrays were blocked in the blocking buffer for 1h on a rocking platform shaker at room temperature. Cell lysates were then diluted and incubated with the Human Phospho-RTK Array at 4°C overnight. Each array was washed by soaking for 10min with the Wash Buffer (provided in the kit). Washing was repeated two times for a total

of three washes. Arrays were incubated with the detection antibody for 2h at room temperature and then were washed three times. Each array was exposed to chemiluminescent reagents and then the film was developed.

2.10 Gene transcription assay

RNA samples were sent to Source BioScience geneservice (Nottingham, UK) and were processed in duplicate using the Illumina's Gene Expression Arrays HumanWG-6 v3 BeadChips. The data was analysed using the Illumina GenomeStudio software v2009.1.

Chapter 3. Immunohistochemical study of intranuclear expression of NRGs

3.1 Introduction

Even though nuclear localisation of NRGs has been reported by independent groups, most of their results are based on a single cell line or a particular tissue type (Section 1.13.5). To our knowledge the immunohistochemical study presented here is the first study which surveyed a wide range of human normal and cancer tissues to determine the frequencies of nuclear staining of NRG1α and NRG1β in various physiological conditions. As nuclear expression of NRG1α and NRG1β was detected in a significant proportion of DCIS cases (Marshall et al., 2006), we further examined their incidences in 119 cases of invasive breast cancer tissues. The frequency of nuclear expression of NRG3 was also examined in normal and breast cancer tissues. Although each member of the NRG family ligands is present in pre-invasive ductal breast cancer, no nuclear staining of either NRG2 or NRG4 was reported (Marshall et al., 2006). Therefore, we prioritised our interests on analysing the nuclear expression of NRG1α, NRG1β and NRG3.

The purpose of this study was to confirm that the observed nuclear localisation patterns of GFP-tagged NRG1β3 were also seen in natural tissues. Using fluorescence microscopy NRG1β3GFP was found to localise to two subnuclear compartments, nucleoli and spliceosomes. Perhaps mainly because it did not fit with classical paradigms of growth factor signalling, it was necessary to demonstrate that intranuclear localisation of NRG1β3 was not an artefact. This immunohistochemistry study not only confirms that intranuclear expression of NRG1 occurs in various physiological conditions, but also provides a rationale for the functional studies at the molecular level described later in this thesis.

3.2 Aims

1. To optimise the anti-NRG1α and anti-NRG1β antibody concentrations in order to produce high quality staining with minimal background.
2. To determine the frequency of intranuclear expression of NRG1α and 1β in a range of normal and cancer tissues by immunohistochemical staining of tissue arrays.
3. To determine the frequency of intranuclear expression of NRG3 in normal and breast cancer tissue samples.

3.3 Results

3.3.1 NRG1 antibody concentration optimisation

To achieve high quality staining with minimal background, optimisation of the concentrations of anti-NRG1α and NRG1β antibodies was performed on a multi-block of rat pancreas tissues prior to use on the tissue arrays. Figure 3-1 shows the comparison of the staining of islets of Langerhan using the anti-NRG1α antibody at concentrations of 1μg/ml and 2μg/ml. Islets of Langerhan are special groups of cells in the pancreas, which make and secrete hormones. There are at least five different types of cells in individual islets. β cells make and release insulin, a hormone that controls the level of glucose in the blood. Anti-NRG1α showed cytoplasmic staining in cells in the centre of the islet of Langerhan. Vascular smooth muscle cells (which compose the majority of the wall of blood vessels) and the endothelium (which is the thin layer of cells that line the interior surface of blood vessels) were also stained. Staining with the anti-NRG1α antibody at 2μg/ml exhibited stronger staining of the islet of Langerhan without any background signal (Figure 3-1b). Figure 3-2 shows staining of islets of Langerhan using the anti-NRG1β antibody at concentrations of 1, 2.5, 3.5 and 5μg/ml. NRG1β showed cytoplasmic staining in cells in the periphery of the islets. The section was under-stained at 1μg/ml (Figure 3-2a), and over-stained at 3.5 and 5μg/ml indicated by the non-specific background (Figure 3-2c and d). This experiment allowed us to detect the lower and higher range of the concentration of the anti-NRG1 antibodies on rat pancreas tissues, which may also apply to other tissue types. The optimal antibody concentration should be the highest concentration that gave the strongest staining without any background signals. The above staining results suggested that NRG1α antibody at 2μg/ml and NRG1β antibody at 2.5μg/ml were the optimal concentrations and were ultimately used in the following study.

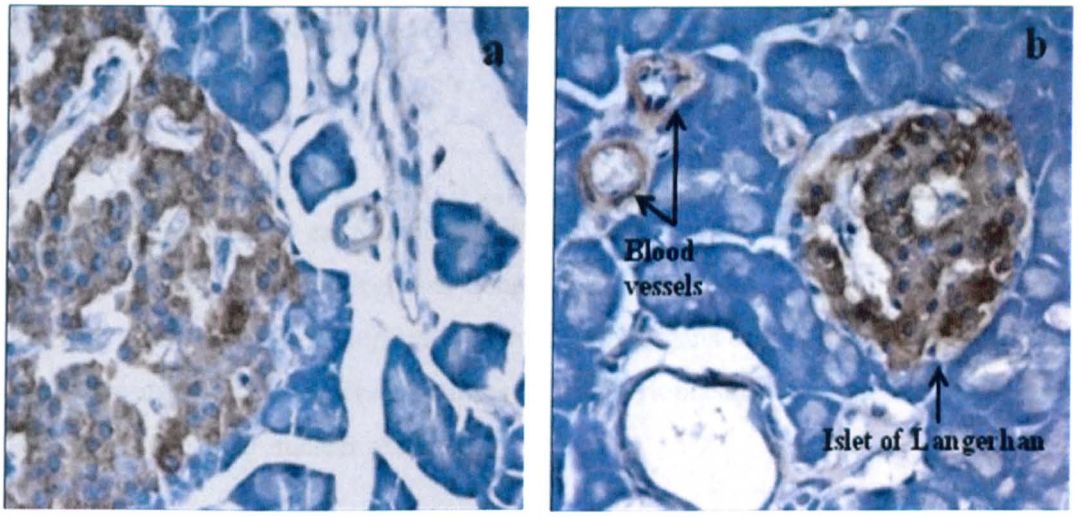

Figure 3-1. Rat pancreas tissues were immunohistochemically stained using anti-NRG1α antibody at 1μg/ml (a) and 2μg/ml (b). Original magnifications: x63.

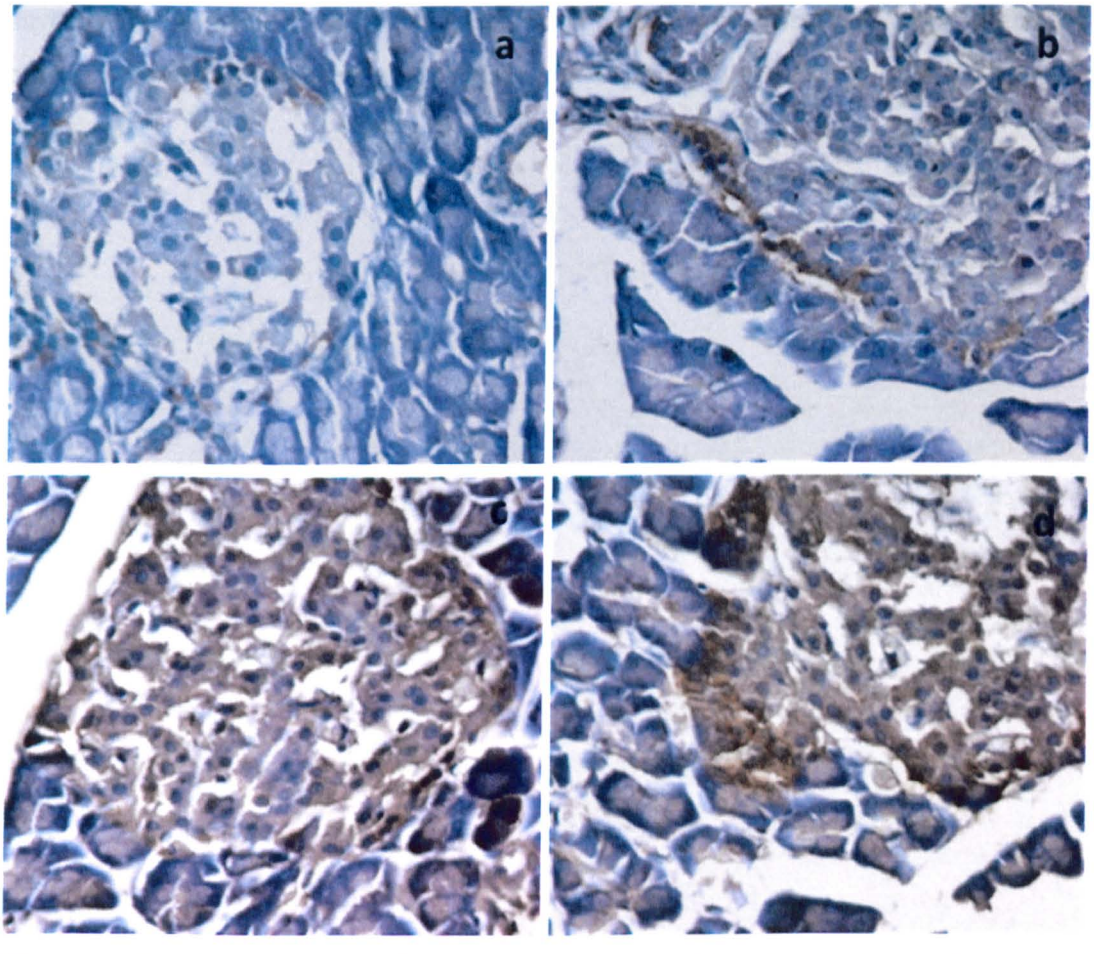

Figure 3-2. Rat pancreas tissues were immunohistochemically stained using anti-NRG1β antibody at 1 (a), 2.5 (b), 3.5 (c) and 5μg/ml (d). Original magnifications: x63.

3.3.2 Intranuclear expression of NRG1α and NRG1β in normal tissues

3.3.2.1 Staining patterns

To analyse the nuclear expression of NRG1α and NRG1β in various normal tissues, immunohistochemical staining was done on a tissue array containing 60 cores (30 different tissue samples in duplicate) from normal organs of non-cancer patients. Most normal tissues showed either no staining or only cytoplasmic staining. However, three tissues did give clear nuclear reactivity.

NRG1α was expressed in normal skin showing a cytoplasmic staining pattern (Figure 3-3a). NRG1β exhibited a similar expression pattern with stronger staining of basal cells in the epidermis (Figure 3-3b). Both NRG1α and NRG1β also showed moderate to strong nuclear staining. Nuclear expression of NRG1α was observed in one of the two cases of human skin tissue, whereas nuclear expression of NRG1β was observed in both cases.

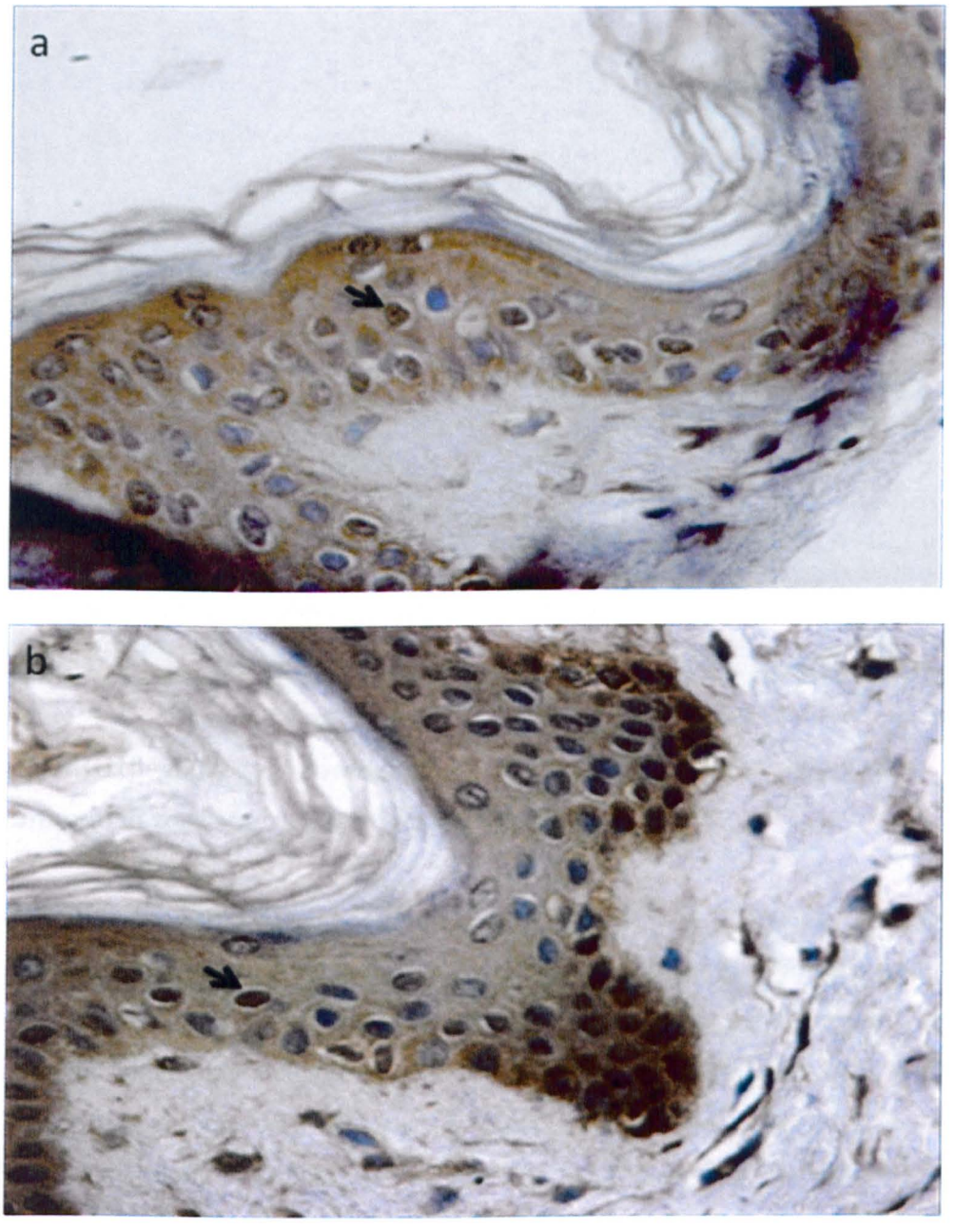

Figure 3-3. Immunohistochemical staining of human skin tissues treated with anti-NRG1α (a) and anti-NRG1β antibody (b), showing moderate to strong cytoplasmic along with nuclear staining (arrowed) in epidermis. Original magnifications: x63.

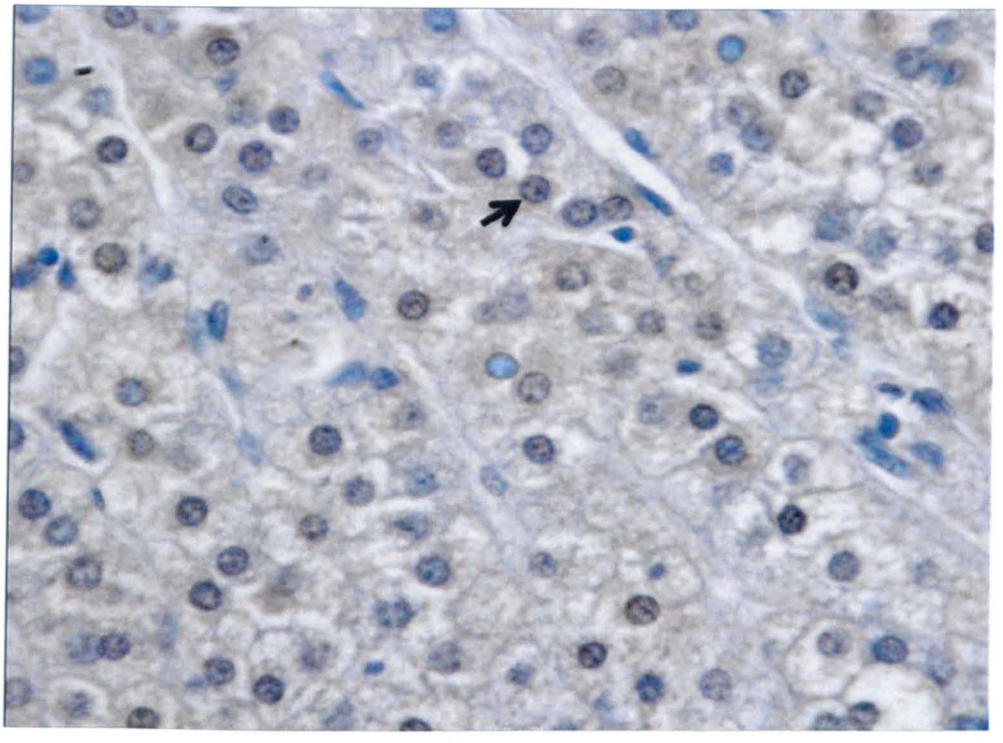

Figure 3-4. Immunohistochemical staining of human adrenal tissue treated with anti-NRG1β antibody, showing moderate cytoplasmic along with nuclear staining (arrowed) in zona reticularis. Original magnifications: x63.

The adrenal cortex consists of three distinct layers: zona reticularis, zona fasiculata and zona glomerulosa, each with distinct hormonal functions. The innermost layer of the adrenal cortex is the zona reticularis. Cells in this layer produce precursor androgens including dehydroepiandrosterone and androstenedione from cholesterol. NRG1β expression was detected in some of these cells, showing a moderate cytoplasmic along with punctated nuclear staining (Figure 3-4). At x63 magnification, intranuclear structure staining was visible.

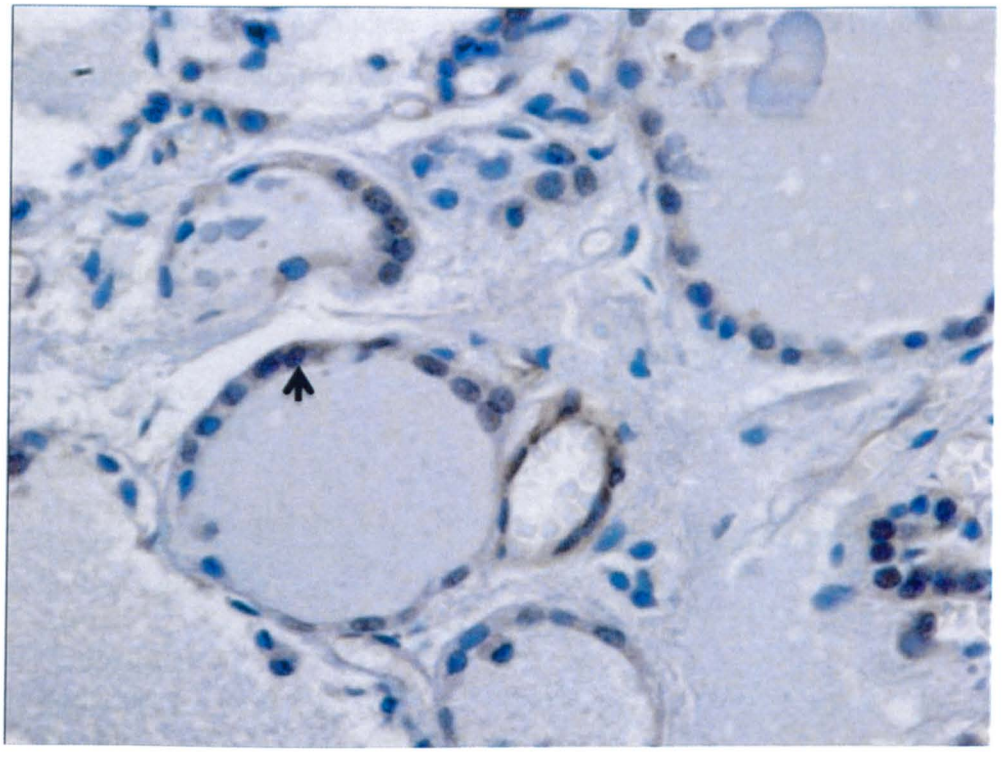

Figure 3-5. Immunohistochemical staining of human thyroid tissue treated with anti-NRG1β antibody, showing weak cytoplasmic along with nuclear staining (arrowed) in thyroid epithelial cells. Original magnifications: x63.

Thyroid gland is one of the largest endocrine glands in the body, which controls metabolism through the production of thyroid hormones. Thyroid gland is composed of spherical follicles that selectively absorb iodine from the blood. The follicles are surrounded by a single layer of thyroid epithelial cells, which secret thyroid hormones. NRG1β showed weak cytoplasmic staining of these epithelial cells (Figure 3-5). Again, nuclear staining was observed.

3.3.2.2 The frequency of intranuclear expression of NRG1α and NRG1β in normal tissues

Nuclear expression of NRG1α was detected in one case of normal skin, whereas nuclear expression of NRG1β was detected in both cases of normal skin, adrenal and thyroid tissues. Table 3-1 lists the tissue types examined and whether nuclear NRG1α and NRG1β were detected in each case.

Table 3-1. Detection of nuclear expression of NRG1α and NRG1β in human normal tissue array. X: uninformative.

	NRG1β		NRG1α	
Organs	Case 1	Case 2	Case 1	Case 2
Skin	+	+	-	+
Subcutis	X	X	X	X
Breast	-	-	-	-
Spleen	-	-	-	-
Lymph node	-	-	-	-
Sketetal muscle	-	-	-	-
Lung	-	-	-	-
Heart	-	-	-	-
Aorta	-	-	-	-
Salivary gland	-	-	-	-
Liver	-	-	-	-
Gallbladder	-	-	-	-
Pancreas	-	-	-	-
Tonsil	-	-	-	-
Esophagus	-	-	-	-
Stomach	-	-	-	-
Small intestine	-	-	-	-
Colon	-	-	-	-
Kidney, cortex	-	-	-	-
Kidney, medulla	-	-	-	-
Uterus	-	-	-	-
Prostate	-	-	-	-
Placenta	-	-	-	-
Umbilical cord	-	-	-	-
Adrenal	+	+	-	-
Thyroid	+	+	-	-
Thymus	-	-	-	-
Gray matter, cerebrum	-	-	-	-
White matter, cerebrum	-	-	-	-
Cerebellum	-	-	-	-

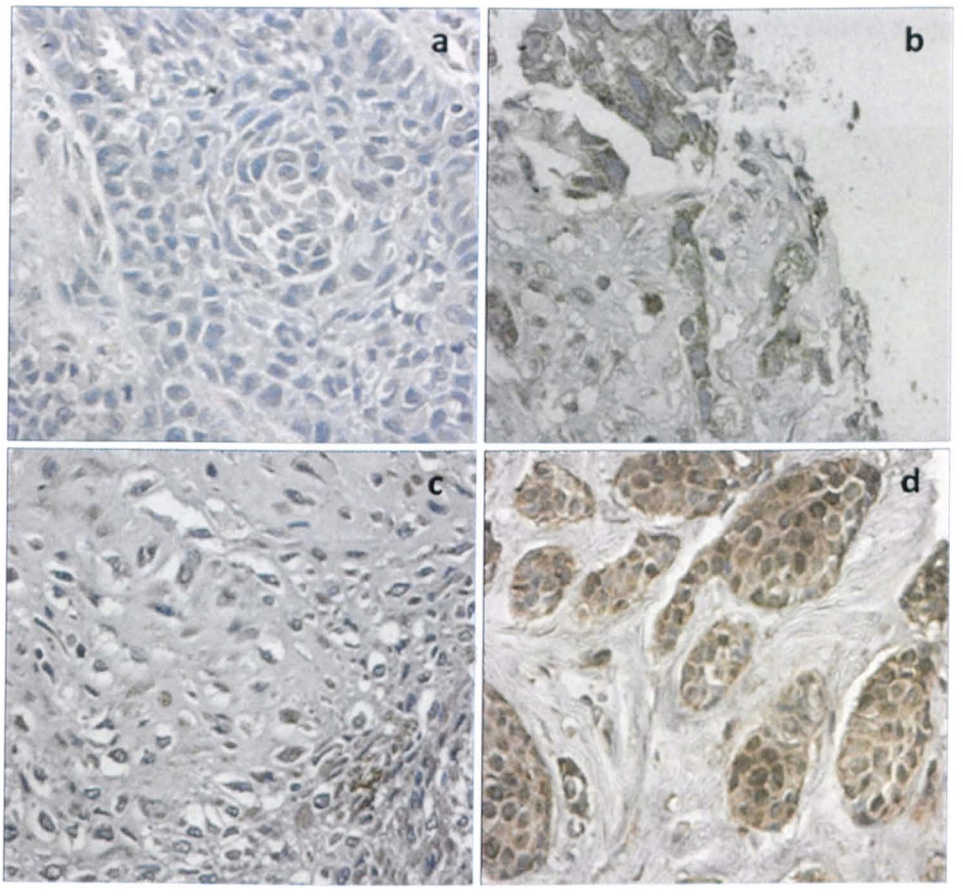

Figure 3-6. Immunohistochemical detection of NRG1α cytoplasmic and nuclear staining in various human cancer tissues. (a) Negative cytoplasmic and nuclear staining (lung cancer); (b) cytoplasmic positive and nuclear negative staining (soft tissue); (c) cytoplasmic negative and nuclear positive staining (soft tissue); (d) cytoplasmic positive with strong nuclear staining (breast cancer). Original magnifications: x63.

3.3.3 Expression of NRG1α and NRG1β in various cancer tissues

3.3.3.1 Staining patterns

Immunohistochemical staining was done on a tissue array containing 150 cores of various human cancers to examine the nuclear expression patterns of NRG1α and NRG1β. Among the various cancer tissues positively stained for NRG1α, its expression patterns were different, with some showing either nuclear or cytoplasmic localisation and others showing both nuclear and cytoplasmic staining. Figure 3-6 shows an example of each staining pattern. Similar expression patterns were also observed in the cancer tissue array stained with anti-NRG1β antibody (data not shown).

A detailed description of positive nuclear staining patterns of NRG1α and NRG1β in each cancer type is given below.

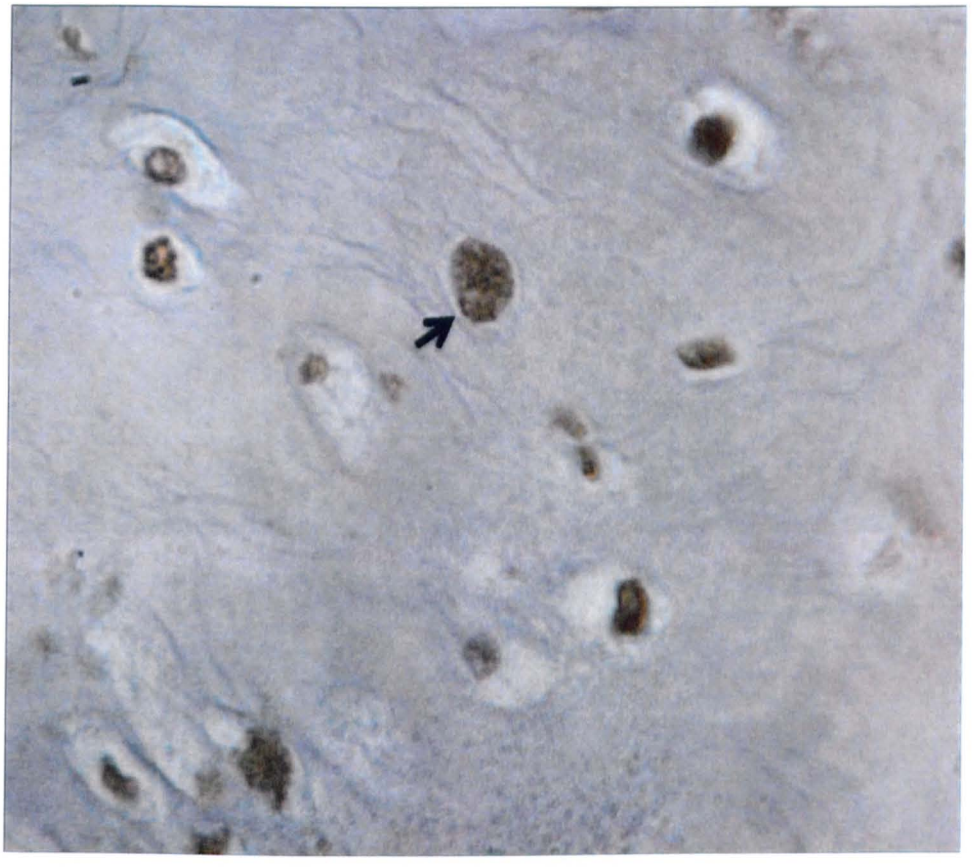

Figure 3-7. Immunohistochemical staining of bone, chondrosarcoma, treated with anti-NRG1α antibody, showing strong nuclear staining (arrowed). Original magnifications: x63.

Chondrosarcoma is a malignant tumour of cartilage-forming cells characterised by chondrocytes with abundant clear, vacuolated cytoplasm and scattered chondroid matrix. When stained with anti-NRG1α antibody, chondrocytes exhibited strong nuclear staining without any detectable cytoplasmic staining (Figure 3-7).

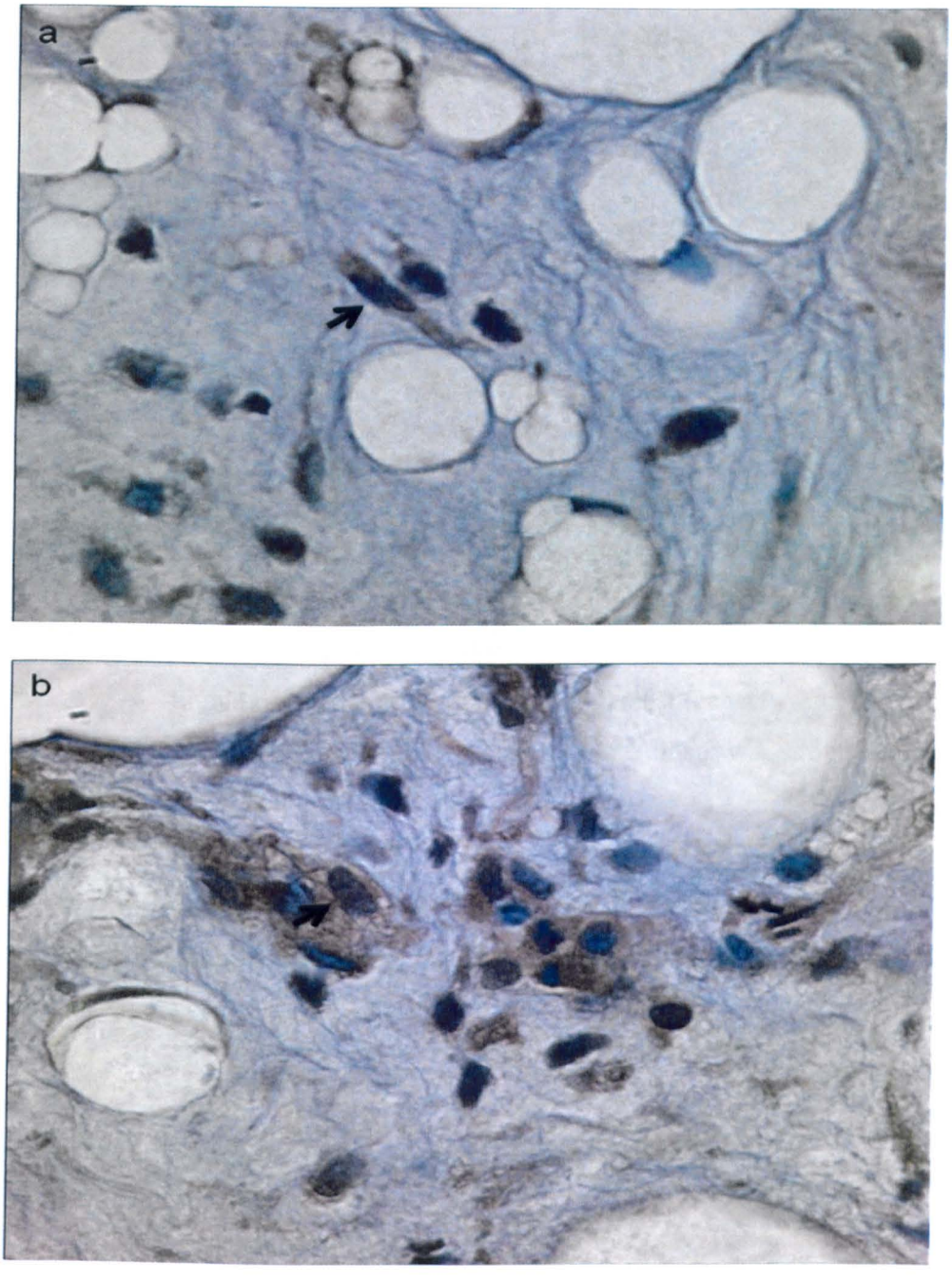

Figure 3-8. Immunohistochemical staining of soft tissue, liposarcoma, treated with anti-NRG1α (a) or anti-NRG1β (b) antibody, showing moderate, cytoplasmic staining together with nuclear staining (arrowed). Original magnifications: x63

Liposarcoma is characterized by small, undifferentiated mesenchymal cells, variable numbers of lipoblasts and thin-walled capillaries. When stained with either anti-NRG1α or anti-NRG1β antibody, among the cells positively stained, some showed both cytoplasmic and nuclear staining whereas others showed only moderate cytoplasmic staining (Figure 3-8).

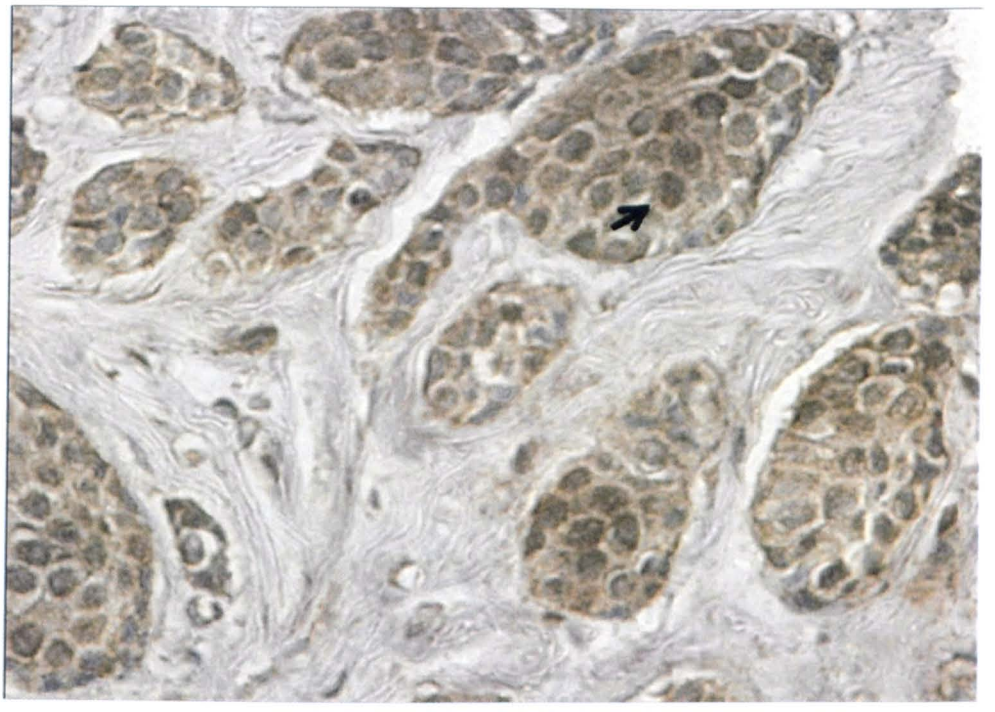

Figure 3-9. Immunohistochemical staining of breast cancer sample, treated with anti-NRG1α antibody showing moderate cytoplasmic along with strong nuclear staining (arrowed). Original magnifications: x63.

Figure 3-9 is an example of NRG1α expression in breast cancer tissue samples showing a predominantly strong nuclear staining pattern in the tumour cells along with moderate cytoplasmic staining.

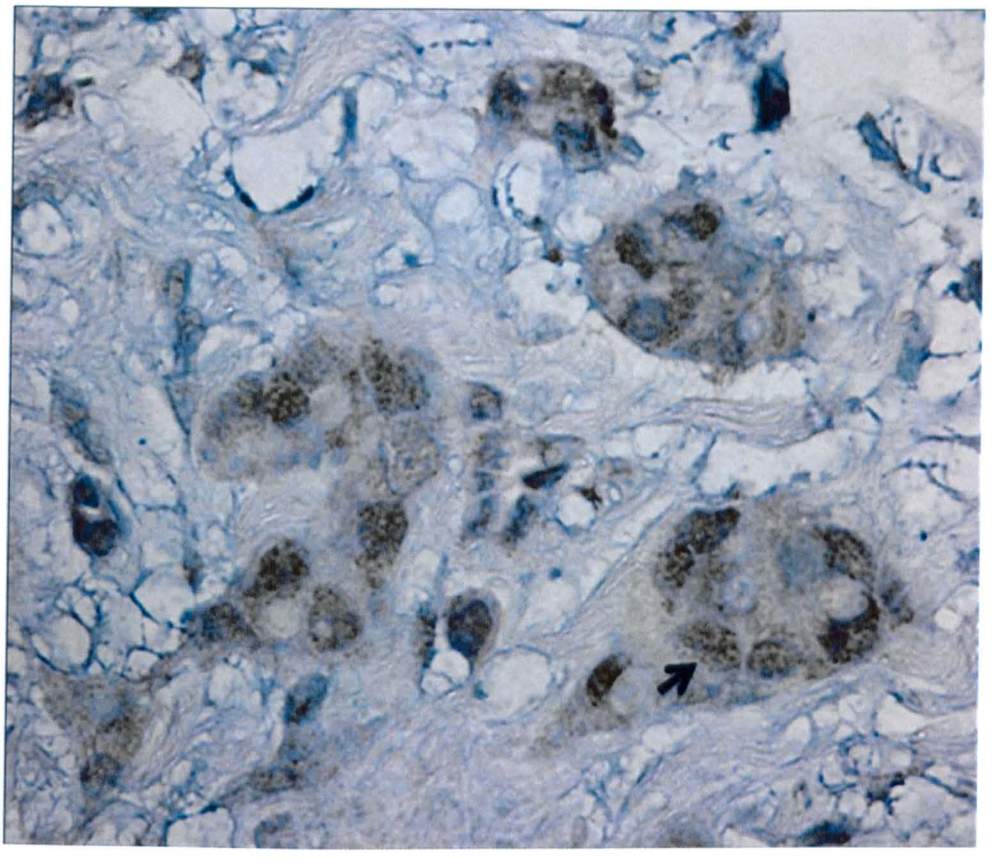

Figure 3-10. Immunohistochemical staining of breast cancer sample, treated with anti-NRG1β antibody, showing weak cytoplasmic along with strong nuclear staining (arrowed). Original magnifications: x63.

NRG1β was expressed in breast cancer tissue samples showing a weak cytoplasmic staining pattern in the tumour cells. Granular nuclear staining was apparent in some cases in conjunction with the cytoplasmic staining (Figure 3-10).

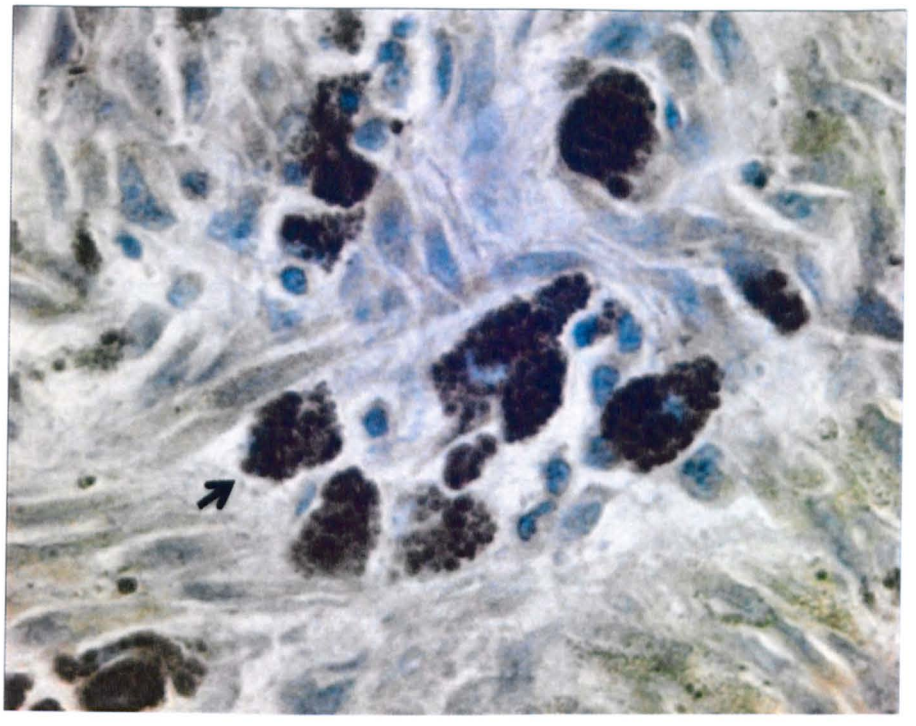

Figure 3-11. Immunohistochemical staining of skin, malignant melanoma, treated with anti-NRG1β antibody. Original magnifications: x63.

Melanoma is a malignant tumour of melanocytes, cells that are derived from the neural crest and migrate to the periphery during fetal life. The tumour cells are not evenly dispersed, but crowd together. When stained with anti-NRG1 antibodies, some clusters of tumour cells exhibited strong brownish colour in both cytoplasm and nucleus (Figure 3-11). However, due to the dark colour of melanin pigmentation dispersed in cells, it was hard to distinguish from the colour used for immuno-detection. Whether the strong brownish colour was a result of NRG1 expression would require further examination.

3.3.3.2 The frequency of intranuclear expression of NRG1α and NRG1β in various cancer tissues

In the array of 146 different human cancer tissue samples, nuclear expression of NRG1β was detected in 3 out of 25 soft tissue cancer samples, whereas nuclear expression of NRG1α was detected in 6 out 16 bone cancer samples, in 6 out of 25 soft tissue samples and in 1 out of 13 skin cancer samples (Table 3-2). The percentage of positive cases of each cancer type was compared by histograms (Figure 3-12).

Table 3-2.The frequency of intranuclear expression of NRG1α and NRG1β in the human various cancer array.

		NRG1β		NRG1α	
Tumours	**# of cases**	**Positive**	**Positivity**	**Positive**	**Positivity**
Lung	24	0	0%	0	0%
Bone	16	0	0%	6	38%
Soft tissue	25	3	12%	6	24%
Skin	13	0	0%	1	8%
Breast	19	0	0%	0	0%
Uterine cervix	26	0	0%	0	0%
Endometrium	12	0	0%	0	0%
Ovary	11	0	0%	0	0%

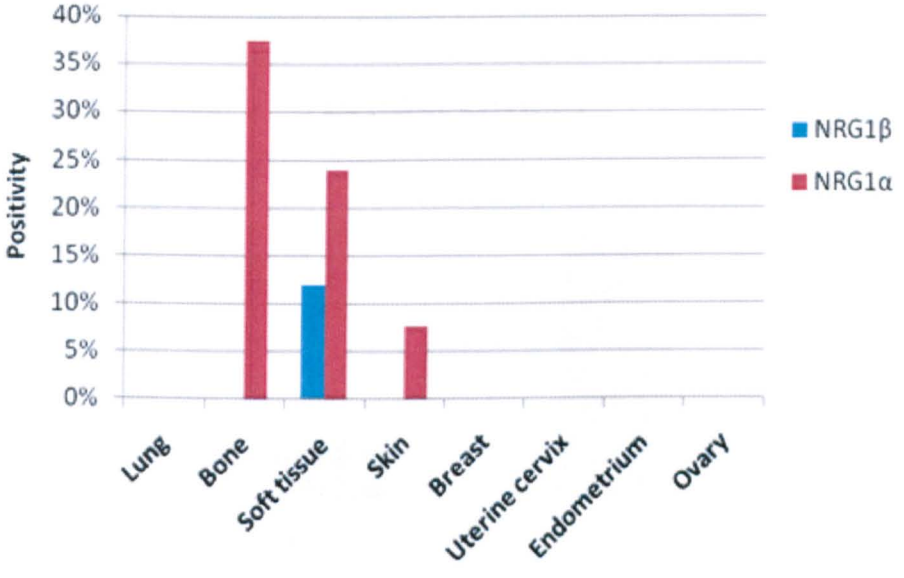

Figure 3-12. Histograms showing nuclear staining of NRG1α and NRG1β in the human cancer tissue array. The graphs show the percentage of cases which exhibited positive nuclear staining in various tumour types.

A tissue array containing one hundred and four human breast cancer tissue samples was immunohistochemically stained with the anti-NRG1α and anti-NRG1β antibodies by Emmet McIntyre, another PhD student in the laboratory. I used this array to score a large number of cases of an individual tumour where the expression had been seen in a minority of cases. Four of the 104 samples on the tissue array were not informative therefore only 100 samples were used. Combined with the 19 breast cancer samples from the human various cancer array, 119 cases were analysed. Nuclear expression of

NRG1β was detected in 3 cases having a positivity of 2.5%, whereas nuclear expression of NRG1α was detected in 14 cases having a positivity of 11.8% (Table 3-3). In summary, amongst the tumour types examined NRG1α had a higher frequency of nuclear expression than NRG1β in bone, soft tissue, skin and breast cancer tissues (Figure 3-12 and Figure 3-13).

Table 3-3. The frequency of intranuclear expression of NRG1α and NRG1β in 119 breast cancer samples.

			NRG1β		NRG1α
	# of cases	# of positive	Positivity	# of positive	Positivity
Breast cancer	119	3	2.5%	14	11.8%

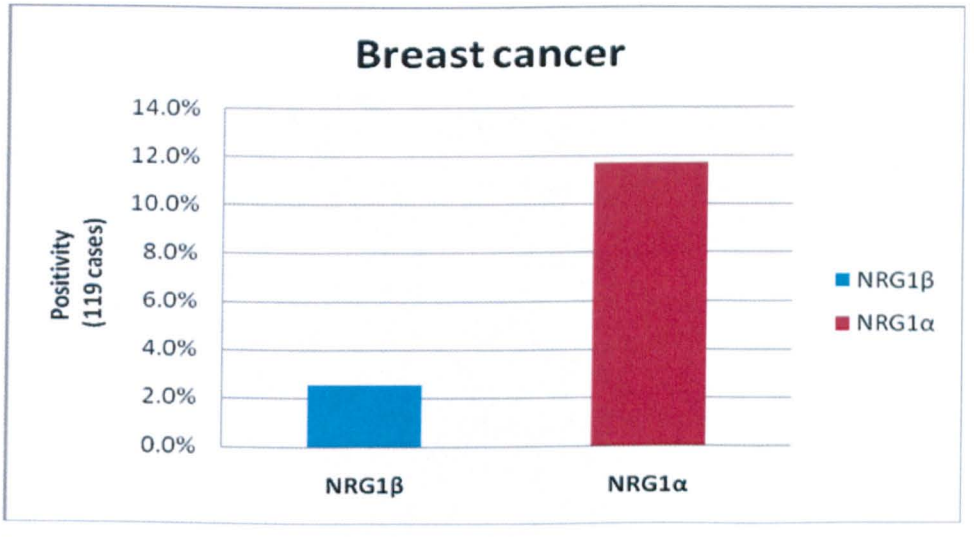

Figure 3-13. Histograms showing the frequency of intranuclear expression of NRG1α and NRG1β in 119 breast cancer samples.

3.3.4 Nuclear expression of NRG3 in normal and breast cancer tissues

The nuclear expression of NRG3 in tissue arrays containing 79 breast cancer samples and 33 normal breast samples were also examined. The immunohistochemical staining was done by Laura Smart, using two NRG3-specific antibodies (NRG3 122 and NRG3 136). Antibody NRG3 122 recognises the EGF domain of NRG3, whereas antibody NRG3 136 recognises the cytoplasmic domain of NRG3 (Figure 3-14).

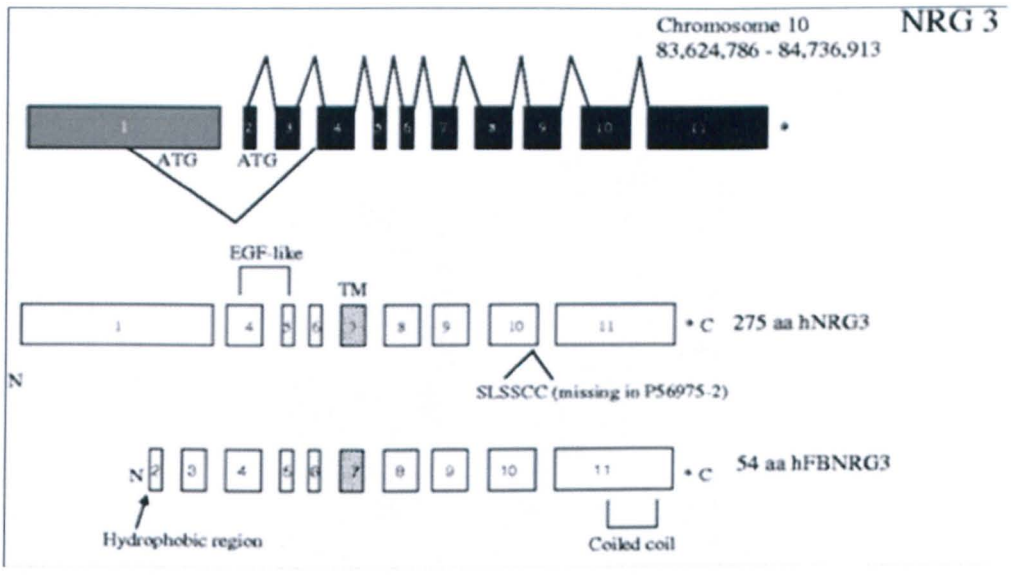

Figure 3-14. Transcript variants of human NRG3. TM: transmembrane. Figure taken from Hayes et al, 2007.

3.3.4.1 Staining patterns

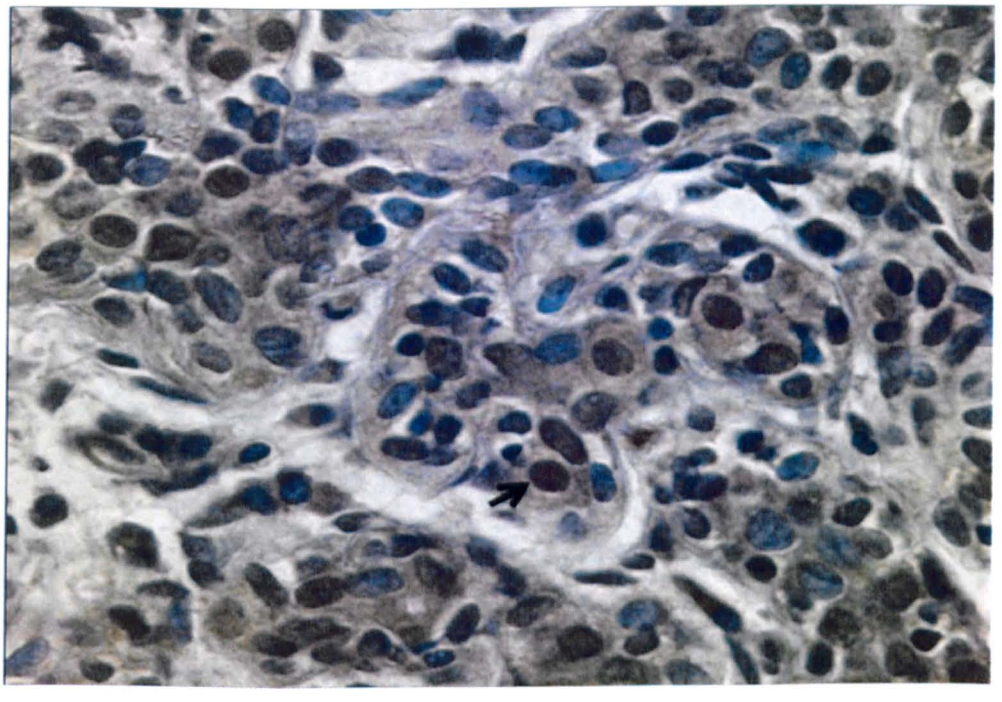

Figure 3-15. Immunohistochemical staining of normal breast sample treated with anti-NRG3 antibody (NRG3 122), showing moderate cytoplasmic along with strong nuclear expression (arrowed). Original magnifications: x63.

NRG3 was expressed in normal breast samples showing moderate cytoplasmic staining along with strong nuclear staining in a high proportion of breast cells (Figure 3-15). Staining with the NRG3 122 and NRG3 136 antibodies showed similar patterns.

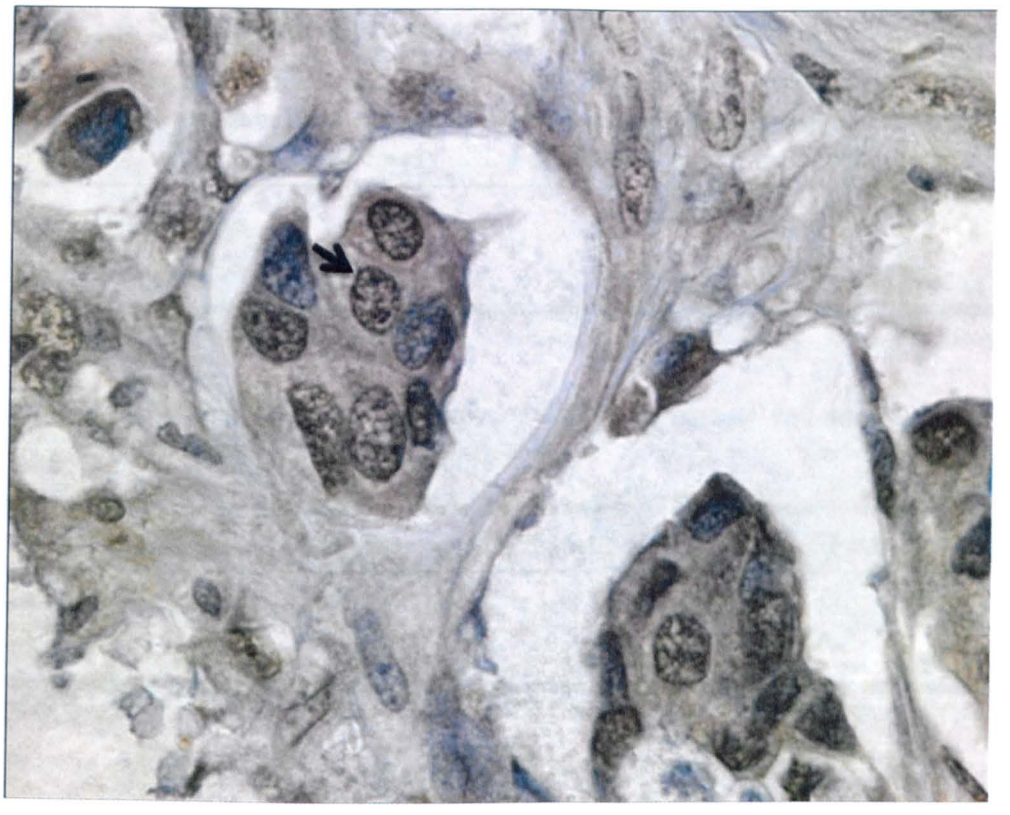

Figure 3-16. Immunohistochemical staining of infiltrating duct carcinoma treated with anti-NRG3 antibody (NRG3 136), showing moderate cytoplasmic along with strong nuclear expression (arrowed) in some of the tumour cells. Original magnifications: x63.

Samples of infiltrating ductal carcinoma of the breast displayed cytoplasmic NRG3 staining. Strong granular nuclear staining was observed in a high proportion of tumour cells (Figure 3-16). The NRG3 122 and NRG3 136 antibodies gave similar staining patterns.

3.3.4.2 The frequency of nuclear expression of NRG3 in normal and breast cancer tissues

The frequency of intranuclear expression of NRG3 in normal and breast cancer tissues is listed in Table 3-4 and Table 3-5 and the percentage of positive cases using each antibody is presented using histograms (Figure 3-17). Using the NRG3 122 antibody, nuclear expression of NRG3 was observed in 14% of breast cancer samples and in 73% of normal breast samples. Using NRG3 136 antibody, nuclear expression of NRG3 was observed in 22% of breast cancer samples and in 36% of normal breast samples.

Table 3-4. Nuclear staining frequency of NRG3 in normal and cancer breast samples when stained with NRG3 122 antibody.

Organ	# of cases	# of positive cases	Positivity
Breast, cancer	79	11	14%
Breast, normal	33	24	73%

Table 3-5. Nuclear staining frequency of NRG3 in normal and cancer breast samples when stained with NRG3 136 antibody.

Organ	# of cases	# of positive cases	Positivity
Breast, cancer	79	17	22%
Breast, normal	33	12	36%

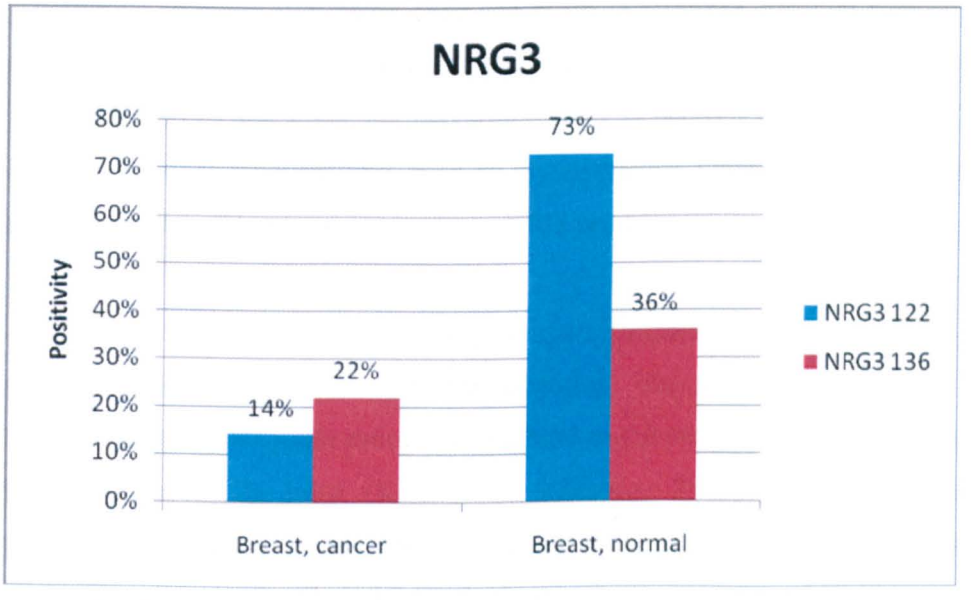

Figure 3-17. Percentage of NRG3 nuclear staining in normal and breast cancer tissue samples using NRG3 122 and 136 antibodies.

In general, a higher frequency of intranuclear expression of NRG3 was detected in normal breast tissue samples than in breast cancer tissue samples, using either the NRG3 122 or NRG3 136 antibody (Figure 3-17). In breast cancer tissue samples, nuclear accumulation of NRG3 was detected in fewer cases using the NRG3 122 antibody than with the NRG3 136 antibody. In contrast, using the NRG3 122 antibody, nuclear expression of NRG3 was detected in 73% of the cases in normal breast tissue samples, twice as high as with the NRG3 136 antibody.

3.4 Discussion

3.4.1 Immunohistochemistry

Immunohistochemistry is the localisaton of antigens in tissue sections through antigen-antibody interactions by the use of labeled antibody. Antibodies are typically made of basic structural units: each with two heavy chains and two light chains. Although the general structure of all antibodies is very similar, a hypervariable region at the tip of the antibody is responsible for specific binding to an antigen. The unique part of the antigen recognised by an antibody is called an epitope which are usually 5-21 amino acids long. Antigens can have different isoforms and different structures due to alternative splicing and posttranslational modifications (Sharp, 1994).

Alternative splicing of a single gene can produce multiple different transcripts, each of which codes for a different protein. NRG1α and NRG1β, whose intranuclear expression was examined in this study, are two splice variants derived from the single *NRG1* gene. Posttranslational modifications such as glycosylation, phosphorylation, and proteolytic processing can add more complexity to NRG proteins.

Antibodies are made by immunizing animals (mouse, rabbit, goat, horse, etc.) with either purified proteins or synthetic peptides. The animal responds by producing antibodies that specifically recognise and bind to the antigen. Monoclonal antibodies are produced mostly in mice (Kohler and Milstein, 1976). Polyclonal antibodies are produced in multiple animal species, particularly rabbit, horse, goat and chicken. The advantage of monoclonal antibodies is their higher specificity which greatly reduces the possibility of cross-reactivity with other antigens (Nielsen *et al.*, 2003). Polyclonal antibodies have higher affinity and wide reactivity (more likely to identify multiple isoforms of the protein) but lower specificity when compared with monoclonal antibodies. Antibodies to NRG1α, NRG1β, and NRG3 used in this immunohistochemical study are polyclonal rabbit antibodies. These antibodies were raised using synthetic peptides to specific epitopes of each neuregulin (i.e., antibody NRG3 122 recognises the EGF-like domain of NRG3, whereas antibody NRG3 136 recognises the cytoplasmic domain of NRG3) and were subject to stringent purification using affinity columns. Nevertheless, all precautions were taken to minimise the occurrence of non-specific background staining by optimising antibody concentrations

on rat pancreas tissues. Moreover, a sensitive detection method was used in this study to detect antigens.

Detection systems are classified as direct or indirect methods (Figure 3-18). The direct method is a one step process with a labelled antibody reacting directly with the antigen in tissue sections. A variety of labels have been used including fluorescent compounds. This method is quick but lacks sufficient sensitivity for detection of some antigens. Compared to direct methods with a labelled primary antibody, indirect methods provide more sensitive antigen detection (Coons and Kaplan, 1950). In the two-step method, the first layer of antibody is unlabeled, but the second layer, raised against the primary antibody, is labelled. The unlabelled primary antibody retains its specificities but the complex results in a stronger signal as the number of labels per molecule of primary antibody is higher thus increasing the intensity of the reaction. The second layer antibody may be labelled with an enzyme such as peroxidase, alkaline phosphatase or glucose oxidase, and this is called an indirect immunoenzyme method. The Avidin-Biotin Complex (ABC) method is a common detection method and was used in this immunohistochemical study. Avidin is a large glycoprotein that has four binding sites per molecule and high affinity for a low-molecular weight vitamin called biotin. Biotin has one binding site for Avidin and can be attached through other sites to an antibody. The increased sensitivity of the avidin-biotin method results from the larger number of biotin molecules that interact with each primary antibody. Thus, the ABC method involves three layers. The first layer is unlabeled primary antibody. The second layer is biotinylated secondary antibody. The third layer is a complex of avidin-biotin peroxidase. The peroxidase is then used to convert 3,3' diaminobenzidine tetrachloride (DAB), which is a soluble chromogen, to an insoluble product giving a brown colour. However, DAB is not the optimal chromogen if melanin pigment is present in the same cell as the antigen being examined. When staining melanoma tissues with anti-NRG1α and anti-NRG1β antibodies, some clusters of tumour cells exhibited a strong brownish colour (Figure 3-11). Without performing control experiments (i.e., staining without primary antibody) in parallel, the interpretation of the specificities of the result turned out to be difficult. To avoid this problem a detection system producing a different colour precipitate could be used for any melanin pigment containing tissues. Alternatively, Giemsa stain or Azure B dye can be used as a counterstain after the immunoreaction is done. In this case the melanin will stain green or blue-green, and DAB product will remain brown (Ramos-Vara and Beissenherz, 2000).

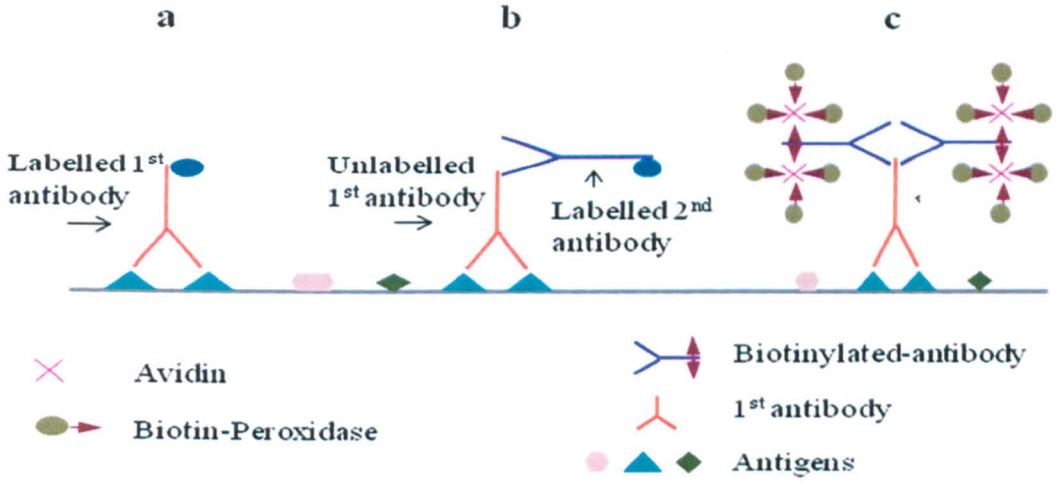

Figure 3-18. Direct (a), indirect (b) and ABC (c) immunohistochemical methods. Figure adapted from Ramos-Vara and Beissenherz, 2000.

3.4.2 Scoring

Usually, scoring by light microscopy can evaluate two parameters: the strength of staining and the area of tissue stained. In this study, only the presence or absence of nuclear staining was recorded. Brown-coloured nuclear staining in tissues samples was visualised by light microscopy and evaluated by two observers and only obvious nuclear immunostaining were considered to be positive. Any ambiguous or not obvious nuclear immunoreactivity was considered as negative. However, even using these quite stringent criteria it was important to test the reproducibility of the scoring. To this end the human, breast cancer-normal array stained with NRG3 122 antibody was re-scored by the same observers in a reproducibility test. There was about 95% agreement in assessing nuclear staining status and therefore, this data can be interpreted with a high level of confidence. The disagreement in occasional cases was partly due to the fact that the status of nuclear staining was inevitably a subjective estimate of the intensity and thus only a semi-quantitative method. Particularly in the weakly staining cases or the cases in which few cells showed nuclear staining, the judgement was more likely to be inconsistent.

3.4.3 Nuclear expression of NRG1

The tissue microarray technology allows simultaneous examination of hundreds of samples on a single microscope slide. In this study, immunohistochemistry was performed using well characterised antibodies against NRG1α and NRG1β proteins

(Srinivasan et al., 1999) analysed on formalin-fixed, paraffin-embedded tissue arrays. We examined the nuclear expression of NRG1α and NRG1β in 60 tissue cores (30 different tissue cores in duplicate) from normal organs of non-cancer patients. Nuclear expression of NRG1α was detected in one case of normal skin, whereas nuclear expression of NRG1β was detected in both cases of normal skin, adrenal cortex and thyroid tissues. We also examined the nuclear expression patterns of NRG1α and NRG1β in 146 tissue cores of various human cancers. Nuclear expression of NRG1β was detected in soft tissue cancers, whereas nuclear expression of NRG1α was detected in soft tissue, bone and skin cancers. Neither was detected in lung, uterine cervix, endometrium and ovarian cancers. The percentage of cases, which exhibited positive nuclear staining of NRG1α and NRG1β in various tumours, is shown in Table 3-2. When analysing 119 breast cancer tissue cores, nuclear expression of NRG1β had a positivity of 2.5%, whereas nuclear NRG1α showed 11.8% positivity (Table 3-3). In summary, NRG1α had a higher frequency of nuclear expression than NRG1β in normal tissues as well as in cancer tissues. The incidence of intranuclear expression of NRG1 in both normal and malignant tissues is relevant to the further investigation on the importance of intranuclear NRG1 in different physiological conditions.

It has recently been shown that NRG1β3, a splicing variant of NRG1, when fused to green fluorescent protein localised to two subnuclear compartments, the nucleoli and spliceosomes (Golding *et al.*, 2004). With the observation of intranuclear expression of NRG1 in different types of tissues it is unlikely that the subnuclear localisation of NRG1β3 is an artefact. Even though nuclear localisation of the EGFR, ErbB2, ErbB3, and proteolytically processed form of ErbB4 has been demonstrated, no evidence has yet suggested that nuclear NRG proteins bind and activate their cognate receptors in the nucleus. The question remains therefore as to what the functions of this molecule are in the nucleus. The answers to this question have been pursued in the following chapters.

3.4.4 Nuclear expression of NRG3

Due to alternative splicing, at least two isoforms of NRG3 (hNRG3 and hFBNRG3) are encoded from the *NRG3* gene as shown in Figure 3-14. Several other splice variants have been identified in our laboratory (Smart and Gullick, unpublished). The hFBNRG3 variant has multiple differences in the presence and absence of exons in the 5' and 3' ends, compared to hNRG3. The translation initiation of hFBNRG3 starts at a unique start codon located at exon 2. The encoded protein has a shorter and distinct N-terminus

and a large C-terminal domain which has been suggested to be involved in DNA binding, protein interaction and trafficking (Carteron *et al.*, 2006). Like other neuregulins, hFBNRG3 is probably a type I transmembrane protein with an extracellular N-terminus and a cytosolic C-terminus. Evidence suggests that after membrane insertion hFBNRG3 is subjected to proteolytic cleavage and can be released into the extracellular space where it may activate the ErbB4 receptor. The existence of multiple splice variants of NRG3 and the possible proteolytic processing following its plasma membrane insertion may explain the observed differences in the frequency of intranuclear expression of NRG3 when staining normal and breast cancer tissues using two antibodies recognising different domains of NRG3. Compared to the NRG3 136 antibody which recognises the cytoplasmic domain of NRG3, the antibody NRG3 122 recognising the EGF-like domain detected a lower percentage of NRG3 in breast cancer tissue samples (14% vs. 22%). In contrast, a higher percentage of nuclear NRG3 (73%) was detected in the normal breast tissues using the NRG3 122 antibody than using the NRG3 136 antibody.

NRG3 expression was thought to be highly restricted to the developing and adult nervous system (Zhang *et al.*, 1997). Our laboratory has previously reported that NRG3 is expressed in DCIS as well as in invasive breast cancers along with other neuregulins (Dunn *et al.*, 2004). When quantifying ErbB ligands in 363 breast tumours NRG3 was detected in 43% of the cases (Revillion *et al.*, 2008). An important function of NRG3 has been suggested in promoting early mammary morphogenesis and in breast cancer (Howard, 2008). On the other hand, nuclear expression of NRG3 was reported to be significantly correlated to low tumour grade (Marshall *et al.*, 2006) and our study detected nuclear NRG3 expression in a higher proportion in normal breast tissues than in breast cancer tissues. NRG3 can only bind to and activate ErbB4 among the members of the ErbB receptor family. Full-length ErbB4 has an established role in postnatal development of the mammary gland during late pregnancy and lactation (Tidcombe *et al.*, 2003) and many studies have found overexpression of membranous ErbB4 as a prognostic indicator for clinical outcome of breast cancer (Aubele *et al.*, 2007). In the kinomic analysis, we have shown that intranuclear NRG1 was able to activate the ErbB4 receptor (see Chapter 6). Whether nuclear NRG3 could have a similar effect on ErbB4 thereby exerting effects on cell proliferation remains to be determined.

Chapter 4. Intranuclear translocation of NRG1β3 studied using photoactivatable GFP

4.1 Introduction

Green fluorescent protein from the jelly fish *Aequorea victoria* and its multicoloured variations have been applied largely as a fluorescent tag to investigate many cellular activities especially in analysing protein localisation and dynamics in living cells (Lippincott-Schwartz and Patterson, 2003). Recently, photoactivatable fluorescent proteins (PAFPs) have been developed. In response to activation with light of a specific wavelength, PAFPs undergo significant changes in their photophysical properties. Some PAFPs convert from a dark to a more bright fluorescence state (photoactivation) (Patterson and Lippincott-Schwartz, 2002), whereas others are capable of changing colour (photoswitching or photoconversion) (Ando *et al.*, 2002).

Patterson and Lippincott-Schwartz have reported a photoactivatable variant of the green fluorescent protein (PAGFP) (Patterson and Lippincott-Schwartz, 2002). The concept of PAGFP design is to develop a variant of GFP with a lower initial minor peak absorbance that greatly increases after photoactivation and thus a more noticeable optical contrast under 488nm excitation. PAGFP is the result of a single residue substitution of histidine for threonine at position 203, in enhanced green fluorescence protein (EGFP). The mechanism of the photoactivation process is based on the photophysical properties of wild type GFP, which shows two peaks in the excitation spectrum, the major absorbance peak at 396nm and the minor one at 476nm. These peaks are produced by the neutral and anionic chromophore forms, respectively (Niwa *et al.*, 1996). When irradiated with ultraviolet or 405nm light, chromophores shift towards the anionic form resulting in an increase in minor peak absorbance (Yokoe and Meyer, 1996). The conversion from the neutral to the anionic form has been shown to be due to Glu222 decarboxylation, which results in rearrangement of the hydrogen bonding and chromophore deprotonation (van Thor *et al.*, 2002). Among several mutations at the threonine 203 position (T203), histidine substitution (T203H) was shown to have minimised minor peak absorbance.

This variant produces the mostly neutral chromophore form. Thus, almost no fluorescence is observed when excited at wavelengths that correspond to the anionic chromophore form (480-510nm). Intense irradiation at 405nm causes PAGFP chromophores to convert from the neutral to the anionic form resulting in a dramatic increase in the green fluorescence of the anionic form. PAGFP photoactivation has been demonstrated to be remarkably stable for days under aerobic conditions (Lippincott-Schwartz and Patterson, 2003). Repeated excitation with 488nm light indicates its photostability is comparable to GFP. These characteristics of PAGFP offer a new tool for exploring intracellular protein dynamics over time by tracking photoactivated molecules that are the only visible GFPs in the cell.

The following study was guided by our interest in understanding intracellular NRG1β3 trafficking in live cells. Using fluorescence microscopy, not only is GFP-tagged NRG1β3 found to localise to two sub-nuclear compartments: nucleoli and spliceosomes, it also has been noticed that NRG1β3 localisation could change from the nucleolar pattern to the speckle pattern or vice versa within two hours (Golding *et al.*, 2004). There are two explanations for the observed interconversion of NRG1β3 localisation patterns. One explanation is that NRG1β3 could redistribute from one site to the other. That is, the interconversion between these two compartments is due to the movement of the protein over time. The other explanation is that NRG1β3 could be degraded in one site at one particular phase of the cell cycle, while being re-synthesised and targeted to the other site in a new phase of the cell cycle. Patterson and Lippincott-Schwartz have demonstrated the uniqueness of PAGFP for analyzing protein dynamics within cultured cells by showing that only photoactivated PAGFP molecules show intense fluorescence whereas newly synthesised molecules do not become fluorescent (Patterson and Lippincott-Schwartz, 2002). If this technique were adapted to our case, PAGFP photoactivation could help to test the hypothesis that the appearance of NRG1β3 at different locations was due to protein movement. That is, if we observed the movement of fluorescent protein after activation, it would demonstrate that NRG1β3 moved from one location to the other. If we did not see any movement and the fluorescent proteins disappeared after a period of time, it was possible that NRG1β3 was degraded at one location and re-synthesised and accumulated at the other location.

4.2 Aims

1. To construct a mammalian cherry vector from a bacterial cherry vector so that it can be co-transfected with the PAGFP construct and used as a marker to help identify cells that have incorporated PAGFP plasmids.

2. To photoactivate unconjugated PAGFP in transiently transfected COS-7 cells and to optimise photoactivation parameters.

3. To subclone NRG1β3 into the pPAGFP vector and express PAGFP-tagged NRG1β3 in COS-7 cells.

4. To monitor the trafficking of PAGFP-tagged NRG1β3 in live cells using confocal microscopy.

4.3 Results

4.3.1 Construction and expression of mCherry

4.3.1.1 Molecular cloning of mammalian vector pmCherry

To express cherry proteins in mammalian cells, we decided to clone mCherry from the bacterial vector pRSET-B (Figure 4-1a) into the pEGFP-N1 vector (Figure 4-1b). The pEGFP-N1 vector is a commonly used mammalian vector which expresses EGFP under the CMV promoter. The CMV promoter is capable of producing relatively high levels of expression of target genes in various mammalian cell types (Wenger *et al.*, 1994). A pair of unique restriction sites was chosen based on the restriction map of vector pEGFP-N1 so that EGFP could be cut out without interfering with the backbone structure. *Sac* II is located at Multiple Cloning Site (MCS) N-terminal to EGFP, whereas *Not* I is next to the C-terminus of EGFP. Double digestions of the pEGFP-N1vector by *Sac* II and *Not* I restriction enzymes should remove EGFP and linearise the vector for subsequent cloning.

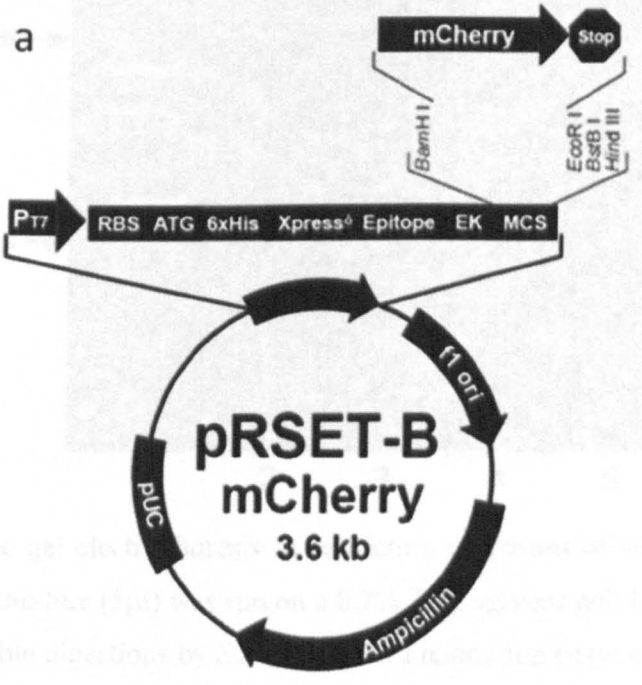

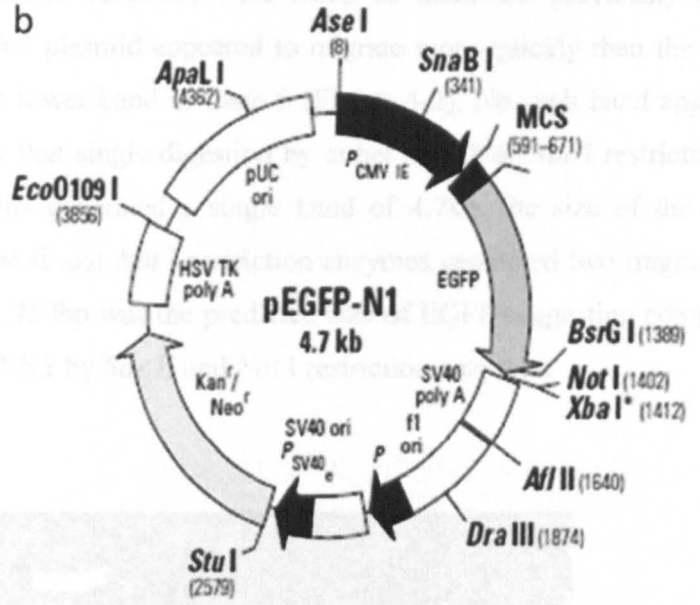

Figure 4-1. Vector maps. Figure taken from www.clontech.com.

a. Bacterial vector pRSET-B mCherry.

b. Mammalian vector pEGFP-N1 used for mCherry sub-cloning.

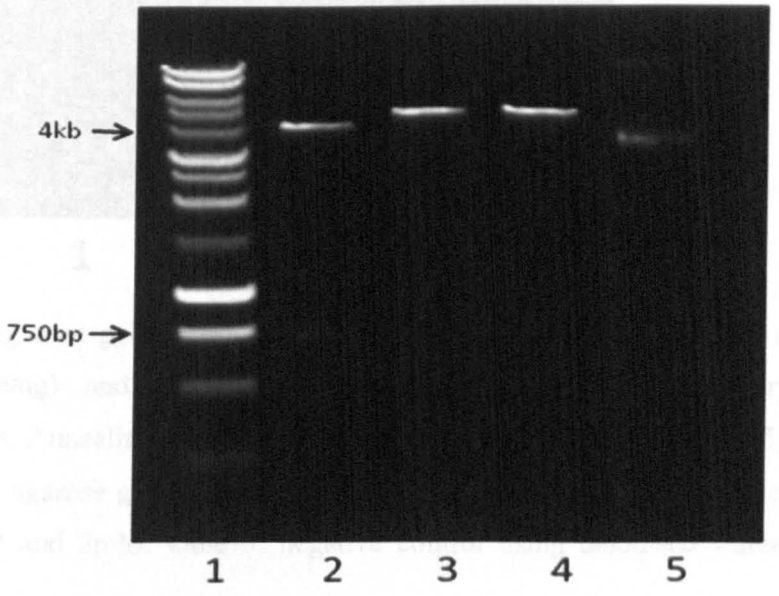

Figure 4-2. Agarose gel electrophoresis of restriction digestions of vector pEGFP-N1. Digestion reaction mixture (5µl) was run on a 0.7% TAE agarose gel. Lane 1: 1kb DNA ladder. Lane 2: double digestions by *Sac* II and *Not* I restriction enzymes. Lane 3: single digestion by *Sac* III only. Lane 4: single digestion by *Not* I only. Lane 5: negative control using deionised water instead of restriction enzymes. Each digestion mixture was incubated at 37°C for 1h.

Restriction digestion reactions were setup as described previously (Section 2.4.4). Uncut supercoiled plasmid appeared to migrate more quickly than the nicked plasmid indicated by the lower band in Lane 5 (Figure 4-2). No such band appeared in lane 3 and 4 indicating that single digestion by either *Sac* II or *Not* I restriction enzyme was complete and this generated a single band of 4.7kb, the size of the vector. Double digestions by *Sac* II and *Not* I restriction enzymes generated two fragments of 4kb and 750bp (Lane 2). 750bp was the predicted size of EGFP suggesting complete digestions of vector pEGFP-N1 by *Sac* II and *Not* I restriction enzymes.

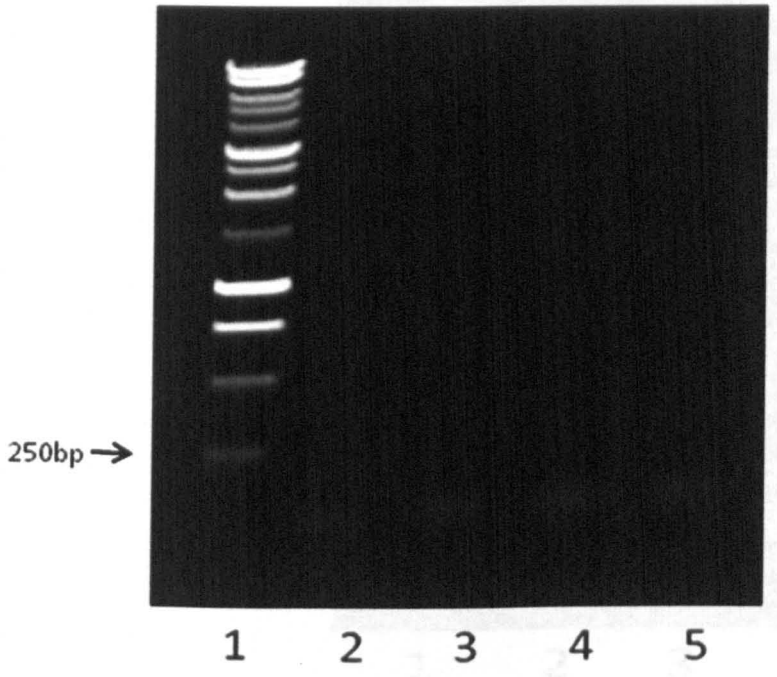

Figure 4-3. Agarose gel electrophoresis of PCR reaction using pRSET-B mCherry as template (100ng) and CherryF and CherryR as primers with varying Mg^{2+} concentrations. Annealing temperature was set up at 55°C. PCR product (5µl) was run on a 2% TAE agarose gel. Lane 1: 1kb DNA ladder. Lane 2-4: Mg^{2+} concentrations at 1mM, 1.5mM and 2mM. Lane 5: negative control using deionised water instead of template DNA.

A pair of primers CherryF and CherryR was designed to amplify mCherry from its vector pRSET-B mCherry with *Sac* II and *Not* I restriction sites added to either end so that the PCR products could subsequently be ligated into the digested pEGFP-N1 vector. Initial PCR reactions were designed to optimise the Mg^{2+} concentration. When the annealing temperature was set up at 55°C, PCR reactions generated short unspecific

products as shown in Figure 4-3. The size of the bands and its presence in the negative control reaction suggested that they were primer dimers. It was possible that the right PCR products were not obtained due to low DNA template concentration. Another PCR reaction was set up with increased DNA template concentrations while keeping other conditions the same. As the DNA template concentration tripled, an intense band of 750bp along with some longer unspecific products was generated as shown in Lane 2 (Figure 4-4). Following gel extraction the 750bp PCR product was digested by *Sac* II and *Not* I restriction enzymes.

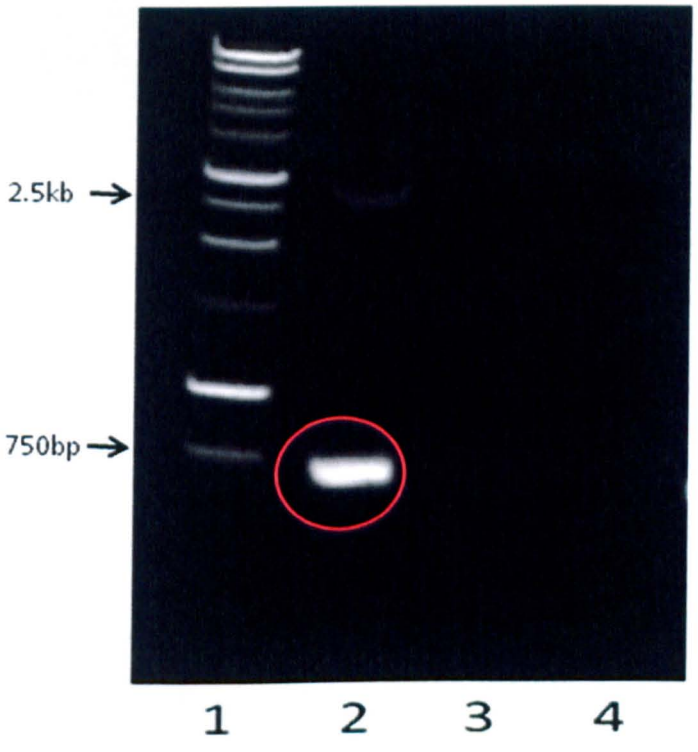

Figure 4-4. Agarose gel electrophoresis of PCR reaction using pRSET-B mCherry as template and CherryF and CherryR primers with varying template concentrations. Annealing temperature was set up at 55°C. PCR product (5µl) was run on a 2% TAE agarose gel. Lane 1: 1kb DNA ladder. Lane 2-3: DNA template concentrations at 600ng and 200ng. Lane 4: negative control using deionised water instead of template DNA.

Ligation and transformation were carried out as previously described (Section 2.4.6). 14 individual colonies were picked 24h after the transformed cells were plated onto LB agar plates supplemented with kanamycin. One colony seemed to be positive by PCR screening using primers CherryF and CherryR (Figure 4-5). The presence of the correct insert was confirmed by sequencing.

Figure 4-5. PCR screening using primers CherryF and CherryR. PCR products (5µl) were run on a 2% TAE agarose gel. Lane 1: 1kb DNA ladder. Lane 2-15: 14 individual colonies were picked and used as templates. Lane 15: positive control using pRSET-B mCherry as template.

4.3.1.2 Expression of mCherry

The newly constructed mammalian cherry expression vector pmCherry was transiently transfected into COS-7 cells. mCherry localised to the cytoplasm and nucleus of the cell when viewed under the microscope (Figure 4-6). As a mutant of GFP (Shaner *et al.*, 2004), mCherry exhibited the same localisation pattern as GFP.

Figure 4-6 Expression of pmCherry in a COS-7 cell. The image was taken by confocal microscopy 24h post transfection. mCherry was excited with 546nm laser light and the image was acquired with a 560nm emission filter.

4.3.2 Photoactivation of PAGFP

COS-7 cells were co-transfected with pPAGFP and pmCherry plasmids using Lipofectamine 2000 transfection reagent. After 24h of incubation, the culture dish was removed from the incubator and examined under the confocal microscope. Initially, an excitation scan with 546nm laser light confirmed the position of mCherry expressing cells (Figure 4-7a-b). When the same cell was scanned with 488nm light at power 13%, no fluorescence was noticeable (Figure 4-7c). Two successive scans with 405nm laser light at 20% power photoactivated PAGFP within the cell. Immediately after the 405nm excitation scans, the photoactivated cell was scanned with 488nm light at power 13% (Figure 4-7d). Consistent with the report of Patterson and Lippincott-Schwartz (2002), upon irradiation with 405nm laser light, the fluorescence in a PAGFP expressing cell increased dramatically under 488nm excitation. To optimise the photoactivation conditions an analysis was performed using a range of 405nm laser power settings (10%-80%) and varying number of scans. It was found that, when scanning with lower 405nm laser power settings (≤20%), the fluorescence signal increased up to two scans and then stabilised up to 6 successive scans. In contrast, when using high laser power settings (>60%), the GFP signal reached the maximum fluorescence intensity at the first two scans. Further scanning reduced the fluorescence intensity. To minimise any possible cell damage caused by 405nm laser scanning, photoactivation conditions described in Figure 4-7 were applied to photoactivate PAGFP in the following experiments. We also tested the photostability of the GFP signal by first photoactivating PAGFP within the cell and then continuously scanning with 488nm excitation wave length. The GFP signal intensity remained bright through consecutive 488nm excitation scans, without further scanning with 405nm laser light.

During this experiment, we observed that cells expressing PAGFP plasmids can be faintly distinguished using UV-light thus co-transfection with pmCherry was not necessary.

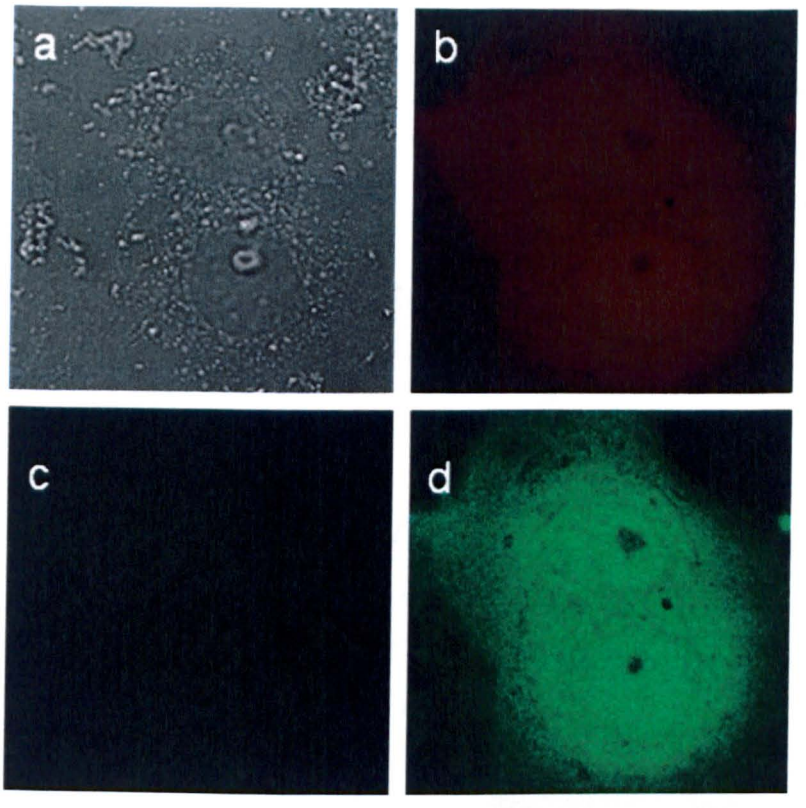

Figure 4-7. Photoactivation of PAGFP in COS-7 cells co-transfected with pmCherry. (a) Bright field image of mCherry expressing cells. (b) mCherry was excited with 546nm laser light at 80% power and collected with a 560nm emission filter. Two successive scans (~1s each at ~1s interval) of the 405nm laser at 20% power were applied to the cells. Images of pre- (c) and post-activation (d) were taken with 488nm laser light at 13% power. Objective: x60. Zoom = 2.2.

4.3.3 Cloning of NRG1β3 into the pPAGFP vector

A PCR based method was chosen to transfer the NRG1β3 sequence from the pQBI25-fN1 NRG1β3 vector (Figure 4-8). Following PCR reactions, the products were run on an agarose gel to confirm that the correct size product of 750bp had been amplified (Figure 4-9). The band was subsequently extracted using the Gel Extraction Kit (Qiagen, UK) and digested with *EcoR* I and *BamH* I restriction enzymes. pPAGFP vector was digested with the same restriction enzymes. Either single or double digestions generated a single band of 4.7kb suggesting that digestions were complete (Figure 4-10).

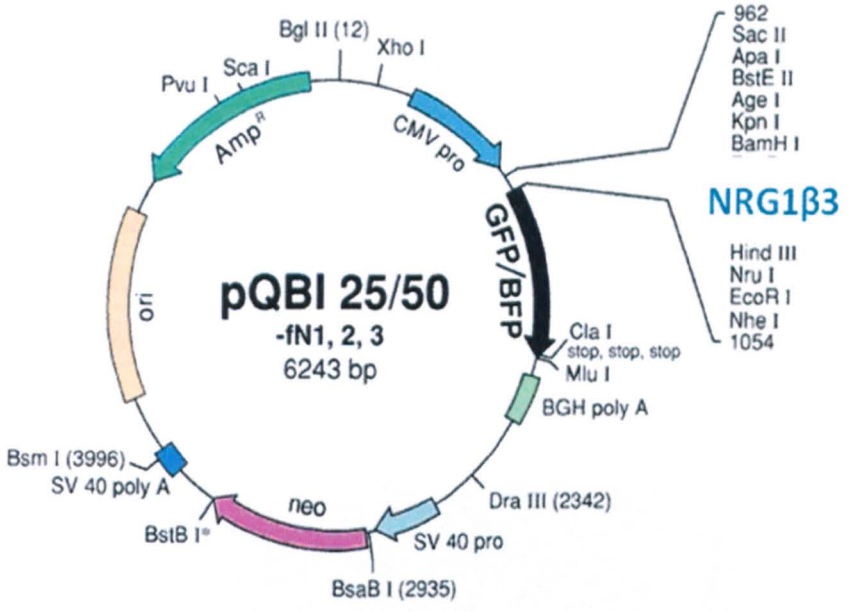

Figure 4-8. Vector map of pQBI25-fN1 showing that NRG1β3 is located between *BamH* I and *Hind* III restriction sites. Figure adapted from www.clontech.com.

Figure 4-9. Agarose gel electrophoresis of PCR reactions by amplifying NRG1β3 from its vector using primers NRG1β3F and NRG1β3R. Annealing temperature was set up at 52°C. PCR products (5μl) were run on a 2% TAE agarose gel. Lane 1: negative control using deionised water instead of template DNA. Lane 2: 1kb DNA ladder. Lane 3: reaction contained 200ng DNA template.

Both the digested pPAGFP vector and NRG1β3 PCR products were cleaned up by PCR Cleanup Kit (Qiagen, UK). The ligation reaction was then performed as described in Section 2.4.6. The plasmid constructs were then transformed into DH5α competent cells and plated onto LB agar plates supplemented with kanamycin. 10 individual colonies from the plates were picked for PCR screening using primers NRG1β3F and NRG1β3R. PCR products were run on an agarose gel to confirm if the insert was present. Three colonies that appeared to contain the insert were sent for DNA sequencing (Figure 4-11).

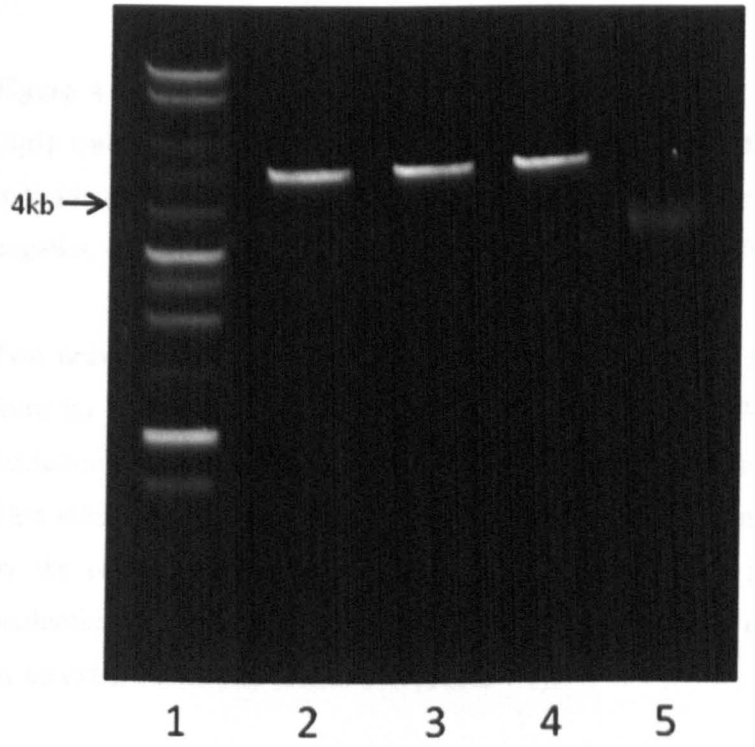

Figure 4-10. Agarose gel electrophoresis of restriction digestions of the vector pEGFP-N1. Digestion reaction mixture (5μl) was run on a 0.7% TAE agarose gel. Lane 1: 1kb DNA ladder. Lane 2: double digestions by *EcoR* I and *BamH* I restriction enzymes. Lane 3: single digestion by *EcoR* I only. Lane 4: single digestion by *BamH* I only. Lane 5: negative control using deionised water instead of restriction enzymes. Each digestion mixture was incubated at 37°C for 1h.

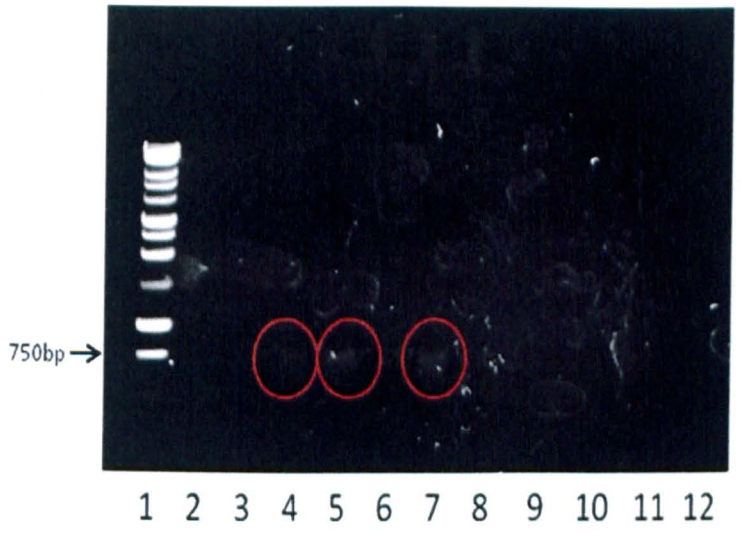

Figure 4-11. PCR screening using primers NRG1β3F and NRG1β3R. PCR products (3μl) were run on a 2% TAE agarose gel. Lane 1: 1kb DNA ladder. Lane 2-11: 10 individual colonies were picked and used as template for PCR reactions. Lane 12: negative control using deionised water instead of template DNA.

Two universal primers CMV F and EBV R were used to sequence NRG1β3-PAGFP from its N-terminus and C-terminus respectively (Figure 4-12). After translating the nucleotide sequence into amino acid sequence, a stop codon was found to be encoded right after the junction of NRG1β3-PAGFP at the very beginning of PAGFP as indicated by the red bar in Figure 4-12. When comparing this to the corresponding PAGFP nucleotide sequence from pPAGFP vector, it was found that this stop codon was caused by an extra nucleotide C insertion (Table 4-1).

The mutated sequence was corrected using the QuickChange Site-Directed Mutagenesis Kit (Stratagene, UK) as described in Section 2.4.9. The mutagenesis primer MP1 was designed to remove the extra nucleotide. Following PCR reaction and parental plasmid digestion, competent cells were transformed and plated on to LB agar plates supplemented with kanamycin. After overnight incubation, 11 individual colonies were picked for PCR screening to verify the insertion. Four out of 11 colonies appeared to be positive (Figure 4-13). They were grown up for plasmid minipreps and then sequenced to ensure that the extra nucleotide had been removed.

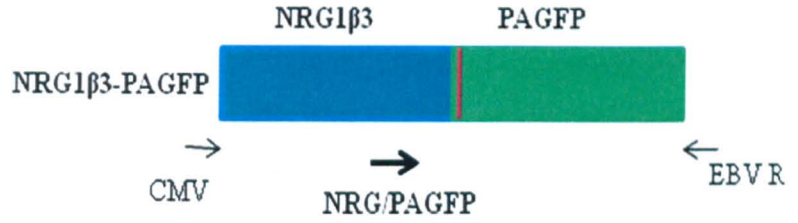

Figure 4-12. Schematic representation of fusion protein NRG1β3-PAGFP and primers used for sequencing NRG1β3-PAGFP. Red bar indicates a stop codon.

Table 4-1. Comparisons of nucleotide and amino acid sequences of pPAGFP and pNRG1β3-PAGFP.

	Nucleotide sequence	Amino acid sequence
pPAGFP	CAA GCT GAC CCT GAA	Q A D P E
pNRG1β3-PAGFP	CAA GCT GAC CCC TGA	Q A D P Stop

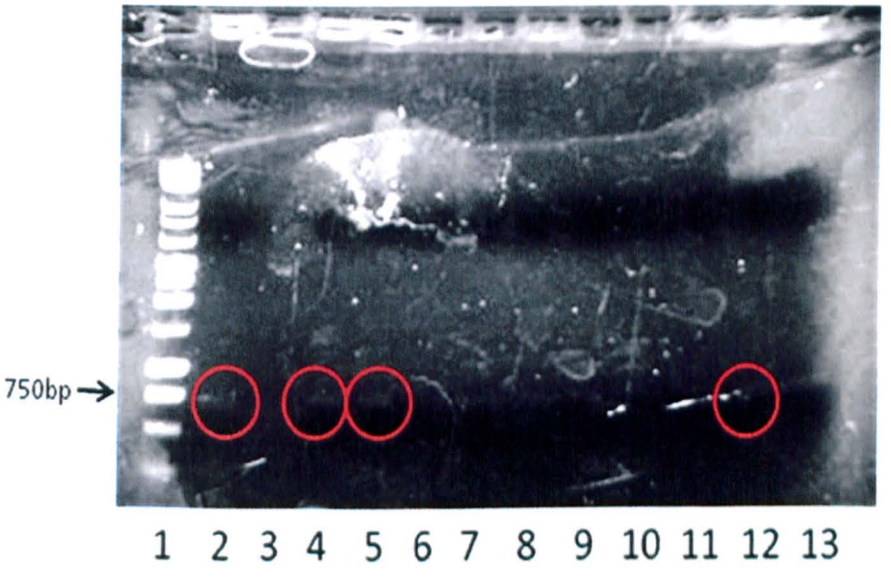

Figure 4-13. PCR screening using primers NRG1β3F and NRG1β3R. PCR products (5μl) were run on a 2% TAE agarose gel. Lane 1: 1kb DNA ladder. Lane 2-12: 11 individual colonies were picked and used as template in PCR reactions. Lane 13: positive control using NRG1β3 as template.

To confirm the expression of the pNRG1β3-PAGFP construct, transient transfections were performed in COS-7 cells using Lipofectamine 2000 transfection reagent (Section 2.1.5.2). Lysate from pPAGFP transfected cells was run in parallel to ensure that the anti-GFP antibody (GFP3E1) recognised PAGFP, a variant of GFP. Also, lysate from pQBI25-fN1 NRG1β3 transfected cells was run as a positive control. If NRG1β3-PAGFP were expressed correctly, it should appear on the blot at the same

molecular size as NRG1β3GFP. The blot was probed with anti-GFP antibody (GFP3E1) at a concentration of 10μg/ml. Bands of the expected size were detected in Lane1 and 2 but not in Lane 3 suggesting that the newly made construct NRG1β3-PAGFP was not expressed (Figure 4-14).

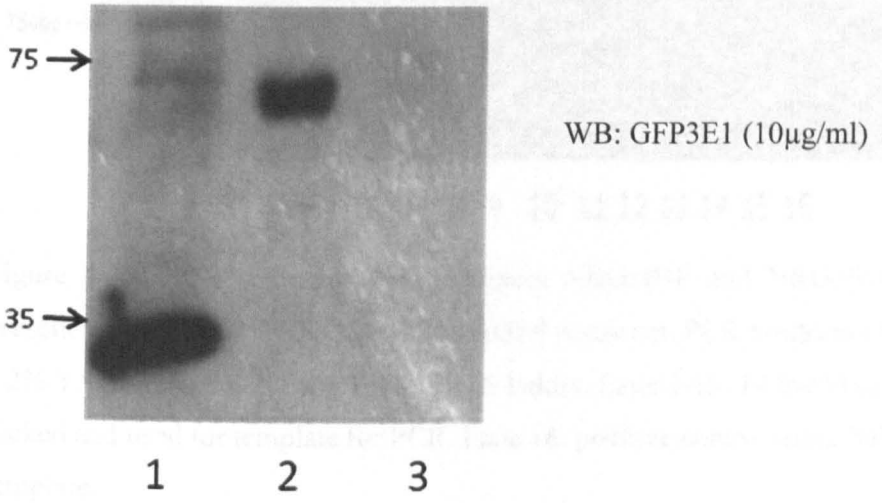

Figure 4-14. Western blot analysis of NRG1β3-PAGFP expression. Cell lysates were run on an 8% SDS-polyacrylamide gel and subjected to western blotting. Lysates included COS-7 cells transfected with pPAGFP (Lane1), pQBI25fN1-NRG1β3 (Lane 2) and the new construct pNRG1β3-PAGFP. Molecular sizes are in kDa.

The universal primers CMV F and EBV R were used to sequence across the flanking vector insert region. Each primer provided reliable sequencing results for up to 700bp. NRG1β3 and PAGFP were about 750bp each. The 3'end of NRG1β3 and the 5' end of PAGFP were not sequenced with high quality indicated by some unspecified nucleotides in the sequencing results. The uncertainty about this region made it suspicious in accounting for the absence of signal of NRG1β3-PAGFP in western blot analysis. To confirm the whole sequence of NRG1β3-PAGFP, we designed a new primer NRG/PAGFP to sequence the junction of NRG β3 and PAGFP (Figure 4-12).

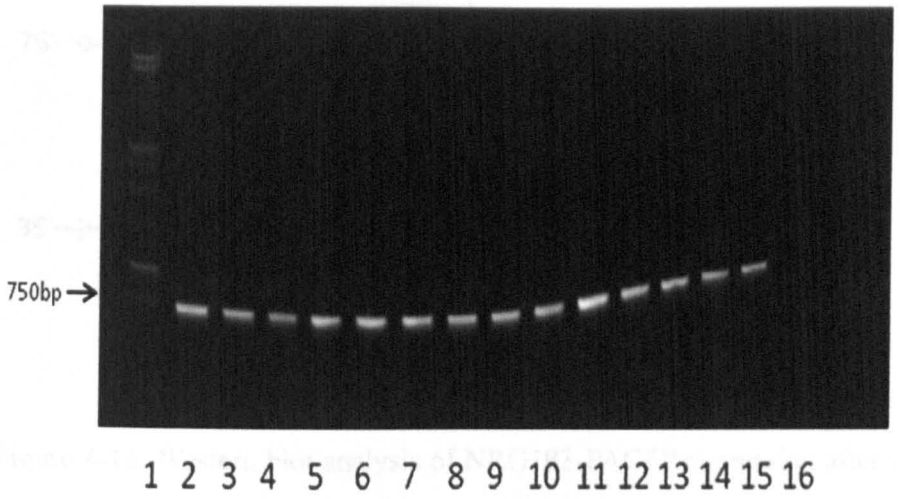

Figure 4-15. PCR screening using primers NRG1β3F and NRG1β3R to verify the presence of NRG1β3 in the NRG1β3-PAGFP construct. PCR products (3μl) were run on a 2% TAE agarose gel. Lane 1: 1kb DNA ladder. Lane 2-15: 14 individual colonies were picked and used for template for PCR. Lane 16: positive control using NRG1β3 cDNA as template.

The sequencing result suggested that NRG1β3 was not in the same reading frame with PAGFP. To resolve this problem, we designed another mutagenesis primer MP2 which introduced two nucleotides at the 3'end of NRG1β3 so that PAGFP could share the same reading frame as NRG1β3. Addition of two nucleotides was done using the QuickChange Site-Directed Mutagenesis Kit (Stratagene, UK) as described in Section 2.4.9. Competent cells were transformed with the products from the mutagenesis reaction and plated on LB agar supplemented with kanamycin. After overnight incubation, 14 individual colonies were picked for PCR screening to verify the presence of NRG1β3 (Figure 4-15). All colonies appeared to be positive. Four of them were grown up for plasmid minipreps and then sequenced to ensure that the extra two nucleotides had been incorporated.

To examine whether NRG1β3-PAGFP was expressed properly after the mutagenesis reaction, COS-7 cells were transfected with pPAGFP, pQBI25fN1-NRG1β3 and the new construct pNRG1β3-PAGFP. Cell lysates were probed with GFP3E1 anti-GFP antibody. Bands of the expected size were detected for all constructs (Figure 4-16). Western blot analysis confirmed the expression of NRG1β3-PAGFP in COS-7 cells.

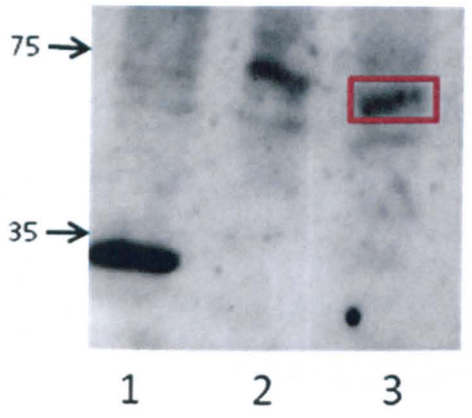

Figure 4-16. Western blot analysis of NRG1β3-PAGFP expression after the mutagenesis reaction. Cell lysates were run on an 8% SDS-polyacrylamide gel and subjected to western blotting. Lysates included COS-7 cells transfected with pPAGFP (Lane1), pQBI25fN1-NRG1β3 (Lane 2) and the new construct pNRG1β3-PAGFP after mutagenesis. Molecular sizes are in kDa.

4.3.4 Microscopy

Since PAGFP alone was successfully photoactivated inside COS-7 cells, it was expected that we could photoactivate NRG1β3-PAGFP in live cells and monitor its intranuclear trafficking over time. To perform this experiment we transiently transfected pNRG1β3-PAGFP into COS-7 cells. 24h post transfection, we selectively photoactivated NRG1β3-PAGFP in expressing cells and observed their behaviour over time. Figure 4-17 illustrates how PAGFP-tagged NRG1β3 changed its localisation patterns over 90min. At first, an NRG1β3-PAGFP expressing cell which showed mainly a nucleolar localisation pattern was chosen to be photoactivated. After two successive scans with 405nm laser light at 20% power, PAGFP-tagged NRG1β3 became highly fluorescent under 488nm excitation as shown at t=0. Continued imaging with 488nm light revealed movement of the photoactivated molecules from nucleoli to speckles. In the cell shown at t=45min, more speckled pattern signals were detected. It seemed that there was a localisation pattern shift of NRG1β3 from a nucleolar-like pattern towards a speckled pattern. This became more obvious after another 45min (t=90min) indicated by the reduced intensity of the signal in the nucleoli and more speckles scattered throughout the nucleus. During this process, only photoactivated NRG1β3-PAGFP molecules exhibited noticeable fluorescence, no newly synthesised molecules became fluorescent. Thus, what we observed suggested that PAGFP-tagged NRG1β3 moved from nucleoli to speckles.

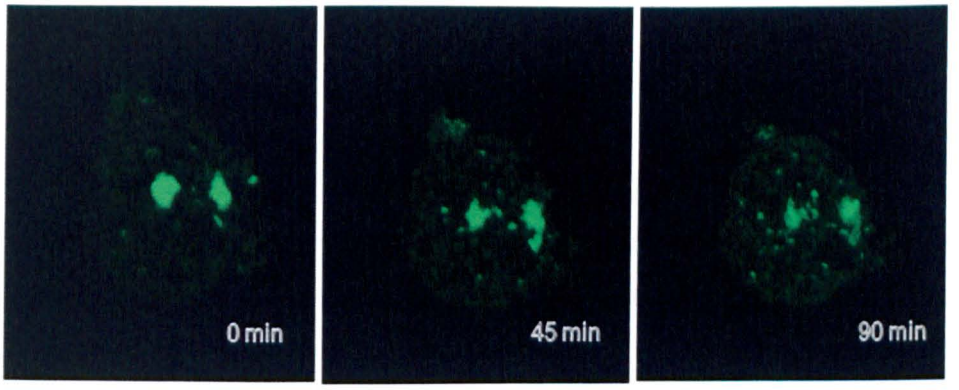

Figure 4-17. Photoactivation and imaging of NRG1β3-PAGFP trafficking in transiently transfected COS-7 cell. NRG1β3-PAGFP was irradiated with 405nm laser light at 20% power. Live cell images were taken every 45min under excitation with low levels (13%) of 488nm laser light post photoactivation.

4.4 Discussion

We have constructed a pmCherry mammalian Cherry expression vector from a bacterial vector and expressed it in COS-7 cells. The initial purpose of this cloning was to use pmCherry as a marker to help localise cells that had incorporated pPAGFP plasmids without photoactivation. The principle was that the cells that took up one plasmid most likely also took up the other plasmid. COS-7 cells were co-transfected with both pmCherry plasmid and pPAGFP plasmid. 24h post transfection, the culture dish was examined under a confocal microscope. mCherry expressing cells were identified by scanning with 546nm laser light. When switched to 405nm laser light, a big proportion of mCherry expressing cells were able to be photoactivated suggesting that cells had incorporated the pmCherry plasmid were very likely to take up pPAGFP plasmid as well. Thus, mCherry could be used as an effective marker to localise PAGFP expressing cells without photoactivation.

We also noticed that PAGFP expressing cells were faintly visible under UV-light which made mCherry co-transfection not necessary. We were able to photoactivate PAGFP in transiently transfected COS-7 cells using low power (20%) 405nm laser light. Images (Figure 4-7c-d) taken pre- and post-photoactivation using 488nm light demonstrate a dramatic increase in the fluorescence signal within a photoactivated cell, as suggested by Patterson and Lippincott-Schwartz (2002). There are a few things worthy of attention when performing photoactivation on a live cell. First, when choosing a target cell, long-term exposure to UV has the potential of activating the PAGFP. Thus, locating PAGFP labelled cells by co-transfecting with a cherry vector could help to avoid the potential harm caused by UV light. Second, photoactivation can be almost instantaneous once the 405nm laser light is applied. Thus, the 405nm laser light should remain off until activation is desired. Third, only a couple of scans of the 405nm laser light at a low power are necessary to activate the PAGFP. A series of 405nm laser light scans could be carried out to detect how bright a cell becomes during the photoactivation process. Last but not least, there is always the trade-off between photoactivation and photobleaching. Photoactivation efficiency is essentially a balance between photoactivation of PAGFP and photobleaching of activated molecules (Testa *et al.*,

2008). Photobleaching of the fluorescence signal in a photoactivated cell may result from a combination of different factors such as the microscope objective used, laser power, number of scans and zoom factors (Stark and Kulesa, 2005). Multiple scans using the 488nm laser contribute to undetectable or an insignificant amount of photobleaching. If a cell is scanned repeatedly with 405nm laser light especially at high power, photodamage is likely to occur. Thus, the combination of laser power and duration and number of scans should be optimised for experimental purpose. In our experiment, two successive scans (~ 1s each at ~1s interval) with 405nm laser light at low power (20%) effectively photoactivated PAGFP in live cells without any noticeable photobleaching.

Here, we took advantage of the PAGFP technique to determine whether PAGFP photoactivation could be used to address a specific question of protein trafficking inside cells. Specifically, we tested our hypothesis of whether the localisation inter-conversion between nucleoli and spliceosome we observed on NRG1β3 was due to protein movement. We started by making an NRG1β3-PAGFP construct by attaching NRG1β3 to the N-terminus of the PAGFP. Following mutagenesis reactions, the expression of this construct was confirmed by western blot analysis (Figure 4-16). COS-7 cells were transfected with pNRG1β3-PAGFP plasmid for 24h. A healthy-looking cell with a clear nucleolar-like pattern or speckled pattern was chosen to photoactivate and monitor for a period of time until its localisation pattern changes became noticeable. Most of the time cells were monitored for hours without showing any pattern changes and then apoptosis occurred (possibly due to repeated exposure to UV light). Even though Figure 4-17 is not a perfect example, it does provide important information in understanding NRG1β3 trafficking in live cells. The photoactivation process was performed under optimised conditions. Pictures were taken every 45min. At the beginning it showed mainly a nucleolar localisation pattern with few speckles scattered in the nucleus. After 45min, more speckles appeared. Another 45min later, the nucleoli dimmed and speckles were present throughout the nucleus. These changes strongly suggested that NRG1β3 moved from nucleoli to speckles and this movement took place in less than 2h which is consistent with previous observation that NRG1β3 localisation pattern changes within 2h (Golding *et al.*, 2004). Furthermore, our findings support the idea that NRG1β3 moves from one intranuclear compartment to the other rather than being degraded in one compartment while re-synthesised and targeted to the other compartment. Future experiments might examine how NRG1β3 localisation patterns are associated with

phases of the cell cycle by labelling NRG1β3 expressing cells with specific cell cycle markers. Addressing these questions would provide more insight into the functions of intranuclear NRG1.

In this study, we have demonstrated that PAGFP photoactivation as an innovative and effective tool for labelling and monitoring the trafficking of proteins in live cells. PAGFPs allow proteins to be tracked without the need for constant imaging. Since only photoactivated PAGFP molecules exhibit noticeable fluorescence, there is no concern that newly synthesised molecules will become fluorescent and complicate the experimental results. In addition to protein labelling and tracking, PAGFPs have a wide range of application at different levels such as visualising RNA and DNA dynamics (Shav-Tal *et al.*, 2004), following exchange of intracellular organelle content (Verkhusha and Sorkin, 2005) and tracking cells during development (Chudakov *et al.*, 2003). With microscopy techniques as an integral tool, PAFPs are anticipated to have more potential applications that have not been realised yet. For example, by using PAGFPs with distinct colours, it should be possible to study the dynamics of several proteins simultaneously. In the future, more studies of biological dynamics will benefit from this technique.

Chapter 5. Establishing an inducible cell line with regulated expression of NRG1β3GFP

5.1 Introduction

Nuclear expression of NRGs has been detected in a range of normal and human cancer tissues (see Chapter 3). However, their functions in the nucleus remain to be determined. Using high-resolution confocal microscopy, we found that NRG1β3GFP localised to nucleoli and SC-35 spliceosomes, nuclear compartments that contribute to ribosome synthesis and RNA splicing, respectively. We hypothesised that such distinct subnuclear localisation may have specific functions in modifying cell behaviour. To facilitate function analysis, we decided to establish a stable cell line in which the expression of NRG1β3GFP would be inducible. Once established, this cell line could allow us to do various small and large scale analyses, including associating NRG1β3GFP nuclear localisation patterns with different phases of the cell cycle, analysing its effect on cell growth, and transcriptomic analysis to investigate how gene transcription profiles are affected by targeting NRG1β3 to specific subnuclear structures.

In this study, a commercially available inducible mammalian expression system was employed: the Tet-Off expression system (Clontech, USA). The Tet-Off system has two critical components, the regulatory protein, encoded by the regulatory plasmid and the response plasmid which expresses a gene of interest under control of the response element (Figure 5-1). In the absence of the inducer doxycycline (Dox, a derivative of tetracycline), the regulatory protein binds the response element and activates transcription of the gene of interest. In contrast, transcription is repressed by the addition of doxycycline. The ultimate goal in setting up a functional Tet System is creating a double-stable Tet cell line which contains both the regulatory and response plasmids. We obtained the MCF-7 Tet-Off cell line which already expresses the regulatory protein (a gift from Dr Paul Edwards, Cambridge, UK). We therefore cloned

the NRG1β3GFP cDNA into the Tet-regulated gene expression system and aimed to establish a stable cell line with inducible expression of the NRG1β3GFP construct. Figure 5-2 is an overview of the general strategy for establishing the Tet-Off system, in which the expression of our gene of interest would be inducible.

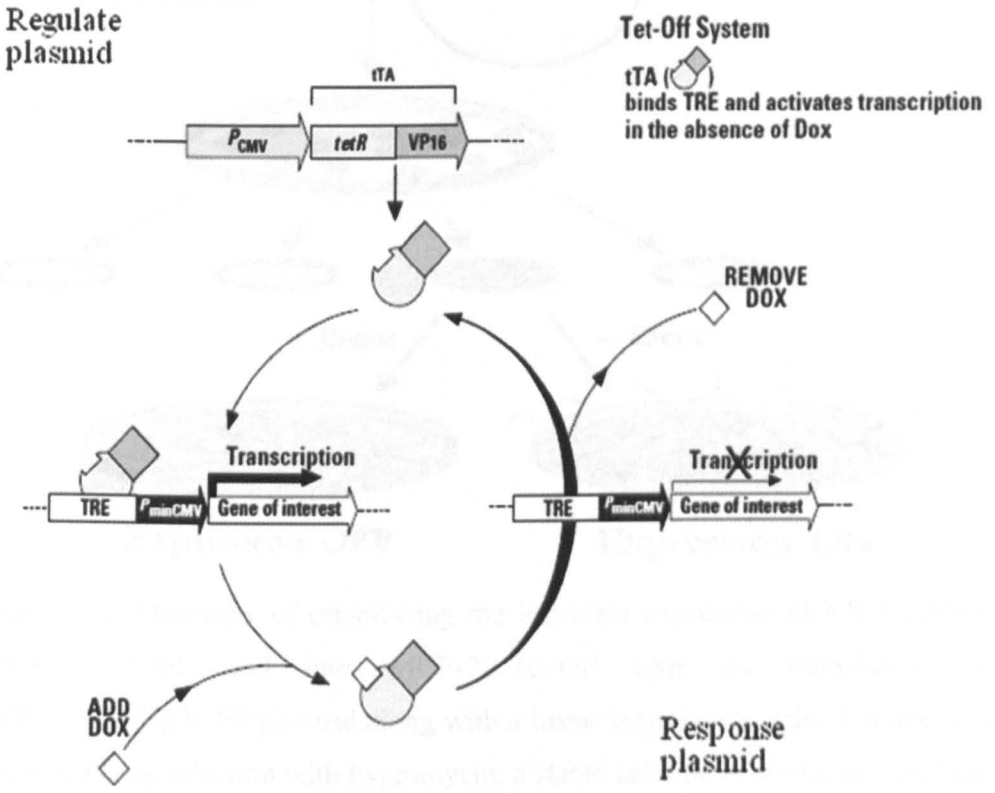

Figure 5-1. Schematic of gene regulation in the Tet-Off System. Figure taken from www.clontech.com.

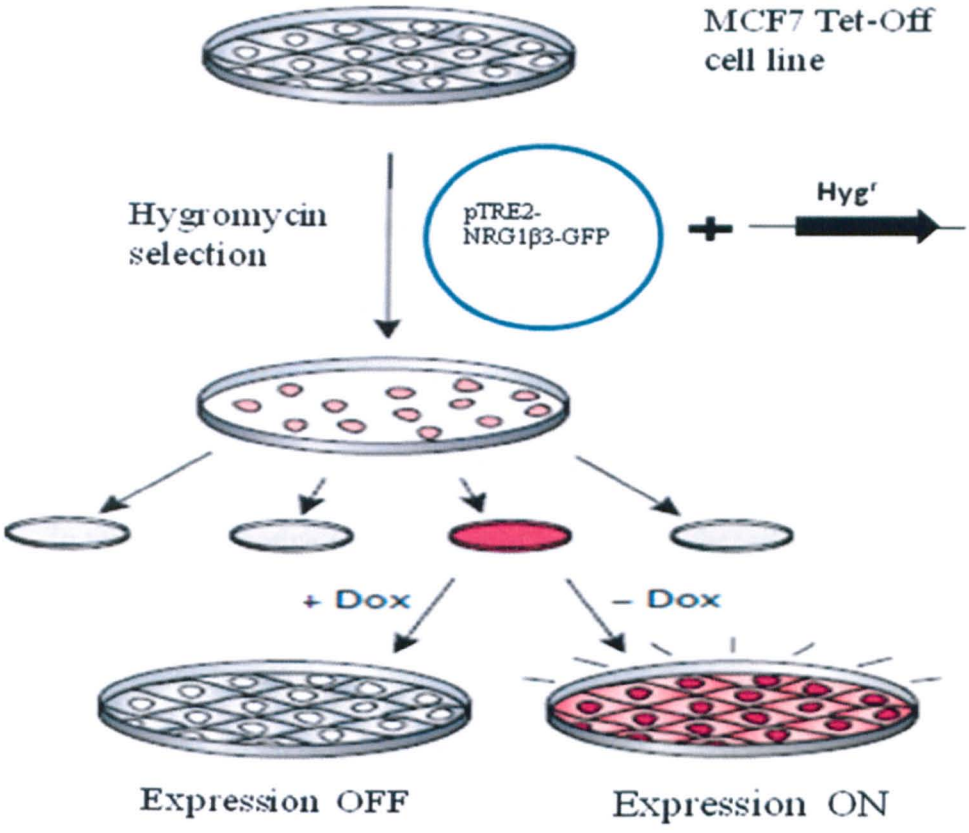

Figure 5-2. Overview of establishing the inducible expression of NRG1β3GFP in the MCF-7 Tet-Off cell line. MCF-7 Tet-Off cells are transfected with the pTRE2-NRG1β3GFP plasmid along with a linear hygromycin selection marker (Hygr). After the drug selection with hygromycin, a stable cell line is produced which expresses NRG1β3GFP in response to the withdrawal of doxycycline (Dox). Figure adapted from www.clontech.com.

5.2 Aims

1. To clone NRG1β3GFP in the multiple cloning site of the response plasmid (pTRE2).
2. To test the inducible expression of NRG1β3GFP in the MCF-7 Tet-Off cell line.
3. To determine the effective concentration of Dox.
4. To test fetal bovine serum for tetracycline contamination.
5. To optimise the transfection efficiency in the MCF-7 Tet-Off cell line.
6. To titrate the effective concentration of hygromycin for cell killing.
7. To co-transfect pTRE2-NRG1β3GFP with the linear hygromycin selection marker and select hygromycin resistant clones.
8. To screen clones for inducible expression of NRG1β3GFP.

5.3 Results

5.3.1 Construction of the pTRE2-NRG1β3GFP vector

To express NRG1β3GFP in the Tet-Off system, we first cloned NRG1β3GFP into the response vector pTRE2. By comparing the vector maps of pQBI25-fN1 NRG1β3GFP and pTRE2, we found that NRG1β3GFP can be cloned into the pTRE2 vector at two compatible restriction sites, *BamH* I and *Mlu* I, that are present on either side of the NRG1β3GFP fragment and in the multiple cloning site of the pTRE2 vector (Figure 5-3).

Restriction digestion reactions were set up as described in Section 2.4.4. Uncut supercoiled plasmid appeared to migrate more quickly than the nicked plasmid indicated by the lower band in Lane 5 as shown in Figure 5-4. No such band appeared in Lane 3 and Lane 4 indicating that single digestion by either *BamH* I or *Mlu* I restriction enzyme was complete, and this generated a single band of 7 kb, the size of the vector. Double digestions by *BamH* I and *Mlu* I restriction enzymes generated two fragments of 5.5 kb and 1.5kb, as shown in Lane 2. 1.5kb was the predicted size of NRG1β3GFP suggesting complete digestions of vector pQBI25-fN1 NRG1β3GFP by *BamH* I and *Mlu* I restriction enzymes. The 1.5kb DNA fragment was purified using QIAEX® II Gel Extraction Kit (as described in Section 2.4.3) for subsequent cloning.

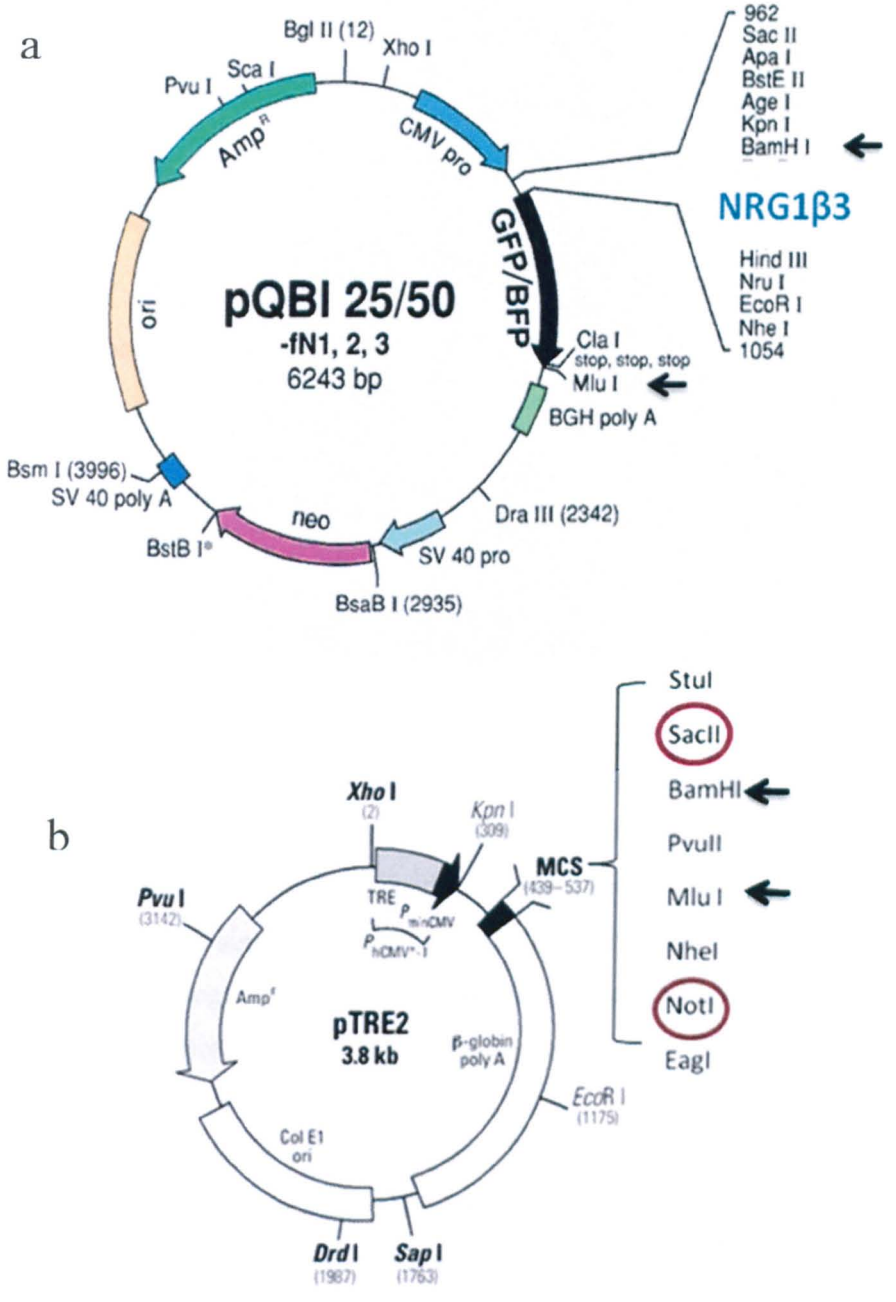

Figure 5-3. Vector maps. (a) Vector pQBI25-fN1 NRG1β3GFP. (b) Response vector pTRE2. Compatible restriction sites are indicated by black arrows. The circled restriction sites were chosen for the subsequent restriction analysis to identify the recombinant plasmids. Figure adapted from www.clontech.com.

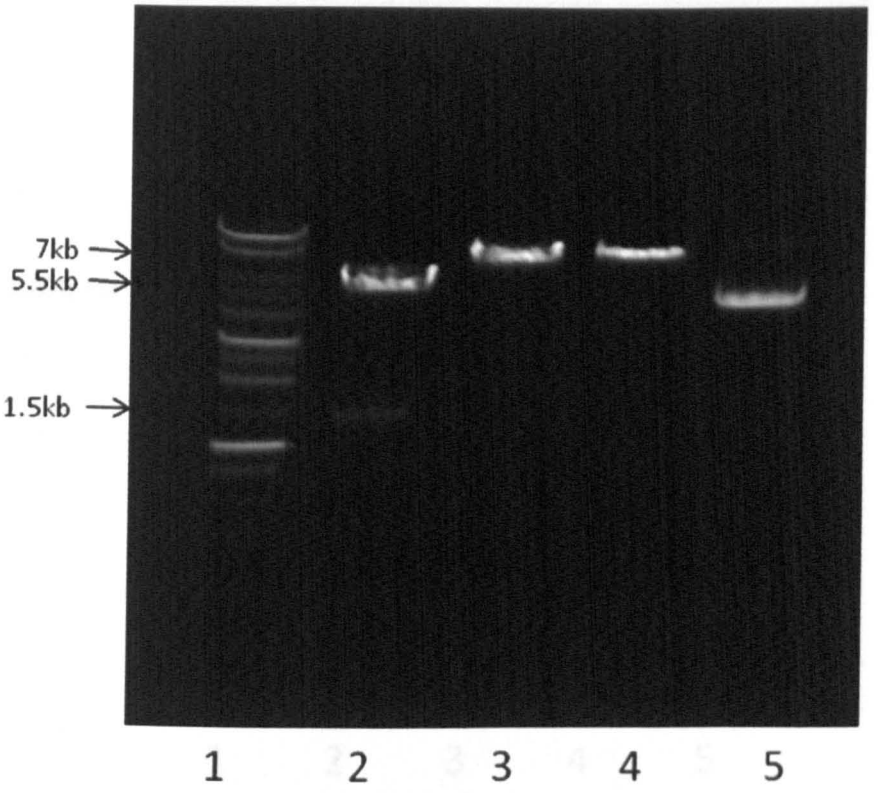

Figure 5-4. Gel of agarose electrophoresis of restriction digestions of the vector pQBI25-fN1 NRG1β3GFP. Digestion reaction mixture (5μl) was run on a 0.7% gel. Lane1: 1kb DNA ladder. Lane 2: double digestions by *BamH* I and *Mlu* I restriction enzymes. Lane 3: single digestion by *BamH* I only. Lane 4: single digestion by *Mlu* I only. Lane 5: negative control of uncut plasmid using deionised water instead of restriction enzymes. Each digestion mixture was incubated at 37°C for 1h.

The response vector pTRE2 was digested under the same conditions. Since only a few nucleotides exist between the two restriction sites in the multiple cloning site of the vector, a single band of the predicted size of the vector (3.8kb) suggested complete digestions (Lane 2 in Figure 5-5). Following gel purification, the digested vector was treated with Calf Intestinal Alkaline Phosphatase (CIAP) (as described in Section 2.4.5) to remove the phosphate group from the 5'-ends to prevent self-ligation of the vector.

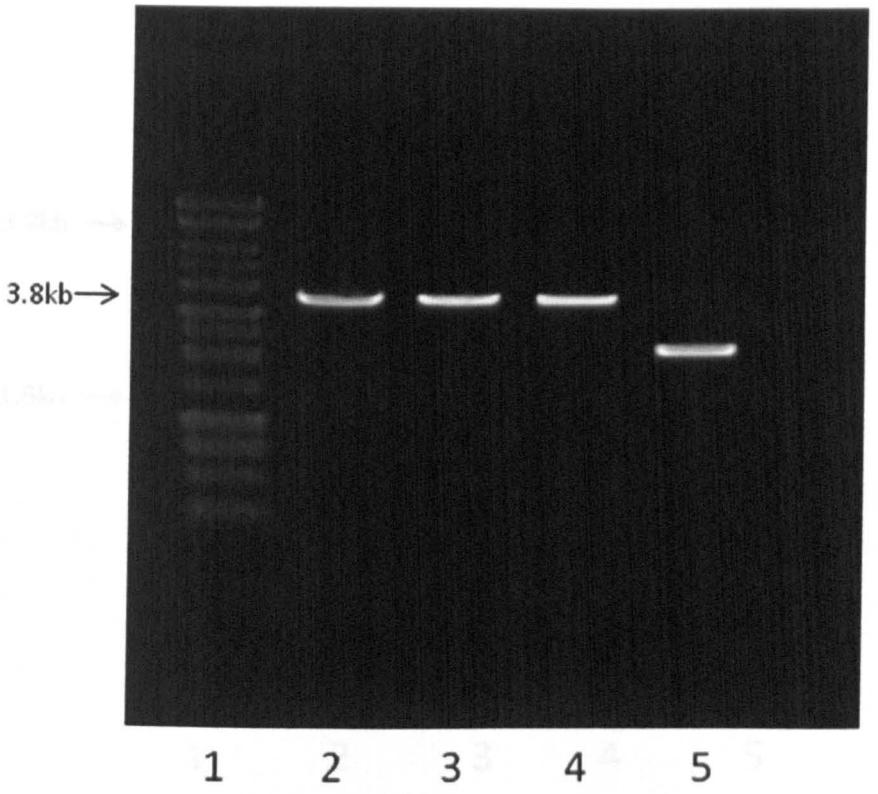

Figure 5-5. Gel of agarose electrophoresis of restriction digestion of the response vector pTRE2. Digestion reaction mixture (5µl) was run on a 0.7% gel. Lane1: 1kb DNA ladder. Lane 2: double digestions by *BamH* I and *Mlu* I restriction enzymes. Lane 3: single digestion by *BamH* I only. Lane 4: single digestion by *Mlu* I only. Lane 5: negative control using deionised water instead of restriction enzymes. Each digestion mixture was incubated at 37°C for 1h.

The ligation reaction was transformed into DH5α competent cells and plated onto LB agar plates supplemented with ampicillin. 10 individual colonies were picked from the plates and the DNA plasmid from each colony was purified using the Qiagen Miniprep Kit (as described in Section 2.4.7). To identify the desired recombinant plasmids, restriction analysis was performed by choosing another two restriction sites (*Sac* II and *Not* I) outside the gene insertion but within the multiple cloning site in the pTRE2 vector (Figure 5-3). Figure 5-6 is a gel picture showing a positive screening by restriction analysis, which generated one fragment of the predicted size of NRG1β3GFP (1.5kb) and another fragment of the predicted size of the vector (3.8kb). Correct orientation and junctions of the insertion were confirmed by sequencing.

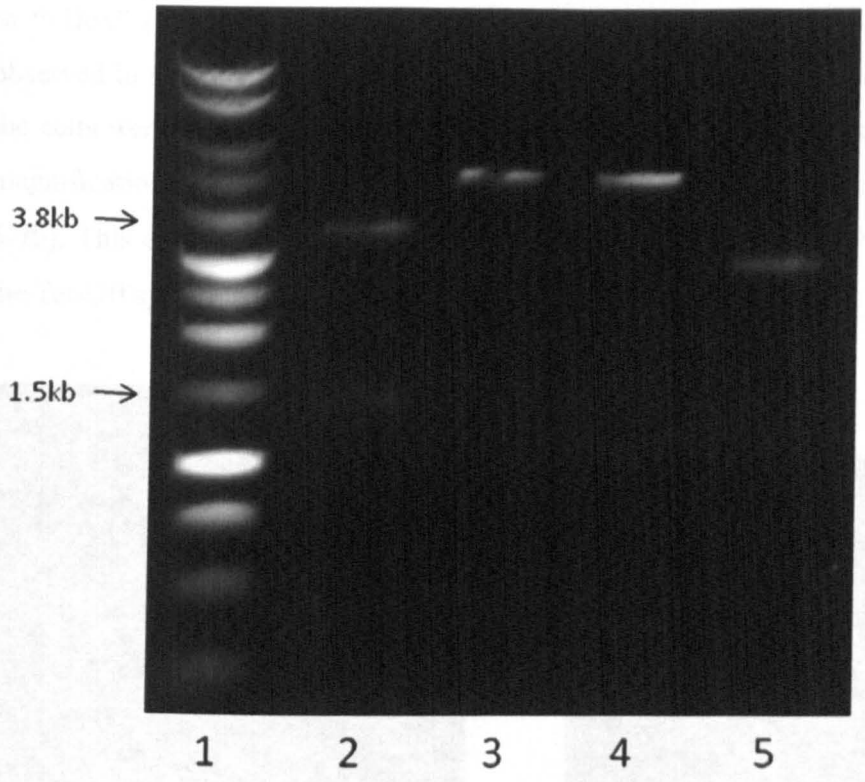

Figure 5-6. Gel of agarose electrophoresis of restriction analysis to identify the recombinant plasmid. Digestion reaction mixture (5µl) was run on a 0.7% gel. Lane1: 1kb DNA ladder. Lane 2: double digestions by *Sac* II and *Not* I restriction enzymes. Lane 3: single digestion by *Sac* II only. Lane 4: single digestion by *Not* I only. Lane 5: negative control using deionised water instead of restriction enzymes. Each digestion mixture was incubated at 37°C for 1h.

5.3.2 Testing of NRG1β3GFP induction in the MCF-7 Tet-Off cell line

Before creating a double stable MCF-7 Tet-Off cell line, a transient induction assay was performed to test whether the expression of NRG1β3GFP was inducible. If the system worked, the expression of NRG1β3GFP would be turned off in the presence of Dox and turned on by the absence of Dox.

Duplicate 35mm tissue culture dishes of MCF-7 Tet-Off cells were transiently transfected with pTRE2-NRG1β3GFP using the FuGENE 6 transfection reagent. When transfection was complete, 1µg/ml Dox (maximum concentration suggested in the literature to achieve full suppression of gene expression) was added to one of the duplicate dishes, leaving the second dish untreated to achieve full induction of NRG1β3GFP expression. After 24h treatment with Dox, "+Dox" cells were compared

to "–Dox" (induced) cells using low light digital microscopy. No fluorescence was observed in the dish treated with 1μg/ml Dox (data not shown). Approximately 10% of the cells were fluorescent in the Dox-free dish (Figure 5-7a). When switched to higher magnification (x63), the localisation pattern of NRG1β3GFP was confirmed (Figure 5-7b). This experiment indicated that the expression of NRG1β3GFP was inducible in the Tet-Off system.

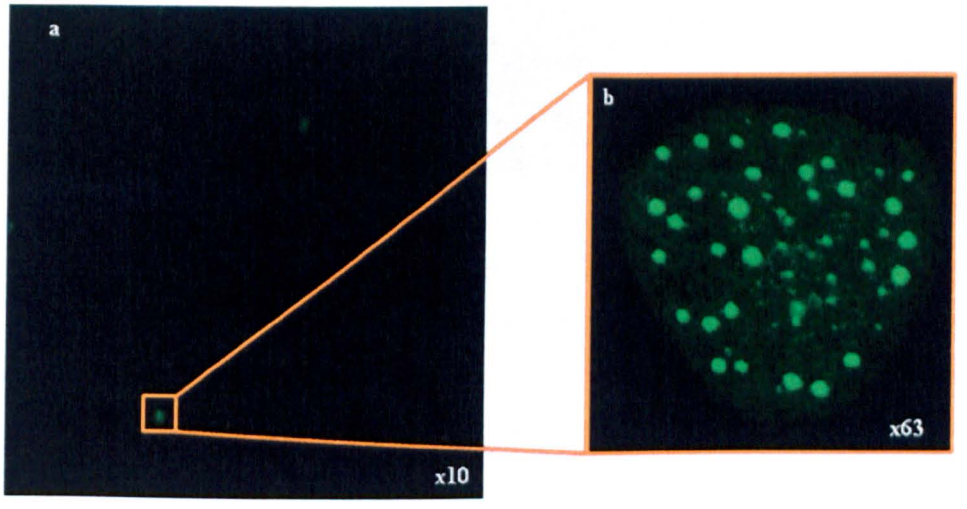

Figure 5-7. Testing of NRG1β3GFP induction in the Tet-Off system. The pTRE2-NRG1β3GFP construct was transiently transfected into MCF-7 Tet-Off cells. In the absence of Dox treatment, NRG1β3GFP expression was induced 24h post transfection. Images were taken at x10 (a) and x63 (b).

5.3.3 Determination of the effective concentration of Dox

Doxycycline was needed for controlling the expression of NRG1β3GFP in the Tet-Off system. A wide range of Dox concentrations are suggested in the literature and the optimal concentration varies with different cell lines. To achieve full repression of gene expression with minimal cytotoxicity, a Dox dose-response experiment was set up to calibrate the effective concentration of Dox in the MCF-7 Tet-Off cell line.

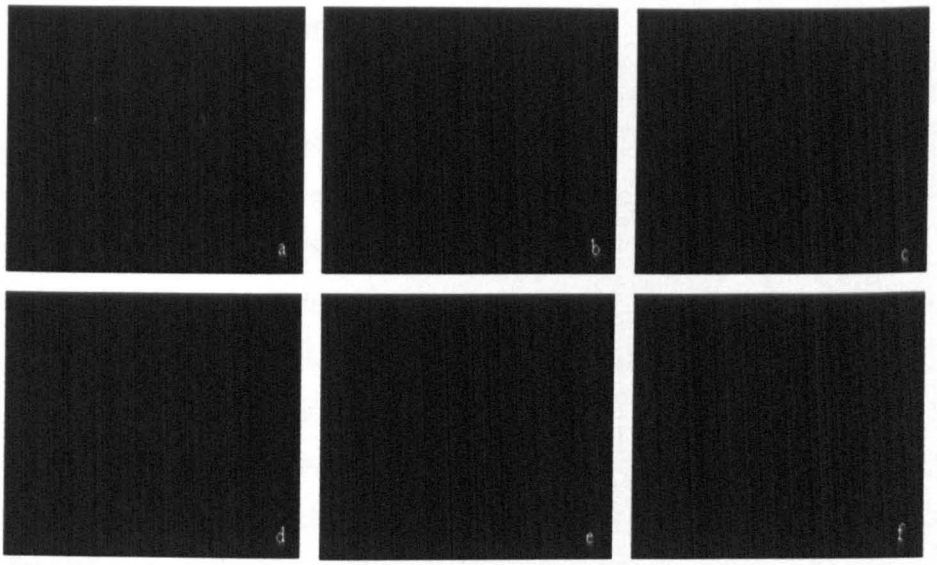

Figure 5-8. Determination of the effective concentration of Dox. 6 dishes of MCF-7 Tet-Off cells were 50% confluent when transiently transfected with the pTRE2-NRG1β3GFP construct. Dox was added to each dish at final concentrations of (a) 50, (b) 100, (c) 200, (d) 400, (e) 600, and (f) 800ng/ml. 24h post transfection cells were visualised using low light digital microscopy. Pictures are representative of each condition. Original magnification: x10.

6 aliquots of MCF-7 Tet-Off cells were plated into 3ml of complete culture medium in 35mm glass-bottom culture dishes. Each dish of cells was 50% confluent when transiently transfected with the pTRE2-NRG1β3GFP construct using FuGENE (Section 2.1.5.1). When transfection was completed, Dox was added to each dish at final concentrations of 50, 100, 200, 400, 600, and 800ng/ml. Cells were left to grow for 24h before examining the expression level of NRG1β3GFP expression in response to varying concentration of Dox. As shown in Figure 5-8, the concentration of Dox at 50, 100, 200ng/ml suppressed gene expression of NRG1β3GFP to some extent (Figure 5-8a-c). Full suppression of NRG1β3GFP expression was achieved when the Dox concentration achieved at 400ng/ml or higher (Figure 5-8e-f). This experiment showed that the level of NRG1β3GFP expression in the Tet-Off system was Dox dose dependent and the effective concentration of Dox to fully suppress NRG1β3GFP expression in the MCF-7 Tet-Off cell line was 400ng/ml.

5.3.4 Testing of serum for tetracycline contamination

Many bovine sera are contaminated with tetracycline or tetracycline-derivatives, presumably due to the use of tetracyclines in the diet of cattle. Tetracycline contamination could affect basal expression or inducibility in Tet systems. Therefore, it was critical that the FBS used for cell culture should not interfere with Tet-responsive expression. Even though these problems could be eliminated by using the Tet System Approved FBS from Clontech which has been tested and found to be free of contaminating tetracycline activity, the cost was high. Another commercially available FBS, from Invitrogen, which was routinely used in tissue culture, was therefore tested in our Tet system to verify tetracycline contamination. Since we were dealing with the Tet-Off system, the traces of tetracycline from FBS were not important in keeping the gene expression silent (in the presence of Dox). However, it might affect the induction level of the gene expression in the absence of Dox.

MCF-7 Tet-Off cells were grown in two 35mm tissue culture dishes containing medium prepared with FBS from Clontech and from Invitrogen, respectively. They were transiently transfected with the pTRE2-NRG1β3GFP construct in the absence of Dox. 24h post transfection, the fluorescence patterns of each dish were examined using low light digital microscopy. No obvious differences were observed in terms of the percentage and the intensity of the green glowing cells. To further examine the induction level of NRG1β3GFP expression, cell lysates from each dish were probed with GFP3E1 anti-GFP antibody (Figure 5-9). Bands of the expected size were detected, and their intensity appeared to be the same. The similar level of induction suggested that the FBS from Invitrogen did not contain tetracycline or at a neglectable level, which would not affect the inducibility of NRG1β3GFP expression in the Tet system.

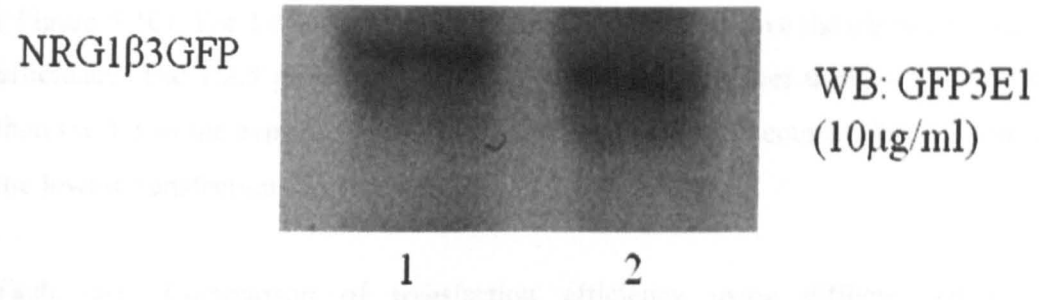

Figure 5-9. Western blot analysis of the level of NRG1β3GFP expression when cultured in different FBS. MCF-7 Tet-Off cells were transiently transfected with the pTRE2-NRG1β3GFP construct in the absence of Dox. Cells were lysed 24h post transfection. Cell lysates were run on an 8% SDS-polyacrylamide gel and probed with an antibody specific for GFP. MCF-7 Tet-Off cells were cultured in the Tet System Approved FBS from Clontech (Lane 1) and in the FBS from Invitrogen (Lane 2).

5.3.5 Optimisation of transfection efficiency in MCF-7 Tet-Off cell line

Developing a stable cell line in which NRG1β3GFP expression would be inducible involved stable transfection of the pTRE2-NRG1β3GFP construct into the MCF-7 Tet-Off cell line. For best results, transfection methods were optimised to achieve high transfection efficiency.

MCF-7 Tet-Off cells were plated out into two 35mm glass bottom dishes the day before transfection. Cells reached about 60% confluency at the time of transfection. The pTRE-NRG1β3GFP construct was transiently transfected into MCF-7 Tet-Off cells using two different transfection reagents: FuGENE 6 (Roche, UK) and Lipofectamine 2000 (Invitrogen, UK). Transfection procedures were carried out according to the supplier's instructions (as described in Section 2.1.5). After 24h incubation in the absence of Dox, each dish was examined using low light digital microscopy. The transfection efficiency was calculated for each transfection reagent, by choosing 3 random fields from which green glowing cells were counted compared to total cells observed, to get a percentage of glowing cells. Lipofectamine 2000 transfection reagent provided higher transfection efficiency (15%) compared to FuGENE 6 (10%).

To further improve the transfection efficiency using the Lipofectamine 2000 transfection reagent, three different ratios of DNA (μg): Lipofectamine 2000 (μl) were

tested as listed in Table 5-1. Transfection efficiency was compared 24h post transfection (Figure 5-10). The 1:5 ratio of DNA: Lipofectamine 2000 gave the highest transfection efficiency. The 1:2.5 produced a transfection efficiency higher than the 1:1 but lower than the 1:5 in the expression of NRG1β3GFP using the cell counts. The 1:1 ratio gave the lowest transfection efficiency.

Table 5-1. Comparison of transfection efficiency using different DNA (μg): Lipofectamine 2000 (μl) ratios.

DNA (μg): Lipofectamine 2000 (μl)	DNA (μg)	Lipofectamine 2000 (μl)	Transfection efficiency
1:1	4	4	10.5%
1:2.5	4	10	15%
1:5	4	20	25%

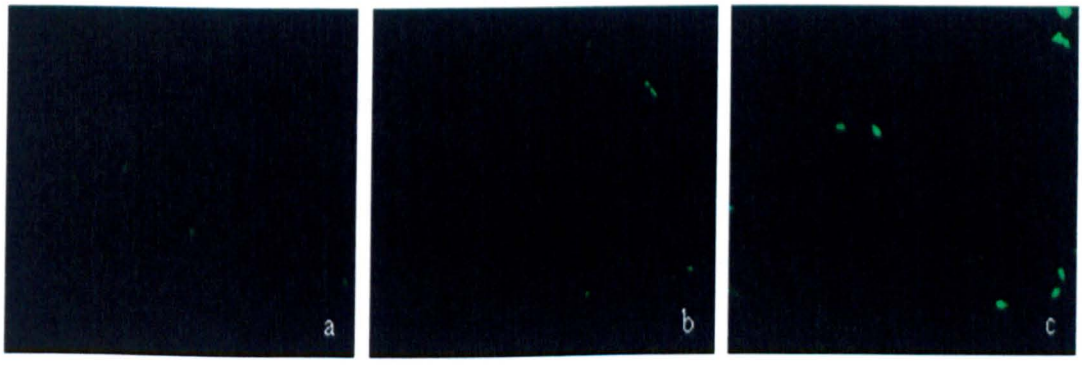

Figure 5-10. Optimisation of transfection efficiency. 3 dishes of MCF-7 Tet-Off cells were 60% confluent when transiently transfected with the pTRE2-NRG1β3GFP construct using DNA (μg): Lipofectamine 2000 (μl) ratios of (a) 1:1, (b) 1:2.5 and (c) 1:5, respectively. After 24h incubation in the absence of Dox, the transfection efficiency of each dish was examined using low light digital microscopy. Pictures are representative of each condition. Original magnification: x10.

5.3.6 Hygromycin titration

Hygromycin was used for the selection of the MCF-7 Tet-Off cell line stably transfected with a linear hygromycin selection marker. Due to variations in the potency of hygromycin it was important to do a titration experiment to determine the optimal concentration necessary to kill untransfected MCF-7 Tet-Off cells.

$3.5x10^4$ MCF-7 Tet-Off cells were plated in each of five 10cm tissue culture dishes containing 10ml of the complete medium plus varying amounts (50, 100, 200, 400, 800μg/ml) of hygromycin. Cells were incubated for 14 days with the selective medium replaced only if nutritional compounds were depleted by the cells cultured, indicated by a colour change from red to yellow. The dishes were examined for viable cells every two days. Cell counting was performed using a hemocytometer (as described in Section 2.1.6). A dose response curve was generated by plotting the number of viable cells on the y-axis versus hygromycin in μg/ml on the x-axis (Figure 5-11). For selecting stable transformants, the optimal hygromycin concentration was the lowest concentration that began to give massive cell death in ~5 days and killed all the cells within two weeks, which was 200μg/ml according to the data shown in Figure 5-11. This optimised hygromycin concentration was subsequently used to block growth of non-transfected cells and select for transfected cells when developing the double stable Tet-Off cell line.

The plating density is another important factor for the selection of stably transfected cells. If cells are plated at too high a density, they will reach confluency before the selection takes effect. Optimal plating density is dependent on cell proliferation rate and cell surface area. For example, large cells that proliferate rapidly have a lower optimal plating density than small cells that proliferate slowly. The plating density of MCF-7 Tet-Off cells was optimised by plating cells at several different densities in the presence of 200μg/ml hygromycin.

MCF-7 Tet-Off cells were plated in each of six 10cm tissue culture dishes containing 10ml of the complete medium at the following densities: $5x10^6$, $1x10^6$, $5x10^5$, $2x10^5$, $1x10^5$, and $5x10^4$. Cells were incubated for 5-14 days in the presence of 200μg/ml hygromycin. The optimal plating density for selecting stable transfectants should allow the cells to reach ~80% confluency before massive cell death begins (at about day 5). For MCF-7 Tet-Off cells, we found $2x10^5$ cells/10cm dish to be an optimal plating density.

Figure 5-11. Hygromycin kill curve showing cell death in relation to increasing concentration of hygromycin over time.

5.3.7 Developing the double-stable Tet-Off inducible cell line

5.3.7.1 Co-transfection of the MCF-7 Tet-Off cells

To generate the double-stable Tet-Off inducible cell line, pTRE2-NRG1β3GFP vector was cotransfected along with the Linear Hygromycin Marker (pTK-Hyg) (Clontech, USA) into the MCF-7 Tet-Off cell line. Transfected MCF-7 Tet-Off cells were cultured in the presence of 400μg/ml Dox in order to keep transcription of NRG1β3GFP turned off. Stable transfectants were selected using hygromycin at 200μg/ml.

MCF-7 Tet-Off cells were grown to 60% confluency in complete medium for transfection. The optimised transfection method described in Section 5.3.5 was followed. The pTRE-NRG1β3GFP vector and the linear hygromycin marker pTK-Hyg were combined at a ratio of 20:1 (according to the manufacturer's instructions). 24μg plasmid DNA and 1.2μg of the linear hygromycin marker were diluted in 1.5ml of Opti-MEM I Reduced Serum Medium. 120μl Lipofectamine 2000 transfection reagent was diluted in 1.5ml of Opti-MEM I Medium. After 5min incubation at room temperature, the diluted DNA was mixed with diluted Lipofectamine 2000. The mixture was incubated for 20min at room temperature and the complexes were added to the MCF-7 Tet-Off cells. The transfected cells were cultured in the absence of Dox for 24h. Following

examining the transfection efficiency under the microscope, Dox was added to the culture medium at a final concentration of 400ng/μl and transfected cells were examined the following day. No fluorescence was observed, suggesting the expression of NRG1β3GFP was fully suppressed. Transfected cells were plated in ten 10cm culture dishes, each containing 15ml of the complete medium, at the optimal plating density determined in Section 5.3.6.

5.3.7.2 Selection of transfected cells

Selection of MCF-7 Tet-Off cells, co-transfected with the pTRE-NRG1β3GFP and the linear hygromycin marker encoding for hygromycin resistance was performed, using culture medium containing hygromycin at a concentration of 400μg/ml.

Transfected cells were allowed to divide for two days before adding hygromycin to the culture medium. Medium was replaced with fresh complete medium containing the hygromycin, when necessary. Fresh Dox was added every two days. After 5-7 days, cells started to die. Drug selection was continued until colonies became visible, indicating that the cell cultures contained only living cells expressing the hygromycin resistant phenotype, and all untransfected cells had died.

For maintenance of the hygromycin resistant phenotype of established transfected cell lines, cells were cultured in hygromycin at a concentration of 200μg/ml recommended for maintenance of human cell lines. Moreover, to eliminate any revertants, cells were cultured in medium containing hygromycin at the same concentration used for the initial selection (400μg/ml) once a month.

5.3.7.3 Cloning by picking and limiting dilution

Colonies became visible in 3-4 weeks. Culture dishes containing colonies were examined with an inverted microscope with a x10 objective. Once average size, healthy and well separated colonies were located, a circle around them was drawn on the bottom of the dish with a marker pen. 35 colonies were isolated and picked from ten culture dishes using 8mm x 8mm cloning cylinders (Millipore, UK) (as described in Section 2.1.7).

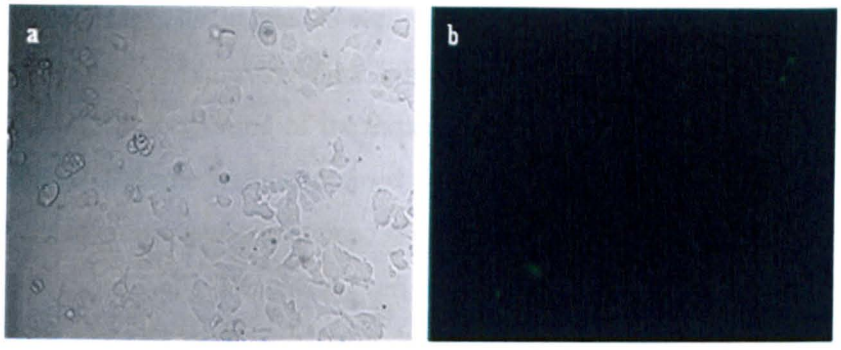

Figure 5-12. Testing individual double-stable clones for expression of NRG1β3GFP. Each clone in a single well of a 96-well plate was examined by removing Dox. Induced NRG1β3GFP expressing cells were indicated by the fluorescence signal.

Individual clones were seeded into single wells of a 96-well plate containing medium with maintenance concentration of hygromycin (200μg/ml) and 400ng/ml Dox. When they had grown sufficiently, clones for induction were tested by removing Dox. When examined using low light digital microscopy, fluorescence was observed in 8 out of 35 clones. However, not all cells from a single isolated clone were fluorescent. Only a few cells were glowing suggesting that NRG1β3GFP was only expressed in a very small proportion of individual cells in the isolated clones (Figure 5-12). To separate individual NRG1β3GFP expressing cells in order to obtain specific clones with expression of our interest gene, single-cell cloning by limiting dilution was carried out.

The fluorescent clones in the separate wells of the 96-well plate were washed twice with PBS buffer and incubated in 0.2ml of EDTA-trypsin solution at 37°C. Once cells detached from the dish bottom, 2ml of fresh medium was added. Before further dilution, 1ml from each promising clone was frozen down as stocks. Another 9ml of complete medium was added to the remaining 1ml and made up to 10ml in total. After performing cell viability count using a hemocytometer, cell density was adjusted to 1 x 10^6 cells/ml. One hundred fold dilution was carried out by transferring 200μl of cell suspension to 20 ml of medium giving 1 x 10^4 cells/ml (10,000 cells per ml). 5ul (50 cells), 10μl (100 cells), 20μl (200 cells) and 50μl (500 cells) of the cell suspension were pipetted respectively into four pre-labelled tubes, each containing 10ml of medium giving 50 cells/10ml, 100 cells/10ml, 200 cells/10ml and 500 cells/10ml. Four 96-well plates were labelled with 50, 100, 200 and 500. 100μl from each 10ml cell suspension was aliquoted into each of the 96 wells in each labelled plate. These dilutions provided at least 5ml of cell suspension containing 0.5, 1, 2 and 5 cells per well.

When the cells in the 96-well plates reached 30% confluency, they were tested for induction by removing Dox from the medium. The number of cells seeded into each well at the beginning of the experiment was indicated by the number of the clusters of the cells. Some wells contained a few clusters of cells suggesting more than 1 cell was seeded; some wells contained no live cells suggesting that probably no cell was seeded into those wells. However, even if some wells seemed to have only one cluster of cells, only a small portion of cells were fluorescent indicating that not every cell in that cluster expressed NRG1β3GFP. Cells from the wells containing fluorescent cells were transferred in sequence from the 96-well plate into a 48-well, 24-well plate in the presence of Dox. When the cells in the 24-well plate reached 30% confluency, the expression of NRG1β3GFP was checked again by removing Dox. Hygromycin resistant clones in culture dishes were examined under low light digital fluorescence microscopy after removing Dox. Although the expression of NRG1β3GFP was apparent, its distribution was heterogeneous. Only a small number of cells exhibited NRG1β3GFP expression within an isolated clone. We also noticed that the number of NRG1β3GFP expressing cells decreased as cells were passaged. At this point, we stopped further attempts at clone isolation.

5.4 Discussion

5.4.1 Functional testing of Tet-Off system

NRG1β3 has been shown to localise to two known intranuclear structures, nucleoli and SC-35 spliceosomes. However, the precise functional correlates of its expression patterns remain unclear. We therefore set out to develop an *in vitro* cell model in which NRG1β3GFP expression in the cell line could be temporally controlled for functional analysis. Several inducible gene expression systems have been developed such as those regulated by hormones, heavy metal ions and heat shock (Yarranton, 1992). However, most of them are limited by nonspecific induction and toxic effects of the inducing agents. The tetracycline (tet)-regulated gene expression system overcomes many of the problems of other inducible systems and has been widely used in mammalian cell culture (Howe *et al.*, 1995), transgenic mice (Ewald *et al.*, 1996) and other species (Thomas *et al.*, 2000). The Tet-Off expression system consists of two separate plasmids, the regulatory plasmid which expresses a transactivation element and the response plasmid which expresses the gene of interest. In the absence of Dox, the transactivator binds to the inducible promoter of the response plasmid, and activates the transcription of the downstream gene of interest. Transcription is turned off by adding Dox to the culture medium. The system is established in target cells by sequentially transfecting them with these two plasmids and selecting stable cell lines. The MCF-7 Tet-Off cell line is a stable cell line that expresses the transactivator. We successfully cloned NRG1β3GFP in the response plasmid pTRE2. This vector was subsequently transiently transfected into the MCF-7 Tet-Off cell line. When treated with Dox, the transcription of NRG1β3GFP was turned off and NRG1β3GFP expression was turned on by removing Dox from the culture medium. This transient expression assay provided a quick indication of the inducibility of NRG1β3GFP expression in the Tet-Off system.

Before developing the double-stable MCF-7 Tet-Off inducible cell line, more pilot experiments were carried out. To calibrate the effective concentration of Dox to achieve full repression of NRG1β3GFP expression, a range of Dox concentration were tested. When Dox reached 400ng/ml, NRG1β3GFP expression was completely shut down as shown in Figure 5-8. Since the tightly controlled induction of the Tet-Off system is

based on the tetracycline-regulated transcription activity, tetracycline contamination in the culture medium might have an effect on the induction level of gene expression. Due to the high cost of Tet Approved FBS (Clontech, UK), the FBS from Invitrogen (UK) was tested in our Tet-Off system for any tetracycline contamination. Using fluorescence microscopy and western blot analysis no obvious differences were observed in the induction level of NRG1β3GFP expression when cultured in these two different FBS (Figure 5-9). To generate the double-stable Tet-Off inducible cell line, the pTRE2-NRG1β3GFP vector was co-transfected along with the linear hygromycin selection marker into the MCF-7 Tet-Off cell line. Before selecting stable transfectants using hygromycin, a titration experiment was carried out to determine the optimal concentration of hygromycin for our particular cell line. By incubating MCF-7 Tet-Off cells with varying hygromycin concentrations, we found 400μg/ml hygromycin to be optimal since it was the lowest concentration that resulted in massive cell death in ~5 days and killed all the cells within two weeks. Also, several plating densities for selecting stable transfectants were tested versus the optimal hygromycin concentration. If cells become too confluent before they begin to die, some clones may be lost if they detach from the plate. Thus, the optimal plating density should allow the cells to reach ~80% confluency before massive cell death begins (at about day 5).

5.4.2 Optimising transfection efficiency

With any transfection reagent or method, there are some important parameters that can greatly influence transfection efficiency, including cell health, degree of confluency, number of passages, contamination, and DNA quality and quantity. In general, cells are recommended to be transfected at 40–80% confluency. Too few cells will cause the culture to grow poorly without cell-to-cell contact. Too many cells results in contact inhibition, making cells resistant to uptake of foreign DNA. Actively dividing cells take up introduced DNA better than non-dividing cells. The optimal amount of DNA to use in the transfection varies depending upon the type of DNA, transfection reagent, the target cell line and number of cells. Thus, optimising transfection efficiency for a particular cell line is important in order to achieve high transfection efficiency. Transfection efficiency is typically measured as the percentage of cells expressing the protein of interest for detection in the total population. In this study, GFP, as a visual marker, allowed the transfection efficiency to be calculated as the percentage of glowing green cells over the total number of cells being counted. Transfection efficiency was first optimised by comparing two different transfection reagents Lipofectamine 2000

and FuGENE 6, both are a proprietary blend of lipids and other components. Following each manufacturer's instructions, Lipofectamine 2000 provided higher transfection efficiency than FuGENE 6. To further optimise the transfection efficiency using Lipofectamine 2000, we transfected the MCF-7 Tet-Off cells at 60% confluency (in 35mm tissue culture dishes) with a fixed amount of DNA (4μg). With cell number and DNA concentration held constant, the amount of Lipofectamine 2000 was varied from 4 to 20μl to determine the optimal concentration. Three different DNA (μg): Lipofectamine 2000 (μl) ratios were tested. 25% transfection efficiency was achieved by transfecting MCF-7 Tet-Off cells with DNA: Lipofectamine 2000 ratio at 1 (4μg): 5 (20μl). The 1:1 ratio gave the lowest transfection efficiency (12.5%). Within the range being tested, it appeared that the lower the DNA: Lipofectamine 2000 ratio the higher the transfection efficiency.

5.4.3 Dilution cloning

Dilution cloning of adherent mammalian cells is a common technique used for isolation of specific mutants (Machatkova *et al.*, 1986). Our particular interest was to separate individual transfected cells in order to obtain specific clones with expression of NRG1β3GFP.

Dilution cloning involves detachment of the adherent cells from the culture dish surface. After counting and diluting to achieve a concentration suitable for obtaining single colonies, the cells are seeded in 96-well plates. To increase the probability of obtaining single cells in the wells, we made a range of dilutions aiming for 0.5, 1, 2, and 5 cells per well. Medium was not changed unless necessary and a small amount of the old medium was left to facilitate cell growth.

After cells had attached, the plates could be examined under the microscope to confirm the presence of individual cells. This procedure, however, could be very time consuming. We adapted a more simple procedure which was to wait for one week and then to examine the plates for the formation of cell colonies. Those wells with visible groups of cells were due to insufficient dilution and those wells containing no cells were due to over dilution. Those wells containing one group of cells were likely due to the proliferation of a single cell. Among the five 96-well plates with serious dilutions, I noticed that the probability of successful cloning was higher if fewer cells were seeded. In plates with lower cell densities (aimed for 0.5 cell/well), one colony can be found in

every six wells. Learning from this experience, dilution of cells to 0.5-1 cell per well would maximise the proportion of wells that contain one single clone. Also, accurate cell counting is important to obtain the best dilution.

Cloning by limiting dilution aimed to isolate individual NRG1β3GFP expressing cells and culture these to produce clones. However, even the wells that appeared to contain one single clone exhibited patchy expression. Even though every attempt was made to ensure that the cells were in single cell suspension prior to plating, it could not be guaranteed that colonies did not arise from two (or more) cells sticking together.

5.4.4 Failures of Tet-based strategies

Two explanations are possible to account for the observed heterogeneous expression patterns of NRG1β3GFP in isolated clones. The first explanation is a lack of selection pressure on NRG1β3GFP expressing cells. Heterogeneity of expression happens in transfection studies using separate transcription units for antibiotic resistance and a gene of interest. We co-transfected a linear hygromycin resistant marker along with the pTRE2-NRG1β3GFP vector into the MCF-7 Tet-Off cells, and in this approach the antibiotic resistance gene and the NRG1β3GFP gene were translated independently. As a consequence, the cells that had one gene incorporated into their genome did not necessarily contain the other gene, and vice versa. Thus selecting with the hygromycin antibiotic those NRG1β3GFP expressing cells without the hygromycin resistance gene were lost. The transfection efficiency of NRG1β3GFP was about 25% so the percentage of cells that had also incorporated the hygromycin resistance gene would be even less. Thus, the cells not expressing NRG1β3GFP but hygromycin resistant might have had a selective advantage and have grown more rapidly, finally leading to a depletion of the desired cell population. Clearly it would therefore have been preferable to use response plasmid containing both the gene of interest and the antibiotic resistance gene which would ensure translation of the two open reading frames, after selection with the antibiotic and all surviving cells should, in theory, stably express the gene of interest in a homogenous manner.

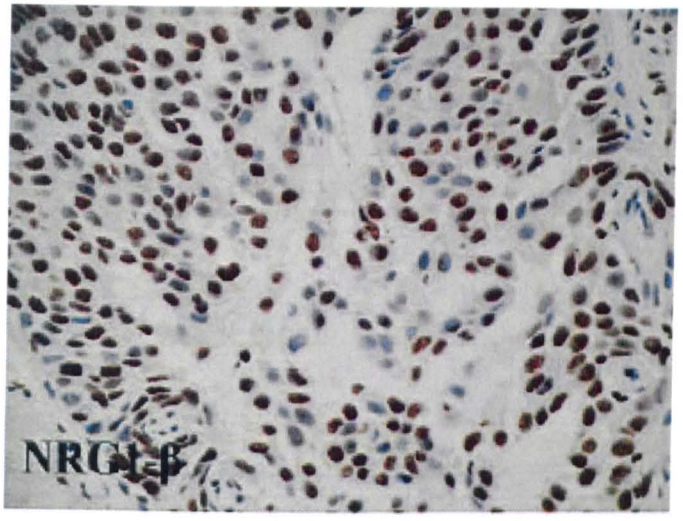

Figure 5-13. Immunohistochemical staining of human ductal carcinoma of the breast with NRG1β antibody. Figure taken from Marshall et al, 2006.

If cells had incorporated both the NRG1β3GFP plasmid and the hygromycin selection marker while showing heterogeneous NRG1β3GFP expression patterns, a second possibility was that the observed expression patterns of NRG1β3GFP were associated with the phases of the cell cycle. This hypothesis is supported by the nuclear expression patterns of NRG1β in immunohistochemical stained human ductal carcinoma tissues (Marshall et al., 2006). As shown in Figure 5-13, nuclear NRG1β expression is strong in some cells but undetectable in the adjacent cells. Similar heterogeneous NRG1β nuclear expression patterns were observed in normal skin, adrenal, thyroid tissues as well as in soft cancer tissues (see Chapter 3). One thing in common in both the immunohistochemical staining and the expression of NRG1β3 *in vitro* is that cells were not synchronised when examined. If the expression of NRG1β3GFP is turned on only at a particular phase of the cell cycle it explains why some cells expressed NRG1β3GFP while the others did not in an isolated clone.

The promising clones showing heterogeneous NRG1β3GFP expression patterns were frozen down once those clones were isolated. In the future, fluorescent activated cell sorting (FACS) (which was not available to us) may help isolate a population of Tet-Off double-stable NRG1β3GFP expressing cells and facilitate functional analysis for NRG1β3GFP expression *in vitro*.

Chapter 6. Exploring the functions of intranuclear expression of NRG1β3

6.1 Introduction

Failure to establish an inducible cell line with regulated expression of NRG1β3 lead us to seek for other approaches to explore the functions of intranuclear expression of NRG1β3. Previous mutational analyses carried out in our laboratory have mapped the amino acids responsible for either the nucleolar or the spliceosome localisation of NRG1β3. Using wild type NRG1β3 and its two mutants which could localise only at spliceosomes (FLAAA) or only in nucleoli (K69A), we explored the functions of nuclear NRG1β3 in each of these compartment separately using two different experimental approaches. One was based on "candidate" effects of intranuclear expression of NRG1β3 such as cell mitogenesis, the level of ribosomal RNA and splicing efficiency. The other screening approach aimed for new discoveries of genes whose expression was altered at either the transcriptional or the protein level.

The most prominent substructure within the nucleus is the nucleolus, which is the site of rRNA transcription and processing. Nucleoli assemble around the tandemly repeated ribosomal DNA gene clusters and 28S, 18S and 5.8S ribosomal RNAs are transcribed as a single precursor, which is processed and assembled with the 5S rRNA into ribosome subunits (Okuwaki, 2006). Cells require large number of ribosomes to meet their needs for proteins synthesis. A parallel effect on increasing cell growth by more rapid synthesis of proteins would also affect the possible rate of the cell cycle. Bouche et al. observed a correlation between the nucleolar localisation of bFGF and the stimulation of ribosomal gene transcription (Bouche et al., 1987). Thus, it would be logical to explore whether nucleolus localised NRG1β3 had any effect on ribosome synthesis. In this study, we therefore investigated how nucleolar localisation of NRG1β3 could affect the ribosomal RNA levels in transiently transfected COS-7 cells using RNA gel electrophoresis.

While the nucleolus is well-known as the centre of ribosome biogenesis, a number of mitogenic growth factors and other growth regulatory proteins have been observed to be localised there. These include parathyroid hormone-related peptide (Nguyen and Karaplis, 1998), basic fibroblast growth factor and acid fibroblast growth factor (Moroianu and Riordan, 1994). In particular, other growth factors such as Schwannoma-derived growth factor (a rat equivalent of the human Amphiregulin protein) and hepatoma-derived growth factors (HDGF) (Everett *et al.*, 2001) are able to stimulate cell growth when localised inside nuclei. Therefore, we hypothesised that nucleolar localisation of NRG1β3 might have a similar mitogenic effect. To test this hypothesis we performed a bromodeoxyuridine (BrdU) incorporation assay on COS-7 cells that were transiently transfected with wild type NRG1β3GFP, the mutant FLAAA which lost the ability to target to nucleoli, and GFP as a control. BrdU is a synthetic thymidine analogue that gets incorporated into newly synthesised DNA strands of actively proliferating cells. Following denaturation of double stranded DNA, antibodies that are conjugated to fluorescent markers bind to BrdU allowing the DNA-synthetic activity of transfected cells to be measured using fluorescence microscopy.

The other subnuclear structure where NRG1β3 accumulates is spliceosomes. Many pre-messenger RNA splicing factors have been localised to nuclear spliceosomes by immunofluorescence. Moreover, this localisation pattern is highly characterised for proteins that are involved in pre-mRNA splicing (Fu, 1995). We therefore also tested the hypothesis that NRG1β3 localised in the spliceosomes could be a component of the splicing machinery. In support of this, Li et al. reported that TGFβ can positively regulate the expression of its own splice variants in cultured trabecular cells (Li et al., 1996a). Based on the fact that at least fifteen different NRG1 isoforms exist due to rich alternative splicing and the use of multiple promoters (Steinthorsdottir et al., 2004), we hypothesised that spliceosome localisation of NRG1β3 might have a role in regulating its own gene splicing. Using the RT-PCR technique, we designed specific primers to detect the mRNA level of NRG1α in NRG1β3GFP transiently transfected MDA-MB-231 cells. Peles et al. showed that this breast cancer cell line expressed NRG1 endogenously (Peles et al., 1992). We further confirmed the transcription of NRG1α splice variant in this cell line.

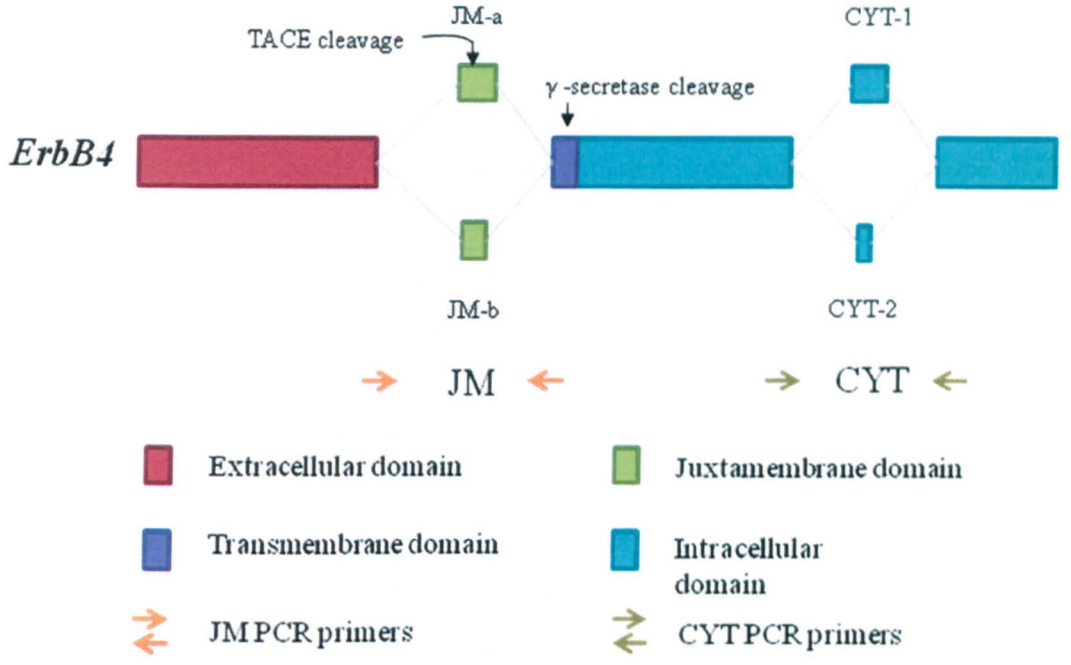

Figure 6-1. Schematic presentation of juxtamembrane (JM-a and JM-b) and cytoplasmic (CYT-1 and CYT-2) ErbB4 isoforms. Sites to which PCR primers are targeted are indicated. Figure adapted from Elenius et al, 1999.

NRG1 is a direct ligand of the ErbB4 receptor and a feature unique among ErbB receptors is that ErbB4 pre-mRNA is alternatively spliced either at the extracellular juxtamembrane region or at the intracellular cytoplasmic tail, generating four structurally different isoforms (Figure 6-1). Evidence has shown that the proteolytic cleavage processing of ErbB4 is promoted by binding of its cognate ligands including neuregulin (Zhou and Carpenter, 2000). There are several examples of EGF-like ligands inducing expression of other ligands of the same family and of their receptors. For instance, an autocrine loop of TGFα has been described in human colon carcinoma cells that express EGF/EGFR (Howell et al., 1995). Here, we hypothesised that the spliceosome localisation of NRG1β3 might be involved in the alternative splicing of ErbB4 pre-mRNA. To investigate the effects of NRG1β3 on ErbB4 splicing RT-PCR was carried out on NRG1β3 transiently transfected breast cancer T47D cell line in which high levels of ErbB4 mRNA have been detected previously (Gilmour *et al.*, 2001).

In addition to the approach based on "candidate" effects aforementioned, we explored the functions of intranuclear localisation of NRG1β3 using the discovery approaches of kinomic and transcriptomic analysis. Growth factors mediate diverse biological

responses by binding to and activating cell surface receptors that have intrinsic protein kinase activity. RTKs are the main mediators of the signalling network that transmit extracellular signals into the cell. They have been viewed as functioning at the cell surface; however, evidence has now accumulated that some cell surface RTKs translocate to the nucleus. Both intact full-length receptors and fragments corresponding to the intracellular domain (ICD) have been identified in the nuclei of various cells and tissues. The best described examples of intact receptors in the nucleoplasm include FGFR1 and the EGFR, ErbB2, and ErbB3 family members (Carpenter, 2003; Wells and Marti, 2002). As mentioned above, the ErbB4 receptor is cleaved constitutively following binding of the ligand NRG (Ni et al., 2001). Two successive proteolytic cleavages release the ICD of ErbB4, which then translocates to the nucleus. Even though nuclear localisation of NRG1β3 has been shown to be receptor independent (Golding et al., 2004), this does not exclude the possibility that a receptor mediated function could occur in the nucleus. Using wild type NRG1β3 and its two mutants which could localise only at spliceosomes (FLAAA) or only in nucleoli (K69A), we investigated whether localisation of the NRG1β3 either in nucleoli or in spliceosomes had any effects on the differential expression or phosphorylation levels of fourty two human RTKs by using the phospho-RTK array technique.

It is not clear yet how the intranuclear expression of NRG1β3 is involved with normal physiological conditions as well as in human cancers; however, several NRG-responsive target genes have been identified to regulate malignant tumour progression (Bagheri-Yarmand et al., 2000; Mandal et al., 2002; Mazumdar et al., 2001). In a yeast two-hybrid screen, NRG was found to interact specifically with several proteins implicated in transcriptional regulation (Breuleux et al., 2006), supporting the hypothesis that nuclear NRG may be directly implicated in transcriptional control. With the availability of the two mutants of NRG1β3 which exhibited exclusive subnuclear localisation patterns we examined how NRG1β3 might directly regulate gene transcription by performing a transcriptomic analysis.

6.2 Aims

1. Using mutants of NRG1 localising to different subnuclear compartments we aimed to quantify the amount of 28S and 18S ribosomal RNA as an assay for possible effects on nucleoli function.

2. To observe the effects of nucleolar localisation of NRG1β3 on cell growth using BrdU labelling followed by immunofluorescence analysis.

3. To investigate the possible effects of intranuclear NRG1β3 on NRG1 and ErbB4 splicing.

4. To examine the effects of differential subnuclear localisation of NRG1β3 on the expression and/or phosphorylation of fourty two RTKs using the Human Phospho-RTK Array.

5. To determine whether localisation of the NRG1β3 protein either in nucleoli or in spliceosomes alters gene transcription profile using the Illumina's Gene Expression Arrays.

6.3 Results

6.3.1 Effects of nucleolar targeting of NRG1β3 on ribosomal RNA levels

To obtain optimal RNA yields and minimise differences due to experimental procedures $5x10^6$ COS-7 cells were plated into five T25 tissue culture flasks. Wild type NRG1β3GFP, the FLAAA mutant or GFP were transiently transfected into the cells. Mock transfection was performed at the same time and one flask of COS-7 cells was left without any treatment. 24h post transfection total cellular RNA was extracted from each of the five samples using the RNeasy Mini Kit (Qiagen, UK) and then treated with DNase I (Invitrogen, UK) to remove genomic DNA contamination. The purity of the RNA was checked by spectrometry to ensure that the A260/A280 ratios ranged between 1.8 and 2.0, typical values for high quality RNA. The extracted total RNA samples were run on a 1% formaldehyde agarose gel which was then stained with SYBR Green (Invitrogen, UK). Figure 6-2 shows that the RNA appeared as two bright discrete bands that represent the 28S and 18S ribosomal species. Since mammalian 28S and 18S rRNA are approximately 5kb and 2kb in size, a 2:1 of 28S:18S ratio of signal intensity is considered as an indication for intact RNA. No background smear behind these bands that gets heavier at lower molecular weights indicated no significant degradation of the RNA had occured. Also, the absence of sharp bands higher than the 28S ribosomal band indicated no genomic DNA contaminations in the sample. After the integrity and purity of the extracted total RNA samples was confirmed, the intensity of ribosomal RNA on the gel image was analysed using ImageJ software.

When quantifying the 28S and 18S rRNA species across all the samples, we used the rRNA level of NRG1β3GFP as a reference against which other rRNA values could be compared. In Figure 6-3, no significant variations existed among samples however taking into account the limited sample number (n=3) and the variances that existed during the experimental procedures, including the amount of RNA loaded, electrophoresis conditions and saturation of SYBR Green fluorescence, we would have to repeat this experiment before drawing any conclusions. However, within the limited time available we did not pursue this question further.

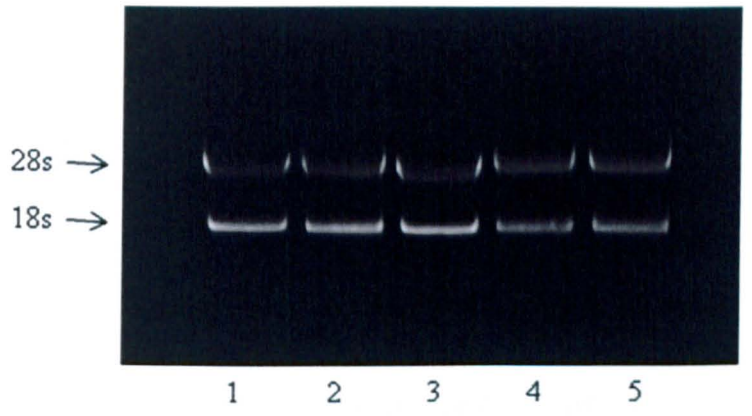

Figure 6-2. Formaldehyde agarose gel (1%) of ribosomal RNA analysis of total RNA extracted from COS-7 cells with or without transfection. Lane 1: NRG1β3GFP. Lane 2: FLAAA. Lane 3: GFP. Lane 4: mock transfection. Lane 5: no treatment. 10μl of total RNA isolated from each sample was loaded per lane. The photograph shows a representative result of triplicate experiments.

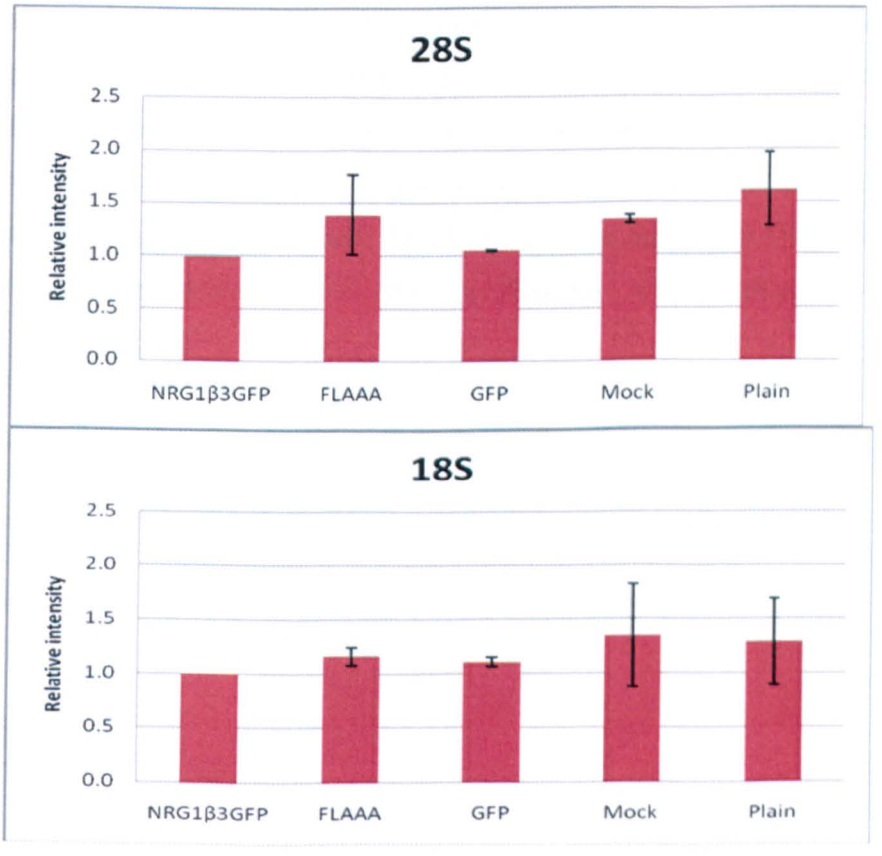

Figure 6-3. Quantitative analyses of rRNA species in COS-7 cells with and without treatments. The rRNA level of NRG1β3GFP was used as a reference for sample comparisons. The data are presented as the mean ± SE (standard deviation). p=0.17 for 28S and p=0.07 for 18S when analysed with the one way analysis of variance (one-way ANOVA).

6.3.2 Effects of nucleolar targeting of NRG1β3 on mitogenesis

To test whether nucleolar targeting of NRG1β3 could be involved in regulating cell mitogenesis, COS-7 cells were transiently transfected with wild type NRG1β3GFP, FLAAA, or GFP as a control. For DNA synthesis analysis, cells were pulsed with 10mM BrdU for 24h. Immunofluorescence staining was performed by incubating the permeablised cells with the monoclonal anti-BrdU antibody (Sigma, UK) followed by the Alexa Fluor 633 secondary antibody (Sigma, UK). The transfected cells were examined using confocal fluorescence microscopy for BrdU incorporation as a marker of DNA synthesis.

BrdU incorporation of each construct in COS-7 cells was measured by counting how many green cells (expressing the transfected gene) were also red (indicating incorporation of BrdU) (indicated by arrows in Figure 6-4a). Cells were counted from 3 randomly selected fields (100 green cells/field). 27% of cells transfected with GFP vector were BrdU positive, 24% of cells transfected with wild type NRG1β3 were BrdU positive, and 22% of cells transfected with FLAAA mutant were BrdU positive (Figure 6-4b). Nucleolar localisation of NRG1β3 increased DNA synthesis by 2% compared to the mutant which lost the ability to target to the nucleolus. If $p<0.05$ was considered statistically significant, these data had a p value equal to 0.13 when analysed with the one-way analysis of variance (one-way ANOVA), which indicated no effect.

a

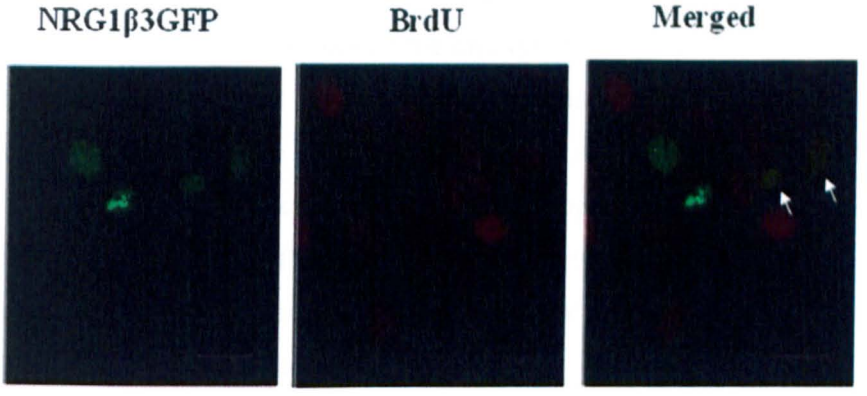

b

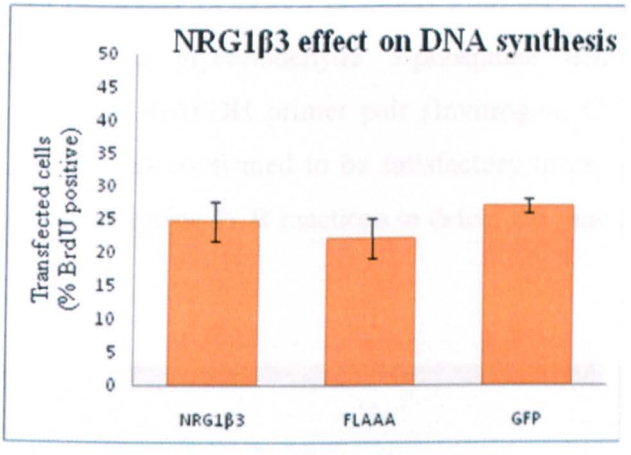

Figure 6-4. Functional effect of NRG1β3 nucleolar localisation on DNA synthesis. (a) Expression of NRG1β3GFP and BrdU incorporation in COS-7 cells. Transfected COS-7 cells were pulsed with 10mM BrdU for 24h. Immunofluorescence staining images of BrdU treated cells are shown. NRG1β3GFP transfected cells are green due to GFP expression, whereas BrdU positive cells are red as they were labelled with the red dye Alexa Fluor 633. The overlap of green and red indicates stimulated BrdU incorporation in the transfected cells. (b) Graphical representation showing percentage of transfected cells that were BrdU-positive (±SE) from immunofluorescence analysis. N=100 cells were counted for each construct and each experiment was repeated twice.

6.3.3 Splicing assay

6.3.3.1 RT-PCR analysis of NRG1 splicing

To examine the effects of subnuclear localisation of NRG1β3 on its own gene splicing we performed a RT-PCR analysis on the MDA-MB-231 cell line which endogenously expresses NRG1. MDA-MB-231 cells were growing in seven T25 tissue culture flasks and were transiently transfected with wild type NRG1β3GFP, the mutants FLAAA and

K69A, or GFP as a control, using the Lipofectamine 2000 transfection reagent. Mock transfection was performed at the same time and one flask of MDA-MB-231 cells was left with no treatment. 24h post transfection total cellular RNA was extracted from the seven samples using the RNeasy Mini Kit (Qiagen, UK) followed by DNase I treatment. The purity of the RNA was checked by spectroscopy. Reverse transcriptions was performed with a First-strand cDNA synthesis kit (Invitrogen, UK) using the oligo-dT primer provided (as described in Section 2.3). 50μl of cDNA from each sample was used for each subsequent PCR reaction.

To verify the reliability of cDNA prepared from each sample, a 500bp region of the house-keeping gene glyceraldehyde 3-phosphate dehydrogenase (GAPDH) was amplified using the GAPDH primer pair (Invitrogen, UK) (data not shown). As the quality of cDNA was confirmed to be satisfactory these cDNA samples were used as templates in the following PCR reactions to detect the transcription level of NRG1α.

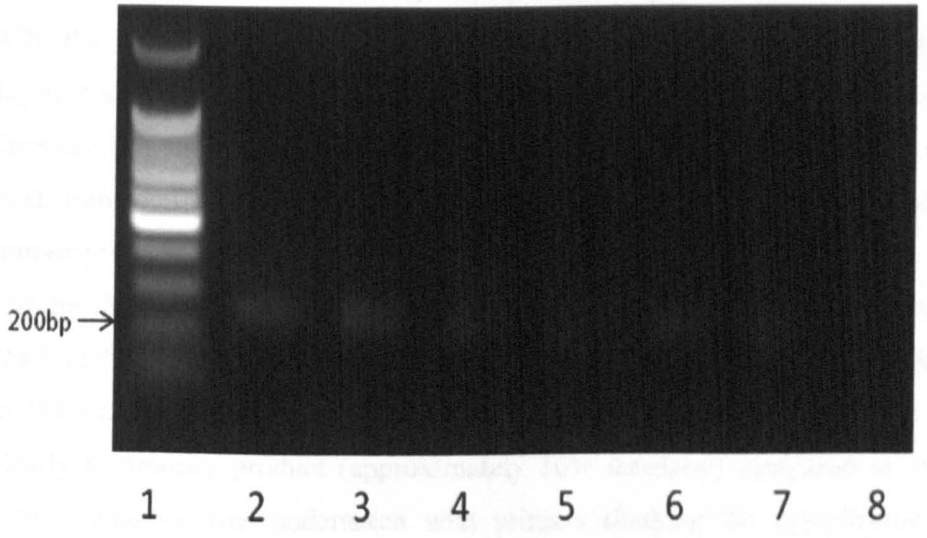

Figure 6-5. RT-PCR analysis of NRG1 isoforms in MDA-MB-231 cells transfected with different constructs. NRG1β3GFP (Lane 2), FLAAA (Lane 3), K69A (Lane 4), GFP (Lane 5), mock (Lane 6), no treatment (Lane 7) and negative control using deionised water instead of cDNA (Lane 8). 10μl samples were loaded each lane. Amplified PCR products were detected using a 2% agarose gel stained with SYBR Green for UV visualisation.

A pair of primers NRG1α-F and NRG1α-R, was designed specifically to detect the NRG1α isoform. The PCR reactions were set up as described in Section 2.4.1(annealing temperature: 52°C) and the products of the reaction were analysed on a 2% agarose gel. A band of 247bp corresponding to NRG1α was observed in all samples as shown in Figure 6-5. The band detected in the MDA-MB-231 cells without any treatment (Figure 6-5, Lane 7) confirmed that NRG1α is expressed endogenously in this cell line. The amount of NRG1α PCR products was very similar in the MDA-MB-231 cells transfected with wild type NRG1β3GFP and mutants FLAAA and K69A, suggesting that neither the nucleolar nor spliceosome localisation of NRG1β3 had any obvious effect on the NRG1α mRNA expression levels.

6.3.3.2 RT-PCR analysis of ErbB4 splicing

Several splice variants of ErbB4 have been reported, which were predicted to initiate different signalling events and to have differing functions (Elenius et al., 1999). It was therefore of interest to examine the effects of intranuclear localisation of NRG1β3 on the transcription level of ErbB4 splice variants. T47D cells were transiently transfected with the wild type NRG1β3GFP, the mutants FLAAA and K69A, or GFP using the Lipofectamine 2000 transfection reagent. Mock transfection was performed at the same time and one flask of cells was left without any treatment. As described previously, 24h post transfection total RNA was isolated from those cells, subjected to reverse transcription and analysed by primers flanking the JM and CYT regions (Figure 6-1). For the JM region, the expected product size for the JM-a cDNA was 414bp and for the JM-b cDNA, 375bp. After separation on a 2% agarose gel, bands corresponding in size to JM-a and JM-b were observed in all samples (Figure 6-6a). The JM-a isoform was clearly a minority product (approximately 10% intensity) compared to JM-b form. A similar analysis was undertaken with primers flanking the cytoplasmic site. In the RT-PCR reactions, products consistent with the CYT-1 (275bp) and CYT-2 (313bp) isoforms were identified (Figure 6-6b). Expression levels appeared to be the same for both isoforms among the samples (Figure 6-6). Taken together, intranuclear localisation of NRG1β3 had no obvious effect on the transcription level of the ErbB4 isoforms.

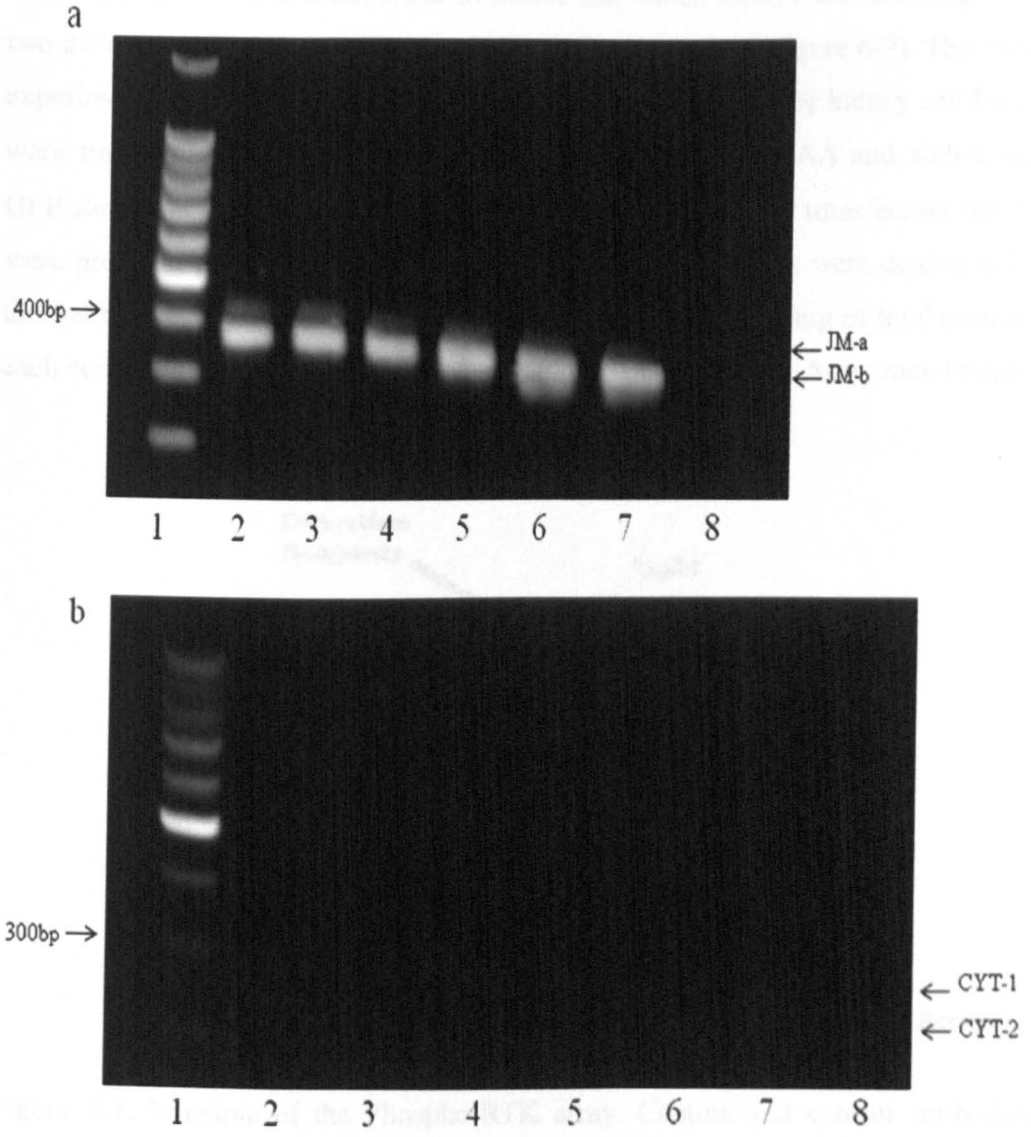

Figure 6-6. RT-PCR analyses of ErbB4 isoforms in T47D cells transfected with different constructs. (a) Expression of the ErbB4 JM-a and JM-b isoforms. (b) Expression of the ErbB4 CYT-isoforms. NRG1β3GFP (Lane 2), FLAAA (Lane 3), K69A (Lane 4), GFP (Lane 5), mock (Lane 6), no treatment (Lane 7) and negative control using deionised water instead of cDNA (Lane 8). 10µl samples were loaded each lane. Amplified PCR products were detected using a 2% agarose gel stained with SYBR Green for UV visualisation.

6.3.4 Intranuclear localisation of NRG1β3 led to differential expression or phosphorylation of RTKs

The Human Phospho-Receptor Tyrosine Kinase (Phospho-RTK) Array (R&D

Biosciences, UK) is a commercial available kit, which allows the screening of fourty two different phosphorylated human RTKs at the same time (Figure 6-7). The following experiment was performed on the HEK-293, a human embryonic kidney cell line. Cells were transiently transfected with NRG1β3GFP, mutants FLAAA and K69A, or with GFP alone using the FuGENE 6 transfection reagent. 24h after transfection cell lysates were prepared using NP-40 lysis buffer. Protein concentrations were determined using the standard Bradford assay (as described in Section 2.5.2). 200μg of total protein from each condition was incubated on separate Human Phospho-RTK Array membranes.

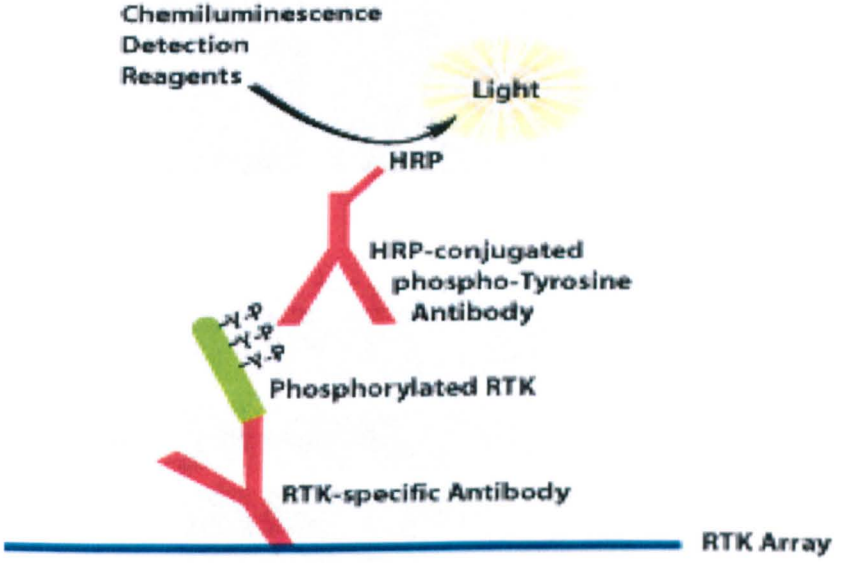

Figure 6-7. Principle of the Phospho-RTK array. Capture and control antibodies are spotted in duplicate on nitrocellulose membranes. Cell lysates are diluted and incubated with the membranes. After binding of both phosphorylated and unphosphorylated RTKs, unbound material is washed away. A pan anti-phospho-tyrosine antibody conjugated to horseradish peroxidase (HRP) is then used to detect phosphorylated tyrosines on activated receptors by chemiluminescence. Figure taken from http://www.rndsystems.com/.

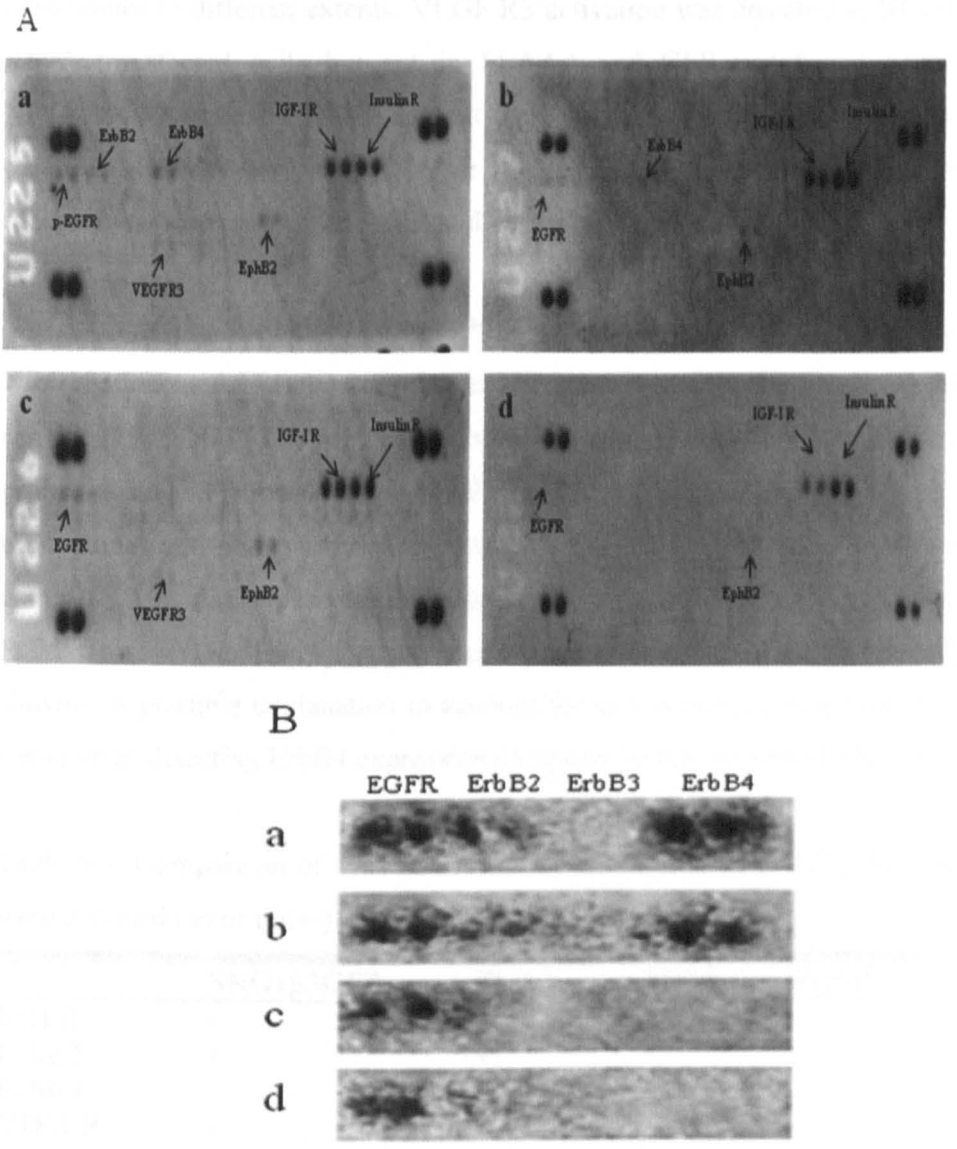

Figure 6-8. Differential phosphorylation of RTKs in transfected HEK-293 cells. HEK-293 cells were transiently transfected with NRG1β3GFP (a), the mutant constructs FLAAA (b) and K69A (c), or with GFP alone (d). Cell lysates were prepared 24h after transfection and analysed by the Human Phospho-RTK Array (R&D Systems). Image B is a closeup of part of image A with brightness increased by 5% and contrast increased by 95%.

The human growth factor receptor tyrosine kinases were differentially expressed and/or activated in HEK-293 cells transfected with different constructs (Figure 6-8). Detected RTK signals are listed in Table 6-1. Of 42 RTKs evaluated on the array membrane for this study, activation of EGFR, IGF-I R, Insulin R and EphB2 were detected on all four

membranes to different extents. VEGF R3 activation was detected in NRG1β3GFP and K69A transfected cells but not in FLAAA and GFP transfected cells. Wild type NRG1β3GFP and the FLAAA mutant increased the phosphorylation and/or expression of the ErbB4 receptor and to a lesser extent the ErbB2 receptor. No increase in either receptor was detected in the K69A and GFP transfected cells.

We attempted to further evaluate ErbB4 expression using western blot analysis. The NRG1β3GFP and FLAAA transfected cell lysates used in the above experiment were run on a 7% SDS PAGE gel. Proteins were transferred to a nitrocellulose membrane and probed using a mouse monoclonal anti-ErbB4 antibody (HFR1) and a mouse monoclonal anti-phospho-tyrosine antibody (PY20), respectively. Blots were labelled using a rabbit anti-mouse HRG-conjugated secondary antibody and developed using ECL. However, no corresponding bands were detected using either antibody (data not shown). A possible explanation to account for this is that western blot analysis is less sensitive in detecting ErbB4 expression compared to the Phospho-RTK Array technique.

Table 6-1. Comparison of activated RTKs in transfected HEK-293 cells. Either signals were detected (+) or not (-).

	NRG1β3GFP	FLAAA	K69A	EGFP
EGFR	+	+	+	+
ErbB2	+	+	-	-
ErbB4	+	+	-	-
IGF-I R	+	+	+	+
Insulin R	+	+	+	+
VEGF R3	+	-	+	-
EphB2	+	+	+	+

6.3.5 No secreted NRG1β3 was detected in the conditioned medium

The Human Phospho-RTK Array analysis showed increased phosphorylation and/or expression of ErbB4 in NRG1β3GFP and FLAAA transfected HEK-293 cells. Whether the anti-ErbB4 antibody spotted on the array membrane recognised the extracellular or the intracellular domain of ErbB4 was unknown as this was not stated in the manufacturer's literature. To our knowledge, only the cytoplasmic domain of ErbB4 has been reported to be present in the nucleus (Williams et al., 2004) and the majority of evidence suggests that no full length ErbB4 translocates to the nucleus. Since NRG1 is a direct ligand of ErbB4, we next investigated whether any secreted form of NRG1β3

might exist that can bind and activate ErbB4 at the cell membrane, even though this could not explain why only one of the mutants of NRG1β3 was able to activate ErbB4 in the kinomic assay. In the following experiments, the conditioned medium of NRG1β3GFP transfected HEK-293 cells was collected and analysed by western blotting.

HEK-293 cells were plated into 35mm culture dish containing 2ml of growth medium and transfected with the NRG1β3GFP construct. 6h after transfection growth medium was changed to 1ml to enrich the protein concentration in the medium. 24h post transfection conditioned medium was collected followed by cell lysis. 30μl of three two-fold cell lysate dilutions were loaded on a 7% SDS PAGE gel along with 30μl of the conditioned medium. Proteins were transferred to a nitrocellulose membrane and probed using a monoclonal anti-GFP antibody, GFP3E1. Based on the running pattern of the conditioned medium (Figure 6-9 Lane 6), we suspected that there was an interference of albumin. Bovine serum albumin (BSA) is a major component of fetal bovine serum, which is a widely used growth supplement for cell culture media (Zunszain et al., 2003). It is the most abundant plasma protein and has a molecular weight of 66kDa, very close to the molecular weight of NRG1β3GFP. To mimimise the interference of albumin on the SDS-PAGE gel, we reduced the FBS concentration from 10% to 0.5% in the culture medium.

HEK-293 cells were transfected with wild type NRG1β3GFP or GFP alone as a control. 6h post transfection, media in both dishes were changed to 1ml containing 0.5% FBS. Conditioned media were collected and cell lysates were prepared 24h after transfection. 1:2, 1:4 and 1:8 dilutions were made from each cell lysate. 30μl of conditioned medium from each condition was loaded on a 7% SDS PAGE gel. After electrophoresis and transfer to nitrocellulose they were probed with the anti-GFP antibody. A signal representing GFP expression was detected in all dilutions of GFP transfected cell lysates (Figure 6-10 Lane 2-4). NRG1β3GFP expression at the predicted molecular weight was detected in the cell lysate with the lowest dilution factor (Figure 6-10 Lane 8). Reducing the FBS concentration from 10% to 0.5% did eliminate the albumin interference. No bands were detected in the conditioned medium of HEK-293 cells transfected with either construct (Figure 6-10 Lane 5 & 11). However, it did not rule out the possibility that NRG1β3 might be secreted from the producing cell but at levels too low to be detected by western blot analysis.

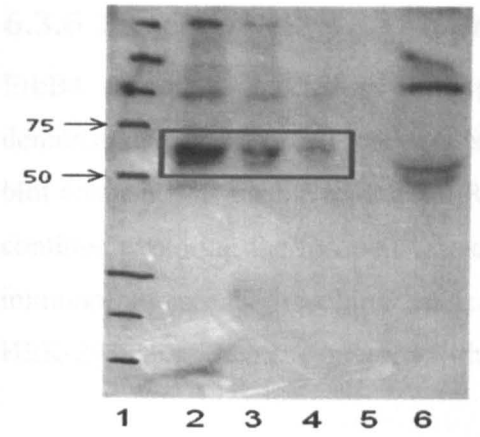

WB: GFP3E1 (10μg/ml)

Figure 6-9 Western blot analysis of NRG1β3 expression in transfected HEK-293 cells and in conditioned medium containing 10% FBS. HEK-293 cells were transiently transfected with the NRG1β3GFP construct. Conditioned medium was collected 24h after transfection and run on a 7% SDS PAGE gel (Lane 6) along with the cell lysates of the transfected cells at 1:2 (Lane 2), 1:4 (Lane 3), and 1:8 (Lane 4) dilutions. The blot was probed with the anti-GFP antibody, GFP3E1. Lane 1: molecular weight markers. Lane 5: blank.

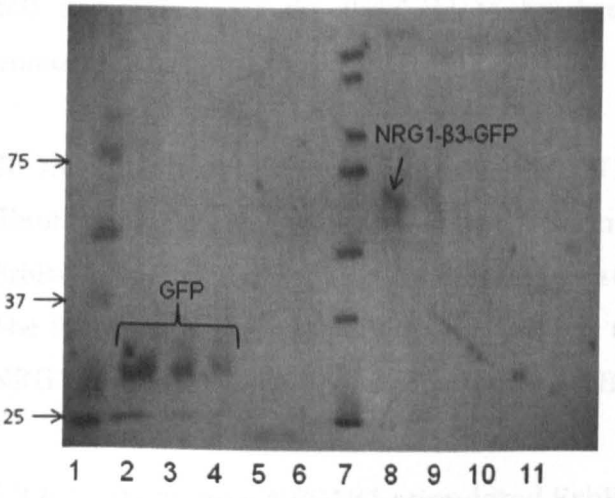

WB: GFP3E1 (10μg/ml)

Figure 6-10. Western blot analysis of NRG1β3 expression in transfected HEK-293 cells and in conditioned medium containing 0.5% FBS. HEK-293 cells were transiently transfected with the NRG1β3GFP construct. Conditioned medium was collected 24h after transfection and run on a 7% SDS PAGE gel (Lane 11) along with cell lysates at 1:2 (Lane 8), 1:4 (Lane 9), and 1:8 (Lane 10) dilutions. HEK-293 cells were also transfected with the GFP construct as a control. Conditioned medium was loaded in Lane 5. Cell lysates from GFP transfected cells were run at 1:2 (Lane 2), 1:4 (Lane 2), and 1:8 (Lane 4) dilutions. Lane 6: blank. Lane 1 and 7: molecular weight markers. The blot was probed with the anti-GFP antibody, GFP3E1.

6.3.6 Effects of NRG1β3 on ErbB4 expression

ErbB4 activation detected in NRG1β3GFP and FLAAA transfected HEK-293 cells demonstrated that this cell line expresses endogenous ErbB4 protein. Previous western blot analysis was unable to detect NRG1β3 expression in the conditioned medium. To continue exploring the location where ErbB4 was activated by NRG1β3 we turned to immunofluorescence labelling to examine the localisation patterns of ErbB4 in HEK-293 cells when coexpressed with NRG1β3GFP.

HEK-293 cells were grown on coverslips and transfected with the NRG1β3GFP construct. 24h post transfection, cells were fixed and permeablised. This would allow receptor expression inside the cell as well as that on the surface to be detected. The cells were incubated with mouse monoclonal antibody HFR-1 which is specific to the cytoplasmic domain of ErbB4, and labelled with rabbit anti-mouse Alexa Fluor 633 secondary antibody (Invitrogen, UK). Using confocal microscopy no fluorescence was detected either in the transfected cells or cells without any transfection (data not shown). We therefore suspected that the level of endogenous ErbB4 expression in the HEK-293 cell line was under the threshold to be detected by either western blotting or immunofluorescence staining.

To solve this problem we turned to the NIH3T3-ErbB4 cell line, which is a mouse fibroblast cell line stably transfected with a plasmid encoding ErbB4. The expression of ErbB4 in this cell line has been confirmed by western blot analysis (Cohen et al., 1996). The following experiments utilised this cell line to continue investigating the effect of NRG1 on the expression and/or activation of ErbB4.

6.3.6.1 Exogenous NRG1β1 stimulated ErbB4 phosphorylation in the NIH3T3-ErbB4 cell line

Before testing the effect of NRG1β3 on ErbB4 activation, the NIH3T3-ErbB4 cells were treated with exogenous NRG1β1 as a positive control. One of the duplicate 35mm tissue culture dishes of NIH3T3-ErbB4 cells was treated with 100 ng/ml of recombinant NRG1β1 for 10min, leaving the second dish untreated. The cell lysates of stimulated and unstimulated NIH3T3-ErbB4 cells were subjected to electrophoresis on a 7% SDS-PAGE gel and were blotted onto a nitrocellulose membrane. Antibodies used in detection were HFR1 (monoclonal anti-ErbB4 antibody), PY20 (monoclonal anti-phosphotyrosine antibody) (Invitrogen, UK), and Ty984 (polyclonal

anti-phospho-ErbB4 antibody) (Cell Signalling, UK), respectively. Under basal growth conditions, basal expression of ErbB4 was detected in the NIH3T3-ErbB4 cell line (Figure 6-11a, Lane 2). Neither tyrosine phosphorylation nor site-specific tyrosine phosphorylation of ErbB4 was detected (Figure 6-11b and c, Lane 2). Following treatment with NRG1β1 (100ng/ml) a band shift was observed in Figure 6-11a Lane 3, suggesting that ErbB4 became phosphorylated upon NRG1 stimulation. Figure 6-11b shows that treatment of NIH3T3-ErbB4 cells with NRG1β1 stimulated tyrosine phosphorylation, indicated by the appearance of a band corresponding to the molecular weight of ErbB4. No signal for the site-specific tyrosine phosphorylation of ErbB4 was detected even with NRG1 stimulation, although many non-specific bands of other molecular weight were seen (Figure 6-11c). The reliability of this commercial antibody remains to be confirmed.

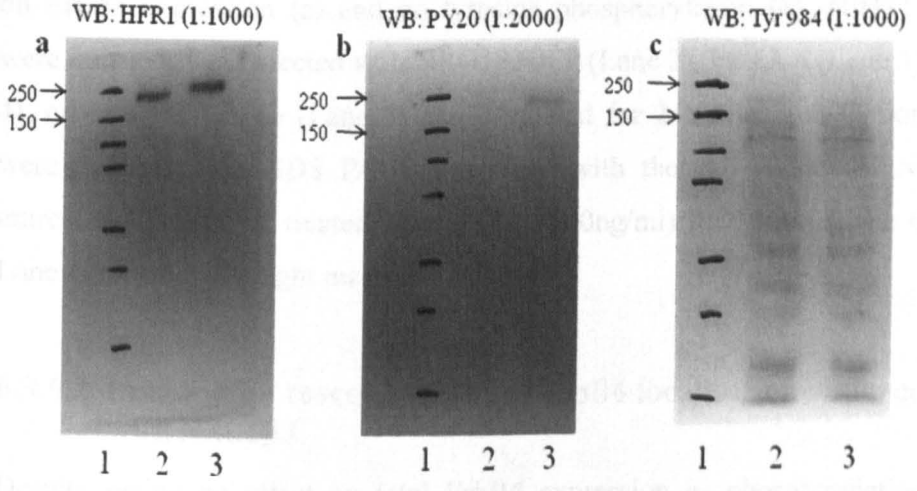

Figure 6-11. Western blot analyses of NIH3T3-ErbB4 cell lysates untreated (Lane 2) or stimulated with NRG1β1 (100ng/ml) for 10min (Lane 3). Lane 1: molecular weight markers.

In order to determine whether expression of NRG1β3 in different subnuclear compartments might affect activation or expression of ErbB4, NIH3T3-ErbB4 cells were transiently transfected with NRG1β3GFP, the mutants FLAAA and K69A, or GFP alone. Cells were lysed 24h after transfection. Cell lysates were run on a 7% SDS PAGE gel, and probed with the HFR1 and PY20 antibodies, respectively. In terms of the expression level of ErbB4, no observable differences were detected due to the expression of any of the four constructs (Figure 6-12a), nor was tyrosine phosphorylation detectable (Figure 6-12b) except in the positive control.

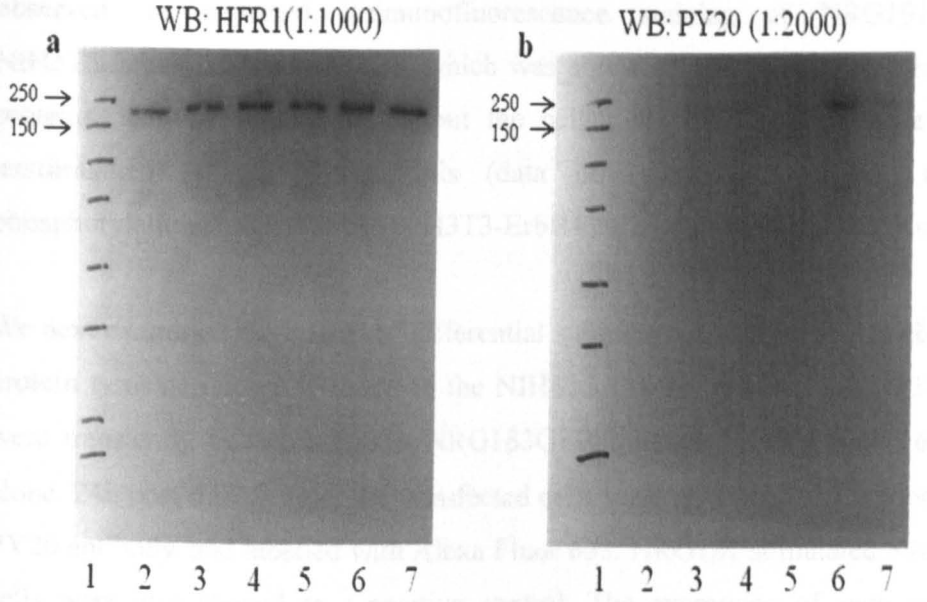

Figure 6-12. Western blot analyses of the effects of intranuclear localisation of NRG1β3 on ErbB4 expression (a) and on tyrosine phosphorylation (b). NIH3T3-ErbB4 cells were transiently transfected with NRG1β3GFP (Lane 2), FLAAA (Lane 3), K69A (Lane 4), or with GFP alone (Lane 5) and incubated for 24h after transfection. Cell lysates were run on a 7% SDS PAGE gel along with the cell lysates of NIH3T3-ErbB4 untreated (Lane 7) or treated with NRG1 (100ng/ml) for 10min (Lane 6) as controls. Lane 1: molecular weight markers.

6.3.6.2 Immunofluorescence study of ErbB4 localisation when coexpressed with NRG1β3

Despite seeing no effect on total ErbB4 expression or phosphorylation it remained possible that a small fraction of the protein might be activated at a specific location in cells. Immunofluorescence staining was therefore carried out to examine the effects of NRG1β1 stimulation on the subcellular localisation of ErbB4 on the NIH3T3-ErbB4 cell line. NIH3T3-ErbB4 cells were grown on coverslips and stimulated with 100ng/ml of recombinant NRG1β1 for 10min. Cells were fixed, permeablised, and incubated with the HFR1 and PY20 antibodies, respectively. Alexa Fluor 633 was used as the secondary antibody for labelling. Negative controls were performed at the same time to ensure that there was no non-specific binding of the antibody.

Subcellular localisation of ErbB4 was examined in NRG1β1 stimulated NIH3T3-ErbB4 cells by confocal immunofluorescence microscopy. Membrane staining of ErbB4 was detected with the HFR1 antibody. Cytoplasmic and peri-nuclear staining was also

observed, as expected. Immunofluorescence staining of NRG1β1 stimulated NIH3T3-ErbB4 cells with PY20, which was able to detect all tyrosine phosphorylated proteins, showed signals throughout the cells. No PY20 signals were detected in unstimulated NIH3T3-ErbB4 cells (data not shown), suggesting the tyrosine phosphorylation detected in the NIH3T3-ErbB4 cells was due to NRG1β1 stimulation.

We next examined the effects of differential subnuclear localisation of NRG1β3 on the protein tyrosine phosphorylation in the NIH3T3-ErbB4 cell line. NIH3T3-ErbB4 cells were transiently transfected with NRG1β3GFP, mutants FLAAA and K69A, or GFP alone. 24h post transfection, the transfected cells were permeablised, incubated with the PY20 antibody, and labelled with Alexa Fluor 633. NRG1β1 stimulated NIH3T3-ErbB4 cells were also stained as a positive control. The expression of each construct was confirmed using confocal microscopy. When excited with He-Ne 633nm laser light, PY20 signals were detected in NRG1β1 stimulated NIH3T3-ErbB4 cells but not in any of the transfected cells (data not shown). The results of kinomic assay demonstrated that NRG1β3 stimulated expression and/or activation of ErbB4. However, we were unable to confirm this using either western blot analysis or immunofluorescence microscopy.

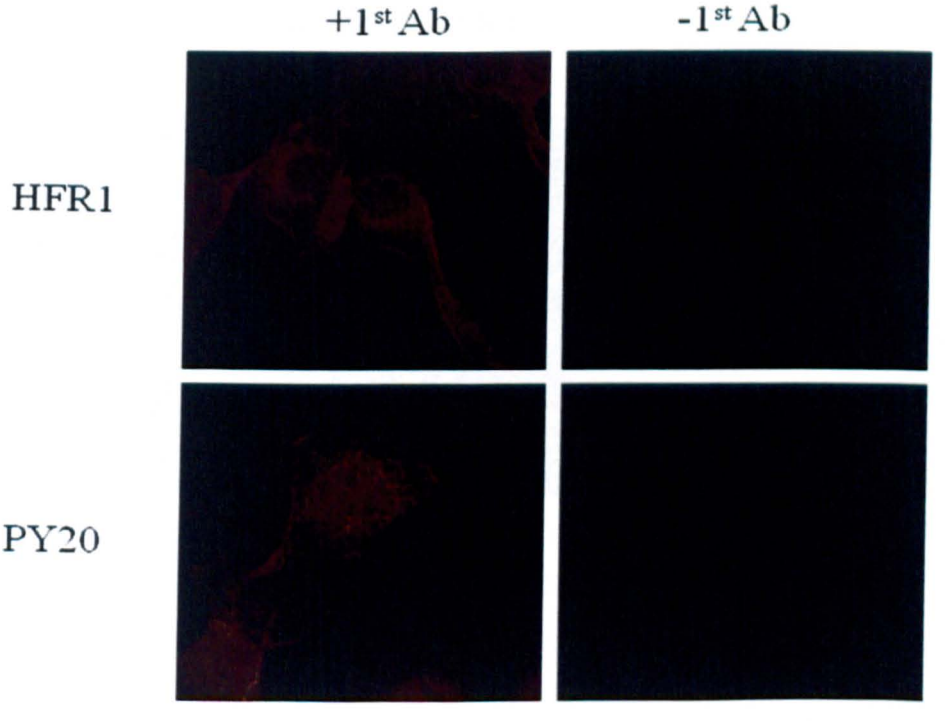

Figure 6-13. Effects of NRG1 stimulation on ErbB4 studied using confocal immunofluorescence microscopy. NIH3T3-ErbB4 cells were treated with recombinant NRG1β1 (100ng/ml) for 10min and immunostained using the HFR1 and PY20 antibodies, and labelled with Alexa Fluor 633. Original magnification: x63.

6.3.7 Analysis of the effect of differential subnuclear localisation of NRG1 on gene transcription

6.3.7.1 Differential subnuclear localisation of NRG1 regulates genes differentially

In order to determine whether localisation of the NRG1β3 protein either in nucleoli or in spliceosomes altered gene transcription we utilised wild type NRG1β3GFP and two mutants which could, as described above, localise only at spliceosomes (K69A) or only in nucleoli (FLAAA). To obtain optimal RNA yields and minimise differences due to experimental procedures, $5x10^6$ HEK-293 cells were plated into three T25 tissue culture flasks. The transient transfections were performed using the Lipofectamine 2000 transfection reagent (as described in Section 2.1.5.2). 24h post transfection, transfection efficiency was approximately 50% in each case when examined under low light digital fluorescence microscopy (Figure 6-14) and the subnuclear localisation patterns of each construct were confirmed. Total cellular RNA was subsequently extracted using the RNeasy Mini Kit (Qiagen, UK) followed by DNase I (Invitrogen, UK) treatment to remove genomic DNA contamination. The purity of the RNA was checked by spectroscopy to ensure that the A_{260}/A_{280} ratios ranged between 1.8 and 2.0 demonstrating the high quality of the RNA.

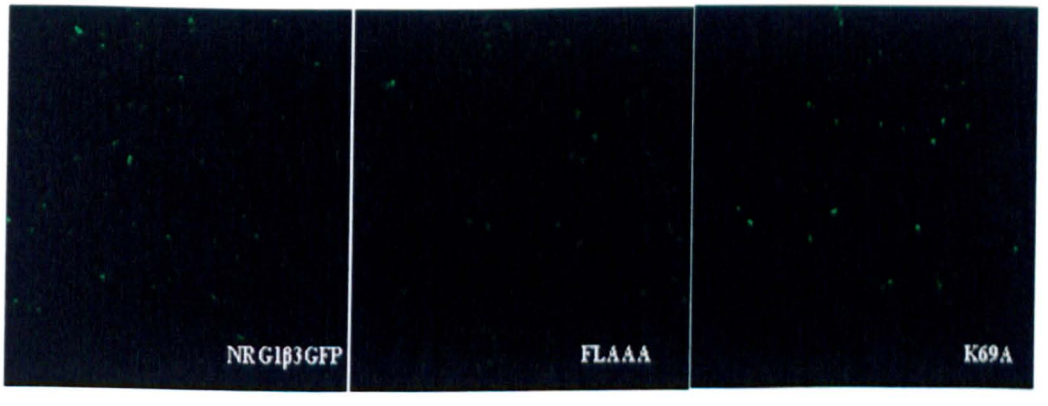

Figure 6-14. Expressions of NRG1β3 and its mutants in HEK-293 cells. HEK-293 cells were transiently transfected with wild type NRG1β3GFP, and the mutants FLAAA and K69A. Transfection efficiency was examined using digital fluorescence microscopy. Original magnification: x10.

Total RNA prepared from each condition was sent to and analysed by Source BioScience Geneservice (Nottingham, UK). The concentration and quality of the total RNA was further assessed by spectrophotometry. Samples in duplicate were normalised and were hybridised to the Illumina's Gene Expression Arrays Human WG-6 v3 BeadChip. The array intensity data was analysed using the Illumina GenomeStudio software v2009.1. Individual mRNA species were quantified. Those which showed statistically different expression between the three conditions are listed in Table 6-2 with a short description of their functions. Among thousands of transcripts analysed, relatively few differences were observed (adjusted p-value =< 0.05) but some were highly significant, in particular the Hsp70B' mRNA was found at 2.5 fold higher levels in cells transfected with the wild type NRG1β3GFP and the FLAAA mutant relative to the K69A transfected cells.

Table 6-2. Comparisons of genes preferentially induced by differential subnuclear localisation of NRG1 determined in transcriptomic assay.

NRG1β3GFP vs FLAAA

Name	GenBank ID	Log fold change	Adjusted p-value	Description
TAF15 RNA polymerase II, TATA box binding protein (TBP)-associated factor	NM_003487	0.641	0.009	A component of the transcription factor complex, which serves as the scaffold for the remainder of the transcription complex and facilitates transcription initiation.
Dynein, axonemal, heavy chain 17	NM_173628	-0.568	0.024	A component of the microtubule-associated motor protein complex.
Denticleless homolog (Drosophila)	NM_016448	-0.516	0.038	Retinoic acid-regulated nuclear matrix-associated protein.
Histone cluster 2, H4b	NM_001034077	-0.523	0.042	A member of the histone H4 family which are basic nuclear proteins responsible for the nucleosome structure of the chromosomal fiber.
SNF8, ESCRT-II complex subunit, homolog (S. cerevisiae)	NM_007241	0.506	0.050	A component associated in a multiprotein complex with RNA polymerase II elongation factor.

NRG1β3GFP vs K69A

Name	GenBank ID	Log fold change	Adjusted p-value	Description
Heat shock 70kDa protein 6 (Hsp70B')	NM_002155	-1.066	4.40E-06	A unique member of the human Hsp70 family of chaperones. It is strictly inducible in response to various cellular stresses.

FLAAA vs K69A

Name	GenBank ID	Log fold change	Adjusted p-value	Description
Heat shock 70kDa protein 6 (Hsp70B')	NM_002155	-1.349	7.23E-08	A unique member of the human Hsp70 family of chaperones. It is strictly inducible in response to heat stress.
Interferon-induced protein with tetratricopeptide repeats 2	NM_001547	0.696	4.38E-03	It binds the translation initiation factor eIF3 and inhibits initiation of protein synthesis.
Ryanodine receptor 1 (skeletal)	NM_000540	-0.591	1.12E-02	It functions as a calcium release channel in sarcoplasmic reticulum.
Heat shock 70kDa protein 1A	NM_005345	-0.517	4.23E-02	A member of the Hsp70 family, involved in stabilising existing proteins against aggregation and mediates the folding of newly translated proteins.

"**Log Fold Change**" is the value of the contrast. Usually this represents a log2-fold change between two or more experimental conditions although sometimes it represents a log2-expression level. Up-regulated genes are indicated by a positive log fold change value. Down regulated genes are accordingly given a negative value.

"**Adjusted p-value**" is the p-value adjusted for multiple testing. It is generally considered that a p-value of 0.05 or less is a reliable indicator of differential expression.

6.3.7.2 Effects of NRG1β3 subnuclear localisation on Hsp70B' expression

To test whether the significant change at the mRNA level was found also at the level of protein expression we repeated the experiment and probed the cell lysates with a Hsp70B' specific monoclonal antibody (Stressgen, UK). Using the concentration (1:1000) recommended by the manufacturer's instruction, no signals were detected in HEK-293 cells transfected with any of the constructs (data not shown).

Noonan et al. detected Hsp70B' expression in the heat shocked HT-29 cells using the same antibody at a concentration of 1:500 (Noonan et al., 2007b). To test the reliability of this commercial antibody we repeated the heat shock experiment on the HT-29 human colon cancer cell line. HT-29 cells were heat stressed for 60min at 42.5°C and returned to 37°C. Cell lysates were prepared at 6h and 12h after the start of heat treatment. As shown in Figure 6-15, Hsp70B' was absent in unstressed cells and was not detectable after 6h following heat shock. At 12h, however, Hsp70B' accumulated to a detectable level.

As the activity of the Hsp70B' antibody was confirmed, HT-29 cells were transiently transfected with NRG1β3GFP, the mutants FLAAA and K69A, or GFP as a control. Cell lysates were prepared 24h after transfection. Immunoblotting detected the Hsp70B' protein in the wild type and FLAAA mutant transfected cells but not in the K69A transfected or in cells transfected with GFP alone (Figure 6-16). The same experiment was repeated on the HEK-293 cell line where similar results were observed, suggesting that NRG1β3 localised in spliceosomes induced the expression of Hsp70B'.

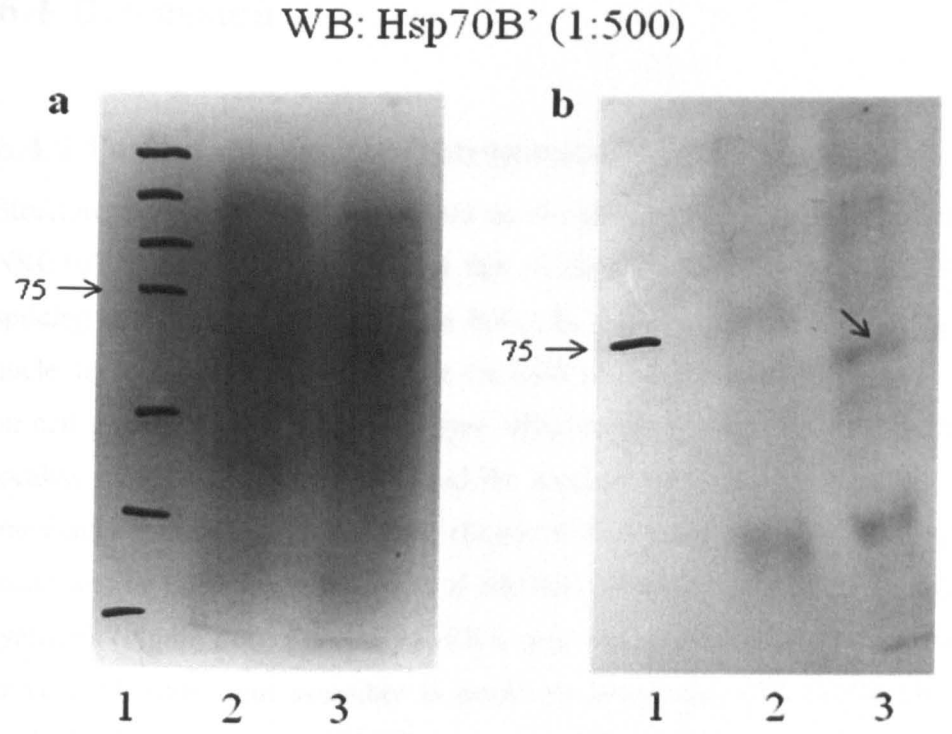

Figure 6-15. Western blot analysis of the expression of Hsp70B'. HT-29 cells were heat shocked under standard conditions, and returned to 37°C. Cells were lysed at 6h (a) or 12h (b) after the heat shock and analysed by immunoblotting using an antibody specific for Hsp70B'. Lane 2: no heat shock. Lane 3: heat shocked. Lane1: molecular weight markers.

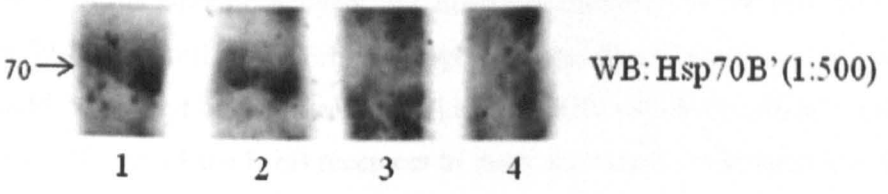

Figure 6-16. Western blot analysis of the expression of Hsp70B' in HT-29 cells transfected with NRG1β3GFP and its mutants. HT-29 cells were transiently transfected with NRG1β3GFP (Lane 1), FLAAA (Lane 2), K69A (Lane 3), or GFP as a control (Lane 4). Cell lysates were prepared 24h after transfection, run on a 7% SDS PAGE gel, and probed with anti-Hsp70B'antibody. Arrow indicates the position of the 70kDa molecular weight marker.

6.4 Discussion

6.4.1 Candidate effects of intranuclear NRG1β3

Structure determines functions. Based on the distinct subnuclear compartments where NRG1β3 localised we hypothesised that its function could be related either to RNA splicing or ribosomal biogenesis (or both). In this study, we examined the effects of nucleolar localisation of NRG1β3 on the level of ribosomal RNA expression as well as on cell growth. Compared to wild type NRG1β3 the mutant FLAAA which could not localise to nucleoli slightly increased the level of the 28S and 18S rRNA species in transiently transfected COS-7 cells (Figure 6-3). However, when measured by BrdU incorporation nucleolar localisation of NRG1β3 resulted in only a 2% increase in DNA synthesis (Figure 6-4). The rate of rRNA gene transcription, pre-rRNA processing and nascent ribosome unit assembly is positively associated with cell growth. Thus, if nucleolar localisation of NRG1β3 stimulated cell growth, we would expect a positive effect on the level of rRNA synthesis. Inversely if NRG1β3 stimulated the efficiency of protein synthesis this might facilitate reduced cell cycle time and increased growth rates. In this respect however our data showed inconsistency. Counting BrdU-labelled proliferating cells was relatively laborious and subjective. Also, variances inevitably existed throughout the process of RNA extraction and quantification which made the data less reliable. Both of these experiments were performed on the COS-7 cell line which, to our knowledge, has limited expression of the ErbB receptors. As shown in the results of the kinomic analysis, intranuclear localisation of NRG1β3 was able to activate the ErbB4 as well as the ErbB2 receptor but the signals were weak. Future experiments could be carried out on a cell line (i.e. the T47D cell line) naturally expressing higher levels of each of the ErbB receptors to study the effects of intranuclear NRG1β3 on cell growth.

Another candidate effect of the spliceosome localisation of NRG1β3 is that it might be involved in RNA splicing. If so, we hypothesised that the first candidates that NRG1β3 could exert its splicing regulation on would be its own gene or its cognate receptor gene. By designing specific primers we identified the NRG1α isoform in the MDA-MB-231 cell line as well as four ErbB4 isoforms in the T47D cell line using the RT-PCR technique. As these experiments required transient transfection of the NRG1β3 construct, we were unable to examine its effect on NRG1β splicing or the ratio of the

two products. Even though no detectable changes of the expression of either the NRG1α or the ErbB4 splice variants were observed, intranuclear localisation of NRG1β3 might be indirectly involved in RNA splicing as a co-factor to facilitate the splicing factors assembly. Breuleux et al. reported similar nuclear localisation patterns of the NRG1α splice variant and in the two hybrid interaction assays, several potential partners were identified including proteins involved in pre-mRNA splicing (Breuleux et al., 2006). It would be of interest in future to explore and explain their possible functional relationship.

6.4.2 Kinomic analysis of intranuclear NRG1β3

The Human Phospho-Receptor Tyrosine Kinase (Phospho-RTK) Array is a rapid and sensitive tool to detect changes in phosphorylation between samples. In this study, HEK-293 cells were transiently transfected with wild type NRG1β3GFP, the FLAAA mutant (which localised to spliceosomes but not nucleoli) and the K69A mutant (which localised to the nucleoli but not spliceosomes), or with GFP as a control. We found that four RTK receptors were activated in all transfected cells, the EGFR, IGF-I R, Insulin R and EphB2 receptors, all of which are involved in cell proliferation and differentiation (Bennasroune et al., 2004). The observed phosphorylation of these receptors could be due to either the basal level expression in HEK-293 cells or the transient expression of GFP. VEGFR3 phosphorylation was detected in NRG1β3GFP and K69A transfected cells, suggesting nucleolar localisation of NRG1 was involved in VEGFR3 expression and/or phosphorylation. VEGFR is one of the receptors for vascular endothelial growth factor, which is an important signalling protein involved in vasculogenesis (the formation of the embryonic circulatory system) and angiogesesis (the growth of blood vessels from pre-existing vasculature) (Stuttfeld and Ballmer-Hofer, 2009). *In vitro*, VEGF has been shown to stimulate endothelial cell mitogenesis and cell migration by binding to tyrosine kinase receptors (the VEGFRs) on the cell surface, causing them to dimerise and become activated through transphosphorylation, a mechanism similar to ErbB activation. Even though NRG1β1 has been shown to induce the expression of VEGF in breast cancer epithelial cells (Bagheri-Yarmand et al., 2000) and there is evidence of nuclear accumulation of VEGF in an experimental wound model (Keresztes and Boonstra, 1999), how VEGFR3 expression and/or phosphorylation are associated with nucleolar localisation of NRG1β3 requires further investigation.

The wild type NRG1β3 and the FLAAA mutant increased the phosphorylation and/or expression of the ErbB2 receptor and to a greater extent of the ErbB4 receptor. NRG1 is a direct ligand of ErbB4 and it can activate the kinase activity of ErbB4. Even though ErbB2 is unable to bind any ligands, it is possible that ErbB2 became phosphorylated by forming heterodimers with ErbB4. While the observed signals of ErbB2 and ErbB4 were not strong, according to the manufacturer's data, the Human Phospho-RTK Array is specific for ErbB2, ErbB3, and ErbB4 and no cross-reactivity occurred. Moreover, they showed that even though NRG1β1 stimulated tyrosine phosphorylation of ErbB2, ErbB3, and ErbB4 was detected by both array and western blot analyses, the Human Phospho-RTK Array was considerably more sensitive than western blot, requiring 20-fold less lysates for the detection of the ErbB4 receptor. This might explain why we were unable to detect ErbB4 expression in western blot analysis using the same lysates.

The results of the kinomic assay showed that ErbB4 was activated by NRG1β3. Since no full-length ErbB4 has been reported to be present in the cell nuclei, it was possible that the observed ErbB4 activation occurred at the cell surface upon NRG1 ligand binding. However this could not explain why NRG1β3 localised only to spliceosomes induced the effect. Western blot analysis of the conditioned medium of NRG1β3GFP transfected HEK-293 cells was unable to detect any corresponding signals of NRG1β3GFP using the anti-GFP antibody. As there is a threshold protein level to be detected by western blot analysis, the absence of signals did not indicate the absence of secreted NRG1β3 proteins in the conditioned medium. Future experiments could be carried out using an antibody that blocks the extracellular domain of ErbB4. If ligand binding is blocked, membrane-bound ErbB4 activation due to secreted NRG1β3 would be inhibited. The kinomic assay would also be repeated under this condition. If similar results are observed, we could conclude that the expression of ErbB4 due to NRG1β3 stimulation occurs inside the nucleus rather than at the cell surface.

The kinomic results did not specify whether the observed ErbB4 activation was due to the increased protein expression, or the phosphorylation of ErbB4, or both. To test these alternatives we purchased a site specific phospho-ErbB4 antibody (Tyr984) from Cell Signalling, UK. The same cell lysates used in the kinomic assay were probed with this commercial antibody, however, no signals were detected. To check the activity of this antibody, untreated and NRG1β1 stimulated NIH3T3-ErbB4 cell lysates were probed with Tyr984, anti-ErbB4 (HFR1) and anti-phosphotyrosine (PY20) antibodies,

respectively (Figure 6-11). In the absence of any treatment ErbB4 expression was detected in NIH3T3-ErbB4 cells, without any tyrosine phosphorylation observed. Upon NRG1β1 stimulation, ErbB4 was phosphorylated, detected by both HFR1 and PY20 antibody. Tyr984 detected no signals in either condition but gave several apparently non-specific bands. Each activated ErbB receptor has unique tyrosine phosphorylation sites. This Tyr984 antibody is reported to detect ErbB4 protein only when phosphorylated on the tyrosine residue 984 and it is possible that NRG1β1 stimulated NIH3T3-ErbB4 may have other tyrosine sites phosphorylated. However, the reliability of this commercial antibody needs to be confirmed.

Western blot analysis showed no observable effects of localisation of NRG1β3 on total ErbB4 expression or phosphorylation. However, it is possible that ErbB4 might be activated by spliceosome localised NRG1β3. Immunofluorescence staining carried out in this study examined the subcellular localisation and activation state of ErbB4 in NRG1β1 stimulated NIH3T3-ErbB4 cells (Figure 6-13). ErbB4 exhibited membrane and cytoplasmic staining, as expected. Tyrosine phosphorylation was observed throughout the cell. No signals of tyrosine phosphorylation were detected in either untreated NIH3T3-ErbB4 cells or in cells expressing NRG1β3 construct, which was inconsistent with the results of kinomic assay. A possible explanation would be, as discussed above, that the RTK-array assay is more sensitive in detected tyrosine phosphorylation than immunofluorescence staining.

6.4.3 Transcriptomic analysis of intranuclear NRG1β3

Gene expression arrays are a powerful tools used in high-throughput experiments to screen for biologically relevant gene expression changes (Yao et al., 2004). In order to determine whether localisation of the NRG1β3 protein either in nucleoli or in spliceosomes altered gene transcription, mRNA prepared from HEK-293 cells transfected with wild type NRG1β3GFP and two mutants which could localise only at spliceosomes (FLAAA) or only in nucleoli (K69A) was analysed by Source BioScience Geneservice. The relative gene expression level was compared between the three conditions. A summary of the results which showed statistically different expression is listed in Table 6-2. Some of the genes identified in Table 6-2 are not informative due to their unidentified functions. We observed however that the level of Hsp70B' (heat shock protein 70B') transcription was 2.5 fold higher in cells transfected with the wild type NRG1β3 and the FLAAA mutant relative to the K69A transfected cells. To test whether

this was found also at the level of protein expression, we analysed the same cell lysates by western blotting with an antibody specific for the Hsp70B' protein. The Hsp70B' protein was detected in the wild type and FLAAA mutant transfected cells but not in the K69A transfected or in cells transfected with GFP alone (Figure 6-16). This data suggests that spliceosome localisation of NRG1β3 induced expression of this protein, which is consistent with the transcriptomic results.

Hsp70B' is a member of the highly conserved heat shock protein 70 family, which is a group of chaperones involved in protein folding, stabilisation, and shuttling functions throughout the cell (Tavaria et al., 1996). Members of this protein family can be induced by various cellular stresses, including heat stress, radiation, heavy metals, certain chemotherapeutics, and other stimuli that are able to activate heat shock transcription factors. To date, knowledge about Hsp70B' is limited. Unlike other members in the Hsp70 family, Hsp70B' is strictly inducible, having no detectable basal level of expression in most cells (Leung et al., 1990). Consistent with this we observed no basal expression of Hsp70B' in the HT-29 human colon cancer cell line. However, 12h post heat shock it reached a detectable level (Figure 6-15). This data suggests that the expression of Hsp70B' is indeed strictly in response to stress. It has been reported that Hsp70B' is essential to survival during intense proteotoxic stress (Noonan et al., 2007a). It is possible that Hsp70B' may contribute to resistance to cell death in pathological conditions where this cellular state exists. In human breast cancer cells, Hsp70 has been identified as one of the NRG-inducible gene products in human breast cancer cells. In addition, a higher expression level of Hsp70 protein was found in human breast tumour samples than from adjacent normal tissue (Mandal et al., 2002). Intranuclear localisation of NRG1β protein has been observed in various human cancer types (Chapter 3). There therefore remains the possibility that nuclear expressions of NRG1β3 may cooperate with Hsp70B' in certain tissues or disease states.

Chapter 7. Investigating the subcellular localisation of ErbB3 when coexpressed with NRG1β3GFP

7.1 Introduction

The *ErbB3* gene is located on chromosome 12q11-13 and transcribed as a 6.2 kb message of 4080 nucleotides (Sithanandam and Anderson, 2008). The ErbB3 mRNA encodes a transmembrane glycoprotein with the same basic structure as the other members of the ErbB family. Due to mutations in the tyrosine kinase domain, ErbB3 has been generally considered as kinase-inactive (Citri et al., 2003). However, a recently published paper demonstrates that despite those sequence alterations ErbB3 retains sufficient kinase activity to transphosphorylate its dimer partner (Shi et al., 2010b).

ErbB3 mRNA has been detected in a number of human tissues including placenta, postnatal skin, stomach, lung, kidney, and brain (Kraus *et al.*, 1989). ErbB3 protein is expressed in various normal tissues and in several cancers (Gullick, 1996; Prigent et al., 1992; Srinivasan et al., 1999). Aberrant increases in ErbB3 expression have been found in breast, ovary, and prostate carcinomas and different cancer cell lines (Leng et al., 1997; Leung et al., 1997; Naidu et al., 1998). Moreover, it has been suggested that high expression of ErbB3 is associated with short patient survival in breast cancer, lung cancer, and oral squamous cell carcinomas (Shintani *et al.*, 1995; Yi *et al.*, 1997).

ErbB receptors are usually located at the cell surface and are activated by extracellular binding of EGF-like growth factors. Unexpectedly, Offterdinger et al. reported high levels of ErbB3 within the nuclei of MTSV1-7 immortalized nonmaligant human mammary epithelial cells (Offterdinger et al., 2002). Two recent studies show that although nuclear expression of ErbB3 was not frequently observed in normal prostate tissues, its expression became more evident in prostate cancer, especially in the advanced hormone-refractory cases (Cheng et al., 2007; Koumakpayi et al., 2006). Immunohistochemically staining of invasive breast cancer tissues using the monoclonal

anti-ErbB3 antibody (RTJ2) showed strong granular nuclear staining (Figure 7-1) (staining was performed by Stefania Zona, a current PhD student in our laboratory). Thus there is accumulating evidence that ErbB3 is indeed present in cell nuclei.

NRG1β1 is a direct ligand of the ErbB3 receptor. In addition, NRG1β1 treatment has previously been reported to affect the subcellular localisation of ErbB3 in human mammary cell lines MTSV1-7 and MCF-7 by shifting ErbB3 from the nucleolus into the nucleoplasm and then into the cytoplasm (Offterdinger *et al.*, 2002). Even though nuclear uptake of NRG1β3 has been shown to be independent of ErbB3 binding (Golding *et al.*, 2004), NRG1β3 might be associated with and/or function through nuclear ErbB3. In this study, we explored any possible effects of NRG1β3 on ErbB3 localisation patterns in cell lines either transiently or stably expressing ErbB3 proteins.

7.2 Aims

1. To subclone ErbB3 into the pmCherry vector.
2. Using confocal microscopy to examine the localisation patterns of Cherry-tagged ErbB3 when coexpressed with NRG1β3GFP in COS-7 cells.
3. Using immunofluorescence staining to investigate ErbB3 localisation in the HEK-293-ErbB3 cell line transiently transfected with the NRG1β3GFP construct.

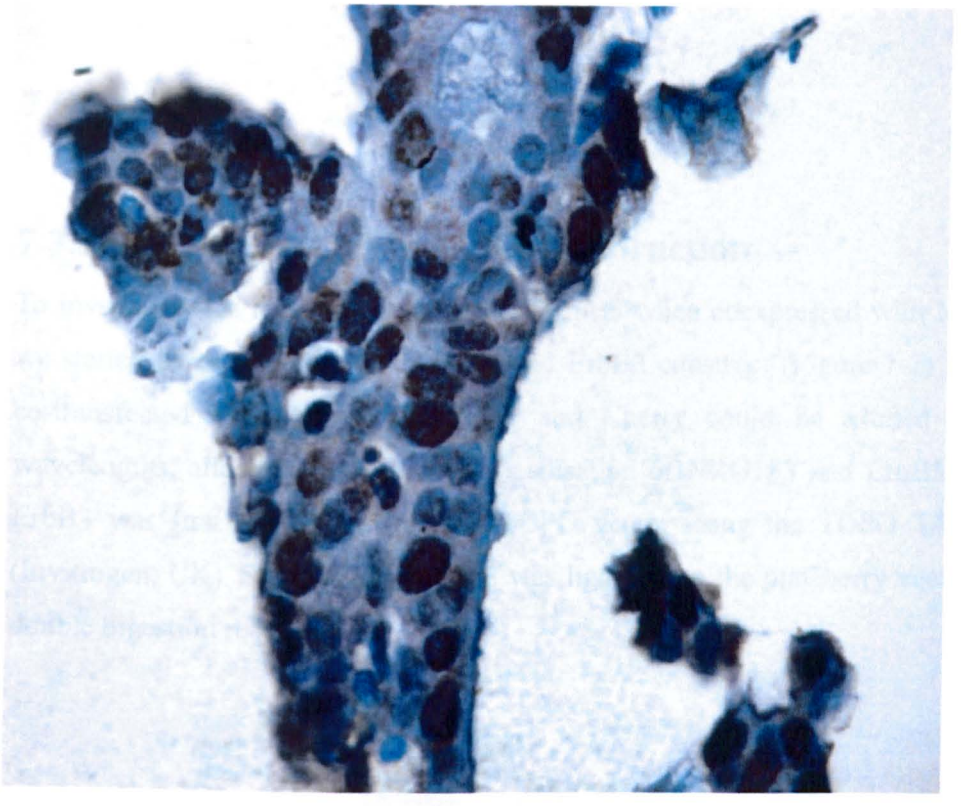

Figure 7-1. Immunohistochemical detection of ErbB3 nuclear staining in breast, infiltrating duct carcinoma tissues using the anti-ErbB3 antibody (RTJ2). Original magnification: x63.

7.3 Results

7.3.1 pmCherry-ErbB3 plasmid construction

To investigate the localisation patterns of ErbB3 when coexpressed with NRG1β3GFP, we started by engineering a Cherry-tagged ErbB3 construct (Figure 7-2) so that when co-transfected into COS-7 cells, GFP and Cherry could be excited by different wavelengths, allowing simultaneous visualisation of NRG1β3 and ErbB3. Full length ErbB3 was first cloned into pCR2.1-TOPO vector using the TOPO TA cloning kit (Invitrogen, UK). Subsequently, ErbB3 was ligated into the pmCherry vector following double digestion reactions.

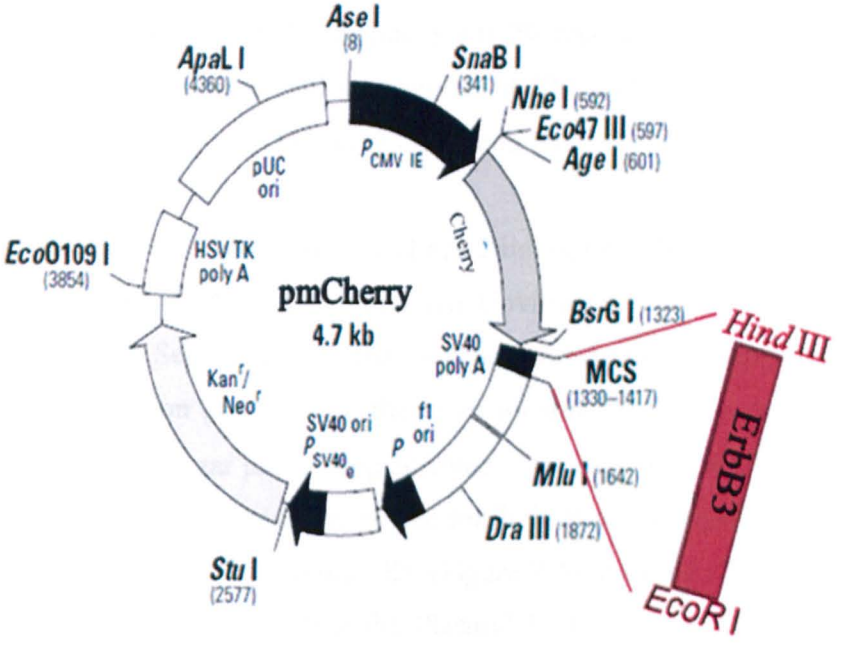

Figure 7-2. Schematic representation of subcloning of ErbB3 into the pmCherry vector at Hind III and EcoR I restriction sites. Figure adapted from www.clontech.com.

A pair of primers ErbB3F and ErbB3R was designed to amplify ErbB3 from its original vector pBABE-puro ErbB3. Initial PCR reactions were designed to optimise the amount of DNA template. When the annealing temperature was set up at 52°C, a single band of 4kb was generated in each of the PCR reaction (Figure 7-3 Lane 2-4) which was the predicted size of ErbB3.

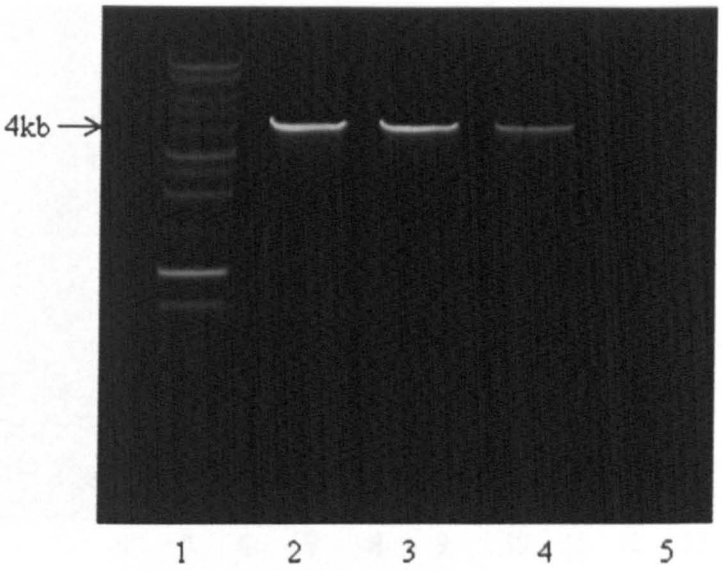

Figure 7-3. Agarose gel electrophoresis of PCR reaction using pBABE-puro ErbB3 as template and ErbB3F and ErbB3R as primers. Annealing temperature was set up at 52°C. PCR product (5µl) was run on a 0.7% TAE agarose gel. Lane 1: 1kb DNA ladder. Lane 2-4: reactions with DNA template at 500, 200 and 50ng. Lane 5: negative control using deionised water instead of DNA template.

Gel purified PCR products (from Lane 2 in Figure 7-3) were cloned into pCR2.1-TOPO vector using TOPO TA Cloning Kit (Invitrogen, UK). The reaction was set up as described in Section 2.4.10 and incubated for 5min at room temperature. The TOPO cloning reaction product was then transformed into DH5α competent cells and these plated onto LB agar plates supplemented with ampicillin and X-gal. 11 individual white colonies from the plates were picked for PCR screening using primers M13F and M13R provided in the TOPO Cloning Kit (Figure 7-4). Purified DNA plasmids were prepared from positive colonies using the Plasmid Miniprep Kit (Qiagen, UK). Subsequently, pCR2.1-TOPO ErbB3 was digested at *Hind* III and *EcoR* I restriction sites present on either end of the ErbB3 insertion (data not shown) to facilitate subsequent ligation into the pmCherry vector.

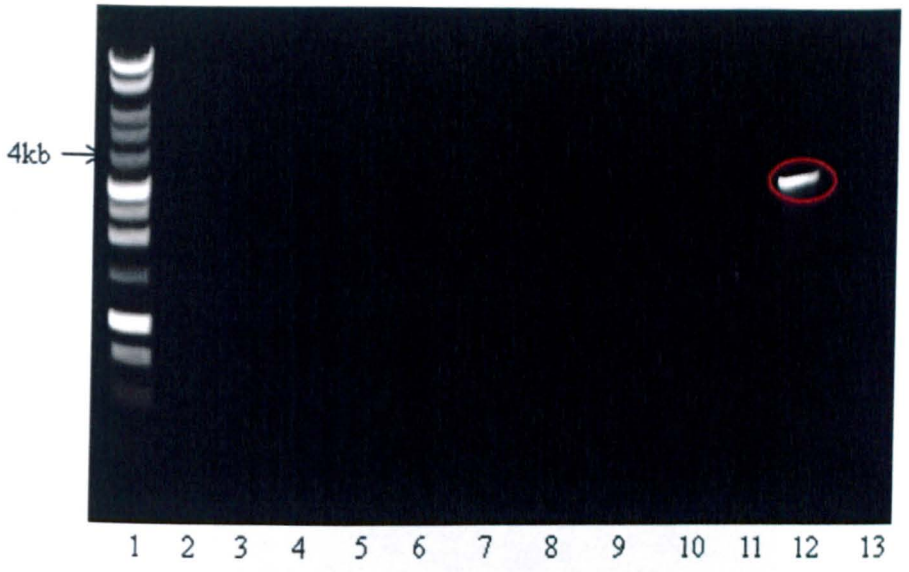

Figure 7-4. PCR screening using primers M13F and M13R. PCR products (3µl) were run on a 0.7% TAE agarose gel. Lane 1: 1kb DNA ladder. Lane 2-12: 11 individual colonies were picked and used as templates for PCR reactions. Lane 13: negative control using deionised water instead of template DNA.

The pmCherry vector was digested at the same restriction sites. Restriction digestion reactions were set up as described in Section 2.4.4. Uncut supercoiled plasmid appeared to migrate more quickly than the nicked plasmid indicated by the lower band in Lane 5 as shown in Figure 7-5. Since only a few nucleotides exist between the two restriction sites in the multiple cloning site of the vector and complete single digestion was achieved by either *Hind* III or *EcoR* I restriction enzyme (Figure 7-5 Lane 3 and Lane 4), we assumed that a single band of the predicted size of the vector (4.7kb) suggested complete double digestions of the pmCherry vector (Figure 7-5 Lane 2). Following gel purification, the digested vector was treated with Calf Intestinal Alkaline Phosphatase (CIAP) (as described in Section 2.4.5) to remove the phosphate group from the 5'- ends to prevent its self-ligation.

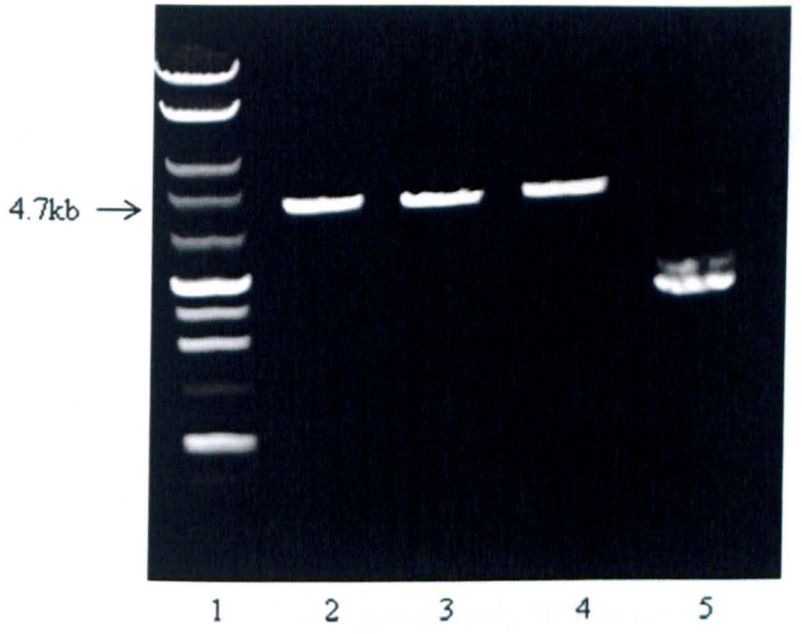

Figure 7-5. Gel of agarose electrophoresis of restriction digestions of the pmCherry vector. Digestion reaction mixture (5µl) was run on a 0.7% gel. Lane1: 1kb DNA ladder. Lane 2: double digestions by *Hind* III and *EcoR* I restriction enzymes. Lane 3: single digestion by *Hind* III only. Lane 4: single digestion by *EcoR* I only. Lane 5: negative control using deionised water instead of restriction enzymes. Each digestion mixture was incubated at 37°C for 1h.

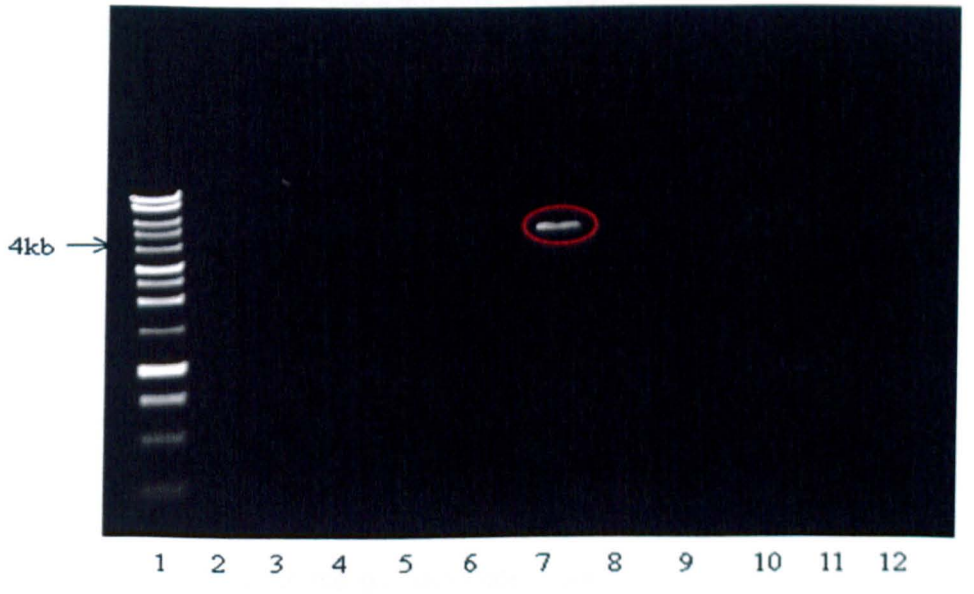

Figure 7-6. PCR screening using primers ErbB3F and ErbB3R. PCR products (3µl) were run on a 0.7% TAE agarose gel. Lane 1: 1kb DNA ladder. Lane 2-11: 10 individual colonies were picked and used as templates for PCR reactions. Lane 12: negative control using deionised water instead of template DNA.

Ligation and transformation were carried out as previously described (Section 2.4.6 and 2.4.7). 10 individual colonies were picked after the transformed cells were plated onto LB agar plates supplemented with kanamycin. One colony seemed positive by PCR screening using primers ErbB3F and ErbB3R (Figure 7-6). The sequence and the junction of the correct insertion were confirmed by sequencing.

To confirm the expression of the newly made pmCherry-ErbB3 construct, transient transfection was performed in COS-7 cells. Lysate from pBABE-puro ErbB3 transfected cells was run in parallel as a control. Cell lysates were probed with RTJ2, a monoclonal antibody directed against a cytoplasmic epitope of ErbB3. Bands of the expected size were detected for both constructs. ErbB3 was approximately 150kDa, whereas Cherry-ErbB3 was approximately 180kDa (Figure 7-7). An extra band was also observed below the expected molecular weights of the two constructs. This could be due to either the proteolytic cleavage or inefficient glycosylation of the protein products.

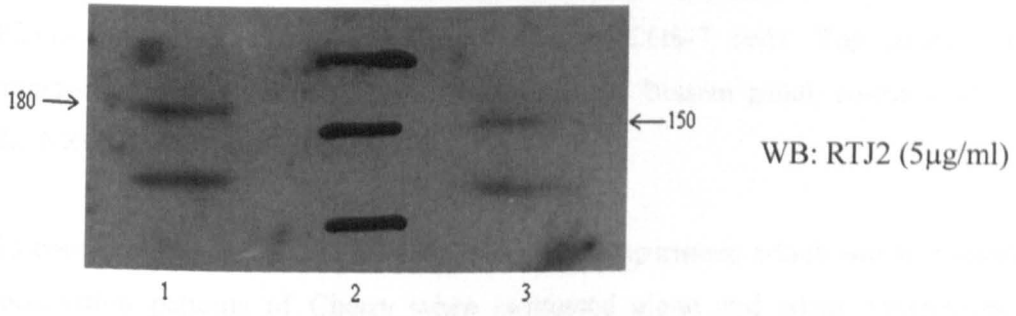

Figure 7-7. Western blot analysis of ErbB3 expression in COS-7 cells transiently transfected with the pmCherry-ErbB3 (Lane 1) or pBABE-puro ErbB3 construct (Lane 3). Lane 2: molecular markers.

7.3.2 Localisation study of Cherry-tagged ErbB3

As western blot analysis confirmed its expression, pmCherry-ErbB3 was transiently transfected into COS-7 cells. The subcellular distribution of ErbB3 was examined using confocal microscopy. Both nuclear and cytoplasmic expression was observed (Figure 7-8, top panel). To examine the localisation patterns of ErbB3 when coexpressed with NRG1β3GFP, the pmCherry-ErbB3 and NRG1β3GFP construct were co-transfected into COS-7 cells. In the bottom panel of Figure 7-8, Cherry-ErbB3 localised to nucleoli and spliceosomes, the same as NRG1β3GFP. It appeared that Cherry-ErbB3 colocalised with NRG1β3GFP in the subnuclear structures.

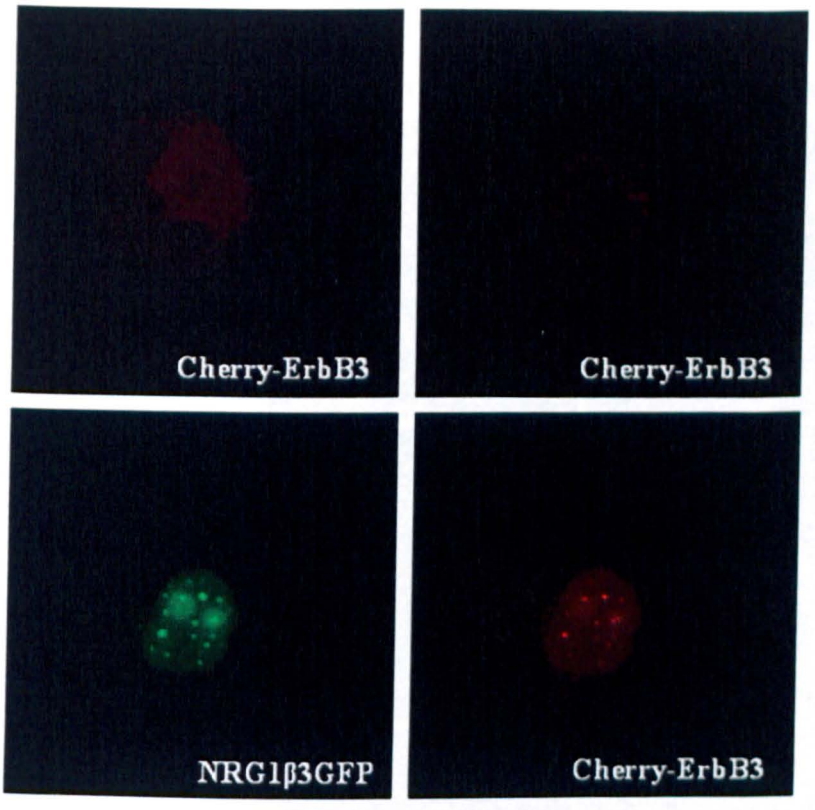

Figure 7-8. Localisation of Cherry-ErbB3 in COS-7 cells. Top panel: transient transfection of the Cherry-ErbB3 construct alone. Bottom panel: co-transfection with the NRG1β3GFP construct.

To complete this study we carried out a control experiment which was to examine the localisation patterns of Cherry when expressed alone and when coexpressed with NRG1β3GFP. In pmCherry transiently transfected COS-7 cells, Cherry localised to the cytoplasm and nucleus of the cell as expected (Figure 7-9 left panel). When coexpressed with NRG1β3GFP, Cherry showed the same subnuclear localisation pattern as NRG1β3GFP (Figure 7-9 right panel), suggesting that the colocalisation of Cherry-ErbB3 and NRG1β3GFP observed previously was an artefact. There are two possible explanations to account for this artefact. One is that Cherry is a mutant of monomer DsRed (Shaner et al., 2004), which might complex with GFP to form a polymer. Thus, when coexpressed in cells, Cherry and GFP exhibited the same localisation pattern. However, no such evidence has been reported in the literature. The other possible explanation is that the observed colocalisation of Cherry and GFP was due to a bleed-through artefact in the confocal fluorescence microscopy. When emission spectra of two fluorophores overlap, emission from one channel could extend to the other channel.

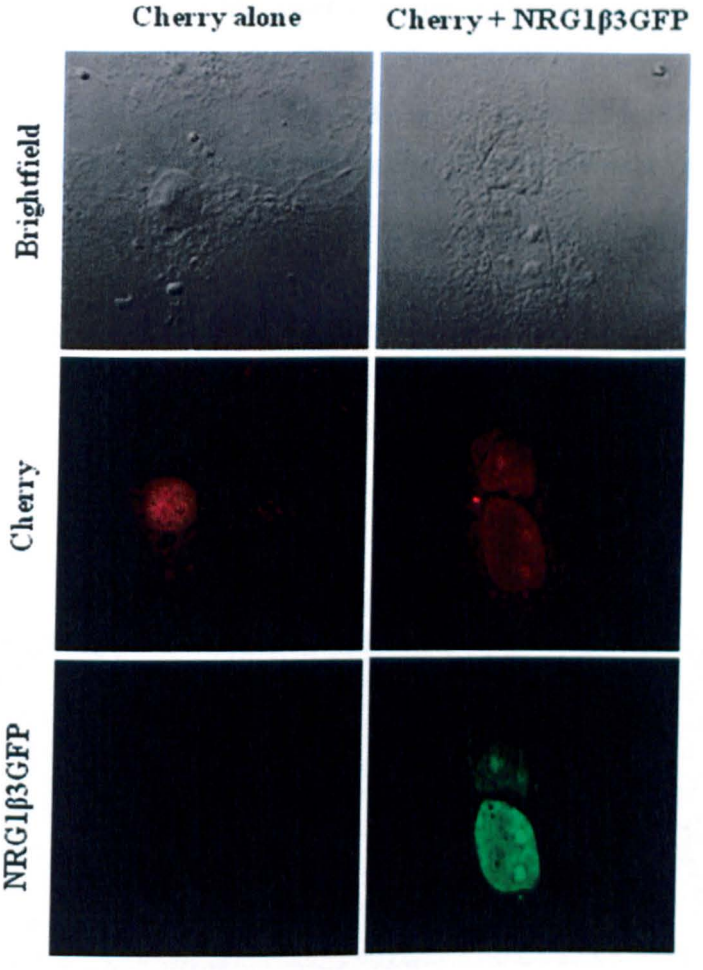

Figure 7-9. Localisation of Cherry in COS-7 cells transiently transfected with (right panel) or without (left panel) the NRG1β3GFP construct.

To examine the emission spectrum of GFP and Cherry, we performed a lamda scan on COS-7 cells transfected with either GFP or Cherry. A lamda scan recorded a series of individual images within a user-defined wavelength range (GFP channel: 490-700nm; Cherry channel: 560-700nm. The bandwidth of the emission filter was set up at 10nm in this experiment), and each image was detected at a specific emission wavelength. When the emission spectrum of GFP and Cherry was depicted by the confocal microscopy software, we noticed that their emission spectra did overlap (within the range of 540-590nm) (data not shown), which explained the observed false positive colocalisation of NRG1β3GFP and Cherry.

Bleed-through artefacts can be corrected to some extent by adjusting laser intensity, gain and offset on the photo multiplier tube (PMT). To establish the level of

bleed-through, the NRG1β3GFP expressing cell was imaged with an argon-ion 488nm laser under the optimum conditions (laser intensity: 13%; offset: -20; gain: 700V) and the amount of signal present in the Cherry channel was recorded at two different conditions (Figure 7-10). When the gain of the red channel was kept at 600V, no bleed-through from the green channel was observed. When the gain value was adjusted to 1300V, a considerable amount of bleed-through was observed in the red channel. This signal represented GFP bleed-through. The procedure was repeated with the Cherry expressing cells to examine any bleed-through into the GFP channel (data not shown). By examining fluorescence once at a time, any signal in other channel would be false and should be removed and this served as reference to change the detector gain level to get rid of emission bleed-through.

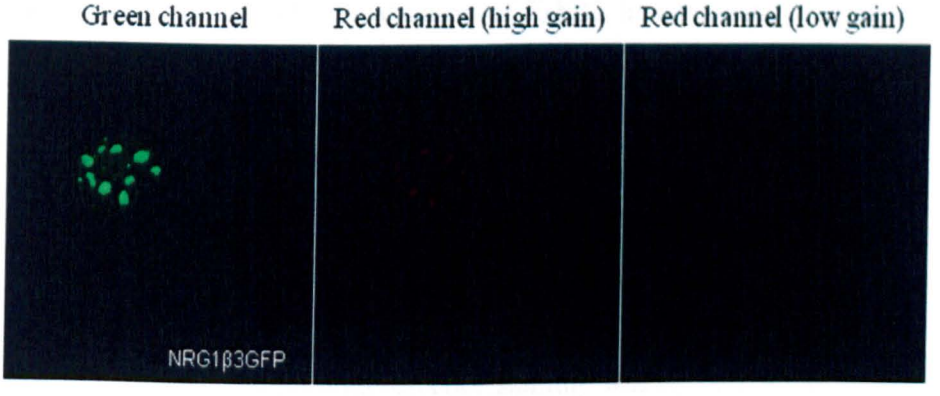

Figure 7-10. Emission bleed-through correction. NRG1β3 was transiently transfected into COS-7 cells. Images were taken by confocal microscopy 24h post transfection. GFP was excited using the 488nm Ar laser at a power of 13%. Emission was collected with a 505nm filter. The 546nm line of He-Ne with a laser power at 80% was active at the same time and the emission was collected with a 560nm filter. While the laser intensity, gain and offset of the GFP channel were kept constant, the gain values of the red channel were adjusted from 1300V (high gain) to 600V (low gain) to eliminate GFP bleed-through signals.

7.3.3 Immunofluorescence study of ErbB3 localisation

To avoid any bleed-through artefacts which could complicate the experimental results, we utilised a far-red fluorescent dye Alexa Fluor 633 (Invitrogen, UK) to label ErbB3 in the following immunofluorescence experiments to study the localisation patterns of ErbB3 when coexpressed with NRG1β3GFP. COS-7 cells were transiently transfected with the pBABE-puro ErbB3 construct. 24h post transfection, cells were fixed,

permeablised and incubated with the anti-ErbB3 antibody RTJ2. A negative control was performed at the same time to ensure that there was no non-specific binding of the antibody. Figure 7-11 shows nuclear immunofluorescence obtained with ErbB3 was found to localise in the nuclei but was excluded from nucleoli.

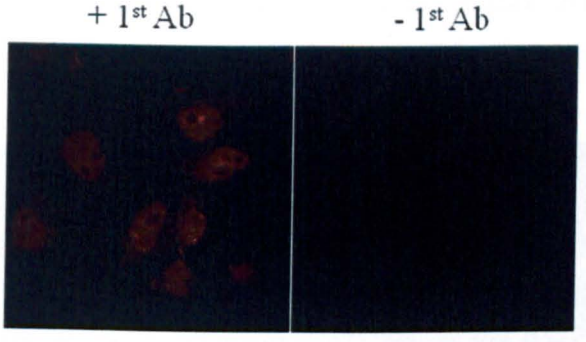

IF: RTJ2 (2.5μg/ml)

Figure 7-11. Subcellular localisation of ErbB3 in transiently transfected COS-7 cells. Confocal immunofluorescent microscopy demonstrating nuclear ErbB3 using the monoclonal RTJ2 antibody. Alexa Fluor 633 was excited with 633nm laser light and the images were acquired with a 647nm emission filter.

We next examined the localisation pattern of ErbB3 when coexpressed with NRG1β3GFP. COS-7 cells were co-transfected with the NRG1β3GFP and pBABE-puro ErbB3 construct. Immunofluorescence staining was carried out as described previously. As Alexa Fluor 633 is not visible to the human eye, the NRG1β3GFP expressing cell was first confirmed by an excitation scan with 488nm laser light. A subsequent scan with 633nm laser light was then performed to examine whether the cell also expressed ErbB3. Figure 7-12 shows the subnuclear localisation patterns of NRG1β3GFP as expected. In the same cell, ErbB3 exhibited nucleoplasm localisation, the same localisation pattern as it gave when expressed alone, suggesting that the expression of NRG1β3 did not cause extra accumulation of ErbB3 in the punctuate structures in the cell nuclei.

As the above experiments were based on the transient expression of ErbB3 in the COS-7 (monkey kidney) cell line, we next examined the localisation pattern of ErbB3 in a human embryonic kidney cell line. The HEK-293-ErbB3 cell line which stably expresses ErbB3 was utilised in the following immunofluorescence experiment. HEK-293-ErbB3 cells were fixed, permeablised and incubated with the RTJ2 antibody. Figure 7-13a shows membrane staining of ErbB3. Apparently, the localisation pattern of

ErbB3 was different in transiently transfected COS-7 cells and in HEK-293 cells stably expressing ErbB3. To examine whether transient or stable transfection had any effects on the subcellular localisation of ErbB3, we repeated the immunofluorescence experiment on the HEK-293 cell line transiently transfected with the pBABE-puro ErbB3 construct. ErbB3 exhibited the same membrane localisation pattern as in the stably transfected HEK-293 cells (Figure 7-13b). These data demonstrated that the localisation pattern of ErbB3 was different in the two tested cell lines.

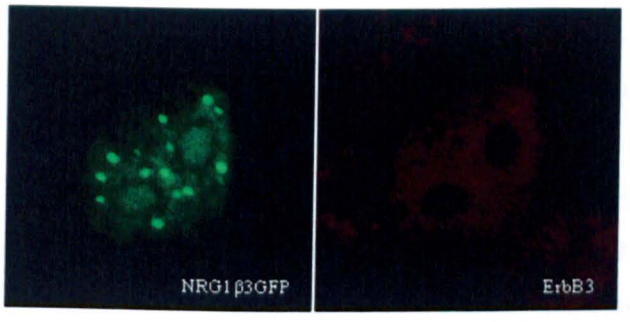

IF: RTJ2 (2.5μg/ml)

Figure 7-12. Localisation pattern of ErbB3 when coexpressed with NRG1β3GFP. COS-7 cells were cotransfected with the NRG1β3GFP and pBABE-puro ErbB3 construct and incubated for 24h. ErbB3 was immunofluorescently labelled with Alexa Fluor 633.

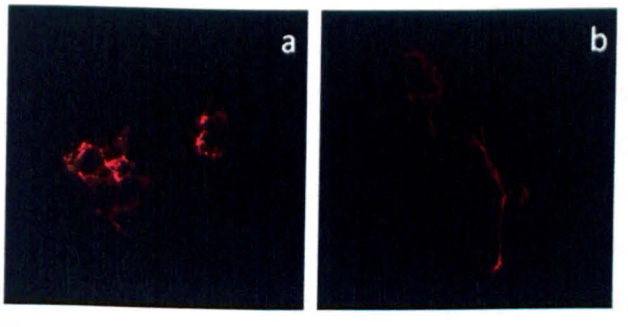

IF: RTJ2 (2.5μg/ml)

Figure 7-13. Localisation patterns of ErbB3 in either stably (a) or transiently (b) transfected HEK-293 cells.

7.4 Discussion

7.4.1 Spectral bleed-through artefacts in confocal microscopy

Imaging experiments having two or more fluorescent labels are often complicated by bleed-through artefacts. Bleed-through can occur during both excitation and emission of the fluorescent proteins and synthetic fluorophores commonly utilised in confocal microscopy. In general, bleed-through between fluorescence excitation spectral profiles occurs toward the blue end (shorter wavelengths) of the spectrum, whereas bleed-through between fluorescence emission spectra occurs in the red (longer wavelengths) region. For example, emission from a green fluorophores can often be detected through red emission filters, but a red dye is not imaged through a green emission filter. This is due to the fact that the absorption and emission spectra for most fluorophores are not symmetrical, but usually display long skewed tails that cover a broad region. A comparison of spectral overlap for GFP, Cherry, and Alexa Fluor 633 that were utilised in this study is presented in the Figure 7-14 (Fluorescence SpecraViewer, adapted from the Invitrogen website). The emission spectra for the GFP and Cherry indicate separation of the peak wavelengths. However, the moderate level of spectral overlap (gray shaded area in Figure 7-14b) illustrates that there is a considerable amount of emission from GFP at the peak emission wavelength of Cherry (denoted by a blue line running from the emission peak to the abscissa). This high level of signal bleed-through makes the separation of the fluorophores difficult since the fluorescence quantum yield of GFP is much higher than that of Cherry. Moreover, due to the fact that these fluorophores have broad excitation and emission spectra, excitation of GFP using the 488nm spectral line of argon-ion laser also produces excitation of Cherry, although to a lesser degree (Figure 7-14a). Thus, the combination of these two fluorescent proteins should be avoided in colocalisation experiments.

The spectral overlap between fluorophores decreases as the bandwidth between emission maxima increases. Alexa Fluor 633 is mostly excited by the 633nm line of a red helium-neon laser and has peak emission at 647nm. As shown in Figure 7-14 GFP and far-red fluorescence Alexa Fluor 633 demonstrate a significantly reduced level of overlap and bleed-through artefacts should be minimal.

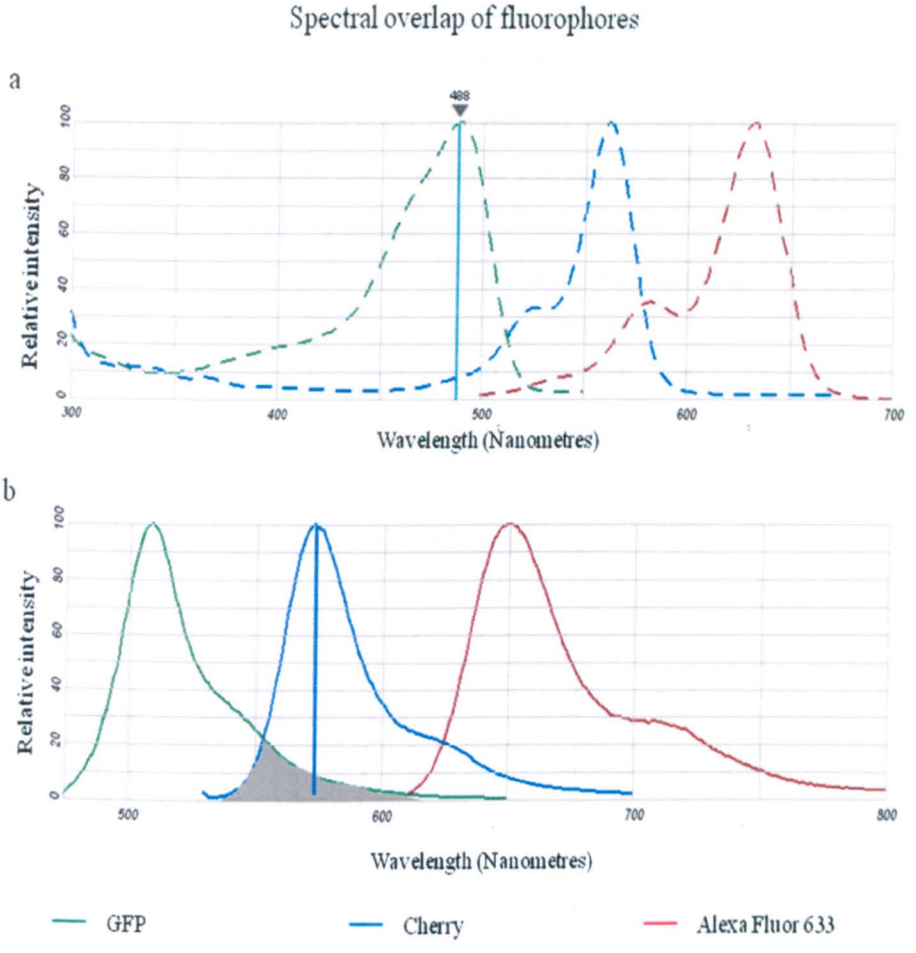

Figure 7-14. Comparison of spectral overlap for fluorophores utilised in the colocalisation experiments. (a) Excitation spectra. (b) Emission spectra. Figure adapted from http://www.invitrogen.com/site/us/en/home.html.

Spectral bleed-through artefacts often complicate the interpretation of experimental results, particularly if colocalisation of fluorophores is under investigation or quantitative measurements are necessary. But the unwanted bleed-through can be minimised in different ways. First, choosing fluorophores with well-separated absorption and emission spectra would avoid bleed-through (i.e. GFP vs. Alexa Fluor 633). In addition, probes with narrow emission spectra may dramatically reduce the problem of bleed-through. Compared to traditional fluorophores, quantum dots, which are semiconductor nanocrystals coated with a hydrophilic polymer shell and conjugated to antibodies, display highly defined spectral profiles (Figure 7-15) (Zorov et al., 2004). The fluorescence emission intensity is confined to a symmetrical peak with a maximum wavelength that is dependent on the dot size, but independent of the excitation wavelength. As a result, all the dots can be efficiently excited at a single wavelength in the UV/violet region (e.g., 405nm). The narrow emission profile enables several

quantum dots to be simultaneously observed with a minimal level of bleed-through. Second, a series of controls should be prepared when performing multiple labelling with two or more fluorophores in order to minimise the confusion in experimental results due to bleed-through artefacts. An important control is to label the specimen or to express the fluorescent proteins separately. This is necessary to determine the amount of signal gain possible in each channel without initiating bleed-through into adjacent channels, as shown in Figure 7-10. Third, the optical filter sets chosen to examine fluorophores emission should be closely matched to the spectral profiles of the probe with regards to bandwidth size and location to avoid any spectral overlap. Last but not least, there are some softwares allowing subtraction of a predetermined percentage of one channel from the other to minimise the effects of bleed-through.

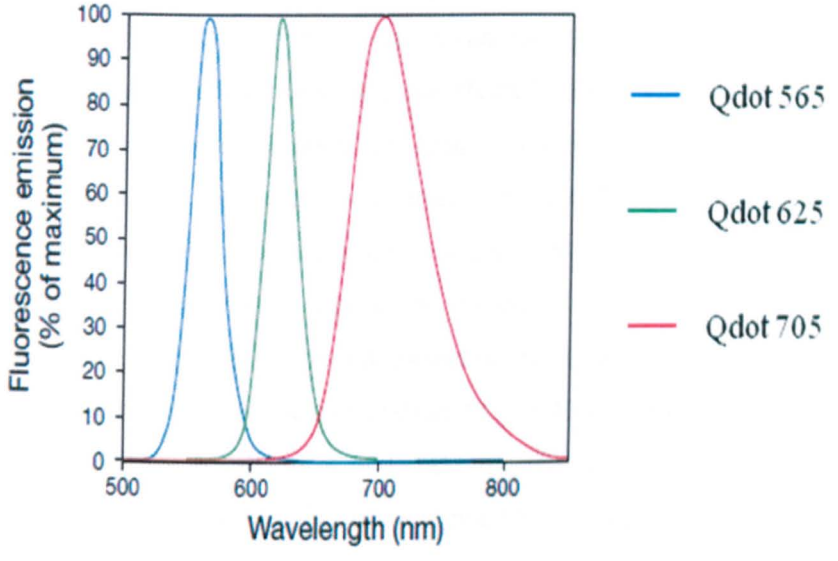

Figure 7-15. Fluorescence emission spectra of quantum dots. Figure taken from http://www.invitrogen.com/site/us/en/home.html.

7.4.2 Nuclear ErbB3

Offterdinger et al. first provided evidence that ErbB3 can be localised in the nucleus of normal and malignant human mammary epithelial cells (Offterdinger et al., 2002). Without adding exogenous NRG1, ErbB3 was concentrated in the nucleoli of MTSV1-7 human mammary epithelial cells. Addition of the NRG1β caused relocation of ErbB3 into the cytoplasm and to the cell membrane. Therefore, we hypothesised that the nuclear localisation of NRG1β3 might also affect the subcellular localisation of ErbB3. A Cherry-tagged ErbB3 plasmid was constructed to examine the localisation pattern of

ErbB3 when coexpressed with NRG1β3GFP. ErbB3 was subcloned into the pmCherry vector downstream of the Cherry encoding region (Figure 7-2). Tagging Cherry to the N-terminus of ErbB3 is very likely to interfere with the protein sorting signals which are usually located at the N-terminus of the protein. This probably explained why inconsistent subcellular localisation patterns of ErbB3 were observed in transiently transfected COS-7 cells. As shown in the top panel of Figure 7-8, both cytoplasmic and nuclear expression of ErbB3 was observed. Also, as discussed above, the colocalisation analysis of GFP and Cherry was complicated by the bleed-through artefacts. Therefore, we turned to other methods to continue the localisation study of ErbB3.

Immunofluorescence labelling ErbB3 with Alexa Fluor 633 avoided bleed-through artefacts. Confocal microscopy demonstrated nucleoplasmic localisation of ErbB3 using the monoclonal RTJ2 antibody (Figure 7-11). Transient co-expression of NRG1β3 did not affect its localisation pattern. Even though both NRG1β3 and ErbB3 exhibited nuclear localisation in transiently transfected COS-7 cells, it appeared that NRG1β3 did not cause any relocalisation of ErbB3 inside the nucleus (Figure 7-12). We also examined the subcellular localisation of ErbB3 in the HEK-293 cell line. ErbB3 exhibited membrane localisation in both stably and transiently transfected HEK-293 cells. The localisation pattern of ErbB3 differed between cell lines (nucleolar localisation of ErbB3 in nonmaliganant human mammary epithelia cells (Offterdinger et al., 2002), nucleoplasm accumulation of ErbB3 in transiently transfected COS-7 cells, and membrane localisation of ErbB3 in HEK-293 cells) implying the importance of the cell type in which ErbB3 was expressed. In support of this hypothesis, Cheng et al. has reported that the bone microenvironment and androgen status could influence the nuclear localisation of ErbB3 in prostate cancer cells (Cheng et al., 2007). Moreover, the significance of nuclear localisation of ErbB3 has been assessed in prostate cancers. Both Cheng et al. and Koumakpayi et al. have provided evidence that nuclear localisation of ErbB3 is associated with prostate cancer cell survival and prostate cancer progression (Cheng et al., 2007; Koumakpayi et al., 2006). Thus, identifying factors that regulate subcellular localisation of ErbB3 would provide new perspectives on the functions of intranuclear ErbB3.

Chapter 8. Discussion

The classical signalling pathway involves membrane bound or secreted growth factors binding to and activating their cognate tyrosine kinase receptors at the cell surface. The phosphorylated tyrosine residues on the activated receptor then recruit and activate second messengers thereby initiating downstream signalling pathways that relay information to the nucleus and other intracellular compartments. Beyond this well established mechanism of growth factor signalling, evidence has accumulated in the past two decades that cell surface growth factor ligands and their cognate receptors are present within cell nuclei. Several lines of evidence demonstrate that FGF, EGF, growth hormone and a number of other ligands, as well as their receptors, are targeted to the nucleus (Bryant and Stow, 2005). Acceptance of intranuclear growth factors and their receptors, however, is not universal and many questions remain regarding the transport and functions of intranuclear growth factor ligands and receptors. Nevertheless, the presence of growth factors and their receptors in the nucleus suggests a novel intracellular signalling activity that might complement the canonical cell surface localised signalling mechanism. In our study, we investigated the action of intranuclear NRG1 in attempt to further understand this new mode of signal transduction.

Immunohistochemical staining of DCIS of the breast showed nuclear expression of NRG1α and NRG1β in 40-50% of the cases examined (Marshall et al., 2006), and we also found them in nuclei when surveying a panel of human normal and invasive cancers tissues (see Chapter 3). However, the functions of NRGs in the nucleus are not yet known. To provide further insight into the mechanism of nuclear translocation, we focused our analysis on the β3 isoform of NRG1. The *NRG1* gene contains at least six promoters and its pre-mRNA is extensively spliced to give more than fifteen different protein products (Steinthorsdottir et al., 2004). Most of them are first synthesised as transmembrane precursors and are trafficked to the cell surface. Upon proteolytic cleavage, they are released as secreted molecules, acting in a paracrine and/or autocrine fashion. Alternatively, there are proteins like NRG1β3 which lacks a transmembrane domain and is not secreted from the producing cell, but harbours a putative nuclear localisation sequence at its N-terminus. Using GFP-tagging and digital fluorescent microscopy, which allows higher resolution than immunohistochemical staining, NRG1β3 was found in two subnuclear structures, nucleoli and spliceosomes (Golding et

al., 2004). Recently, Breuleux et al. reported similar results of another splice variant of NRG1 (Breuleux et al., 2006).

As some NRG isoforms can translocate to the nucleus, one question that needs to be addressed is whether nuclear NRGs function through its cognate receptors or by some other process. These two alternative mechanisms are not of course mutually exclusive. Even though it has been shown that localisation of NRG1β3 to the nucleus is receptor independent as it occurs in cells lacking its cognate receptors, ErbB3 and ErbB4, and is unaffected by removal of the receptor-binding domain (Golding et al., 2004), this does not rule out the possibility that a receptor-mediated function could take place in the nucleus. Accumulating evidence has shown that ErbB receptor family members are present in the nucleus. Among the ErbB family members, EGFR (Marti *et al.*, 1991), ErbB2 (Xie and Hung, 1994) and ErbB3 (Offterdinger *et al.*, 2002) are detected in the nucleus as full length receptors. ErbB4 undergoes sequential proteolytic processing producing an intracellular domain (ICD), which translocates to the nucleus and functions as a transcription factor (Ni *et al.*, 2001). Full length ErbB4 was once been detected in the nucleus of human umbilical venous epithelial cells and arterial endothelial cells (Bueter *et al.*, 2006). Using immunohistochemically staining we observed strong nuclear expression of ErbB3 in invasive breast cancer tissues. Moreover, confocal immunofluorescence microscopy showed nucleoplasmic localisation of ErbB3 in transiently transfected COS-7 cells (see Chapter 7).

There are examples of growth factors functioning through their cognate receptors in the nucleus. For instance, it has been demonstrated that nuclear EGF binds EGFR in comparable fashion to surface EGFR and this nuclear ligand/receptor complex could induce tyrosine autophosphorylation of EGFR (Cao et al., 1995). In this study, we used two experimental approaches to investigate the receptor-mediated effects of intranuclear expression of NRG1. One was based on "candidate" effects. As quite a few growth factors localised in the nucleolus show mitogenic functions and nucleolus is well-known as the centre of ribosome biogenesis, we looked at the effect of differential subnuclear localisation of NRG1β3 on cell mitogenesis which was measured by bromodeoxyuridine incorporation and on the level of ribosomal RNA using RNA gel electrophoresis. The other structure where NRG1β3 accumulates is spliceosomes. This localisation pattern is highly characteristic for proteins that are involved in pre-mRNA splicing. Moreover, the spliceosome exhibits exceptional compositional dynamics (Wahl

et al., 2009). It contains many proteins that are loosely associated and are only called into action or required in certain situations. As demonstrated by Golding et al., (2004) as well as our findings, NRG1β3 is a dynamic protein which could relocalise from nucleoli to spliceosomes within 90min, suggesting that NRG1β3 might be involved in the spliceosome activities such as to prepare for the splicing of pre-mRNA and/or to react to changes in the state of the cell or its environment. As the mRNA of both *NRG1* and *ErbB4* its cognate receptor genes are subjected to alternative splicing and there are examples that the system can regulate itself, we looked at the splicing efficiency of subnuclear localisation of NRG1β3 on its own gene and on the *ErbB4* gene products using the RT-PCR technique. No significant effect was however observed in any of the above experiments. While these techniques are only semiquantitative the lack of an obvious effect inclined us to explore other possible activities and we did not pursue these experiments further due to time constraints.

The other screening approach utilised in my project aimed for new discoveries of genes whose expression was altered at either the transcription or the protein level. In our attempt to identify genes regulated due to differential subnuclear localisation of NRG1, we observed induced Hsp70B' transcription only when the protein was present in the spliceosomes. Moreover, we were able to confirm its expression at the protein level by performing western blot analysis with an antibody specific to the Hsp70B' protein. Consistent with our transcriptomic results, Hsp70B' was identified as one of the NRG-inducible gene products in human breast cancer cells (Mandal et al., 2002).

Mammalian heat shock proteins have been classified into different families according to their molecular size and each family of heat shock proteins is composed of members expressed either constitutively or those which may be regulated inductively. Under non-stressed conditions, the expression of Hsp70B' is usually very low. In contrast, the expression of Hsp70B' is induced after many different kinds of stresses such as heat, irradiation, oxidative stress, or anticancer chemotherapy. High expression of Hsp70B' has been reported in high grade malignant tumours such as breast, endometrial and gastric cancer (Brondani Da Rocha et al., 2004; Vargas-Roig et al., 1998) and it appears to be a factor in tumour pathogenesis largely explained by its anti-apoptotic functions which permit malignant cells to arise despite the triggering of apoptotic signals during transformation. Moreover, a molecular link has been shown between Hsp70B' expression and tumour progression in prostate cancer (Grossmann et al., 2001).

As reported by Marshall et al. NRG1 and NRG3 were found expressed at quite high levels in up to half of cases of DCIS of the breast and we observed relatively high incidence of nuclear NRG1 expression in invasive cancers such as bone and soft tissue cancers (Marshall et al., 2006). One hypothesis consistent with our observations is that those cells may be in a stressed state due to hypoxia and accumulation of waste products. Our transcriptomic results for the first time linked spliceosome localised NRG1 with the highly conserved heat shock response. At this stage, we do not know if stresses have any effect on the nuclear splice variants of the *NRG1* gene as they have on the translation control of some cytokine mRNA products (Cully and Downward, 2009) and if spliceosome accumulation of NRG1 could increase the tumourigenicity of cancer cells by utilising the cytoprotective effects of molecular chaperone genes or even is associated with poor prognosis and resistance to chemotherapy or radiation therapy; given this, however, it will be of interest to explore the underlying mechanisms.

Another important finding of my study is that using mutants of NRG1β3 which localised exclusively to spliceosomes or to nucleoli we demonstrated that spliceosome localisation increased the expression and/or phosphorylation of the ErbB4 receptor, and to a less extent the ErbB2 receptor (see Chapter 5). NRG1 is a direct ligand of ErbB4 which can activate the kinase activity of ErbB4. Even though NRG1 does not bind to ErbB2, it is possible that ErbB2 became phosphorylated by forming heterodimers with ErbB4. However, we were unable to confirm these results by western blot analysis. One possible explanation to account for this is that the Human Phospho-RTK Array is more sensitive than western blot in detecting the phosphorylation/expression level changes. To distinguish whether the observed ErbB4 activation in the kinomic results was due to the increased protein expression or the phosphorylation of ErbB4, we purchased a site specific phopho-ErbB4 antibody, which should be able to detect ErbB4 phosphorylation. However, no specific signals were observed when blotting the cell lysates with this antibody, although many non-specific bands of other molecular weight were seen. The reliability of this commercial available antibody needs to be confirmed.

ErbB3 is another cognate receptor of NRG1. It has been reported that NRG1β1 treatment could affect the subcellular localisation of ErbB3 in human mammary cell lines by shifting ErbB3 from the nucleolus into the nucleoplasm and then into the cytoplasm (Offterdinger *et al.*, 2002). In our experiments, when NRG1β3 and ErbB3 were coexpressed and examined by confocal immunofluorescence microscopy, we

observed nucleoplasmic localisation of ErbB3, without any extra accumulation in spliceosomes where NRG1β3 localised. Our results suggest that spliceosomes are the site where activation of the nuclear ErbB receptors occurs upon NRG1β3 binding. Also, we noticed that ErbB3 exhibited either nucleoplasmic or membrane localisation depending on the type of cell line in which it was expressed, which is supported by the findings of other research groups, that ErbB3 localisation patterns are greatly affected by the microenvironment of the expressing cell (Cheng et al., 2007; Koumakpayi et al., 2006). More specifically, it has been demonstrated that ErbB3 nuclear localisation discriminated normal from malignant prostate tissues and between tumours from hormone-sensitive versus hormone-refractory prostate cancer. Taken together the kinomic results and the regulated nuclear localisation of ErbB3, we hypothesised that activation of the ErbB receptor family members in different subcellular compartments might engage and activate different second messengers thus leading to different cellular responses. There is, indeed, evidence to support this hypothesis.

At the cell surface, ligand binding triggers receptor dimerisation which subsequently activates many downstream signalling pathways, including the ERK-MAPK pathway, the PI3K pathway, and the pathways that regulate small GTPases (Schlessinger, 2000). Signals transmitted through these pathways regulate transcription of the immediate-response genes, such as those encoding the transcription factors Myc and Fos, which greatly affect nuclear events such as mitogenesis and changes in gene expression.

In the cytosol, it has been shown that activated EGFR tightly controls its overall endocytosis by modulating the trafficking of the clathrin-coated pit associated proteins such as epsin and Eps15 (Vecchi et al., 2001). These endocytic proteins shuttle in and out of the nucleus where they are believed to regulate a limited and specific set of genes implicated in specific processes, for example in this instance in clathrin-coated pits or endosome formation. The possibility that activated receptors organise their own endocytosis has been considered as an extension of membrane receptor function in terms of the assembly of signalling cascades.

Inside the nucleus, the C-terminal regions of EGFR (Lin *et al.*, 2001), ErbB2 (Xie and Hung, 1994), and ErbB4 (Ni *et al.*, 2001) have been reported to possess transactivation activity and multiple promoters have been identified as the targets of nuclear ErbB

receptors. As EGFR lacks a DNA binding domain, it can physically interact with signal transducers and activators of transcription 3 (STAT3) in the nucleus. This complex was shown to bind to the AT-rich sequence of the promoters leading to transcriptional activation of several genes, including cyclin D1 and inducible nitric oxide synthase (Lo *et al.*, 2005). Nuclear ErbB2 forms a complex at a specific nucleotide sequence of the cyclooxygenase enzyme COX-2 gene promoter and is able to stimulate its transcription (Wang *et al.*, 2004). COX-2 affects cell proliferation and has been shown to be important in carcinogenesis (Soslow *et al.*, 2000). ErbB4 conveys its transcriptional function through its ICD domain. Ligand binding activates ErbB4 leading to the recruitment of STAT5A to a phosphorylated receptor tyrosine residue. The cleaved ICD conveys STAT5A to the nucleus which in turn transactivates the β-casein gene promoter (Williams *et al.*, 2004). In addition to a role of RTKs in the control of gene regulation, modification of nuclear proteins is another function for nuclear-localised receptors or their cytoplasmic domain fragments. EGFR phosphorylates the chromatin-bound DNA replication and damage repair factor proliferating cell nuclear antigen (PCNA). Increased PCNA phosphorylation is associated with increased cell proliferation and is correlated with poor survival of breast cancer patients (Wang et al., 2006a). ErbB2 has been shown to colocalise with and bind to cyclin B-Cdc2 complexes and phosphorylates Cdc2 in the nucleus. Increased phosphorylation of Cdc-2 in ErbB2 overexpressing cells inhibits the kinase activity of Cdc-2 and delays M-phase entry, leading to taxol resistance in breast cancer (Tan *et al.*, 2002). Expression of ErbB4 ICD phosphorylates and inhibits the nuclear protein Mdm2 and consequently increases the levels of p53 and p21 expression (Arasada and Carpenter, 2005).

Despite the evidence of localisation of full length ErbB receptors in the nucleus as well as their hypothesised or demonstrated molecular functions, the mechanistic basis of how intrinsic membrane proteins translocate to the nucleoplasm, unassociated with the nuclear envelope, has remained to be identified. A mechanism termed "retro-translocation" has been proposed by a number of investigators. It is an alternative application of the endoplasmic reticulum (ER) associated degradation (ERAD) pathway (Tsai *et al.*, 2002), which functions to move unfolded or misfolded proteins from the ER lumen to the cytoplasm for ubiquitin-dependent degradation. The assumption that ERAD facilitates the movement of cell surface proteins to the cytoplasm or to the nucleus is based on several toxins entering cells by this route (Sandvig and van Deurs, 2000). For example, following binding to cell surface receptors, the plant toxin ricin is

endocytosed then moves from the endosome through the Golgi to the ER, where it is transported to the cytoplasm. The typical fate of proteins moving through the ERAD pathway is that they get ubiquitinated and degraded. The ability of ricin to escape the normal degradative fate of ERAD substrates suggests there are alternative fates but it is unclear that how normal cellular proteins can exploit such a retrograde transport system in the manner demonstrated by toxins. It has been proposed that the retro-translocation model involves the internalisation of the surface receptor through the clathrin-coated endocytotic vesicle, which then merges with the ER through the Golgi. The retro-translocation of ER-bound EGFR into the cytosol involves the Sec61 translocon (Liao and Carpenter, 2007) which forms a channel across the ER membrane for protein transport (Wiertz *et al.*, 1996). The membrane protein in the cytosol is stabilised by the chaperone protein HSP70, and then directed by the nuclear transporter importin proteins to the nucleus through the nuclear pore complex (Giri *et al.*, 2005). The above scenario provides the only currently available plausible hypothese for liberation from a lipid bilayer and transport to the nucleus but does not define the complete process of how these receptors make their way to the nucleus. A completely different hypothesis argues that full length growth factor receptors are located at the nuclear membrane (envelope) rather than in a soluble form in the nucleoplasm. As nascent receptors are synthesised by nuclear membrane associated ribosomes, the newly synthesised receptors will be found in the outer leaflet of the nuclear envelope which could have multiple intranuclear invaginations and pores (Fricker et al., 1997). However, without being glycosylated in the Golgi apparatus the functionality of these receptors remain questionable. All these proposed mechanisms remain speculative and thus need to be demonstrated experimentally.

Considering that the double nuclear membrane with nuclear invaginations are surrounded by the endoplasmic reticulum, plasma membrane, and other various exocytotic and endocytotic vesicular structures, it is not surprising that researchers using microscopy techniques find identifying true intra-nucleoplasmic proteins rather difficult. The membrane structures within a cell grown in tissue culture as a monolayer are remarkably flat and as such the actual localisation of these growth factor receptors needs to be examined with extra care. Thus while there is some evidence and much speculation regarding the presence of truly nucleoplasmic growth factor receptors it must also be considered that they are not present. If we assume that there are no full length ErbB receptors in the nucleus, the most intriguing question needs to be

considered is what is intranuclear NRG1 doing?

In the experiment exploring intranuclear trafficking of NRG1β3 using the photoactivateable GFP-tagged protein, we observed that when the fusion protein located in nucleoli was activated it gradually disappeared from this site and reappeared in spliceosomes over a ninety minute period, which is consistent with previous findings that NRG1β3 localisation patterns interconverted within two hours (Golding et al., 2004). Furthermore, this observation provides evidence in support of the hypothesis that NRG1β3 moves from one intranuclear compartment to the other rather than being degraded in one compartment while re-synthesised and targeted to the other compartment. We suspected that relocalisation of NRG1β3 might be associated with other nuclear proteins in each subnuclear compartment. Using a yeast two-hybrid screen Breuleux et al. identified several spliceosome located proteins that interacted with NRG1α in spliceosomes (Breuleux et al., 2006). In a mutational analysis performed in our laboratory by Dr C. Trim, four positively charged resides were identified which were necessary for spliceosome localisation of NRG1β3. Molecular modelling suggested that three of these may form a binding site for interaction with structures within the spliceosome (Wang et al., 2010, submitted). Therefore, it is possible that the two localisation sequences of NRG1β3 identified to be responsible for each subnuclear structure localisation are involved in protein-protein interactions. When NRG1β3 needs to relocate, associated nuclear proteins presumably dissociate from it, allowing it to move. Several proteins have been reported with the similar behaviour of moving between different subnuclear compartments. One such example is Cdc14, which is sequestered in the nucleolus for most of the cell cycle and then is released from the nucleolus during nuclear division, allowing it to reach its targets (Visintin et al., 1999). It is possible therefore that controlled relocalisation of NRG1β3 is associated with the cell cycle, and its interacting proteins might be cell cycle regulators.

The conventional view that ligands and their membrane receptors fulfil their signalling roles uniquely at the cell membrane and that signals are subsequently relayed on to the nucleus through pathways involving common second messengers and phosphorylation cascades fail to explain the wide diversity of ligands/receptors and their corresponding unique and specific gene expression profiles (Subramaniam et al., 2001). Direct action within the nucleus of specific ligand and/or ligand/receptor complexes provides an additional level of regulation in terms of selectivity, specificity, and efficiency of gene

transcription control. To leap to the next step in understanding these processes, we will have to discover the mechanistic basis of the molecular and cellular functions of these nuclear ligands and receptors before they will be generally accepted. Now the weight of evidence has tipped the scales towards the belief that these events do occur in at least some cells under specific circumstances. We expect an expanding effort by many more investigators in the next few years and the findings are likely to be as unexpected as they have been so far.

References

Abbott, B.D., Lin, T.M., Rasmussen, N.T., Albrecht, R.M., Schmid, J.E., and Peterson, R.E. (2003). Lack of expression of EGF and TGF-alpha in the fetal mouse alters formation of prostatic epithelial buds and influences the response to TCDD. Toxicol Sci *76*, 427-436.

Adam, R.M., Danciu, T., McLellan, D.L., Borer, J.G., Lin, J., Zurakowski, D., Weinstein, M.H., Rajjayabun, P.H., Mellon, J.K., and Freeman, M.R. (2003). A nuclear form of the heparin-binding epidermal growth factor-like growth factor precursor is a feature of aggressive transitional cell carcinoma. Cancer Res *63*, 484-490.

Adnane, J., Gaudray, P., Dionne, C.A., Crumley, G., Jaye, M., Schlessinger, J., Jeanteur, P., Birnbaum, D., and Theillet, C. (1991). BEK and FLG, two receptors to members of the FGF family, are amplified in subsets of human breast cancers. Oncogene *6*, 659-663.

Aguilar, Z., and Slamon, D.J. (2001). The transmembrane heregulin precursor is functionally active. J Biol Chem *276*, 44099-44107.

Amit, I., Wides, R., and Yarden, Y. (2007). Evolvable signaling networks of receptor tyrosine kinases: relevance of robustness to malignancy and to cancer therapy. Mol Syst Biol *3*, 151.

Ando, R., Hama, H., Yamamoto-Hino, M., Mizuno, H., and Miyawaki, A. (2002). An optical marker based on the UV-induced green-to-red photoconversion of a fluorescent protein. Proc Natl Acad Sci U S A *99*, 12651-12656.

Arasada, R.R., and Carpenter, G. (2005). Secretase-dependent tyrosine phosphorylation of Mdm2 by the ErbB-4 intracellular domain fragment. J Biol Chem *280*, 30783-30787.

Aubele, M., Auer, G., Walch, A.K., Munro, A., Atkinson, M.J., Braselmann, H., Fornander, T., and Bartlett, J.M. (2007). PTK (protein tyrosine kinase)-6 and HER2 and 4, but not HER1 and 3 predict long-term survival in breast carcinomas. Br J Cancer *96*, 801-807.

Bagheri-Yarmand, R., Vadlamudi, R.K., Wang, R.A., Mendelsohn, J., and Kumar, R. (2000). Vascular endothelial growth factor up-regulation via p21-activated kinase-1 signaling regulates heregulin-beta1-mediated angiogenesis. J Biol Chem *275*, 39451-39457.

Bao, J., Wolpowitz, D., Role, L.W., and Talmage, D.A. (2003). Back signaling by the Nrg-1 intracellular domain. J Cell Biol *161*, 1133-1141.

Baselga, J., and Averbuch, S.D. (2000). ZD1839 ('Iressa') as an anticancer agent. Drugs *60 Suppl 1*, 33-40; discussion 41-32.

Baselga, J., Mendelsohn, J., Kim, Y.M., and Pandiella, A. (1996). Autocrine regulation of membrane transforming growth factor-alpha cleavage. J Biol Chem *271*, 3279-3284.

Bennasroune, A., Gardin, A., Aunis, D., Cremel, G., and Hubert, P. (2004). Tyrosine

kinase receptors as attractive targets of cancer therapy. Crit Rev Oncol Hematol *50*, 23-38.

Birchmeier, C. (2009). ErbB receptors and the development of the nervous system. Exp Cell Res *315*, 611-618.

Bouche, G., Gas, N., Prats, H., Baldin, V., Tauber, J.P., Teissie, J., and Amalric, F. (1987). Basic fibroblast growth factor enters the nucleolus and stimulates the transcription of ribosomal genes in ABAE cells undergoing G0----G1 transition. Proc Natl Acad Sci U S A *84*, 6770-6774.

Breuleux, M. (2007). Role of heregulin in human cancer. Cell Mol Life Sci *64*, 2358-2377.

Breuleux, M., Schoumacher, F., Rehn, D., Kung, W., Mueller, H., and Eppenberger, U. (2006). Heregulins implicated in cellular functions other than receptor activation. Mol Cancer Res *4*, 27-37.

Brondani Da Rocha, A., Regner, A., Grivicich, I., Pretto Schunemann, D., Diel, C., Kovaleski, G., Brunetto De Farias, C., Mondadori, E., Almeida, L., Braga Filho, A., *et al.* (2004). Radioresistance is associated to increased Hsp70 content in human glioblastoma cell lines. Int J Oncol *25*, 777-785.

Bryant, D.M., and Stow, J.L. (2005). Nuclear translocation of cell-surface receptors: lessons from fibroblast growth factor. Traffic *6*, 947-954.

Bueter, W., Dammann, O., Zscheppang, K., Korenbaum, E., and Dammann, C.E. (2006). ErbB receptors in fetal endothelium--a potential linkage point for inflammation-associated neonatal disorders. Cytokine *36*, 267-275.

Burgess, T.L., Ross, S.L., Qian, Y.X., Brankow, D., and Hu, S. (1995). Biosynthetic processing of neu differentiation factor. Glycosylation trafficking, and regulated cleavage from the cell surface. J Biol Chem *270*, 19188-19196.

Busfield, S.J., Michnick, D.A., Chickering, T.W., Revett, T.L., Ma, J., Woolf, E.A., Comrack, C.A., Dussault, B.J., Woolf, J., Goodearl, A.D., *et al.* (1997). Characterization of a neuregulin-related gene, Don-1, that is highly expressed in restricted regions of the cerebellum and hippocampus. Mol Cell Biol *17*, 4007-4014.

Camirand, A., Lu, Y., and Pollak, M. (2002). Co-targeting HER2/ErbB2 and insulin-like growth factor-1 receptors causes synergistic inhibition of growth in HER2-overexpressing breast cancer cells. Med Sci Monit *8*, BR521-526.

Cao, H., Lei, Z.M., Bian, L., and Rao, C.V. (1995). Functional nuclear epidermal growth factor receptors in human choriocarcinoma JEG-3 cells and normal human placenta. Endocrinology *136*, 3163-3172.

Carpenter, G. (2003). Nuclear localization and possible functions of receptor tyrosine kinases. Curr Opin Cell Biol *15*, 143-148.

Carraway, K.L., 3rd, and Burden, S.J. (1995). Neuregulins and their receptors. Curr Opin Neurobiol *5*, 606-612.

Carraway, K.L., 3rd, Weber, J.L., Unger, M.J., Ledesma, J., Yu, N., Gassmann, M., and Lai, C. (1997). Neuregulin-2, a new ligand of ErbB3/ErbB4-receptor tyrosine kinases. Nature *387*, 512-516.

Carteron, C., Ferrer-Montiel, A., and Cabedo, H. (2006). Characterization of a neural-specific splicing form of the human neuregulin 3 gene involved in oligodendrocyte survival. J Cell Sci *119*, 898-909.

Cheng, C.J., Ye, X.C., Vakar-Lopez, F., Kim, J., Tu, S.M., Chen, D.T., Navone, N.M., Yu-Lee, L.Y., Lin, S.H., and Hu, M.C. (2007). Bone microenvironment and androgen status modulate subcellular localization of ErbB3 in prostate cancer cells. Mol Cancer Res *5*, 675-684.

Chudakov, D.M., Belousov, V.V., Zaraisky, A.G., Novoselov, V.V., Staroverov, D.B., Zorov, D.B., Lukyanov, S., and Lukyanov, K.A. (2003). Kindling fluorescent proteins for precise in vivo photolabeling. Nat Biotechnol *21*, 191-194.

Ciardiello, F., and Tortora, G. (2003). Epidermal growth factor receptor (EGFR) as a target in cancer therapy: understanding the role of receptor expression and other molecular determinants that could influence the response to anti-EGFR drugs. Eur J Cancer *39*, 1348-1354.

Citri, A., Alroy, I., Lavi, S., Rubin, C., Xu, W., Grammatikakis, N., Patterson, C., Neckers, L., Fry, D.W., and Yarden, Y. (2002). Drug-induced ubiquitylation and degradation of ErbB receptor tyrosine kinases: implications for cancer therapy. Embo J *21*, 2407-2417.

Citri, A., Skaria, K.B., and Yarden, Y. (2003). The deaf and the dumb: the biology of ErbB-2 and ErbB-3. Exp Cell Res *284*, 54-65.

Cohen, B.D., Green, J.M., Foy, L., and Fell, H.P. (1996). HER4-mediated biological and biochemical properties in NIH 3T3 cells. Evidence for HER1-HER4 heterodimers. J Biol Chem *271*, 4813-4818.

Cohen, G.B., Ren, R., and Baltimore, D. (1995). Modular binding domains in signal transduction proteins. Cell *80*, 237-248.

Coons, A.H., and Kaplan, M.H. (1950). Localization of antigen in tissue cells; improvements in a method for the detection of antigen by means of fluorescent antibody. J Exp Med *91*, 1-13.

Cully, M., and Downward, J. (2009). Translational responses to growth factors and stress. Biochem Soc Trans *37*, 284-288.

Daneshmand, M., Parolin, D.A., Hirte, H.W., Major, P., Goss, G., Stewart, D., Batist, G., Miller, W.H., Jr., Matthews, S., Seymour, L., *et al.* (2003). A pharmacodynamic study of the epidermal growth factor receptor tyrosine kinase inhibitor ZD1839 in metastatic colorectal cancer patients. Clin Cancer Res *9*, 2457-2464.

Dapson, R.W. (1993). Fixation for the 1990's: a review of needs and accomplishments. Biotech Histochem *68*, 75-82.

Daub, H., Weiss, F.U., Wallasch, C., and Ullrich, A. (1996). Role of transactivation of the EGF receptor in signalling by G-protein-coupled receptors. Nature *379*, 557-560.

Derynck, R., Goeddel, D.V., Ullrich, A., Gutterman, J.U., Williams, R.D., Bringman, T.S., and Berger, W.H. (1987). Synthesis of messenger RNAs for transforming growth factors alpha and beta and the epidermal growth factor receptor by human tumors. Cancer Res *47*, 707-712.

Diaz-Rodriguez, E., Esparis-Ogando, A., Montero, J.C., Yuste, L., and Pandiella, A. (2000). Stimulation of cleavage of membrane proteins by calmodulin inhibitors. Biochem J *346 Pt 2*, 359-367.

Donepudi, M., and Resh, M.D. (2008). c-Src trafficking and co-localization with the EGF receptor promotes EGF ligand-independent EGF receptor activation and signaling. Cell Signal *20*, 1359-1367.

Dunn, M., Sinha, P., Campbell, R., Blackburn, E., Levinson, N., Rampaul, R., Bates, T., Humphreys, S., and Gullick, W.J. (2004). Co-expression of neuregulins 1, 2, 3 and 4 in human breast cancer. J Pathol *203*, 672-680.

Eck, M.J., Dhe-Paganon, S., Trub, T., Nolte, R.T., and Shoelson, S.E. (1996). Structure of the IRS-1 PTB domain bound to the juxtamembrane region of the insulin receptor. Cell *85*, 695-705.

Eib, D.W., and Martens, G.J. (1996). A novel transmembrane protein with epidermal growth factor and follistatin domains expressed in the hypothalamo-hypophysial axis of Xenopus laevis. J Neurochem *67*, 1047-1055.

Elenius, K., Choi, C.J., Paul, S., Santiestevan, E., Nishi, E., and Klagsbrun, M. (1999). Characterization of a naturally occurring ErbB4 isoform that does not bind or activate phosphatidyl inositol 3-kinase. Oncogene *18*, 2607-2615.

Engelman, J.A., Janne, P.A., Mermel, C., Pearlberg, J., Mukohara, T., Fleet, C., Cichowski, K., Johnson, B.E., and Cantley, L.C. (2005). ErbB-3 mediates phosphoinositide 3-kinase activity in gefitinib-sensitive non-small cell lung cancer cell lines. Proc Natl Acad Sci U S A *102*, 3788-3793.

Erickson, S.L., O'Shea, K.S., Ghaboosi, N., Loverro, L., Frantz, G., Bauer, M., Lu, L.H., and Moore, M.W. (1997). ErbB3 is required for normal cerebellar and cardiac development: a comparison with ErbB2-and heregulin-deficient mice. Development *124*, 4999-5011.

Eto, K., Eda, K., Kanemoto, S., and Abe, S. (2006). The immunoglobulin-like domain is involved in interaction of Neuregulin1 with ErbB. Biochem Biophys Res Commun *350*, 263-271.

Everett, A.D., Stoops, T., and McNamara, C.A. (2001). Nuclear targeting is required for hepatoma-derived growth factor-stimulated mitogenesis in vascular smooth muscle cells. J Biol Chem *276*, 37564-37568.

Ewald, D., Li, M., Efrat, S., Auer, G., Wall, R.J., Furth, P.A., and Hennighausen, L. (1996). Time-sensitive reversal of hyperplasia in transgenic mice expressing SV40 T

antigen. Science *273*, 1384-1386.

Falls, D.L. (2003). Neuregulins: functions, forms, and signaling strategies. Exp Cell Res *284*, 14-30.

Fan, H., Turck, C.W., and Derynck, R. (2003). Characterization of growth factor-induced serine phosphorylation of tumor necrosis factor-alpha converting enzyme and of an alternatively translated polypeptide. J Biol Chem *278*, 18617-18627.

Fedi, P., Pierce, J.H., di Fiore, P.P., and Kraus, M.H. (1994). Efficient coupling with phosphatidylinositol 3-kinase, but not phospholipase C gamma or GTPase-activating protein, distinguishes ErbB-3 signaling from that of other ErbB/EGFR family members. Mol Cell Biol *14*, 492-500.

Fischer, E.H. (1999). Cell signaling by protein tyrosine phosphorylation. Adv Enzyme Regul *39*, 359-369.

Fluge, O., Akslen, L.A., Haugen, D.R., Varhaug, J.E., and Lillehaug, J.R. (2000). Expression of heregulins and associations with the ErbB family of tyrosine kinase receptors in papillary thyroid carcinomas. Int J Cancer *87*, 763-770.

Fowler, K.J., Walker, F., Alexander, W., Hibbs, M.L., Nice, E.C., Bohmer, R.M., Mann, G.B., Thumwood, C., Maglitto, R., Danks, J.A., *et al.* (1995). A mutation in the epidermal growth factor receptor in waved-2 mice has a profound effect on receptor biochemistry that results in impaired lactation. Proc Natl Acad Sci U S A *92*, 1465-1469.

Fricker, M., Hollinshead, M., White, N., and Vaux, D. (1997). Interphase nuclei of many mammalian cell types contain deep, dynamic, tubular membrane-bound invaginations of the nuclear envelope. J Cell Biol *136*, 531-544.

Fu, X.D. (1995). The superfamily of arginine/serine-rich splicing factors. Rna *1*, 663-680.

Garrett, T.P., McKern, N.M., Lou, M., Elleman, T.C., Adams, T.E., Lovrecz, G.O., Zhu, H.J., Walker, F., Frenkel, M.J., Hoyne, P.A., *et al.* (2002). Crystal structure of a truncated epidermal growth factor receptor extracellular domain bound to transforming growth factor alpha. Cell *110*, 763-773.

Gassmann, M., Casagranda, F., Orioli, D., Simon, H., Lai, C., Klein, R., and Lemke, G. (1995). Aberrant neural and cardiac development in mice lacking the ErbB4 neuregulin receptor. Nature *378*, 390-394.

Gilbertson, R.J., Clifford, S.C., MacMeekin, W., Meekin, W., Wright, C., Perry, R.H., Kelly, P., Pearson, A.D., and Lunec, J. (1998). Expression of the ErbB-neuregulin signaling network during human cerebellar development: implications for the biology of medulloblastoma. Cancer Res *58*, 3932-3941.

Gilmour, L.M., Macleod, K.G., McCaig, A., Gullick, W.J., Smyth, J.F., and Langdon, S.P. (2001). Expression of erbB-4/HER-4 growth factor receptor isoforms in ovarian cancer. Cancer Res *61*, 2169-2176.

Gilmour, L.M., Macleod, K.G., McCaig, A., Sewell, J.M., Gullick, W.J., Smyth, J.F., and Langdon, S.P. (2002). Neuregulin expression, function, and signaling in human ovarian cancer cells. Clin Cancer Res *8*, 3933-3942.

Giri, D.K., Ali-Seyed, M., Li, L.Y., Lee, D.F., Ling, P., Bartholomeusz, G., Wang, S.C., and Hung, M.C. (2005). Endosomal transport of ErbB-2: mechanism for nuclear entry of the cell surface receptor. Mol Cell Biol *25*, 11005-11018.

Gizatullin, R.Z., Muravenko, O.V., Al-Amin, A.N., Wang, F., Protopopov, A.I., Kashuba, V.I., Zelenin, A.V., and Zabarovsky, E.R. (2000). Human NRG3 gene Map position 10q22-q23. Chromosome Res *8*, 560.

Golding, M., Ruhrberg, C., Sandle, J., and Gullick, W.J. (2004). Mapping nucleolar and spliceosome localization sequences of neuregulin1-beta3. Exp Cell Res *299*, 110-118.
Gollamudi, M., Nethery, D., Liu, J., and Kern, J.A. (2004). Autocrine activation of ErbB2/ErbB3 receptor complex by NRG-1 in non-small cell lung cancer cell lines. Lung Cancer *43*, 135-143.
Grossmann, M.E., Huang, H., and Tindall, D.J. (2001). Androgen receptor signaling in androgen-refractory prostate cancer. J Natl Cancer Inst *93*, 1687-1697.

Gullick, W.J. (1996). The c-erbB3/HER3 receptor in human cancer. Cancer Surv *27*, 339-349.

Gullick, W.J. (2001). The Type 1 growth factor receptors and their ligands considered as a complex system. Endocr Relat Cancer *8*, 75-82.

Hanahan, D., and Weinberg, R.A. (2000). The hallmarks of cancer. Cell *100*, 57-70.

Hansen, M.R., Roehm, P.C., Chatterjee, P., and Green, S.H. (2006). Constitutive neuregulin-1/ErbB signaling contributes to human vestibular schwannoma proliferation. Glia *53*, 593-600.

Harari, D., Tzahar, E., Romano, J., Shelly, M., Pierce, J.H., Andrews, G.C., and Yarden, Y. (1999). Neuregulin-4: a novel growth factor that acts through the ErbB-4 receptor tyrosine kinase. Oncogene *18*, 2681-2689.

Hayes, N.V., Blackburn, E., Smart, L.V., Boyle, M.M., Russell, G.A., Frost, T.M., Morgan, B.J., Baines, A.J., and Gullick, W.J. (2007). Identification and characterization of novel spliced variants of neuregulin 4 in prostate cancer. Clin Cancer Res *13*, 3147-3155.

Hayes, N.V., and Gullick, W.J. (2008). The neuregulin family of genes and their multiple splice variants in breast cancer. J Mammary Gland Biol Neoplasia *13*, 205-214.
Heldin, C.H. (1995). Dimerization of cell surface receptors in signal transduction. Cell *80*, 213-223.

Higashiyama, S., Horikawa, M., Yamada, K., Ichino, N., Nakano, N., Nakagawa, T., Miyagawa, J., Matsushita, N., Nagatsu, T., Taniguchi, N., *et al.* (1997). A novel brain-derived member of the epidermal growth factor family that interacts with ErbB3 and ErbB4. J Biochem *122*, 675-680.

Holbro, T., Beerli, R.R., Maurer, F., Koziczak, M., Barbas, C.F., 3rd, and Hynes, N.E.

(2003). The ErbB2/ErbB3 heterodimer functions as an oncogenic unit: ErbB2 requires ErbB3 to drive breast tumor cell proliferation. Proc Natl Acad Sci U S A *100*, 8933-8938.

Holmes, W.E., Sliwkowski, M.X., Akita, R.W., Henzel, W.J., Lee, J., Park, J.W., Yansura, D., Abadi, N., Raab, H., Lewis, G.D., *et al.* (1992). Identification of heregulin, a specific activator of p185erbB2. Science *256*, 1205-1210.

Howard, B.A. (2008). The role of NRG3 in mammary development. J Mammary Gland Biol Neoplasia *13*, 195-203.

Howe, J.R., Skryabin, B.V., Belcher, S.M., Zerillo, C.A., and Schmauss, C. (1995). The responsiveness of a tetracycline-sensitive expression system differs in different cell lines. J Biol Chem *270*, 14168-14174.

Howell, G.M., Ziober, B.L., Humphrey, L.E., Willson, J.K., Sun, L., Lynch, M., and Brattain, M.G. (1995). Regulation of autocrine gastrin expression by the TGF alpha autocrine loop. J Cell Physiol *162*, 256-265.

Hubbard, S.R. (2009). The juxtamembrane region of EGFR takes center stage. Cell *137*, 1181-1183.

Hubbard, S.R., and Till, J.H. (2000). Protein tyrosine kinase structure and function. Annu Rev Biochem *69*, 373-398.

Ito, Y., Takeda, T., Higashiyama, S., Noguchi, S., and Matsuura, N. (2001). Expression of heparin-binding epidermal growth factor-like growth factor in breast carcinoma. Breast Cancer Res Treat *67*, 81-85.

Janmaat, M.L., Kruyt, F.A., Rodriguez, J.A., and Giaccone, G. (2003). Response to epidermal growth factor receptor inhibitors in non-small cell lung cancer cells: limited antiproliferative effects and absence of apoptosis associated with persistent activity of extracellular signal-regulated kinase or Akt kinase pathways. Clin Cancer Res *9*, 2316-2326.

Jans, D.A., and Hassan, G. (1998). Nuclear targeting by growth factors, cytokines, and their receptors: a role in signaling? Bioessays *20*, 400-411.

Jeong, E.G., Soung, Y.H., Lee, J.W., Lee, S.H., Nam, S.W., Lee, J.Y., Yoo, N.J., and Lee, S.H. (2006). ERBB3 kinase domain mutations are rare in lung, breast and colon carcinomas. Int J Cancer *119*, 2986-2987.

Johnson, G.R., Saeki, T., Auersperg, N., Gordon, A.W., Shoyab, M., Salomon, D.S., and Stromberg, K. (1991). Response to and expression of amphiregulin by ovarian carcinoma and normal ovarian surface epithelial cells: nuclear localization of endogenous amphiregulin. Biochem Biophys Res Commun *180*, 481-488.

Jones, F.E., and Stern, D.F. (1999). Expression of dominant-negative ErbB2 in the mammary gland of transgenic mice reveals a role in lobuloalveolar development and lactation. Oncogene *18*, 3481-3490.

Jones, J.T., Akita, R.W., and Sliwkowski, M.X. (1999). Binding specificities and

affinities of egf domains for ErbB receptors. FEBS Lett *447*, 227-231.

Joo, C.K., Kim, H.S., Park, J.Y., Seomun, Y., Son, M.J., and Kim, J.T. (2008). Ligand release-independent transactivation of epidermal growth factor receptor by transforming growth factor-beta involves multiple signaling pathways. Oncogene *27*, 614-628.

Jura, N., Endres, N.F., Engel, K., Deindl, S., Das, R., Lamers, M.H., Wemmer, D.E., Zhang, X., and Kuriyan, J. (2009). Mechanism for activation of the EGF receptor catalytic domain by the juxtamembrane segment. Cell *137*, 1293-1307.

Kario, E., Marmor, M.D., Adamsky, K., Citri, A., Amit, I., Amariglio, N., Rechavi, G., and Yarden, Y. (2005). Suppressors of cytokine signaling 4 and 5 regulate epidermal growth factor receptor signaling. J Biol Chem *280*, 7038-7048.

Kataoka, H. (2009). EGFR ligands and their signaling scissors, ADAMs, as new molecular targets for anticancer treatments. J Dermatol Sci *56*, 148-153.

Keresztes, M., and Boonstra, J. (1999). Import(ance) of growth factors in(to) the nucleus. J Cell Biol *145*, 421-424.

Kim, E.S., Khuri, F.R., and Herbst, R.S. (2001). Epidermal growth factor receptor biology (IMC-C225). Curr Opin Oncol *13*, 506-513.

Kimura, H. (1993). Schwannoma-derived growth factor must be transported into the nucleus to exert its mitogenic activity. Proc Natl Acad Sci U S A *90*, 2165-2169.

Kinugasa, Y., Ishiguro, H., Tokita, Y., Oohira, A., Ohmoto, H., and Higashiyama, S. (2004). Neuroglycan C, a novel member of the neuregulin family. Biochem Biophys Res Commun *321*, 1045-1049.

Kochupurakkal, B.S., Harari, D., Di-Segni, A., Maik-Rachline, G., Lyass, L., Gur, G., Kerber, G., Citri, A., Lavi, S., Eilam, R., *et al.* (2005). Epigen, the last ligand of ErbB receptors, reveals intricate relationships between affinity and mitogenicity. J Biol Chem *280*, 8503-8512.

Kohler, G., and Milstein, C. (1976). Derivation of specific antibody-producing tissue culture and tumor lines by cell fusion. Eur J Immunol *6*, 511-519.

Koumakpayi, I.H., Diallo, J.S., Le Page, C., Lessard, L., Gleave, M., Begin, L.R., Mes-Masson, A.M., and Saad, F. (2006). Expression and nuclear localization of ErbB3 in prostate cancer. Clin Cancer Res *12*, 2730-2737.

Kraus, M.H., Issing, W., Miki, T., Popescu, N.C., and Aaronson, S.A. (1989). Isolation and characterization of ERBB3, a third member of the ERBB/epidermal growth factor receptor family: evidence for overexpression in a subset of human mammary tumors. Proc Natl Acad Sci U S A *86*, 9193-9197.

Laban, C., Bustin, S.A., and Jenkins, P.J. (2003). The GH-IGF-I axis and breast cancer. Trends Endocrinol Metab *14*, 28-34.

Lane, H.A., Beuvink, I., Motoyama, A.B., Daly, J.M., Neve, R.M., and Hynes, N.E. (2000). ErbB2 potentiates breast tumor proliferation through modulation of

p27(Kip1)-Cdk2 complex formation: receptor overexpression does not determine growth dependency. Mol Cell Biol *20*, 3210-3223.

Lee, J., and Wood, W.I. (1993). Assignment of heregulin (HGL) to human chromosome 8p22-p11 by PCR analysis of somatic cell hybrid DNA. Genomics *16*, 790-791.

Lee, K.F., Simon, H., Chen, H., Bates, B., Hung, M.C., and Hauser, C. (1995). Requirement for neuregulin receptor erbB2 in neural and cardiac development. Nature *378*, 394-398.

Lemmens, K., Doggen, K., and De Keulenaer, G.W. (2007). Role of neuregulin-1/ErbB signaling in cardiovascular physiology and disease: implications for therapy of heart failure. Circulation *116*, 954-960.

Leng, J., Lang, J., Shen, K., and Guo, L. (1997). Overexpression of p53, EGFR, c-erbB2 and c-erbB3 in endometrioid carcinoma of the ovary. Chin Med Sci J *12*, 67-70.

Leu, M., Bellmunt, E., Schwander, M., Farinas, I., Brenner, H.R., and Muller, U. (2003). Erbb2 regulates neuromuscular synapse formation and is essential for muscle spindle development. Development *130*, 2291-2301.

Leung, A.K., Andersen, J.S., Mann, M., and Lamond, A.I. (2003). Bioinformatic analysis of the nucleolus. Biochem J *376*, 553-569.

Leung, H.Y., Weston, J., Gullick, W.J., and Williams, G. (1997). A potential autocrine loop between heregulin-alpha and erbB-3 receptor in human prostatic adenocarcinoma. Br J Urol *79*, 212-216.

Leung, T.K., Rajendran, M.Y., Monfries, C., Hall, C., and Lim, L. (1990). The human heat-shock protein family. Expression of a novel heat-inducible HSP70 (HSP70B') and isolation of its cDNA and genomic DNA. Biochem J *267*, 125-132.

Li, J., Tripathi, B.J., Chalam, K.V., and Tripathi, R.C. (1996a). Transforming growth factor-beta 1 and -beta 2 positively regulate TGF-beta 1 mRNA expression in trabecular cells. Invest Ophthalmol Vis Sci *37*, 2778-2782.

Li, Q., Ahmed, S., and Loeb, J.A. (2004). Development of an autocrine neuregulin signaling loop with malignant transformation of human breast epithelial cells. Cancer Res *64*, 7078-7085.

Li, W., Park, J.W., Nuijens, A., Sliwkowski, M.X., and Keller, G.A. (1996b). Heregulin is rapidly translocated to the nucleus and its transport is correlated with c-myc induction in breast cancer cells. Oncogene *12*, 2473-2477.

Liao, H.J., and Carpenter, G. (2007). Role of the Sec61 translocon in EGF receptor trafficking to the nucleus and gene expression. Mol Biol Cell *18*, 1064-1072.

Lin, S.Y., Makino, K., Xia, W., Matin, A., Wen, Y., Kwong, K.Y., Bourguignon, L., and Hung, M.C. (2001). Nuclear localization of EGF receptor and its potential new role as a transcription factor. Nat Cell Biol *3*, 802-808.

Lippincott-Schwartz, J., and Patterson, G.H. (2003). Development and use of fluorescent protein markers in living cells. Science *300*, 87-91.

Liu, X., Hwang, H., Cao, L., Wen, D., Liu, N., Graham, R.M., and Zhou, M. (1998). Release of the neuregulin functional polypeptide requires its cytoplasmic tail. J Biol Chem *273*, 34335-34340.

Lo, H.W., Hsu, S.C., Ali-Seyed, M., Gunduz, M., Xia, W., Wei, Y., Bartholomeusz, G., Shih, J.Y., and Hung, M.C. (2005). Nuclear interaction of EGFR and STAT3 in the activation of the iNOS/NO pathway. Cancer Cell *7*, 575-589.

Longart, M., Liu, Y., Karavanova, I., and Buonanno, A. (2004). Neuregulin-2 is developmentally regulated and targeted to dendrites of central neurons. J Comp Neurol *472*, 156-172.

Lu, H.S., Chang, D., Philo, J.S., Zhang, K., Narhi, L.O., Liu, N., Zhang, M., Sun, J., Wen, J., Yanagihara, D., *et al.* (1995). Studies on the structure and function of glycosylated and nonglycosylated neu differentiation factors. Similarities and differences of the alpha and beta isoforms. J Biol Chem *270*, 4784-4791.

Lu, Y., Zi, X., Zhao, Y., Mascarenhas, D., and Pollak, M. (2001). Insulin-like growth factor-I receptor signaling and resistance to trastuzumab (Herceptin). J Natl Cancer Inst *93*, 1852-1857.

Luetteke, N.C., Qiu, T.H., Fenton, S.E., Troyer, K.L., Riedel, R.F., Chang, A., and Lee, D.C. (1999). Targeted inactivation of the EGF and amphiregulin genes reveals distinct roles for EGF receptor ligands in mouse mammary gland development. Development *126*, 2739-2750.

Lupu, R., Cardillo, M., Cho, C., Harris, L., Hijazi, M., Perez, C., Rosenberg, K., Yang, D., and Tang, C. (1996). The significance of heregulin in breast cancer tumor progression and drug resistance. Breast Cancer Res Treat *38*, 57-66.

Lynch, T.J., Bell, D.W., Sordella, R., Gurubhagavatula, S., Okimoto, R.A., Brannigan, B.W., Harris, P.L., Haserlat, S.M., Supko, J.G., Haluska, F.G., *et al.* (2004). Activating mutations in the epidermal growth factor receptor underlying responsiveness of non-small-cell lung cancer to gefitinib. N Engl J Med *350*, 2129-2139.

Machatkova, M., Jurmanova, K., and Snejdar, V. (1986). [Decontamination of continual cell lines spontaneously infected with mycoplasmas]. Vet Med (Praha) *31*, 415-422.

Mandal, M., Li, F., and Kumar, R. (2002). Heregulin up-regulates heat shock protein-70 expression in breast cancer cells. Anticancer Res *22*, 1965-1969.

Marchionni, M.A., Goodearl, A.D., Chen, M.S., Bermingham-McDonogh, O., Kirk, C., Hendricks, M., Danehy, F., Misumi, D., Sudhalter, J., Kobayashi, K., *et al.* (1993). Glial growth factors are alternatively spliced erbB2 ligands expressed in the nervous system. Nature *362*, 312-318.

Marshall, C., Blackburn, E., Clark, M., Humphreys, S., and Gullick, W.J. (2006). Neuregulins 1-4 are expressed in the cytoplasm or nuclei of ductal carcinoma (in situ) of the human breast. Breast Cancer Res Treat *96*, 163-168.

Marti, U., Burwen, S.J., Wells, A., Barker, M.E., Huling, S., Feren, A.M., and Jones, A.L. (1991). Localization of epidermal growth factor receptor in hepatocyte nuclei. Hepatology *13*, 15-20.

Mazumdar, A., Adam, L., Boyd, D., and Kumar, R. (2001). Heregulin regulation of urokinase plasminogen activator and its receptor: human breast epithelial cell invasion. Cancer Res *61*, 400-405.

McIntyre, E., Blackburn, E., Brown, P.J., Johnson, C.G., and Gullick, W.J. (2010). The complete family of epidermal growth factor receptors and their ligands are co-ordinately expressed in breast cancer. Breast Cancer Res Treat *122*, 105-110.

Meier, T., Masciulli, F., Moore, C., Schoumacher, F., Eppenberger, U., Denzer, A.J., Jones, G., and Brenner, H.R. (1998). Agrin can mediate acetylcholine receptor gene expression in muscle by aggregation of muscle-derived neuregulins. J Cell Biol *141*, 715-726.

Miettinen, P.J., Berger, J.E., Meneses, J., Phung, Y., Pedersen, R.A., Werb, Z., and Derynck, R. (1995). Epithelial immaturity and multiorgan failure in mice lacking epidermal growth factor receptor. Nature *376*, 337-341.

Mills, G.B., Kohn, E., Lu, Y., Eder, A., Fang, X., Wang, H., Bast, R.C., Gray, J., Jaffe, R., and Hortobagyi, G. (2003). Linking molecular diagnostics to molecular therapeutics: targeting the PI3K pathway in breast cancer. Semin Oncol *30*, 93-104.

Mitsiades, C.S., Mitsiades, N.S., McMullan, C.J., Poulaki, V., Shringarpure, R., Akiyama, M., Hideshima, T., Chauhan, D., Joseph, M., Libermann, T.A., *et al.* (2004). Inhibition of the insulin-like growth factor receptor-1 tyrosine kinase activity as a therapeutic strategy for multiple myeloma, other hematologic malignancies, and solid tumors. Cancer Cell *5*, 221-230.

Montero, J.C., Rodriguez-Barrueco, R., Yuste, L., Juanes, P.P., Borges, J., Esparis-Ogando, A., and Pandiella, A. (2007). The extracellular linker of pro-neuregulin-alpha2c is required for efficient sorting and juxtacrine function. Mol Biol Cell *18*, 380-393.

Montero, J.C., Yuste, L., Diaz-Rodriguez, E., Esparis-Ogando, A., and Pandiella, A. (2000). Differential shedding of transmembrane neuregulin isoforms by the tumor necrosis factor-alpha-converting enzyme. Mol Cell Neurosci *16*, 631-648.

Moroianu, J., and Riordan, J.F. (1994). Nuclear translocation of angiogenin in proliferating endothelial cells is essential to its angiogenic activity. Proc Natl Acad Sci U S A *91*, 1677-1681.

Moscoso, L.M., Chu, G.C., Gautam, M., Noakes, P.G., Merlie, J.P., and Sanes, J.R. (1995). Synapse-associated expression of an acetylcholine receptor-inducing protein, ARIA/heregulin, and its putative receptors, ErbB2 and ErbB3, in developing mammalian muscle. Dev Biol *172*, 158-169.

Motoyama, A.B., Hynes, N.E., and Lane, H.A. (2002). The efficacy of ErbB receptor-targeted anticancer therapeutics is influenced by the availability of epidermal growth factor-related peptides. Cancer Res *62*, 3151-3158.

Naidu, R., Yadav, M., Nair, S., and Kutty, M.K. (1998). Expression of c-erbB3 protein in primary breast carcinomas. Br J Cancer *78*, 1385-1390.

Nathan, C., and Muller, W.A. (2001). Putting the brakes on innate immunity: a regulatory role for CD200? Nat Immunol *2*, 17-19.

Nguyen, M.T., and Karaplis, A.C. (1998). The nucleus: a target site for parathyroid hormone-related peptide (PTHrP) action. J Cell Biochem *70*, 193-199.

Ni, C.Y., Murphy, M.P., Golde, T.E., and Carpenter, G. (2001). gamma -Secretase cleavage and nuclear localization of ErbB-4 receptor tyrosine kinase. Science *294*, 2179-2181.

Nielsen, T.O., Hsu, F.D., O'Connell, J.X., Gilks, C.B., Sorensen, P.H., Linn, S., West, R.B., Liu, C.L., Botstein, D., Brown, P.O., *et al.* (2003). Tissue microarray validation of epidermal growth factor receptor and SALL2 in synovial sarcoma with comparison to tumors of similar histology. Am J Pathol *163*, 1449-1456.

Niwa, H., Inouye, S., Hirano, T., Matsuno, T., Kojima, S., Kubota, M., Ohashi, M., and Tsuji, F.I. (1996). Chemical nature of the light emitter of the Aequorea green fluorescent protein. Proc Natl Acad Sci U S A *93*, 13617-13622.

Noonan, E.J., Place, R.F., Giardina, C., and Hightower, L.E. (2007a). Hsp70B' regulation and function. Cell Stress Chaperones *12*, 393-402.

Noonan, E.J., Place, R.F., Rasoulpour, R.J., Giardina, C., and Hightower, L.E. (2007b). Cell number-dependent regulation of Hsp70B' expression: evidence of an extracellular regulator. J Cell Physiol *210*, 201-211.

Normanno, N., Bianco, C., De Luca, A., Maiello, M.R., and Salomon, D.S. (2003). Target-based agents against ErbB receptors and their ligands: a novel approach to cancer treatment. Endocr Relat Cancer *10*, 1-21.

Normanno, N., Bianco, C., De Luca, A., and Salomon, D.S. (2001). The role of EGF-related peptides in tumor growth. Front Biosci *6*, D685-707.

Normanno, N., De Luca, A., Bianco, C., Strizzi, L., Mancino, M., Maiello, M.R., Carotenuto, A., De Feo, G., Caponigro, F., and Salomon, D.S. (2006). Epidermal growth factor receptor (EGFR) signaling in cancer. Gene *366*, 2-16.

Nyati, M.K., Maheshwari, D., Hanasoge, S., Sreekumar, A., Rynkiewicz, S.D., Chinnaiyan, A.M., Leopold, W.R., Ethier, S.P., and Lawrence, T.S. (2004). Radiosensitization by pan ErbB inhibitor CI-1033 in vitro and in vivo. Clin Cancer Res *10*, 691-700.

Offterdinger, M., Schofer, C., Weipoltshammer, K., and Grunt, T.W. (2002). c-erbB-3: a nuclear protein in mammary epithelial cells. J Cell Biol *157*, 929-939.

Ogiso, H., Ishitani, R., Nureki, O., Fukai, S., Yamanaka, M., Kim, J.H., Saito, K., Sakamoto, A., Inoue, M., Shirouzu, M., *et al.* (2002). Crystal structure of the complex of human epidermal growth factor and receptor extracellular domains. Cell *110*, 775-787.

Okuwaki, M. (2006). [Structure and function of the nucleolus]. Tanpakushitsu Kakusan Koso *51*, 1950-1956.

Olayioye, M.A., Graus-Porta, D., Beerli, R.R., Rohrer, J., Gay, B., and Hynes, N.E. (1998). ErbB-1 and ErbB-2 acquire distinct signaling properties dependent upon their dimerization partner. Mol Cell Biol *18*, 5042-5051.

Olayioye, M.A., Neve, R.M., Lane, H.A., and Hynes, N.E. (2000). The ErbB signaling network: receptor heterodimerization in development and cancer. Embo J *19*, 3159-3167.

Olsnes, S., Klingenberg, O., and Wiedlocha, A. (2003). Transport of exogenous growth factors and cytokines to the cytosol and to the nucleus. Physiol Rev *83*, 163-182.

Paez, J.G., Janne, P.A., Lee, J.C., Tracy, S., Greulich, H., Gabriel, S., Herman, P., Kaye, F.J., Lindeman, N., Boggon, T.J., *et al.* (2004). EGFR mutations in lung cancer: correlation with clinical response to gefitinib therapy. Science *304*, 1497-1500.

Pao, W., Miller, V.A., Politi, K.A., Riely, G.J., Somwar, R., Zakowski, M.F., Kris, M.G., and Varmus, H. (2005). Acquired resistance of lung adenocarcinomas to gefitinib or erlotinib is associated with a second mutation in the EGFR kinase domain. PLoS Med *2*, e73.

Patterson, G.H., and Lippincott-Schwartz, J. (2002). A photoactivatable GFP for selective photolabeling of proteins and cells. Science *297*, 1873-1877.

Pedersen, M.W., Meltorn, M., Damstrup, L., and Poulsen, H.S. (2001). The type III epidermal growth factor receptor mutation. Biological significance and potential target for anti-cancer therapy. Ann Oncol *12*, 745-760.

Peles, E., Bacus, S.S., Koski, R.A., Lu, H.S., Wen, D., Ogden, S.G., Levy, R.B., and Yarden, Y. (1992). Isolation of the neu/HER-2 stimulatory ligand: a 44 kd glycoprotein that induces differentiation of mammary tumor cells. Cell *69*, 205-216.

Prickett, T.D., Agrawal, N.S., Wei, X., Yates, K.E., Lin, J.C., Wunderlich, J.R., Cronin, J.C., Cruz, P., Rosenberg, S.A., and Samuels, Y. (2009). Analysis of the tyrosine kinome in melanoma reveals recurrent mutations in ERBB4. Nat Genet *41*, 1127-1132.

Prigent, S.A., and Gullick, W.J. (1994). Identification of c-erbB-3 binding sites for phosphatidylinositol 3'-kinase and SHC using an EGF receptor/c-erbB-3 chimera. Embo J *13*, 2831-2841.

Prigent, S.A., Lemoine, N.R., Hughes, C.M., Plowman, G.D., Selden, C., and Gullick, W.J. (1992). Expression of the c-erbB-3 protein in normal human adult and fetal tissues. Oncogene *7*, 1273-1278.

Qi, C.F., Liscia, D.S., Normanno, N., Merlo, G., Johnson, G.R., Gullick, W.J., Ciardiello, F., Saeki, T., Brandt, R., Kim, N., *et al.* (1994). Expression of transforming growth factor alpha, amphiregulin and cripto-1 in human breast carcinomas. Br J Cancer *69*, 903-910.

Qian, X., LeVea, C.M., Freeman, J.K., Dougall, W.C., and Greene, M.I. (1994).

Heterodimerization of epidermal growth factor receptor and wild-type or kinase-deficient Neu: a mechanism of interreceptor kinase activation and transphosphorylation. Proc Natl Acad Sci U S A *91*, 1500-1504.

Rajkumar, T., Stamp, G.W., Hughes, C.M., and Gullick, W.J. (1996). c-erbB3 protein expression in ovarian cancer. Clin Mol Pathol *49*, M199-M202.

Ramos-Vara, J.A., and Beissenherz, M.E. (2000). Optimization of immunohistochemical methods using two different antigen retrieval methods on formalin-fixed paraffin-embedded tissues: experience with 63 markers. J Vet Diagn Invest *12*, 307-311.

Red Brewer, M., Choi, S.H., Alvarado, D., Moravcevic, K., Pozzi, A., Lemmon, M.A., and Carpenter, G. (2009). The juxtamembrane region of the EGF receptor functions as an activation domain. Mol Cell *34*, 641-651.

Revillion, F., Lhotellier, V., Hornez, L., Bonneterre, J., and Peyrat, J.P. (2008). ErbB/HER ligands in human breast cancer, and relationships with their receptors, the bio-pathological features and prognosis. Ann Oncol *19*, 73-80.

Rimer, M., Prieto, A.L., Weber, J.L., Colasante, C., Ponomareva, O., Fromm, L., Schwab, M.H., Lai, C., and Burden, S.J. (2004). Neuregulin-2 is synthesized by motor neurons and terminal Schwann cells and activates acetylcholine receptor transcription in muscle cells expressing ErbB4. Mol Cell Neurosci *26*, 271-281.

Ring, H.Z., Chang, H., Guilbot, A., Brice, A., LeGuern, E., and Francke, U. (1999). The human neuregulin-2 (NRG2) gene: cloning, mapping and evaluation as a candidate for the autosomal recessive form of Charcot-Marie-Tooth disease linked to 5q. Hum Genet *104*, 326-332.

Robertson, S.C., Tynan, J.A., and Donoghue, D.J. (2000). RTK mutations and human syndromeswhen good receptors turn bad. Trends Genet *16*, 265-271.

Rowan, M.J., Klyubin, I., Cullen, W.K., and Anwyl, R. (2003). Synaptic plasticity in animal models of early Alzheimer's disease. Philos Trans R Soc Lond B Biol Sci *358*, 821-828.

Saeki, T., Stromberg, K., Qi, C.F., Gullick, W.J., Tahara, E., Normanno, N., Ciardiello, F., Kenney, N., Johnson, G.R., and Salomon, D.S. (1992). Differential immunohistochemical detection of amphiregulin and cripto in human normal colon and colorectal tumors. Cancer Res *52*, 3467-3473.

Salomon, D.S., Brandt, R., Ciardiello, F., and Normanno, N. (1995). Epidermal growth factor-related peptides and their receptors in human malignancies. Crit Rev Oncol Hematol *19*, 183-232.

Sandgren, E.P., Schroeder, J.A., Qui, T.H., Palmiter, R.D., Brinster, R.L., and Lee, D.C. (1995). Inhibition of mammary gland involution is associated with transforming growth factor alpha but not c-myc-induced tumorigenesis in transgenic mice. Cancer Res *55*, 3915-3927.

Sandvig, K., and van Deurs, B. (2000). Entry of ricin and Shiga toxin into cells:

molecular mechanisms and medical perspectives. Embo J *19*, 5943-5950.

Sartor, C.I., Zhou, H., Kozlowska, E., Guttridge, K., Kawata, E., Caskey, L., Harrelson, J., Hynes, N., Ethier, S., Calvo, B., *et al.* (2001). Her4 mediates ligand-dependent antiproliferative and differentiation responses in human breast cancer cells. Mol Cell Biol *21*, 4265-4275.

Schlessinger, J. (2000). Cell signaling by receptor tyrosine kinases. Cell *103*, 211-225.

Sergina, N.V., Rausch, M., Wang, D., Blair, J., Hann, B., Shokat, K.M., and Moasser, M.M. (2007). Escape from HER-family tyrosine kinase inhibitor therapy by the kinase-inactive HER3. Nature *445*, 437-441.

Shaner, N.C., Campbell, R.E., Steinbach, P.A., Giepmans, B.N., Palmer, A.E., and Tsien, R.Y. (2004). Improved monomeric red, orange and yellow fluorescent proteins derived from Discosoma sp. red fluorescent protein. Nat Biotechnol *22*, 1567-1572.

Sharp, P.A. (1994). Split genes and RNA splicing. Cell *77*, 805-815.

Shav-Tal, Y., Darzacq, X., Shenoy, S.M., Fusco, D., Janicki, S.M., Spector, D.L., and Singer, R.H. (2004). Dynamics of single mRNPs in nuclei of living cells. Science *304*, 1797-1800.

She, Q.B., Solit, D., Basso, A., and Moasser, M.M. (2003). Resistance to gefitinib in PTEN-null HER-overexpressing tumor cells can be overcome through restoration of PTEN function or pharmacologic modulation of constitutive phosphatidylinositol 3'-kinase/Akt pathway signaling. Clin Cancer Res *9*, 4340-4346.

Shi, F., Telesco, S.E., Liu, Y., Radhakrishnan, R., and Lemmon, M.A. (2010a). ErbB3/HER3 intracellular domain is competent to bind ATP and catalyze autophosphorylation. Proc Natl Acad Sci U S A *107*, 7692-7697.

Shi, F., Telesco, S.E., Liu, Y., Radhakrishnan, R., and Lemmon, M.A. (2010b). ErbB3/HER3 intracellular domain is competent to bind ATP and catalyze autophosphorylation. Proc Natl Acad Sci U S A.

Shintani, S., Funayama, T., Yoshihama, Y., Alcalde, R.E., and Matsumura, T. (1995). Prognostic significance of ERBB3 overexpression in oral squamous cell carcinoma. Cancer Lett *95*, 79-83.

Shirakabe, K., Wakatsuki, S., Kurisaki, T., and Fujisawa-Sehara, A. (2001). Roles of Meltrin beta /ADAM19 in the processing of neuregulin. J Biol Chem *276*, 9352-9358.

Sibilia, M., Steinbach, J.P., Stingl, L., Aguzzi, A., and Wagner, E.F. (1998). A strain-independent postnatal neurodegeneration in mice lacking the EGF receptor. Embo J *17*, 719-731.

Sibilia, M., and Wagner, E.F. (1995). Strain-dependent epithelial defects in mice lacking the EGF receptor. Science *269*, 234-238.

Siegel, P.M., Ryan, E.D., Cardiff, R.D., and Muller, W.J. (1999). Elevated expression of activated forms of Neu/ErbB-2 and ErbB-3 are involved in the induction of mammary

tumors in transgenic mice: implications for human breast cancer. Embo J *18*, 2149-2164.

Sithanandam, G., and Anderson, L.M. (2008). The ERBB3 receptor in cancer and cancer gene therapy. Cancer Gene Ther *15*, 413-448.

Slamon, D.J., Clark, G.M., Wong, S.G., Levin, W.J., Ullrich, A., and McGuire, W.L. (1987). Human breast cancer: correlation of relapse and survival with amplification of the HER-2/neu oncogene. Science *235*, 177-182.

Soltoff, S.P., and Cantley, L.C. (1996). p120cbl is a cytosolic adapter protein that associates with phosphoinositide 3-kinase in response to epidermal growth factor in PC12 and other cells. J Biol Chem *271*, 563-567.

Soslow, R.A., Dannenberg, A.J., Rush, D., Woerner, B.M., Khan, K.N., Masferrer, J., and Koki, A.T. (2000). COX-2 is expressed in human pulmonary, colonic, and mammary tumors. Cancer *89*, 2637-2645.

Soung, Y.H., Lee, J.W., Kim, S.Y., Wang, Y.P., Jo, K.H., Moon, S.W., Park, W.S., Nam, S.W., Lee, J.Y., Yoo, N.J., *et al.* (2006). Somatic mutations of the ERBB4 kinase domain in human cancers. Int J Cancer *118*, 1426-1429.

Srinivasan, R., Benton, E., McCormick, F., Thomas, H., and Gullick, W.J. (1999). Expression of the c-erbB-3/HER-3 and c-erbB-4/HER-4 growth factor receptors and their ligands, neuregulin-1 alpha, neuregulin-1 beta, and betacellulin, in normal endometrium and endometrial cancer. Clin Cancer Res *5*, 2877-2883.

Srinivasan, R., Poulsom, R., Hurst, H.C., and Gullick, W.J. (1998). Expression of the c-erbB-4/HER4 protein and mRNA in normal human fetal and adult tissues and in a survey of nine solid tumour types. J Pathol *185*, 236-245.

Stark, D.A., and Kulesa, P.M. (2005). Photoactivatable green fluorescent protein as a single-cell marker in living embryos. Dev Dyn *233*, 983-992.

Stefansson, H., Sigurdsson, E., Steinthorsdottir, V., Bjornsdottir, S., Sigmundsson, T., Ghosh, S., Brynjolfsson, J., Gunnarsdottir, S., Ivarsson, O., Chou, T.T., *et al.* (2002). Neuregulin 1 and susceptibility to schizophrenia. Am J Hum Genet *71*, 877-892.

Stein, R.A., and Staros, J.V. (2000). Evolutionary analysis of the ErbB receptor and ligand families. J Mol Evol *50*, 397-412.

Stein, R.A., and Staros, J.V. (2006). Insights into the evolution of the ErbB receptor family and their ligands from sequence analysis. BMC Evol Biol *6*, 79.

Steinthorsdottir, V., Stefansson, H., Ghosh, S., Birgisdottir, B., Bjornsdottir, S., Fasquel, A.C., Olafsson, O., Stefansson, K., and Gulcher, J.R. (2004). Multiple novel transcription initiation sites for NRG1. Gene *342*, 97-105.

Stephens, P., Hunter, C., Bignell, G., Edkins, S., Davies, H., Teague, J., Stevens, C., O'Meara, S., Smith, R., Parker, A., *et al.* (2004). Lung cancer: intragenic ERBB2 kinase mutations in tumours. Nature *431*, 525-526.

Stuttfeld, E., and Ballmer-Hofer, K. (2009). Structure and function of VEGF receptors. IUBMB Life *61*, 915-922.

Subramaniam, P.S., Torres, B.A., and Johnson, H.M. (2001). So many ligands, so few transcription factors: a new paradigm for signaling through the STAT transcription factors. Cytokine *15*, 175-187.

Sweeney, C., and Carraway, K.L., 3rd (2000). Ligand discrimination by ErbB receptors: differential signaling through differential phosphorylation site usage. Oncogene *19*, 5568-5573.

Tan, M., Jing, T., Lan, K.H., Neal, C.L., Li, P., Lee, S., Fang, D., Nagata, Y., Liu, J., Arlinghaus, R., *et al.* (2002). Phosphorylation on tyrosine-15 of p34(Cdc2) by ErbB2 inhibits p34(Cdc2) activation and is involved in resistance to taxol-induced apoptosis. Mol Cell *9*, 993-1004.

Tateishi, M., Ishida, T., Mitsudomi, T., Kaneko, S., and Sugimachi, K. (1990). Immunohistochemical evidence of autocrine growth factors in adenocarcinoma of the human lung. Cancer Res *50*, 7077-7080.

Tavaria, M., Gabriele, T., Kola, I., and Anderson, R.L. (1996). A hitchhiker's guide to the human Hsp70 family. Cell Stress Chaperones *1*, 23-28.

Testa, I., Garre, M., Parazzoli, D., Barozzi, S., Ponzanelli, I., Mazza, D., Faretta, M., and Diaspro, A. (2008). Photoactivation of pa-GFP in 3D: optical tools for spatial confinement. Eur Biophys J *37*, 1219-1227.

Thatcher, N., Chang, A., Parikh, P., Rodrigues Pereira, J., Ciuleanu, T., von Pawel, J., Thongprasert, S., Tan, E.H., Pemberton, K., Archer, V., *et al.* (2005). Gefitinib plus best supportive care in previously treated patients with refractory advanced non-small-cell lung cancer: results from a randomised, placebo-controlled, multicentre study (Iressa Survival Evaluation in Lung Cancer). Lancet *366*, 1527-1537.

Thomas, D.D., Donnelly, C.A., Wood, R.J., and Alphey, L.S. (2000). Insect population control using a dominant, repressible, lethal genetic system. Science *287*, 2474-2476.

Threadgill, D.W., Dlugosz, A.A., Hansen, L.A., Tennenbaum, T., Lichti, U., Yee, D., LaMantia, C., Mourton, T., Herrup, K., Harris, R.C., *et al.* (1995). Targeted disruption of mouse EGF receptor: effect of genetic background on mutant phenotype. Science *269*, 230-234.

Tidcombe, H., Jackson-Fisher, A., Mathers, K., Stern, D.F., Gassmann, M., and Golding, J.P. (2003). Neural and mammary gland defects in ErbB4 knockout mice genetically rescued from embryonic lethality. Proc Natl Acad Sci U S A *100*, 8281-8286.

Tokunaga, E., Kimura, Y., Oki, E., Ueda, N., Futatsugi, M., Mashino, K., Yamamoto, M., Ikebe, M., Kakeji, Y., Baba, H., *et al.* (2006). Akt is frequently activated in HER2/neu-positive breast cancers and associated with poor prognosis among hormone-treated patients. Int J Cancer *118*, 284-289.

Troyer, K.L., and Lee, D.C. (2001). Regulation of mouse mammary gland development and tumorigenesis by the ERBB signaling network. J Mammary Gland Biol Neoplasia *6*,

7-21.

Tsai, B., Ye, Y., and Rapoport, T.A. (2002). Retro-translocation of proteins from the endoplasmic reticulum into the cytosol. Nat Rev Mol Cell Biol *3*, 246-255.

Tsai, M.S., Shamon-Taylor, L.A., Mehmi, I., Tang, C.K., and Lupu, R. (2003). Blockage of heregulin expression inhibits tumorigenicity and metastasis of breast cancer. Oncogene *22*, 761-768.

Ursini-Siegel, J., Schade, B., Cardiff, R.D., and Muller, W.J. (2007). Insights from transgenic mouse models of ERBB2-induced breast cancer. Nat Rev Cancer *7*, 389-397.
van Thor, J.J., Gensch, T., Hellingwerf, K.J., and Johnson, L.N. (2002). Phototransformation of green fluorescent protein with UV and visible light leads to decarboxylation of glutamate 222. Nat Struct Biol *9*, 37-41.

Vargas-Roig, L.M., Gago, F.E., Tello, O., Aznar, J.C., and Ciocca, D.R. (1998). Heat shock protein expression and drug resistance in breast cancer patients treated with induction chemotherapy. Int J Cancer *79*, 468-475.

Vecchi, M., Polo, S., Poupon, V., van de Loo, J.W., Benmerah, A., and Di Fiore, P.P. (2001). Nucleocytoplasmic shuttling of endocytic proteins. J Cell Biol *153*, 1511-1517.

Verkhusha, V.V., and Sorkin, A. (2005). Conversion of the monomeric red fluorescent protein into a photoactivatable probe. Chem Biol *12*, 279-285.

Visintin, R., Hwang, E.S., and Amon, A. (1999). Cfi1 prevents premature exit from mitosis by anchoring Cdc14 phosphatase in the nucleolus. Nature *398*, 818-823.

Vogel, C.L., Cobleigh, M.A., Tripathy, D., Gutheil, J.C., Harris, L.N., Fehrenbacher, L., Slamon, D.J., Murphy, M., Novotny, W.F., Burchmore, M., *et al.* (2002). Efficacy and safety of trastuzumab as a single agent in first-line treatment of HER2-overexpressing metastatic breast cancer. J Clin Oncol *20*, 719-726.

Wahl, M.C., Will, C.L., and Luhrmann, R. (2009). The spliceosome: design principles of a dynamic RNP machine. Cell *136*, 701-718.

Waksman, G., Kominos, D., Robertson, S.C., Pant, N., Baltimore, D., Birge, R.B., Cowburn, D., Hanafusa, H., Mayer, B.J., Overduin, M., *et al.* (1992). Crystal structure of the phosphotyrosine recognition domain SH2 of v-src complexed with tyrosine-phosphorylated peptides. Nature *358*, 646-653.

Wang, J.Y., Miller, S.J., and Falls, D.L. (2001). The N-terminal region of neuregulin isoforms determines the accumulation of cell surface and released neuregulin ectodomain. J Biol Chem *276*, 2841-2851.

Wang, S.C., Lien, H.C., Xia, W., Chen, I.F., Lo, H.W., Wang, Z., Ali-Seyed, M., Lee, D.F., Bartholomeusz, G., Ou-Yang, F., *et al.* (2004). Binding at and transactivation of the COX-2 promoter by nuclear tyrosine kinase receptor ErbB-2. Cancer Cell *6*, 251-261.

Wang, S.C., Nakajima, Y., Yu, Y.L., Xia, W., Chen, C.T., Yang, C.C., McIntush, E.W., Li, L.Y., Hawke, D.H., Kobayashi, R., *et al.* (2006a). Tyrosine phosphorylation controls

PCNA function through protein stability. Nat Cell Biol *8*, 1359-1368.

Wang, S.E., Narasanna, A., Perez-Torres, M., Xiang, B., Wu, F.Y., Yang, S., Carpenter, G., Gazdar, A.F., Muthuswamy, S.K., and Arteaga, C.L. (2006b). HER2 kinase domain mutation results in constitutive phosphorylation and activation of HER2 and EGFR and resistance to EGFR tyrosine kinase inhibitors. Cancer Cell *10*, 25-38.

Wells, A., and Marti, U. (2002). Signalling shortcuts: cell-surface receptors in the nucleus? Nat Rev Mol Cell Biol *3*, 697-702.

Wen, D., Suggs, S.V., Karunagaran, D., Liu, N., Cupples, R.L., Luo, Y., Janssen, A.M., Ben-Baruch, N., Trollinger, D.B., Jacobsen, V.L., *et al.* (1994). Structural and functional aspects of the multiplicity of Neu differentiation factors. Mol Cell Biol *14*, 1909-1919.

Wenger, R.H., Moreau, H., and Nielsen, P.J. (1994). A comparison of different promoter, enhancer, and cell type combinations in transient transfections. Anal Biochem *221*, 416-418.

Wiertz, E.J., Tortorella, D., Bogyo, M., Yu, J., Mothes, W., Jones, T.R., Rapoport, T.A., and Ploegh, H.L. (1996). Sec61-mediated transfer of a membrane protein from the endoplasmic reticulum to the proteasome for destruction. Nature *384*, 432-438.

Wiley, H.S. (2003). Trafficking of the ErbB receptors and its influence on signaling. Exp Cell Res *284*, 78-88.

Williams, C.C., Allison, J.G., Vidal, G.A., Burow, M.E., Beckman, B.S., Marrero, L., and Jones, F.E. (2004). The ERBB4/HER4 receptor tyrosine kinase regulates gene expression by functioning as a STAT5A nuclear chaperone. J Cell Biol *167*, 469-478.

Xian, C.J., and Zhou, X.F. (2004). EGF family of growth factors: essential roles and functional redundancy in the nerve system. Front Biosci *9*, 85-92.

Xie, Y., and Hung, M.C. (1994). Nuclear localization of p185neu tyrosine kinase and its association with transcriptional transactivation. Biochem Biophys Res Commun *203*, 1589-1598.

Yaffe, M.B. (2002). Phosphotyrosine-binding domains in signal transduction. Nat Rev Mol Cell Biol *3*, 177-186.

Yao, B., Rakhade, S.N., Li, Q., Ahmed, S., Krauss, R., Draghici, S., and Loeb, J.A. (2004). Accuracy of cDNA microarray methods to detect small gene expression changes induced by neuregulin on breast epithelial cells. BMC Bioinformatics *5*, 99.

Yarden, Y. (2001). The EGFR family and its ligands in human cancer. signalling mechanisms and therapeutic opportunities. Eur J Cancer *37 Suppl 4*, S3-8.

Yarden, Y., and Sliwkowski, M.X. (2001). Untangling the ErbB signalling network. Nat Rev Mol Cell Biol *2*, 127-137.

Yarranton, G.T. (1992). Inducible vectors for expression in mammalian cells. Curr Opin Biotechnol *3*, 506-511.

Yi, E.S., Harclerode, D., Gondo, M., Stephenson, M., Brown, R.W., Younes, M., and Cagle, P.T. (1997). High c-erbB-3 protein expression is associated with shorter survival in advanced non-small cell lung carcinomas. Mod Pathol *10*, 142-148.

Yokoe, H., and Meyer, T. (1996). Spatial dynamics of GFP-tagged proteins investigated by local fluorescence enhancement. Nat Biotechnol *14*, 1252-1256.

Zhang, D., Sliwkowski, M.X., Mark, M., Frantz, G., Akita, R., Sun, Y., Hillan, K., Crowley, C., Brush, J., and Godowski, P.J. (1997). Neuregulin-3 (NRG3): a novel neural tissue-enriched protein that binds and activates ErbB4. Proc Natl Acad Sci U S A *94*, 9562-9567.

Zhang, X., Gureasko, J., Shen, K., Cole, P.A., and Kuriyan, J. (2006). An allosteric mechanism for activation of the kinase domain of epidermal growth factor receptor. Cell *125*, 1137-1149.

Zhang, X., Pickin, K.A., Bose, R., Jura, N., Cole, P.A., and Kuriyan, J. (2007). Inhibition of the EGF receptor by binding of MIG6 to an activating kinase domain interface. Nature *450*, 741-744.

Zhou, B.B., Peyton, M., He, B., Liu, C., Girard, L., Caudler, E., Lo, Y., Baribaud, F., Mikami, I., Reguart, N., *et al.* (2006). Targeting ADAM-mediated ligand cleavage to inhibit HER3 and EGFR pathways in non-small cell lung cancer. Cancer Cell *10*, 39-50.
Zhou, W., and Carpenter, G. (2000). Heregulin-dependent trafficking and cleavage of ErbB-4. J Biol Chem *275*, 34737-34743.

Zorov, D.B., Kobrinsky, E., Juhaszova, M., and Sollott, S.J. (2004). Examining intracellular organelle function using fluorescent probes: from animalcules to quantum dots. Circ Res *95*, 239-252.

Zunszain, P.A., Ghuman, J., Komatsu, T., Tsuchida, E., and Curry, S. (2003). Crystal structural analysis of human serum albumin complexed with hemin and fatty acid. BMC Struct Biol *3*, 6.